DOCTORAL THESIS

Innovative nanosystems for diagnosis and treatment of colorectal cancer

Surasa Nagachinta

NanoFar, Erasmus Mundus Joint Doctorate in Nanomedicine and Pharmaceutical Innovation

University of Santiago de Compostela

Santiago de Compostela, Spain

2018

Education and Culture DG

ERASMUS MUNDUS

USC
UNIVERSIDADE
DE SANTIAGO
DE COMPOSTELA

TESIS DOCTORAL

Nanosistemas innovadores para el diagnóstico y tratamiento del cáncer de colon

Surasa Nagachinta

Programa de doctorado en Nanomedicina e Innovación Farmacéutica

Universidad de Santiago de Compostela

Santiago de Compostela, España

2018

Education and Culture DG

ERASMUS MUNDUS

USC
UNIVERSIDADE
DE SANTIAGO
DE COMPOSTELA

AUTHORIZATION OF THE THESIS SUPERVISORS

Innovative nanosystems for diagnosis and treatment of colorectal cancer

Dr. María de la Fuente Freire, Full time Researcher (Miguel Servet program). Head of the Nano-Oncology Unit, Health Research Institute of Santiago de Compostela (IDIS), Servizo Galego de Saúde (SERGAS). Santiago de Compostela, Spain.

Prof. Rafael López López, Associate Professor, Department of Medicine, University of Santiago de Compostela, Spain.

Prof. André Luxen, Full Professor, Laboratory of Radiochemistry, Cyclotron Research Center (CRC), University of Liége, Belgium

REPORT:

That the present thesis, corresponds to the work carried out by Miss Surasa Nagachinta, under our supervision, and that we authorize its presentation considering it gathers the necessary requirements of article 34 of the USC Doctoral Studies regulation, and that as supervisors of this thesis, it does not incur in the abstention causes established by the law 40/2015.

At Santiago de Compostela on _____ 2018

Dr. María de la Fuente Freire Prof. Rafael López López Prof. André Luxen

USC
UNIVERSIDADE
DE SANTIAGO
DE COMPOSTELA

AUTORIZACIÓN DEL DIRECTOR / TUTOR DE LA TESIS

Nanosistemas innovadores para el diagnóstico y tratamiento del cáncer de colon

Dra María de la Fuente Freire, Investigadora (programa Miguel Servet). Directora de la Unidad de Nano-Oncología del Instituto de Investigación Sanitaria de Santiago de Compostela (IDIS), SERGAS, Santiago de Compostela, España.

Prof. Rafael López López, profesor asociado, departamento de Medicina, Universidad de Santiago de Compostela, España.

Prof. André Luxen, Full Professor, Laboratory of Radiochemistry, Cyclotron Research Center (CRC), Universidad de Liége, Belgium

INFORMA/N:

Que la presente tesis, se corresponde con el trabajo realizado por Dña. Surasa Nagachinta, bajo mi dirección, y autorizo su presentación, considerando que reúne los requisitos exigidos en la Regulación de Estudios de Doctorado de la USC, y que como director de esta no incurre en las causas de abstención establecidas en la Ley 40/2015.

En Santiago de Compostela a _____ de 2018

Dr. María de la Fuente Freire Prof. Rafael López López Prof. André Luxen

USC
UNIVERSIDADE
DE SANTIAGO
DE COMPOSTELA

PhD CANDIDATE STATEMENT

Innovative nanosystems for diagnosis and treatment of colorectal cancer

Miss Surasa Nagachinta

I submit my Doctoral thesis, following the procedure according to the Regulation, stating that:

1) This thesis gathers the results corresponding to my work.
2) When necessary, explicit mention is given to the collaborations the work may have had.
3) The present document is the final version submitted for its defense and coincide with the document sent in electronic format.
4) I confirm that this thesis does not incur in any plagiarism of any other authors or documents submitted by me for obtaining other degrees.

At Santiago de Compostela, _____ 2018

Miss Surasa Nagachinta

USC
UNIVERSIDADE
DE SANTIAGO
DE COMPOSTELA

DECLARACIÓN DEL AUTOR/A DE LA TESIS

Nanosistemas innovadores para el diagnóstico y tratamiento del cáncer de colon

Dña. Surasa Nagachinta

Presento mi tesis, siguiendo el procedimiento adecuado a la Regulación, y declaro que:

1) La tesis abarca los resultados de la elaboración de mi trabajo.
2) De ser el caso, en la tesis se hace referencia a las colaboraciones que tuvo este trabajo.
3) La tesis es la versión definitiva presentada para su defensa y coincide con la versión enviada en formato electrónico.
4) Confirmo que la tesis no incurre en ningún tipo de plagio de otros autores ni de trabajos presentados por mí para la obtención de otros títulos.

En Santiago de Compostela a _____ *de 2018*

Dña. Surasa Nagachinta

USC
UNIVERSIDADE
DE SANTIAGO
DE COMPOSTELA

Dedicated to my beloved family

Surasa Nagachinta 2018

USC
UNIVERSIDADE
DE SANTIAGO
DE COMPOSTELA

Imagination is more important than knowledge

Albert Einstein

USC
UNIVERSIDADE
DE SANTIAGO
DE COMPOSTELA

Acknowledgements

First and foremost, I extend my gratitude to the European Commission (EACEA) for the Erasmus Mundus grant under the Nanofar Joint Doctoral Program. I would like to thank deeply Prof. Frank Boury and related NanoFar members for their dedication to this European doctorate program. This also includes my NanoFar friends with whom I had incredible times during NanoFar classes and meetings. I was very happy to be part of this great PhD programme. I wish to all of my friends the best for their future and hopefully to stay in touch for the upcoming years.

I would like to gratefully thank Dr. María de la Fuente Freire, Prof. Rafael López López, and Prof. André Luxen for giving me this opportunity to undertake this PhD in their groups during the past three years. I cordially appreciate their continued guidance, enthusiasm and help throughout my thesis. Dr. María de la Fuente Freire gave me a lot of her time as well as invaluable advice for my research. She made a lot of efforts on the revision of my thesis, letting me learn many excellent skills in academic writing. I really appreciate all of her inspiration and contribution. I would also like to thank Prof. Rafael López López for his prompt support, especially when I had a health problem. I express my sincere appreciation to my supervisor, Prof. André Luxen. He strongly supported me with the best resource for my scientific adventure in Belgium. Despite his busy schedule, he took the time needed and went out of his way to discuss my experimental works. I really appreciate all of his supportive contributions.

Also, I would like to thank my colleagues in Lab18 and Lab13 at IDIS for the fruitful collaboration during my work. In special, thanks to Belen, Abi, Marta, Sai, Sandra10, Sandra, Raneem for your constant support, inside and outside of the lab. Thanks to the members of our neighbor lab, Sabella, Alba, Pablo, Mariajo, Miguel, Eloi, Maria, and Ana for always helping me with all the lab equipment and cell experiments. My gratitude also goes to all the researchers in the hospital for their continued welcome and support. I learned and grew a lot from their experience and guidance. Their friendship made these years so much fun and brought about some of the most unforgettable times of my life.

Many thanks to all the people who have collaborated with me in CIMUS, CACTUS, and the hospital, Balby, Belen, Lucia, Estaban, and Marta for your scientific guidance and support. Marta devoted a lot of time and effort to take good pictures from confocal. Balby supported me every time for the freeze-dry cycle. To people in CIMUS, Lena, Nataliya, Sonia, Adriana, Jose, Tamara, Irene, Carla, Sofia, Sara, Andrea, and German: thank you so much for sharing your knowledge and ideas with me. To Puri thank you so much for your help with all administrative works. All the time you have been very kind, helpful and resourceful.

I would like to thank my Asian friends, Howl, Paul, Maruthi, Ulung, and Muhammad for having such a big heart and for letting me be a part of the Asian family. You are enormous. In special, thanks to Maruthi for walking alongside me since we started this “camino” in PhD. I would like to thank also Mehtap, Yuki and Carla for all the friendship and support wherever we are! Thank you so much for being with me during the hard times.

To all the cyclotron members, you are an amazing team. I would like to thank Sylvestre for all your help. You greatly improved my knowledge in chemistry and taught me several radiolabeling techniques. Thank you for being patient, especially at the beginning of my labelling experiment. I would also like to thank Christian for his support during the labelling experiment. I am grateful to my PET-MRI team, Guillaume, Mohamed, and Alain for your advice in the biodistribution study. Of course, Melisa and Natacha, for all the experiments we performed together and for sharing your mice-working experience. I owe a huge thanks to Agostinho, Jerome and Nicolas. Thank you for all the fun moments, you are awesome!

I would like to thank Brigitte and Annick for helping me with all the paper works in Belgium and for ordering our chemicals. Christine, for her help and many practical things in the lab. Charlotte, for her technical support for DLS. Besides, I would like to thank all the people of both the cyclotron center and the chemistry building with whom I had to chance to work during my PhD. In special, thanks to Jeremie, Paul, and Shabnam for the time that we studied together during animal lectures and for being great colleagues. Yes! we passed the exam.

Certainly, I warmly thank my NanoFar friends in Liège. Bathabile for the first introduction to the city and the information about the accommodation. Rahmet and Zeynep for all the time we spent in both scientific study and leisure activities. And all my international lunchmates at the cafeteria, John, Ruben, and Nikola for sharing great talks and interesting topics during lunch time.

Of course, my deepest gratitude goes to my parents and my big family. Even though we are far away from each other by distance, I always feel their presence and support. Their eternal guidance is beyond words. Finally, I thank all my proofreaders, Air, Rob, and Martin, who have been very kind during the tight schedule I had to submit my thesis.

This PhD programme is now hopefully coming to an end. I am grateful for this great opportunity to build up my academic experience and for all the people it has enabled me to meet and cooperate with. As much as I enjoy reaching its destination, I want to thank each and every one of you for making this journey unforgettable.

USC
UNIVERSIDADE
DE SANTIAGO
DE COMPOSTELA

CONFLICT OF INTEREST

I declare no conflicts of interest with the subject, matter or materials discussed in this thesis.

Miss Surasa Nagachinta

USC
UNIVERSIDADE
DE SANTIAGO
DE COMPOSTELA

Table of contents

USC
UNIVERSIDADE
DE SANTIAGO
DE COMPOSTELA

Abstract / Resumen

USC
UNIVERSIDADE
DE SANTIAGO
DE COMPOSTELA

Abstract

The main goal of this thesis has been the engineering of innovative nanosystems of application in the treatment and molecular diagnosis of colorectal cancer. Sphingomyelin nanoemulsions (SNs) were selected for this purpose, and their composition adapted to and efficient association of oncosuppressor miRNAs for development of anticancer gene therapies able to stop tumor growth and proliferation. Additionally, a procedure for developing ^{18}F-radiolabelled SNs for imaging and diagnosis purposes was optimized, and validated by PET.

SNs, formulated by the ethanol injection method, provide ideal conditions for the incorporation of sensitive biomolecules such as nucleic acids. For miRNA association two approaches were followed. First, it was incorporated a cationic lipid, stearylamine, to allow further miRNA association to the surface of nanoemulsions via electrostatic interactions. Second method involved the preformation of lipid complexes (miRNA and DOTAP) and subsequent encapsulation into SNs. Both approaches demonstrated to mediate an efficient association and delivery of oncosuppressor miRNA145 to colorectal cancer cells. The second strategy rendered an improved uptake and subsequent increase in the intracellular levels of miRNA145. Functional assays confirmed that this formulation was able to exert an anti-tumor activity, through the inhibition of cell proliferation, colony-forming, and cell migration capacities, highlighting the potential of this approach for the development of miRNAs gene replacement therapies.

Secondly, it was attempted the radiolabelling of SNs with ^{18}F, following an indirect method that uses 4-[^{18}F]fluorobenzamido-N-ethylmaleimide ([^{18}F]FBEM) as a ^{18}F-prosthetic group. The chemical reaction was performed between the maleimide group of [^{18}F]FBEM and the thiol functional groups located at the surface of either SNs bearing PEG-SH, or SNs decorated with the RPM peptide. Biodistribution studies and PET images allowed us to conclude that it is possible to track the radiolabelled SNs after intravenous injection to mice.

In conclusion, it has been proved that SNs are versatile nanosystems that can be adapted to different medical needs. SNs are efficient nanosystems for the delivery of innovative-targeted gene therapies, and can be successfully radiolabeled allowing whole-body read-outs by PET. Altogether, SNs are a promising platform for therapy and diagnosis of colorectal cancer, and have potential for further development of nanotheranostics.

USC
UNIVERSIDADE
DE SANTIAGO
DE COMPOSTELA

Resumen

El objetivo principal de esta tesis ha sido el desarrollo de nanosistemas innovadores de aplicación en el tratamiento y diagnóstico molecular del cáncer colorrectal. En este trabajo se exploró el potencial de nanoemulsiones de esfingomielina (SNs) para la asociación de miRNAs oncosupresores como estrategia para detener el crecimiento y la proliferación tumoral. Por otro lado, se optimizó un procedimiento para desarrollar SNs radiomarcadas con ^{18}F con fines diagnósticos mediante imagen molecular por Tomografía de Emisión de Positrones (PET).

Para la asociación del miRNA se propusieron dos enfoques. En primer lugar, la incorporación de un lípido catiónico, la estearilamina, de modo que se vea favorecida la asociación del miRNA mediante el establecimiento de interacciones electrostáticas. En segundo lugar, la formación previa de complejos lipídicos (miRNA-DOTAP) para su posterior encapsulación en SNs. Ambos enfoques demostraron ser adecuados para la asociación y la administración del miRNA oncosupresor (miR145) a células de cáncer colorrectal. La segunda estrategia produjo un mayor aumento en los niveles intracelulares de miR145. Ensayos funcionales confirmaron a su vez que esta formulación presenta un gran potencial para el desarrollo de terapias antitumorales, dado es capaz de mediar una inhibición de la proliferación celular, capacidad de formación de colonias, y migración.

Se procedió además a marcar las SNs con ^{18}F, para su uso en imagen diagnóstica (PET), empleando un método indirecto que utiliza 4-[^{18}F]fluorobenzamido-N-etilmaleimida ([^{18}F]FBEM) como grupo protésico ^{18}F. La conjugación química se realizó mediante la reacción del grupo maleimida del [^{18}F]FBEM, con grupos funcionales tiol, introducidos en SNs en forma de lípido C_{18}-PEG_{12}-SH, o tras ser decoradas con el péptido RMP. Los estudios de biodistribución y las imágenes permitieron rastrear las SNs tras ser inyectadas por vía intravenosa en ratones.

En conclusión, ha sido demostrado que las SNs son nanosistemas versátiles que pueden adaptarse a diferentes necesidades médicas. Las SNs han demostrado ser eficientes para la administración de terapias antitumorales basadas en la miRNAs, y pueden ser radiomarcadas para aplicación en imagen molecular. En conjunto, SNs son una plataforma prometedora para la terapia y el diagnóstico del cáncer colorrectal, y potencial desarrollo de nanoteranósticos

USC
UNIVERSIDADE
DE SANTIAGO
DE COMPOSTELA

Resumen in extenso

USC
UNIVERSIDADE
DE SANTIAGO
DE COMPOSTELA

Resumen in extenso

El cáncer colorrectal es la tercera causa principal de fallecimiento asociado al cáncer. La tasa de supervivencia disminuye drásticamente cuando se produce la diseminación tumoral y formación de metástasis. Aunque diversas estrategias han sido desarrolladas para el tratamiento del cáncer de colon, existe una considerable diferencia en lo que respecta a la supervivencia del paciente cuando es tratado desde la etapa temprana de la enfermedad, o cuando el cáncer se encuentra en estadio avanzado[1-3]. Asimismo, debido a la administración no específica de los fármacos quimioterapéuticos convencionales, casi la totalidad de los pacientes sufren amplios efectos secundarios[4,5]. Para mejorar el pronóstico y supervivencia de los pacientes, es necesario desarrollar nuevos métodos de diagnóstico y monitorización de la enfermedad, que detecten la formación de metástasis de manera temprana, así como nuevas terapias más efectivas y dirigidas, para abordar la aparición de resistencias a medicamentos, y disminuir la toxicidad de los tratamientos.

En las últimas décadas, la nanotecnología ha desempeñado un papel significativo en la administración de fármacos antitumorales dada la alta versatilidad y potencial de los nanosistemas para el transporte de fármacos clásicos y de nuevos biofármacos[6-8]. Además de moléculas terapéuticas, los nanosistemas pueden asociar agentes de diagnóstico para ser monitorizados mediante el uso de modalidades avanzadas de imagen, como Resonancia Magnética Nuclear (RMN), Tomografía Computarizada (TC), Tomografía por Emisión de Positrones (PET), Tomografía Computarizada por Emisión de Fotones Individuales (SPECT) y ultrasonidos (US)[9,10].

Esta tesis doctoral se ha centrado esencialmente en el desarrollo de nanoemulsiones lipídicas para el diseño de nuevas estrategias terapéuticas y de diagnóstico del cáncer de colon. Partiendo de una composición sencilla, nanoemulsiones compuestas a base de vitamina E y esfigomielina (nanoemulsiones de esfingomielina, SNs), se ha procedido a i) adaptar la formulación para favorecer la asociación de miRNAs oncosupresores, con el objeto de determinar la eficacia de esta estrategia para interferir la progresión tumoral, y ii) proceder a su radiomarcaje con ^{18}F para su aplicación en imagen molecular (PET).

SNs para la liberación de miRNAs oncosupresores capaces de interrumpir la progresión tumoral en cáncer colorrectal.

La irrupción de nanofármacos en el mercado, junto con los éxitos obtenidos en ensayos clínicos, conjuntamente con la aparición de varias terapias novedosas basadas en polinucleótidos, están impulsando una creciente demanda de nanovehículos de transporte de fármacos más eficientes y seguros[11,12]. A pesar de que la administración de material genético basada en partículas virales ha sido extensamente evaluada, a día de hoy todavía presenta inconvenientes como la seguridad a largo plazo y limitaciones en su capacidad de carga[13]. Por ello, el desarrollo de sistemas no virales de administración de polinucleótidos se presenta como una opción alternativa para el transporte de material genético como el ADN plasmídico (pDNA), ARN interferente (siRNA) y micro-ARN (miRNA). Entre ellos, los nanosistemas lipídicos poseen varias ventajas en comparación con los vectores virales, en términos de seguridad, metodología de preparación, producción a gran escala y posible modificación química[14]. Las formulaciones compuestas por núcleos oleosos poseen dificultades para inmovilizar a los polinucleótidos ya que estas moléculas exhiben una tendencia natural a migrar a las interfaces agua-aceite y difundir en el medio externo. El empleo de nanoemulsiones catiónicas se ha estudiado en este trabajo para abordar este problema. De esta forma el grupo amino del lípido cargado positivamente puede interaccionar con la carga negativa del grupo fosfato de los polinucleótidos, lo que resulta en una eficiente asociación del material genético[15]. Este trabajo se centra en dos estrategias principales. Por un lado, la inclusión de un lípido catiónico (estearilamina (ST)) como un componente adicional de SNs, para favorecer la asociación del miRNA mediante el establecimiento de interacciones electrostáticas (SNs-ST-miRNA). Por otro lado, la preparación previa de complejos DOTAP-miRNA para su posterior inclusión en el núcleo oleoso de la nanoemulsión (SNs-DOTAP-miRNA) (**Figura 1**). Estas dos nanoemulsiones basadas en miRNA han sido sintetizadas con una sencilla técnica, ampliamente caracterizadas, y su potencial terapéutico evaluado en células de cáncer colorrectal (SW480).

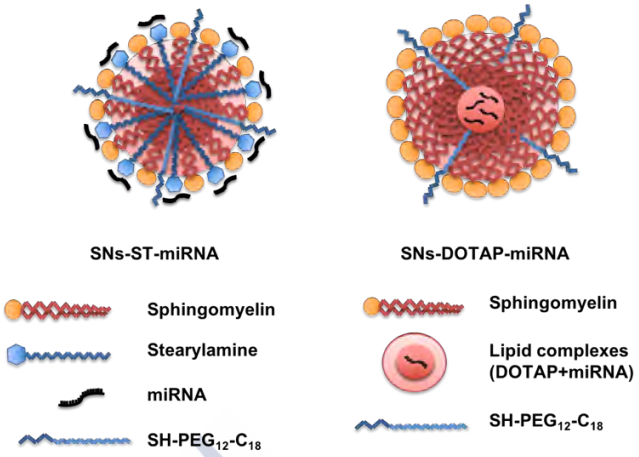

Figura 1. Ilustración esquemática de los componentes de las nanoemulsiones con estearilamina, (SNs-ST-miRNA) y DOTAP (SNs-DOTAP-miRNA).

SNs son formulaciones sencillas, biocompatibles y biodegradables, producidas mediante el método de inyección de etanol. Se componen principalmente de un aceite, vitamina E (VitE), y un surfactante de naturaleza esfingoide, esfingomielina (SM). Se han incluido además derivados lipídicos de polietilengliol (PEG) ($SH\text{-}PEG_{12}\text{-}C_{18}$) en una menor proporción, con el objetivo de mejorar la estabilidad de la formulación, y para permitir una posterior funcionalización con ligandos o radioisótipos[16,17]. Además, como se ha descrito anteriormente, también se han incorporado pequeñas cantidades de lípidos catiónicos, ST y DOTAP, para aumentar la eficacia de asociación de miRNAs.

Para la preparación de SNs, en primer lugar se disuelven los componentes lipídicos en etanol, VitE:SM:PEG en una proporción 10:1:0,1 p/p. Posteriormente un volumen de 110µl se inyecta sobre 1ml de agua ultrapura, y de forma espontánea se obtienen las nanoemulsiones, que presentan un tamaño promedio de 131 + 8 nm, un índice de polidispersión (PDI) de 0.2 y una carga superficial ligeramente negativa de -13 ± 7mV. El análisis fisicoquímico complementario realizado mediante la técnica de Nanoparticle Tracking Analysis (NTA) muestra correlación con los parámetros determinados previamente, confirmando así el tamaño y la distribución relativamente monodispersa de las SNs desarrolladas, y aportando a mayores un dato de concentración de $4.2x10^{12} \pm 2.1x10^{10}$ partículas/ml.

La formulación denominada SNs-ST-miRNA se desarrolló tras incorporar ST en la composición de SNs. La interacción entre los lípidos catiónicos y los ácidos nucleicos está intensamente influenciada por su interacción carga-carga. Por lo tanto la selección de ST se realizó en base a la presencia en su estructura de un grupo amino primario con carga positiva en un amplio rango de pH[18,19]. Se prepararon y caracterizaron nanoemulsiones con relaciones VitE:SM:PEG:ST de 10:1:0.1:0.1 a 10:1:0.1:2 (p/p). En base a sus propiedades fisicoquímicas (tamaño y carga superficial), la formulación con ratio VitE:SM:PEG:ST 10:1:0.1:1 (SNs-ST) fue seleccionada para estudios posteriores.

A continuación se evaluaron en detalle las condiciones de asociación de miRNA. Para ello se agregaron cantidades crecientes de SNs-ST sobre una solución de miRNA (10 µg) (relaciones miRNA: ST de 1: 1 a 1:10) y se incubaron bajo agitación magnética. Se observó que el aumento de la proporción de SNs-ST (y por lo tanto de grupos catiónicos) afecta principalmente a las propiedades superficiales de los nanosistemas. Todos los tamaños obtenidos se mantuvieron alrededor de 150-170 nm, con bajos índices de polidispersión en todos los casos, excepto en las relaciones miRNA:ST 1:5 y 1:7 para las cuales se observó una agregación masiva. Esto puede ser debido a la neutralización de la carga superficial, como se ha observado para otros nanosistemas catiónicos lipídicos[20-22]. La asociación eficaz del miRNA a la superficie de SNs-ST se confirmó mediante un ensayo de electroforesis en gel. Tras los experimentos de asociación, las nanoemulsiones SNs-ST-miRNA con una relación de masa miRNA:ST 1:10 se seleccionaron para los siguientes experimentos de transfección (**Tabla 1**).

Por otro lado se prepararon las nanoemulsiones denominadas SNs-DOTAP-miRNA a partir de complejos lipídicos preformados. Estos complejos se sintetizaron haciendo interaccionar miRNA con dos lípidos catiónicos previamente seleccionados (ST y DOTAP) a distintos ratios. Tras una evaluación en cuanto a características fisicoquímicas se consideró a los complejos de miRNA:DOTAP en una proporción de 1:15 (p/p) como candidatos ideales para su incorporación adicional en las SNs. Los nanosistemas SNs-DOTAP-miRNA fueron a su vez caracterizados exhibiendo un tamaño de partícula promedio de 124 ± 9 nm, un PDI de 0.2 y una carga superficial de +37 ± 3 mV (**Tabla 1**). Adicionalmente se realizó un análisis de electroforesis en gel para

demostrar que el miRNA es complejado de manera eficiente con el lípido catiónico DOTAP, y que la asociación a SNs efectivamente proporciona una protección adicional.

Tabla 1. Tamaño (nm), PDI (índice de polidispersión) y carga superficial (mV) de las nanoemulsiones SNs-ST-miRNA y SNs-DOTAP-miRNA.

Formulación	Tamaño (nm)	PDI	Carga Superficial (mV)
SNs-ST-miRNA	148 ± 8	0.2	+26 ± 3
SNs-DOTAP-miRNA	124 ± 9	0.2	+37 ± 3

Se realizaron estudios de internalización celular mediante microscopía confocal (se muestran los núcleos celulares de células SW480 teñidos en azul) con los dos prototipos desarrollados (SNs-ST-miRNA y SNs-DOTAP-miRNA), empleando un doble marcaje fluorescente (miRNA marcado con Cy5, Cy5-miRNA, y esfigomielina (SM) con TopFluor®, TopFluor®-SM). Ambas formulaciones fueron internalizadas eficientemente por las células (señal verde) siendo el Cy5-miRNA conjuntamente transportado a los citoplasmas celulares (señal roja) (**Figura 2)**. Es destacable que las imágenes combinadas de ambos canales (rojo y verde) ilustran que tanto las SNs-ST-miRNA como las SNs-DOTAP-miRNA se incorporan en forma de nanoemulsiones estables, ya que se puede observar una co-localización de las señales en ambos casos. Posteriormente, se llevaron a cabo estudios cuantitativos mediante análisis por citometría de flujo (FACS). Las formulaciones SNs-DOTAP-miRNA mostraron una mayor co-localización de Cy5-miRNA y TopFluor®-SM en comparación con las SNs-ST-miRNA. Esto puso de manifiesto que la formación de complejos con miRNA y posterior asociación a SNs favorece una mayor protección y median de esta forma su administración intracelular mejorada respecto a cuando este se dispone en la superficie de las nanoemulsiones[23].

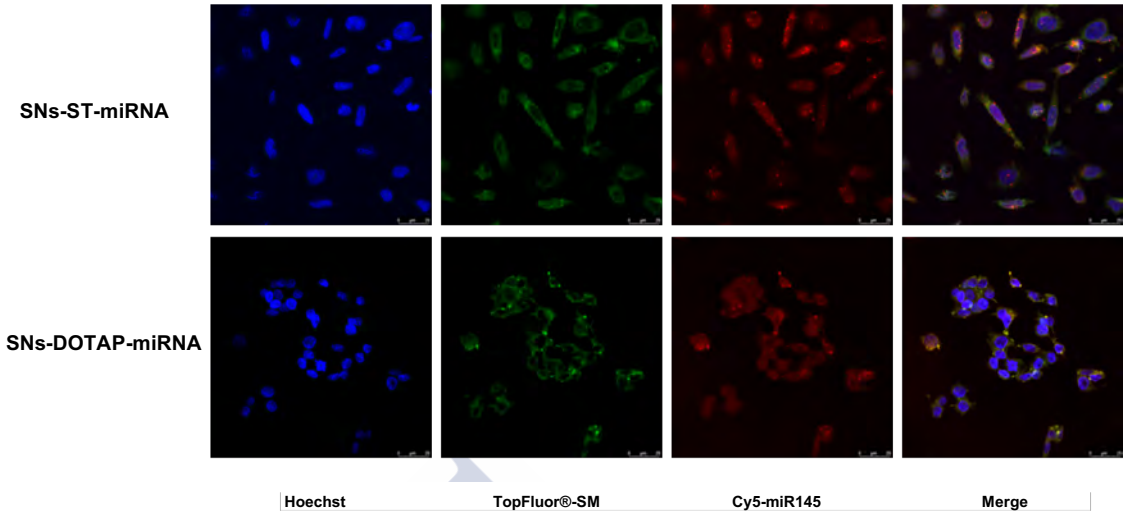

Figura 2. Internalización de nanoemulsiones SNs-ST-miRNA y SNs-DOTAP-miRNA en células SW480. Proyección máxima de las imágenes de microscopía confocal de nanoemulsiones marcadas con TopFluor® esfingomielina (TopFluor®-SM, verde), y miR145 marcado con Cy5 (Cy5-miR145, rojo) (4 h a 37ºC). Núcleo celular teñido con Hoechst (azul).

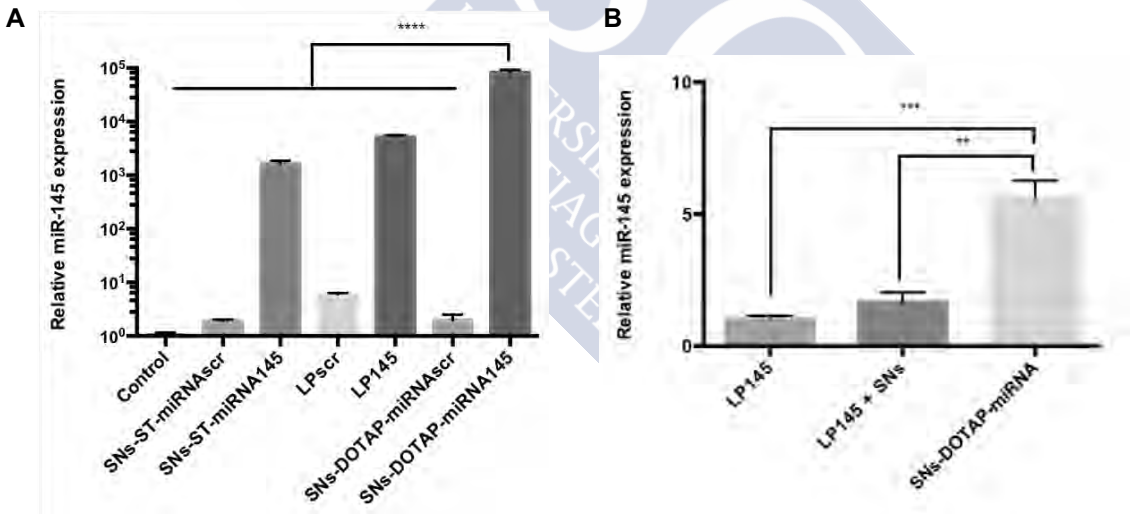

Figura 3. Expresión de miR145 después de la transfección con SNs-ST-miRNA145, complejos lipídicos 145 (LP145) y SNs-DOTAP-miRNA145 (así como con nanosistemas preparados con la secuencia truncada, SNs-ST-miRNAscr, LPscr, y SNs-DOTAP-miRNAscr) (A). Expresión relativa de miR145 después de la transfección con LP145, mezcla física de LP145 y SNs, y SNs-DOTAP-miRNA145 en células SW480 (B). (2 µg miRNA/pocillo en placas de 6 pocillos, 4 h incubación, 72 horas post-transfección, datos normalizados frente al control interno RNU6) (**** $p \leq 0.0001$, *** $p \leq 0.001$, and ** $p \leq 0.01$).

Los datos de transfección muestran, de manera coherente, una mayor eficacia para SNs-DOTAP-miRNA145 (64 veces más que las SNs-ST-miRNA). Además, comparando la eficiencia de transfección de los complejos lipídicos (LP145), una mezcla física de complejos y nanoemulsiones (LP145 + SNs) y SNs-DOTAP-miRNA, los resultados destacan los beneficios de integrar dichos complejos con SNs (**Figura 3A y 3B**).

Finalmente, se evaluó la capacidad de las SNs-DOTAP-miRNA145 para suprimir el crecimiento tumoral en células de cáncer colorrectal SW480. Se realizaron para ello tanto ensayos de proliferación como de migración. En los estudios de proliferación se observó que tanto el número de células como el de colonias celulares transfectadas con SNs-DOTAP-miRNA145 se redujo significativamente con respecto a las células control no tratadas y las células tratadas con la secuencia control (**Figura 4A y 4B**). Los estudios de cicatrización o "*wound healing*" también confirmaron sus efectos en términos de migración. La herida creada artificialmente en la placa de células SW480 tratadas con SNs-DOTAP-miRNA145 permaneció con una mayor abertura al final del estudio que la herida control y la tratada con las SNs-DOTAP-miRNAscr (**Figura 4C**). Estos resultados indican claramente que los SNs-DOTAP-miRNA145 inhiben el crecimiento y la migración en células de cáncer colorrectal (SW480), en línea con estudios previos[24,25].

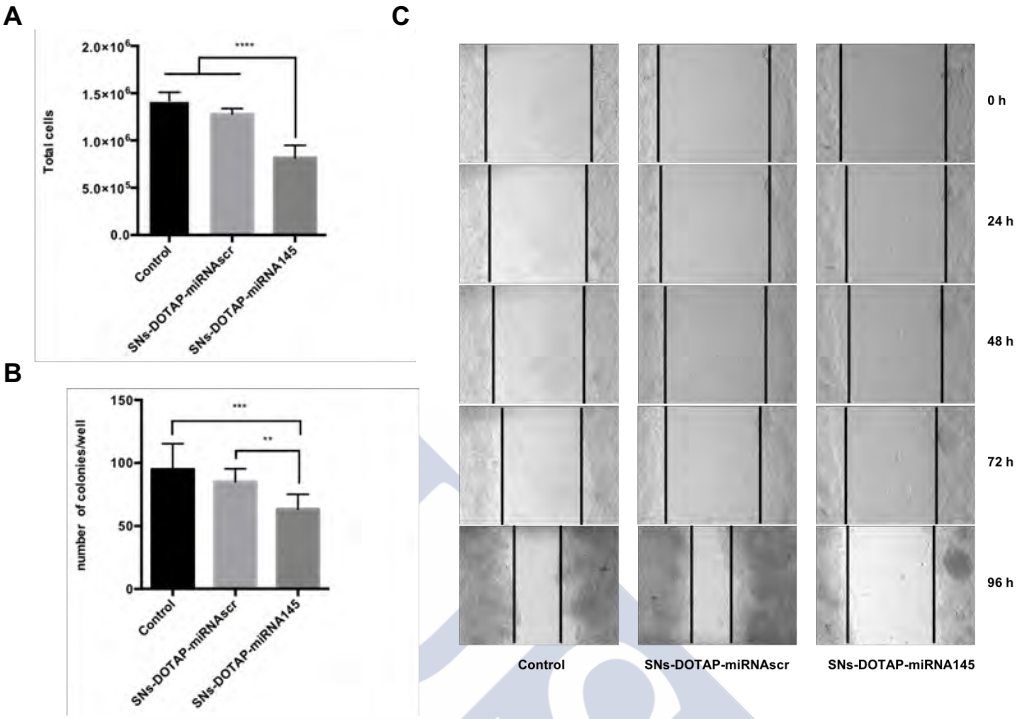

Figura. 4. Actividad citostática de las nanoemulsiones SNs-DOTAP-miRNA145 en células transfectadas SW480. Proliferación de células SW480 72 h post-transfección (**** $p \leq 0.0001$) (A). Análisis cuantitativo de recuento de número de columnas, 2 semanas después de la transfección (*** $p \leq 0.001$ y ** $p \leq 0.01$) (B). Imágenes representativas mostrando la migración celular observada en el estudio de *wound healing* para las células control, células tratadas con SNs-DOTAP-miRNA145 y la misma formulación con la secuencia truncada (SNs-DOTAP-miRNAscr). Las imágenes se obtuvieron a tiempos 0, 24, 48, 72 y 96 horas tras el tratamiento. Las líneas negras delimitan los márgenes establecidos (C).

En conclusión, en este trabajo se han desarrollado con éxito SNs que asocian y encapsulan eficientemente miRNA145, SNs-ST-miRNA y SNs-DOTAP-miRNA. Ambas formulaciones poseen un tamaño comprendido entre 120-150 nm y presentan poblaciones monodispersas. Estudios *in vitro* confirman su capacidad para acceder al citoplasma celular, liberar eficientemente su carga (miRNA145), y posteriormente restaurar su expresión de manera eficaz. La restitución de los niveles de miRNA145 posterior a la administración de SNs-DOTAP-miRNA demostró ser efectiva, suprimiendo la proliferación de las células tumorales, la formación de colonias y la migración. Estudios adicionales de este estas nanoemulsiones SNs-DOTAP-miRNA en un modelo animal de cáncer de colon podrán confirmar el potencial de esta plataforma para el diseño de terapias antitumorales de reemplazo de miRNAs.

Radiomarcaje de SNs con ^{18}F para PET

Actualmente las técnicas de imagen guiada están desempeñando un papel muy importante para el estudio de la biodistribución y la farmacocinética de fármacos. Además de las modalidades de imagen anatómica, como la Tomografía Computarizada (TC) y la Imagen por Resonancia Magnética (IRM), las estrategias de imagen molecular pueden a su vez facilitar la localización y cuantificación de las sondas radiomarcadas. Las imágenes de Tomografía por Emisión de Positrones (PET), técnica de imagen molecular no invasiva, se utilizan ampliamente en la práctica clínica diaria para el diagnóstico debido a su accesibilidad, alta sensibilidad y exactitud cuantitativa[26,27]. La ^{18}F-fluorodeoxiglucosa (^{18}F-FDG), análogo fluorado de la glucosa, es usada clínicamente para la obtención de imágenes en oncología en base a su amplia incorporación a tejidos tumorales que presentan un aumento del metabolismo de la glucosa. Este agente de diagnóstico clínico, aprobado por la agencia americana de alimentos y medicamentos (FDA), es el radiofármaco que ha permitido la entrada de la técnica de PET a nivel hospitalario y por lo tanto ha ayudado a mejorar el diagnóstico y el tratamiento del cáncer[28,29]. No obstante, en ciertos casos, las imágenes obtenidas con ^{18}F-FDG pueden incurrir en falsos positivos, ya que este radiofármaco no es un marcador específico de proliferación de células neoplásicas, sino cuantificador del elevado metabolismo glucídico existente en tejidos. Por este motivo, puede ser difícil alcanzar cantidades suficientes de ^{18}F-FDG en el área diana. En consecuencia, esto ha llevado al desarrollo de sistemas de administración más específicos para la obtención de imágenes tumorales[30,31].

Es posible desarrollar nanosistemas radiomarcados capaces de aumentar la señal, la sensibilidad y la resolución de la imagen adquirida en comparación con los radiofármacos estándares actuales como por ejemplo la ^{18}F-FDG[32]. Además, es posible adaptar su composición para lograr incrementar su estabilidad en plasma y su vida media en circulación, por lo que tienen un gran potencial para aplicaciones clínicas[33-35]. Entre los radioisótopos, el ^{18}F puede considerarse como un prometedor emisor de positrones para imagen por PET debido varios factores como una vida media de 110 min que permite tomar imágenes durante varias horas, su baja energía de positrones que genera imágenes de alta resolución, y su producción a gran escala con una elevada eficiencia[36-38]. Por lo tanto la utilización del ^{18}F para el radiomarcaje de nanosistemas se presenta como una alternativa interesante.

En esta tesis hemos desarrollo un método para el marcaje de nanoemulsiones lipídicas con ^{18}F. En primer lugar se comenzó con la síntesis de un grupo protésico marcado con ^{18}F, [^{18}F]FBEM, que posteriormente se conjugó con grupos tiol (-SH) mediante la reacción de adición de Michael, localizados bien en la superficie de las nanoemulsiones de esfingomielina que incorporan SH-PEG_{12}-C_{18} en su composición (SNs), o bien con el residuo cisteína en SNs decoradas con el péptido RPM (SNs-RPM), Posteriormente, ambas nanoemulsiones radiomarcadas (SNs-[^{18}F]FBEM y SNs-RPM-[^{18}F]FBEM) fueron purificadas, caracterizadas, e inyectadas en ratones sanos, para determinar su potencial para futuros estudios de imagen molecular por PET.

Las nanoemulsiones evaluadas en este estudio fueron preparadas mediante un método de baja energía utilizando el procedimiento de inyección de etanol[39]. Tanto las SNs como las SN-RPM se formaron espontáneamente después de la inyección de la fase lipídica sobre la fase acuosa bajo agitación magnética. La síntesis de [^{18}F]FBEM se realizó a partir de una metodología publicada anteriormente[40]. [^{18}F]FBEM fue sintetizado y se llevó a completa evaporación formando una fina película. Después de reducir el enlace disulfuro para reactivar la función tiol libre en SNs y SNs-RPM, estas fueron añadidas sobre la película de [^{18}F]FBEM para su marcaje, seguido de un paso de purificación para eliminar el agente reductor.

El radiomarcaje se llevó a cabo mediante la reacción química entre el grupo maleimida de [^{18}F]FBEM y los grupos tiol libres en la superficie de las SNs y las SNs-RPM. Las nanoemulsiones radiomarcadas fueron de nuevo purificadas obteniéndose los dos prototipos de nanoemulsión SNs-[^{18}F]FBEM y SNs-RPM-[^{18}F]FBEM. El rendimiento radioquímico (RRQ) obtenido (corrigiendo la desintegración) fue de un 35.1 $\pm$ 5.7% (n=4) y 39.4 $\pm$ 5.5% (n=4) para SNs-[^{18}F]FBEM and SNs-RPM-[^{18}F]FBEM respectivamente. Ambas nanoemulsiones marcadas con [^{18}F]FBEM exhiben tamaños hidrodinámicos entre 130-150 nm con bajo PDI y carga superficial positiva. No se observan cambios significativos con respecto a las nanoemulsiones no marcadas, lo que nos permite concluir que el proceso de radiomarcaje es respetuoso y no compromete la estructura ni la estabilidad de los nanosistemas. Ambas formulaciones poseen un pH entre 7-8 y una osmolaridad de entre 280-290 mOsm/kg, características que los hacen adecuados para inyección parenteral (**Tabla 2**). La confirmación de la posición del radiomarcaje, bien en el lípido o el péptido asociado a las nanoemulsiones, se analizó mediante un detector gamma y UV en UPLC con respecto a sus

estándares predeterminados (Ref); Ref-[^{18}F]FBEM, Ref-SH-PEG12-C18 (Ref-lipid), y Ref-RPMpeptide-PEG8-C18 (Ref-peptide) (**Figura 5**). Este experimento confirmó que la posición de radiomarcaje se produjo en los grupos funcionales tiol tanto de lípidos como péptidos. Por otro lado, no se observó marcaje inespecífico en ninguna de las formulaciones. Finalmente, el proceso de purificación fue realizado con éxito obteniéndose nanoemulsiones marcadas y purificadas.

Tabla 2. Rendimiento radioquímico (RRQ), tamaño en nm, índice de polidispersión (PDI), carga superficial (mV), pH, y osmolaridad de SNs-[^{18}F]FBEM y SNs-RPM-[^{18}F]FBEM (n=4).

Formulación	RRQ	Tamaño (nm)	PDI	Carga superficial (mV)	pH	Osmolaridad (mOsm/kg)
SNs-[^{18}F]FBEM	35.1 ± 5.7	136 ± 9	0.2	+38 ± 6	7.6 ± 0.2	287 ± 5
SNs-RPM-[^{18}F]FBEM	39.4 ± 5.5	149 ± 8	0.2	+37 ± 5	7.8 ± 0.3	285 ± 6

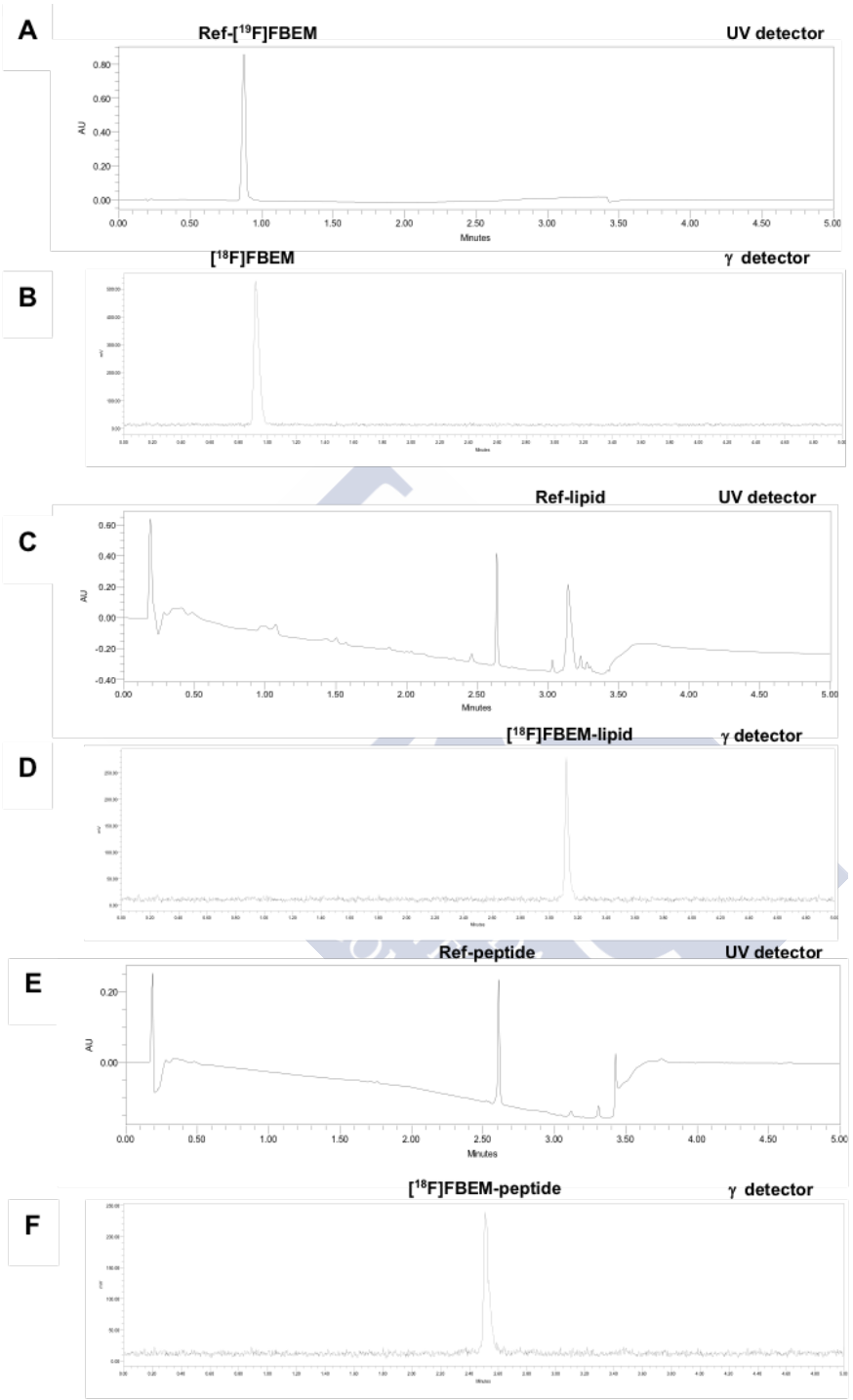

Figura 5. Representación esquemática de cromatogramas de UPLC mostrando señales de los detectores UV y gamma de los compuestos Ref-[^{19}F]FBEM) (A), [^{18}F]FBEM (B), Ref-lipid(C), [^{18}F]FBEM-lipid (D), Ref-peptide (E) y [^{18}F]FBEM-peptide (F).

Este estudio es un ejemplo del correcto marcaje de nanoemulsiones de esfingomielina con [^{18}F]FBEM usando un método de marcaje indirecto y en ausencia de solventes orgánicos. La unión se basa en la reacción de adición de Michael entre grupos tiol-maleimida. Este radiomarcaje de nanoemulsiones puede realizarse tanto antes como después de la formulación de estas. Ejemplos de marcaje con diferentes grupos protésicos ^{18}F antes y después de la formación de nanosistemas pueden encontrarse en la literatura[41-44]. Debido a la corta vida media del ^{18}F, el método de radiomarcaje a posteriori muestra una ventaja al permitir obtener altos rendimientos radioquímicos con respecto al radiomarcaje previo. El proceso de radiomarcaje de estas nanoemulsiones se realizó controlando los valores de osmolaridad y pH para alcanzar las características apropiadas de las para su inyección en animales[45].

Para determinar el comportamiento *in vivo* de las nanoemulsiones radiomarcadas estas fueron administradas mediante inyección en cola a ratones sanos. Por un lado, se midió la radioactividad en los órganos diseccionados para determinar la biodistribución *ex vivo.* Por otro lado, se realizaron estudios PET-MRI tanto para realizar estudios farmacocinéticos como para demostrar el potencial de las nanoemulsiones desarrolladas como agentes de contraste para la obtención de imágenes *in vivo*.

El patrón *ex vivo* indicó que ambas nanoemulsiones parecen ser capturadas por el sistema retículo-endotelial (SRE). Patrones de biodistribución similares han sido descritos para otras nanopartículas lipídicas[46-48]. Una posible estrategia para modular la biodistribución y la interacción con las células del SRE podría ser la modificación de su superficie, por ejemplo con polietilenglicol (PEG) o otras moléculas hidrofilicas[49-51]. De hecho, las SNs decoradas con el péptido RPM (SNs-RPM-[^{18}F]FBEM) dieron lugar a una menor acumulación tanto en bazo como en hígado. Se observó además la acumulación de las nanoemulsiones en intestino, riñón y pulmón. La captación en los pulmones podría estar relacionada con su tamaño un fenómeno de agregación que haga que se acumulen en los capilares pulmonares. La presencia de radiactividad en el intestino podría deberse a su excreción hepática a través de la vesícula biliar en las heces. La baja cantidad de radioactividad detectada en hueso indica la ausencia de defluoración, ya que el ^{18}F libre tiene direccionalidad hacia tejido óseo, lo que sugiere que la mayor parte del radiomarcaje ^{18}F permanece

en las formulaciones y que las nanoemulsiones radiomarcadas son estables tras la inyección intravenosa[52,53] (**Figura 6**).

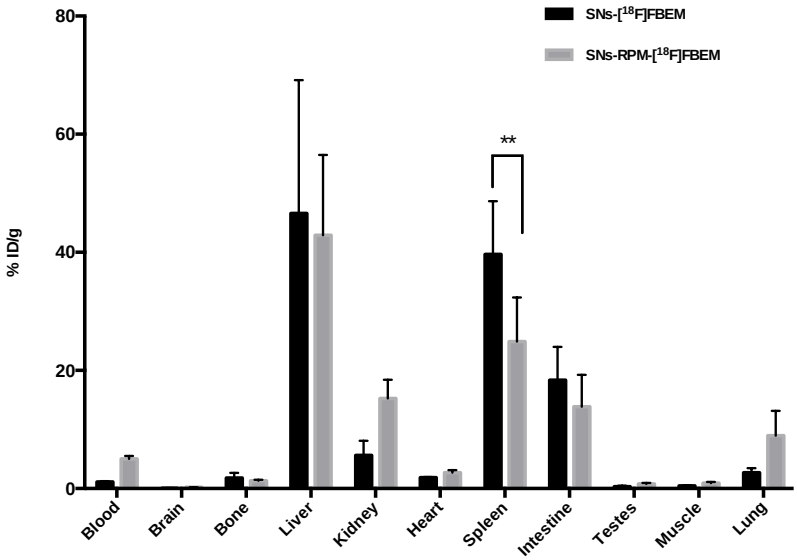

Figure 6. Perfil de biodistribución *ex vivo* de SNs-[^{18}F]FBEM and SNs-RPM-[^{18}F]FBEM en órganos de ratones BALB/c 3 horas post-inyección.

Se realizaron estudios de biodistribución (**Figura 7**) y farmacocinética *in vivo* empleando PET-MRI. La región de interés dibujada en los ventrículos del corazón confirmó el éxito de la inyección en la vena de la cola, ya que la radioactividad disminuyó después de la administración. Por otro lado, las curvas de actividad-tiempo revelaron una rápida captación en el hígado y el bazo. Se pudieron observar dos rutas de eliminación (hígado y riñón), primando la excrección hepática. La biodistribución y la farmacocinética de las formulaciones desarrolladas en este trabajo indican que esta metodología puede sentar las bases para el radiomarcaje de nanosistemas lipídicos para diagnóstico del cáncer.

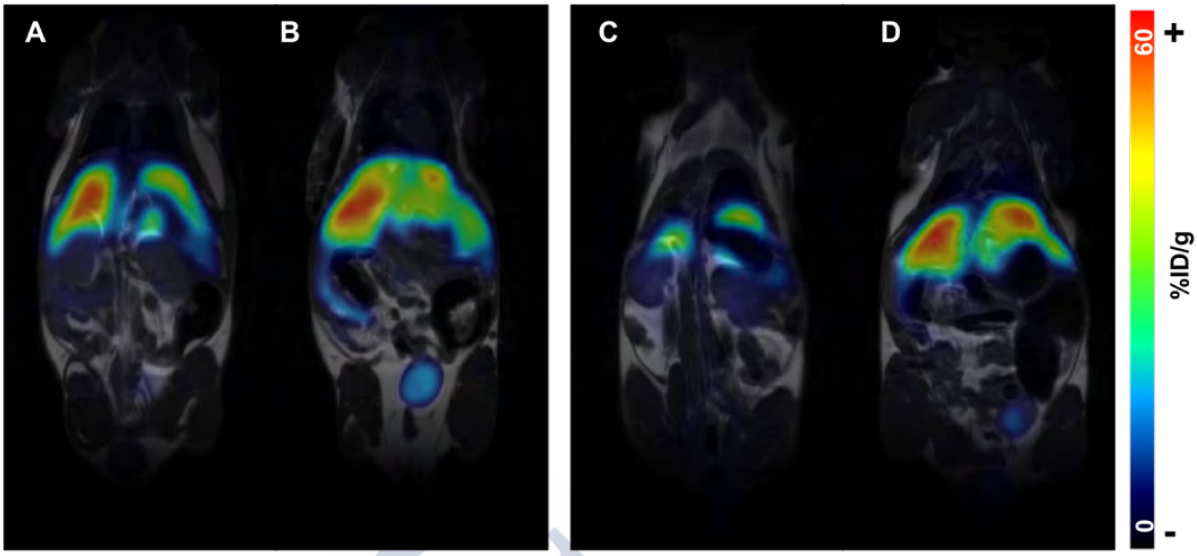

Figura 7. Biodistribución *in vivo* de SNs-[^{18}F]FBEM (izquierda) y SNs-RPM-[^{18}F]FBEM (derecha) en ratones macho BALB/c 2 horas post-inyección usando la técnica de imagen PET-IRM: dos diferentes secciones del plano coronal muestran respectivamente los riñones (A,C) y el hígado y la vejiga (B,D).

En conclusión, el radiomarcaje de nanosistemas lipídicos se desarrolló con éxito tanto para nanoemulsiones de esfingomielina (SNs-[^{18}F]FBEM) como para nanoemulsiones decoradas con péptidos (SNs-RPM-[^{18}F]FBEM) usando un método sencillo y condiciones suaves, sin alterar sus propiedades fisicoquímicas. Las nanoemulsiones radiomarcadas pueden ser monitorizadas por PET-MRI abriendo la puerta al desarrollo de nanosistemas lipídicos para su uso en diagnóstico por imagen molecular. Asimismo, esta estrategia puede ser aplicada a otro tipo de nanoestructuras, siempre y cuando presenten un grupo tiol en su superficie.

Referencias

(1) Ferlay, J.; Colombet, M.; Soerjomataram, I.; Dyba, T.; Randi, G.; Bettio, M.; Gavin, A.; Visser, O.; Bray, F. Cancer Incidence and Mortality Patterns in Europe: Estimates for 40 Countries and 25 Major Cancers in 2018. *Eur. J. Cancer* **2018**, *103*, 356–387.

(2) Arnold, M.; Sierra, M. S.; Laversanne, M.; Soerjomataram, I.; Jemal, A.; Bray, F. Global Patterns and Trends in Colorectal Cancer Incidence and Mortality. *Gut* **2017**, *66*, 683–691.

(3) Fribert, P.; Paulová, L.; Patáková, P.; Rychtera, M.; Melzoch, K. Alternativní Metody Separace Kapalných Biopaliv z Média Při Fermentaci. *Chem. List.* **2013**, *107*, 843–847.

(4) Colagiuri, B.; Dhillon, H.; Butow, P. N.; Jansen, J.; Cox, K.; Jacquet, J. Does Assessing Patients' Expectancies about Chemotherapy Side Effects Influence Their Occurrence? *J. Pain Symptom Manage.* **2013**, *46*, 275–281.

(5) Devlin, E. J.; Denson, L. A.; Whitford, H. S. Cancer Treatment Side Effects: A Meta-Analysis of the Relationship Between Response Expectancies and Experience. *J. Pain Symptom Manage.* **2017**, *54*, 245–258.

(6) Pérez-Herrero, E.; Fernández-Medarde, A. Advanced Targeted Therapies in Cancer: Drug Nanocarriers, the Future of Chemotherapy. *Eur. J. Pharm. Biopharm.* **2015**, *93*, 52–79.

(7) Muthiah, M.; Park, I.-K.; Cho, C.-S. Nanoparticle-Mediated Delivery of Therapeutic Genes: Focus on MiRNA Therapeutics. *Expert Opin. Drug Deliv.* **2013**, *10*, 1259–1273.

(8) Wang, H.; Jiang, Y.; Peng, H.; Chen, Y.; Zhu, P.; Huang, Y. Recent Progress in MicroRNA Delivery for Cancer Therapy by Non-Viral Synthetic Vectors. *Adv. Drug Deliv. Rev.* **2015**, *81*, 142–160.

(9) Hong, H.; Zhang, Y.; Sun, J.; Cai, W. Molecular Imaging and Therapy of Cancer with Radiolabeled Nanoparticles. *Nano Today* **2009**, *4*, 399–413.

(10) Ostermayer, G.; Pohl, A.; Hausleitner, C.; Reindl, L.; Seifert, F. CDMA for Wireless SAW Sensor Applications. *Spread Spectr. Tech. Appl. Proceedings, 1996., IEEE 4th Int. Symp.* **2002**, *2*, 795–799.

(11) Jeanmonod, D. J.; Rebecca; Suzuki, K. et al. Non-Viral Delivery Systems in Gene Therapy. *Intech open* **2018**, *2*, 1-33.

(12) Yin, H.; Kanasty, R. L.; Eltoukhy, A. A.; Vegas, A. J.; Dorkin, J. R.; Anderson, D. G. Non-Viral Vectors for Gene-Based Therapy. *Nat. Rev. Genet.* **2014**, *15*, 541–555.

(13) Titze-de-Almeida, R.; David, C.; Titze-de-Almeida, S. S. The Race of 10 Synthetic RNAi-Based Drugs to the Pharmaceutical Market. *Pharm. Res.* **2017**, *34*, 1339–1363.

(14) Chen, J.; Guo, Z.; Tian, H.; Chen, X. Production and Clinical Development of Nanoparticles for Gene Delivery. *Mol. Ther. - Methods Clin. Dev.* **2016**, *3*, 16023.

(15) Golan, S.; Talmon, Y. Nanostructure of Complexes between Cationic Lipids and an Oppositely Charged Polyelectrolyte. *Langmuir* **2012**, *28*, 1668–1672.

(16) Kolate, A.; Baradia, D.; Patil, S.; Vhora, I.; Kore, G.; Misra, A. PEG - A Versatile Conjugating Ligand for Drugs and Drug Delivery Systems. *J. Control. Release* **2014**, *192*, 67–81.

(17) Suk, J. S.; Xu, Q.; Kim, N.; Hanes, J.; Ensign, L. M. PEGylation as a Strategy for Improving Nanoparticle-Based Drug and Gene Delivery. *Adv. Drug Deliv. Rev.* **2016**, *99*, 28–51.

(18) Zhang, J.; Fan, H.; Levorse, D. A.; Crocker, L. S. Ionization Behavior of Amino Lipids for SiRNA Delivery: Determination of Ionization Constants, SAR, and the Impact of Lipid p K a on Cationic Lipid-Biomembrane Interactions. *Langmuir* **2011**, *27*, 1907–1914.

(19) Jeong, M. W.; Oh, S. G.; Kim, Y. C. Effects of Amine and Amine Oxide Compounds on the Zeta-Potential of Emulsion Droplets Stabilized by Phosphatidylcholine. *Colloids Surfaces A Physicochem. Eng. Asp.* **2001**, *181*, 247–253.

(20) Liu, J.; Meng, T.; Yuan, M.; Wen, L. J.; Cheng, B. L.; Liu, N.; Huang, X.; Hong, Y.; Yuan, H.; Hu, F. Q. MicroRNA-200c Delivered by Solid Lipid Nanoparticles Enhances the Effect of Paclitaxel on Breast Cancer Stem Cell. *Int. J. Nanomedicine* **2016**, *11*, 6713–6725.

(21) Martini, É.; Fattal, E.; de Oliveira, M. C.; Teixeira, H. Effect of Cationic Lipid Composition on Properties of Oligonucleotide/Emulsion Complexes: Physico-Chemical and Release Studies. *Int. J. Pharm.* **2008**, *352*, 280–286.

(22) Teixeira, H.; Dubernet, C.; Puisieux, F. ; Benita, F. ; Couvreur, P. ; Submicron Cationic Emulsions as a New Delivery System for Oligonucleotides. *Pharmaceutical Research*. **1999,** *16*, 1.

(23) Hauptstein, S.; Prüfert, F.; Bernkop-Schnürch, A. Self-Nanoemulsifying Drug Delivery Systems as Novel Approach for PDNA Drug Delivery. *Int. J. Pharm.* **2015**, *487*, 25–31.

(24) Liang, G.; Zhu, Y.; Jing, A.; Wang, J.; Hu, F.; Feng, W.; Xiao, Z.; Chen, B. Cationic MicroRNA-Delivering Nanocarriers for Efficient Treatment of Colon Carcinoma in Xenograft Model. *Gene Ther.* **2016**, *23*. 829-838.

(25) Setua, S.; Khan, S.; Yallapu, M. M.; Behrman, S. W.; Sikander, M.; Khan, S. S.; Jaggi, M.; Chauhan, S. C. Restitution of Tumor Suppressor MicroRNA-145 Using Magnetic Nanoformulation for Pancreatic Cancer Therapy. *J. Gastrointest. Surg.* **2017**, *21*. 94-105.

(26) Ding, H.; Wu, F. Image Guided Biodistribution and Pharmacokinetic Studies of Theranostics. *Theranostics* **2012**, *2*, 1040–1053.

(27) De Jong, M.; Essers, J.; Van Weerden, W. M. Imaging Preclinical Tumour Models: Improving Translational Power. *Nat. Rev. Cancer* **2014**, *14*, 481–493.

(28) Zhu, A.; Daniel Lee, A.; Shim, H. Metabolic PET Imaging in Cancer Detection and Therapy Response. *Semin Oncol* **2011**, *38* (1), 55–69.

(29) Jadvar, H; Is There Utility for FDG PET in Prosate Cancer. *Semin Nucl Med* . **2016**, *46* (6), 502–506.

(30) Goel,S.; England, C. G.; Chen, F.; Cai, W.; Positron emission tomography and nanotechnology: A dynamic duo for cancer theranostics. *Adv. Drug Deliv. Rev.* **2017.** *113* 157–176

(31) Gambhir, S. S.; Molecular Imaging of Cancer with Positron Emission Tomography. *Nature Rev. Cancer.* **2002**, *2* 683-693

(32) Thakor, A. S.; Jokerst, J. V.; Ghanouni, P.; Campbell, J. L.; Mittra, E.; Gambhir, S. S. Clinically Approved Nanoparticle Imaging Agents. *J. Nucl. Med.* **2016**, *57*, 1833–1837.

(33) Madru, R.; Kjellman, P.; Olsson, F.; Wingardh, K.; Ingvar, C.; Stahlberg, F.; Olsrud, J.; Latt, J.; Fredriksson, S.; Knutsson, L.; et al. 99mTc-Labeled Superparamagnetic Iron Oxide Nanoparticles for Multimodality SPECT/MRI of Sentinel Lymph Nodes. *J. Nucl. Med.* **2012**, *53*. 459-463.

(34) Psimadas, D.; Baldi, G.; Ravagli, C.; Bouziotis, P.; Xanthopoulos, S.; Franchini, M. C.; Georgoulias, P.; Loudos, G. Preliminary Evaluation of a 99mTc Labeled Hybrid Nanoparticle Bearing a Cobalt Ferrite Core: In Vivo Biodistribution. *J. Biomed. Nanotechnol.* **2012**, *8*. 575-585.

(35) Zeng, J.; Jia, B.; Qiao, R.; Wang, C.; Jing, L.; Wang, F.; Gao, M. In situ111In-Doping for Achieving Biocompatible and Non-Leachable 111In-Labeled Fe3O4 Nanoparticles. *Chem. Commun.* **2014**.

(36) Okarvi, S. M. Recent Progress in Fluorine-18 Labeled Peptide Radiopharmaceuticals. *Eur. J. Nucl. Med.* **2001**, *28*, 929–938.

(37) Pretze, M.; Große-Gehling, P.; Mamat, C. Cross-Coupling Reactions as Valuable Tool for the Preparation of PET Radiotracers. *Molecules* **2011**, *16*, 1129–1165.

(38) Van der Born, D.; Pees, A.; Poot, A. J.; Orru, R. V. A.; Windhorst, A. D.; Vugts, D. J. Fluorine-18 Labeled Building Blocks for PET Tracer Synthesis. *Chem. Soc. Rev.* **2017**, *46*, 4709–4773.

(39) Shin, G. H.; Chung, S. K.; Kim, J. T.; Joung, H. J.; Park, H. J. Preparation of Chitosan-Coated Nanoliposomes for Improving the Mucoadhesive Property of Curcumin Using the Ethanol Injection Method. *J. Agric. Food Chem.* **2013**, *61*, 11119–11126.

(40) Dammicco, S.; Goux, M.; Lemaire, C.; Becker, G.; Bahri, M. A.; Plenevaux, A.; Cinier, M.; Luxen, A. Regiospecific Radiolabeling of Nanofitin on Ni Magnetic Beads with [^{18}F]FBEM and in Vivo PET Studies. *Nucl. Med. Biol.* **2017**, *51*, 33–39.

(41) Rojas, S.; Gispert, J. D.; Martín, R.; Abad, S.; Menchón, C.; Pareto, D.; Víctor, V. M.; Álvaro, M.; García, H.; Herance, J. R. Biodistribution of Amino-Functionalized Diamond Nanoparticles. in Vivo Studies Based On18F Radionuclide Emission. *ACS Nano* **2011**, *5*, 5552–5559.

(42) Rojas, S.; Gispert, J. D.; Abad, S.; Buaki-Sogo, M.; Victor, V. M.; Garcia, H.; Herance, J. R. In Vivo Biodistribution of Amino-Functionalized Ceria Nanoparticles in Rats Using Positron Emission Tomography. *Mol. Pharm.* **2012**, *9*, 3543–3550.

(43) Guerrero, S.; Herance, J. R.; Rojas, S.; Mena, J. F.; Gispert, J. D.; Acosta, G. A.; Albericio, F.; Kogan, M. J. Synthesis and in Vivo Evaluation of the Biodistribution of a 18F-Labeled Conjugate Gold-Nanoparticle-Peptide with Potential Biomedical Application. *Bioconjug. Chem.* **2012**, *23*, 399–408.

(44) Di Mauro, P. P.; Gómez-Vallejo, V.; Baz Maldonado, Z.; Llop Roig, J.; Borrós, S. Novel 18F Labeling Strategy for Polyester-Based NPs for in Vivo PET-CT Imaging. *Bioconjug. Chem.* **2015**, *26*, 582–592.

(45) Stranz, M.; Kastango, E. S. A Review of pH and Osmolarity. *International Journal of Pharmaceutical Compounding.* **2013**, *6.* 216-220

(46) Jensen, A. I.; Severin, G. W.; Hansen, A. E.; Fliedner, F. P.; Eliasen, R.; Parhamifar, L.; Kjær, A.; Andresen, T. L. Remote-Loading of Liposomes with Manganese-52 and in Vivo Evaluation of the Stabilities of 52 Mn-DOTA and 64 Cu-DOTA Using Radiolabelled Liposomes and PET Imaging. *J. Control. Release* **2018**, *269*, 100–109.

(47) Crístian, D.; Soares, F.; Oliveira, M. C. De; Luís, A.; Barros, B. De; Cardoso, V. N.; Ramaldes, G. A. European Journal of Pharmaceutical Sciences Liposomes Radiolabeled with 159 Gd : In Vitro Antitumoral Activity , Biodistribution Study and Scintigraphic Image in Ehrlich Tumor Bearing Mice. **2011**, *43*, 290–296.

(48) Eroglu, H.; Yenilmez, A. An Investigation of the Usability of Solid Lipid Nanoparticles Radiolabelled with Tc-99m as Imaging Agents in Liver-Spleen Scintigraphy. **2016**, *12*, 1501–1509.

(49) Blanco, E.; Shen, H.; Ferrari, M. Principles of Nanoparticle Design for Overcoming Biological Barriers to Drug Delivery. *Nat. Biotechnol.* **2015**, *33*, 941–951.

(50) Rao, L.; Xu, J. H.; Cai, B.; Liu, H.; Li, M.; Jia, Y.; Xiao, L.; Guo, S. S.; Liu, W.; Zhao, X. Z. Synthetic Nanoparticles Camouflaged with Biomimetic Erythrocyte Membranes for Reduced Reticuloendothelial System Uptake. *Nanotechnology* **2016**, *27*, 85106.

(51) Ducongé, F.; Pons, T.; Pestourie, C.; Hérin, L.; Thézé, B.; Gombert, K.; Mahler, B.; Hinnen, F.; Kühnast, B.; Dollé, F.; *et al.* Fluorine-18-Labeled Phospholipid Quantum Dot Micelles for in Vivo Multimodal Imaging from Whole Body to Cellular Scales. *Bioconjug. Chem.* **2008**, *19*, 1921–1926.

(52) Schirrmeister, H.; Guhlmann, A.; Elsner, K.; Kotzerke, J.; Glatting, G.; Rentschler, M.; Neumaier, B.; Träger, H.; Nüssle, K.; Reske, S. N. Sensitivity in Detecting Osseous Lesions Depends on Anatomic Localization: Planar Bone Scintigraphy versus 18F PET. *J. Nucl. Med.* **1999**, *40*, 1623–1629.

(53) Zhou, J.; Yu, M.; Sun, Y.; Zhang, X.; Zhu, X.; Wu, Z.; Wu, D.; Li, F. Fluorine-18-Labeled Gd3+/Yb3+/Er3+ Co-Doped NaYF4 Nanophosphors for Multimodality PET/MR/UCL Imaging. *Biomaterials* **2011**, *32*, 1148–1156.

USC
UNIVERSIDADE
DE SANTIAGO
DE COMPOSTELA

Chapter 1

Introduction

USC
UNIVERSIDADE
DE SANTIAGO
DE COMPOSTELA

Introduction Contents

1. Colorectal cancer

Cancer is a major public-health disease worldwide. Despite progress in cancer treatment in terms of surgery and chemotherapy, cancer is a leading cause of death[1]. Estimated data from GLOBOCAN 2018 showed that colorectal cancer (CRC) is on the third place for incidence and second place for mortality among 36 human malignancies in 185 Countries (**Figure 1**)[2].

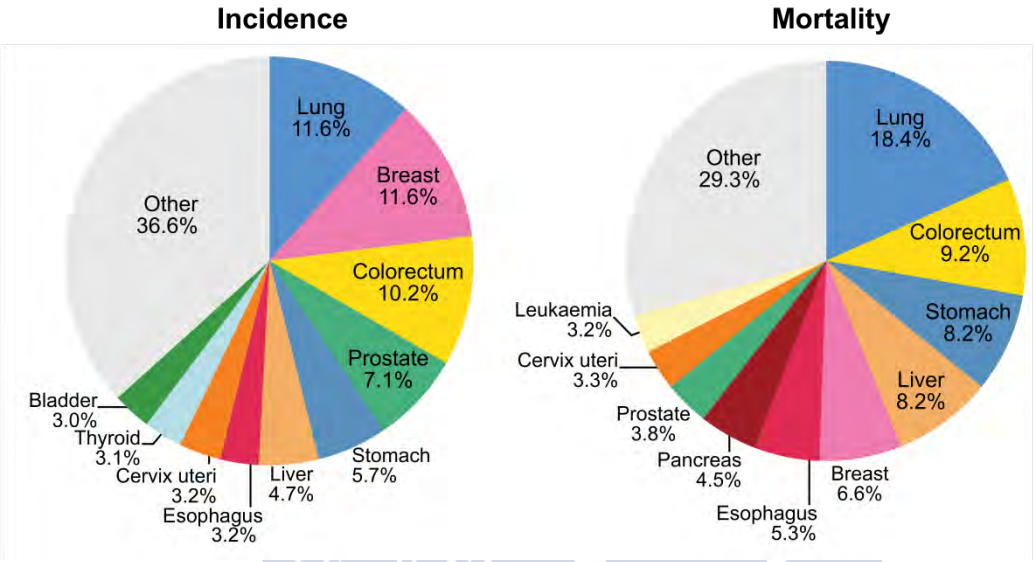

Figure 1. Distribution of Cases and Deaths for the 10 Most Common Cancers in 2018. [Reproduced from Bray, F., et al. (2018). GLOBOCAN 2018[2] with permission.]

It is well known that there are two major pathways of genetic alterations in colorectal carcinogenesis. One is the chromosomal instability (CIN) and the other is microsatellite instability (MSI). CIN is characterized by allelic losses on chromosome which stimulates clonal diversity. MSI refers to replication errors in primary sequences of chromosomes, either by aberrant methylation or by somatic mutation. Owing to recent progress in molecular biology, other routes, including the transforming growth factor-β/SMAD, the serrated, and the epigenetic pathway have been reported[3]. In the invasion and metastasis steps of colorectal cancers, various genes have now been identified as being involved in proteolysis, adhesion, angiogenesis, and cell growth[4].

Generally, development of colorectal cancer initiates when the normal epithelium transforms to a small adenoma by the activation of the Wnt/β-catenin pathway. Further K-RAS mutation leads to the formation of a large adenoma. The final step involves p53 inactivation and transforming growth factor beta (TGF-β) signaling pathway mutation (**Figure 2)**[5].

Apart from genetics, age is one of the major factors in the development of CRC especially in elderly people. Other causes are obesity, diabetes, dietary, smoking, and consuming of alcohol. To screen colon cancer, several tests can be performed such as colonoscopy, sigmoidoscopy, fecal occult blood test, fecal immunochemical test, DNA testing, and CT colonography (**Figure 3**)[6,7].

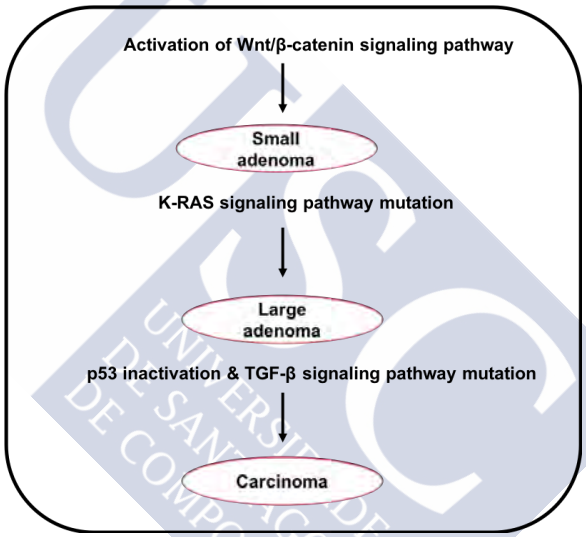

Figure 2. Steps involved in CRC progression.

The American Joint Committee on Cancer (AJCC)/ TNM system clarifies the stage of CRC by the letters T, N, and M, describing the areas of cancer growth. The T score means the growth of the primary tumor. The N score refers to nearby cancer growth within the colon or lymph nodes. Lastly, the M score states if the cancer has spread to distant sites. These scores are combined to give the stage of cancer (**Table 1)**. Stage 0, the carcinoma has not grown beyond the first layer of its wall. This is a noninvasive cancer. If all the cancer was removed during an endoscopic polypectomy, it may not need more treatment. During stage I, the carcinoma has developed into either the second or third layer of the colon wall. Stage II represents the cancer that reaches the

fourth layer of or outside the colon wall. However, there is no cancer in nearby or distant sites. For Stage III, the cancer has spread from the colon to nearby lymph nodes or there are tumor deposits (small secondary tumors within the colon). Stage IV demonstrates the colon cancer that has spread to distant organs. Common distant sites are liver and lungs. Generally, it is rated twice. The first rate before treatment is called the clinical stage. It defines how far the cancer has spread and how many lymph nodes have cancer. Nevertheless, some cancers could be found after surgery. Thus, a second rate is performed, named the pathologic stage[8].

Figure 3. Overview of colorectal cancer. [Adapted from Benerjee, A., et al. (2017). Drug Discov. Today[6] with permission.]

2. Therapeutic approaches for colorectal cancer

Generally, the therapeutic methods for CRC are surgery, cryosurgery, radiation therapy, and chemotherapy. Surgery and radiotherapy are the most effective treatments for local and non-metastatic cancers, while chemotherapy, hormone, and biological therapies are commonly used with metastatic tumors.

2.1. Surgery and radiotherapy

When tumor is still at a local site, surgery is the standard procedure for Stage I-III CRC. Usually, the surgeon removes not only the tumor but also colon sections including fat and lymph nodes. The healthy parts of colon are generally reconnected at the end. However, if they are not

able to be re-joined, a rerouted colon surgery will be carried out. This procedure is called colostomy which results in an opening in the abdomen. It is often a temporary method while the bowel is healing. Radiation therapy eradicates the tumor via high-energy rays. This treatment could be utilized alone or combined with other therapies either to reduce tumor volume before surgery or to abolish the remaining cancer cells after chemotherapy. In some cases, it may also be used to relieve the pain by diminishing cancer size when tumor removal is not possible[9,10].

Table 1. TNM classification and AJCC 8th edition Staging of Colon Cancer. [Reproduced from Vogel, JD., et al. (2017). Dis. Colon Rectum[7] with permission.]

	Definition of primary tumor (T)		
T Category	T Criteria		
TX	Primary tumor cannot be assessed		
T0	No evidence of primary tumor		
Tis	Carcinoma in situ, intramucosal adenocarcinoma (involvement of lamina propria, no extension through the muscularis mucosae)		
T1	Tumor invades submucosa		
T2	Tumor invades muscularis propria		
T3	Tumor invades through the muscularis propria into the pericolonic tissue		
T4a	Tumor penetrates to the surface of the visceral peritoneum (serosa)		
T4b	Tumor invades and/or is adherent to other organs or structures		
	Regional lymph node staging (N)		
NX	Regional lymph nodes cannot be assessed		
N0	No regional lymph node metastasis		
N1	1 to 3 regional lymph nodes are positive (tumor in lymph nodes measuring ≥0.2mm), or any number of tumor deposits are present and all identifiable lymph nodes are negative		
N1a	1 regional lymph node is positive		
N1b	2–3 regional lymph nodes are positive		
N1c	No regional lymph nodes are positive, but there are tumor deposits in subserosa, mesentery, or nonperitonealized pericolic or perirectal tissues without regional nodal metastases		
N2a	4 or more regional lymph nodes are positive		
N2b	7 or more regional lymph nodes are positive		
	Distant metastasis staging (M)		
M0	No distant metastasis		
M1a	Metastasis confined to 1 organ or site is identified without peritoneal metastasis		
M1b	Metastasis confined to 2 or more organs or sites is identified without peritoneal metastasis		
M1c	Metastasis to the peritoneal surface is identified alone or with other site or organ metastases		
Stage	*T*	*N*	*M*
0	Tis	N0	M0
I	1–2	N0	M0
IIA	T3	N0	M0
IIB	T4a	N0	M0
IIC	T4b	N0	M0
IIIA	T1-T2	N1-N1c	M0
	T1	N2a	M0
IIIB	T3-T4a	N1-N1c	M0
	T2-T3	N2a	M0
	T1-2	N2b	M0
IIIC	T4a	N2a	M0
	T3-T4a	N2b	M0
	T4b	N1-N2	M0
IVA	Any T	Any N	M1a
IVB	Any T	Any N	M1b
IVC	Any T	Any N	M1C

AJCC = American Joint Committee on Cancer.

2.2. Chemotherapy

To lessen cancer cell division, different drugs or drug combinations are utilized as a principal therapeutic strategy. Chemotherapeutic drugs disrupt the life cycle of cancer cells in different ways such as damaging their DNA or interfering with the process of DNA synthesis. Most of them are administrated through vein, whereas the others are taken orally. Typically, chemotherapeutic drugs are given in combination to reduce the chance of drug resistance compared with using a single drug. Chemotherapy is used in cycles of treatment days followed by days of rest. Depending on which drugs are used, the cycles are varied; for example, 14 or 21 days long offering a chance for the body to recover. Nonetheless, this conventional chemotherapy still has pitfalls related to the delivery of drugs to the non-target site, and unwanted side effects. For instance, neutropenia, anemia, mucositis, gastrointestinal toxicity, diarrhea, nausea, vomiting, fatigue, hand-foot syndrome, hematologic disorders, and liver toxicity are major drawbacks suffered by a number of patients[11,12]. Chemotherapy regimens used for colon cancer are shown in **Table 2.**

Table 2. Chemotherapy regimens used for colon cancer[13,14].

Single agent or combination	Generic name	Brand name
5-FU/LV	5-FU = fluorouracil	-
	LV = leucovorin*	-
Capecitabine	Capecitabine Xeloda®	Xeloda®
CAPEOX	CAPE = capecitabine	Xeloda®
	OX = oxaliplatin	Eloxatin®
FOLFIRI	FOL = leucovorin*	-
	F = fluorouracil	-
	IRI = irinotecan	Camptosar®
FOLFOX	FOL = leucovorin*	-
	F = fluorouracil	-
	OX = oxaliplatin	Eloxatin®
FOLFOXIRI	FOL = leucovorin*	-
	F = fluorouracil	-
	OX = oxaliplatin	Eloxatin®
	IRI = irinotecan	Camptosar®
Irinotecan	Irinotecan	Camptosar®
Trifluridine + tipiracil	Trifluridine + tipiracil	Lonsurf®

*Levoleucovorin can be used instead of leucovorin

2.3. Targeted therapies

Targeted cancer therapies are molecules that impede the spreading of tumor by targeting or interfering with specific molecules that play an essential role in tumor progression and growth. Targeted therapy is considered less harmful to normal cells than conventional chemotherapy drugs. Many of the substances are considered biologic therapies because they are derived from antibodies, Y-shaped proteins. Targeted therapy for colon cancer basically targets the VEGF (vascular endothelial growth factor) and EGFR (epidermal growth factor receptor) pathways (**Figure 4**).

Normally, cancer cells receive food and oxygen from blood for growing. VEGF is one of the substances created by cancer cells which attaches to surface receptors of endothelial cells to stimulate the growth of blood vessels. Thus, VEGF pathway works as anti-angiogenic therapies to stop the growth of abnormal blood vessels that feed tumors. Currently, there are three kinds of drugs in the line for treating metastatic colorectal cancer cancer including antibody, fusion protein, and tyrosine kinase inhibitor. Bevacizumab (Avastin®) is an antibody, which binds to VEGF before reaching its receptors at endothelial cells. As a result, VEGF cannot attach to its endothelial surface receptors and no growth signals being produced. Ramucirumab (Cyramza®) binds to VEGF receptors on the outside of endothelial cells blocking VEGF from attaching its receptors. Regorafenib (Stivarga®) is a tyrosine kinase inhibitor (TKI), in oral dosage form. TKI attaches to VEGF receptors on the inside of endothelial cells or surface receptors within cancer cells and stops growth signals. Ziv-aflibercept (Zaltrap®) is a fusion protein designed to target multiple growth factors involved in cancer and angiogenesis. It acts as a decoy and traps VEGF. As a consequence, it is unable to bind to the real receptor.

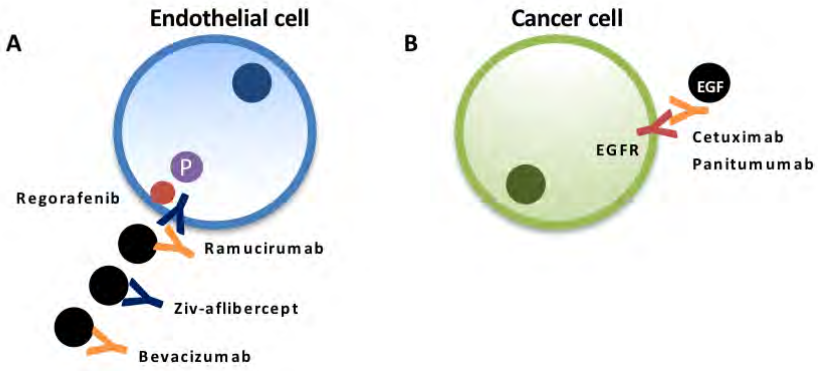

Figure 4. Targeted therapy. vascular endothelial growth factor (VEGF) (A) and epidermal growth factor receptor (EGFR) (B) pathways.

The epidermal growth factor receptor (EGFR) is one of the surface receptors on cancer cells that can trigger tumor development. When EGF (epidermal growth factor) binds to EGFR, the chemical pathway of growth signals is turned on. EGFR signaling plays an important role in the development of the disease especially with an abnormality of gene. Anti-EGFR treatment targets this receptor to interrupt its signal and hamper tumor growth[15]. Cetuximab (Erbitux®) and Panitumumab (Vectibix®) bind to the ends of EGFRs that are outside of the cell; hence, EGF is blocked from attaching and triggering growth signals. Moreover, it also attracts immune cells triggering the killing system for cancer.

To date, the therapeutic results have not yet reached satisfactory outcomes due to drug resistance. As primary treatment, surgery has shown a good effectiveness; however, patients still confront recurrence, which is a main shortcoming and frequently leads to death. The attempts to achieve early diagnosis and efficient treatment are ultimate goals to improve patient survival[16]. The severe adverse effects of cancer drugs to the non-cancer cells greatly limit the maximal allowable systemic dose, resulting in insufficient drug concentrations reaching the carcinoma. Therefore, improvements of anticancer delivery are necessary to target specifically tumor cells and differentiate normal cells in order to overcome the side effects and systemic toxicity. An overview regarding the potential of nanotechnology to improve delivery of anticancer drugs is provided in **section 4**.

3. Gene therapies

Nowadays, nucleic acid-based therapies are being proposed for the treatment of prevalent and rare diseases[17,18]. There are numerous kinds of nucleic acid drugs that affect at a specific step of the gene expression process such as protein-expressing plasmid DNA (pDNA) and messenger RNA (mRNA), antisense oligonucleotides (ASOs), microRNA (miRNA), small interfering RNA (siRNA), and genome editing systems (the CRISPR-Cas9 system). Each of them plays a role at a different level, e.g., genomic, transcriptional, and post-transcriptional step contributing to upregulation of gene expression or disruption of gene expression[19]. Therefore, the main advantage of gene therapy is that it can be precisely designed to achieve the desired therapeutic effect. Gene therapy has also been suggested for the development of improved and specific treatments against CRC. Various gene therapy methods include gene correction, immunogenetic manipulation and virotherapy[20]. Common mutations in CRC, such as those of the tumor suppressor, p53 or the proto-oncogene, K-RAS have also been assessed as therapeutic targets[21,22]. A closer description of the main gene therapy approaches is provided in the next epigraph, with some specific examples of different approaches specifically designed to treat CRC:

3.1. Upregulation of gene expression with plasmid DNA (pDNA)

A plasmid DNA is a small, circular, double-stranded DNA molecule between 5 and 20 kbp. It naturally exists in bacterial cells and some eukaryotes. Generally, the genes carried in plasmids provide bacteria with genetic benefits, thus pDNA are introduced into cells to restore the deficiency or insufficient production of a specific protein. Until now, there are more than 100 plasmid-based therapies being tested in clinical trials. A recent study of targeted lipoplex loading recombinant interleukin-15 plasmid (pIL15) demonstrated *in vivo* antitumor effect, suppression tumor growth in CT26 colon cancer mouse model[23].

3.2. Messenger RNA (mRNA)

mRNA is a natural biomolecule that carries a portion of the DNA code to other parts of the cell for processing. It is a single-stranded nucleotides known as ribonucleic acid. During the transcription step, a single strand of DNA is decoded by RNA polymerase, and mRNA is produced.

The feasibility of using mRNA for therapeutic protein expression *in vivo* has been studied as an alternative to DNA-based gene therapy. Though mRNA is less stable than DNA, it offers several merits such as higher transfection efficiency in non-dividing cells (no nuclear localization required), no potential for mutagenesis in the genome, predictable kinetics, rapid expression, decreased immunogenicity, and increased safety profile (lack of CpG motifs)[24]. Commonly, mRNAs are employed in vaccination strategies targeting dendritic cells (DCs) resulting in the development of a tumor vaccine[25]. An example related to the use of mRNA for CRC treatment refers to immunizations mediated by mRNA-loaded DCs in patients with resected hepatic metastases of colon cancer[26].

3.3 Disruption of gene expression

The concept of RNA interference (RNAi) is to disrupt disease-related gene and protein expression. Such a method is straightforward and evolutionary regulates gene expression. From Watson-Crick base-pair hybridization, a sequence that is complementary to a specific mRNA inhibits the expression of that mRNA and blocks the translation of genetic information from DNA to protein[27]. RNAi is based on a post-transcriptional regulation activated by a double-stranded RNA (dsRNA), which pave the way for sequence-specific silencing of a mRNA. It was discovered in Caenorhabditis elegans by Fire and Mello in 1998 including endogenous (miRNA) or exogenous (siRNA and shRNA) RNAs[28]. When the double-stranded RNA molecules incorporate into the RNA-induced silencing complex (RISC), gene silencing begins. While miRNAs bind partially to their target mRNAs causing degradation or translational inhibition, siRNAs and shRNAs bind completely to and cleave the complementary strand[29]. Though toxicity related with siRNA and shRNA overexpression is being debated, miRNA could be a safer choice because it does not compromise the gene knockdown efficacy.

3.4 microRNA (miRNA)

MicroRNAs (miRNAs) are small non-coding RNAs. They can regulate post-transcriptional gene expression and silence a broad set of target genes via diverse mechanisms, either restoring or repressing miRNA expression and activity[30]. They are often 18–25 nucleotides in length, which endogenously synthesized and promote mRNA degradation and/or translational inhibition.

Because of significant changes of their expression in cancer, miRNAs are supposed to be key factors in cancer genetics and to have potential as anticancer drugs. Their functions include cell survival, proliferation, apoptosis, tumor growth, and metastasis.

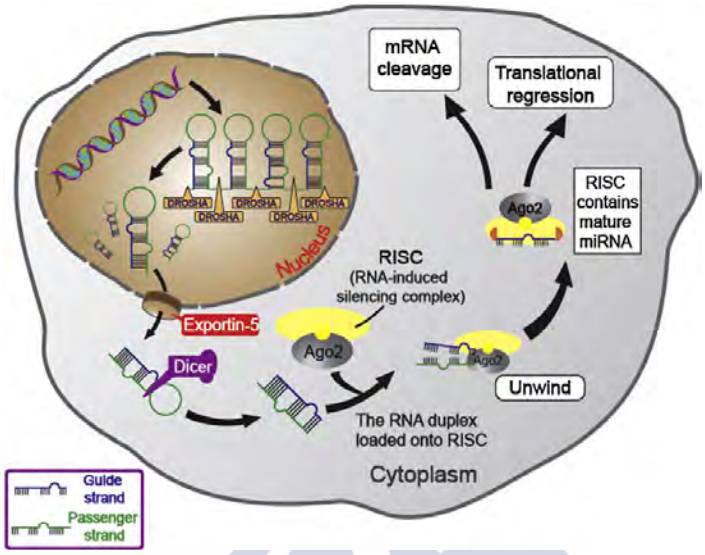

Figure 5. microRNA generation and silencing mechanisms. [Reproduced from Chen, Y., et al. (2015). Adv. Drug Deliv. Rev.[29] with permission]

In mammalian cells, primary miRNA precursors (pri-miRNAs) are initially produced as short hairpin structures in the nucleus by RNA polymerase II. They are further cleaved by Drosha in the nucleus, transported into the cytoplasm by exportin-5, and finally converted into double-stranded duplexes by the RNAse Dicer[31]. Mature miRNAs are recognized by Argonaute 2 (AGO2) and incorporated into the RISC complex. They are unwounded and annealed to the target mRNAs carrying complementary sequences causing an inhibition of translation and degradation of mRNA[32]. miRNAs are capable of regulating tens to hundreds of mRNAs through the imperfect base pairing between miRNAs and the 3′ or 5′ untranslated region of the target mRNAs (**Figure 5)**.

In cancer, the roles of miRNAs include manipulating gene expressions, regulating downstream signaling pathways, and thus controlling cancer formation and progression. Therefore, they have been utilized in cancer therapy as therapeutic agents or biomarkers to regulate multiple cancer-related genes in terms of cell cycle progression, metabolism, cell death, angiogenesis,

metastasis, and immunosuppression[33]. Two strategies are currently used to regulate the function of miRNAs in cancers. miRNAs can be downregulated when they function as tumor suppressors or overexpressed when they function as oncogenes[34] (**Figure 6)**.

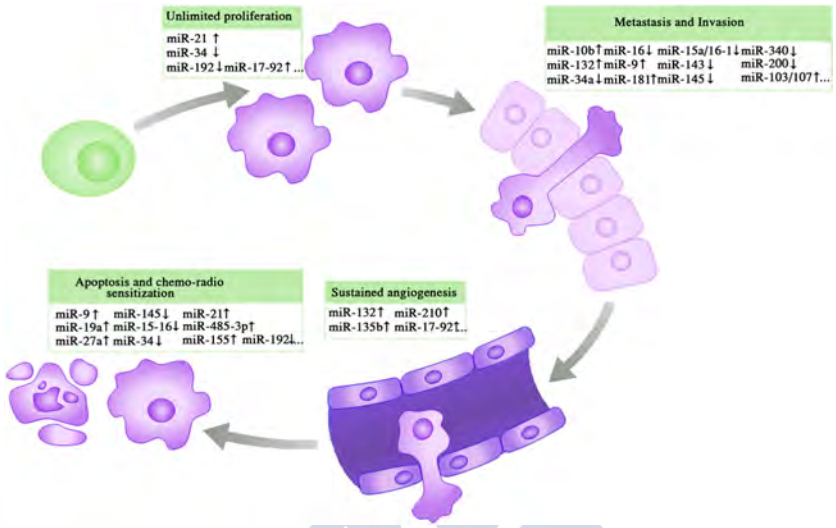

Figure 6. miRNAs targeting the hallmarks of cancer at various progression stages (The up arrows represent oncomiRs and the down arrows indicate tumor-suppressive miRNAs). [Reproduced from Wang, H., et al. (2015). Adv. Drug Deliv. Rev.[34] with permission]

In case miRNAs are downregulated, replacement therapy with miRNA mimics is used to restore miRNA levels and their tumor suppressive functions. For instance, miR-34a, miR-15a, miR-16, miR-17, miR-29, miR-126, miR-143/145, and the let-7 family are under-expressed in many human cancers. Hence, up-regulation of these tumor-suppressive molecules reprograms cancer cells by incorporation into the RISC and silencing their target mRNAs[35,36]. Additionally, the mimics of duplex structures are preferred over single-stranded mimics because the double-stranded miRNA mimics have been found to facilitate RISC loading and so enhance the gene-silencing efficacy[37]. Furthermore, plasmid DNAs, which encode hairpin pre-miRNA can be utilized to reactivate cellular pathways and induce therapeutic responses[38]. Different approaches related to restoring of miRNA levels to decrease tumor growing and progression have been proposed as novel therapeutic strategies for CRC, for example, miR-200c by targeting ZEB1 mRNA, miR-4458 by targeting hexokinase2 mRNA, and miR-145 by targeting fascin-1 mRNA[39-41].

On the contrary, oncomiRs (e.g., miR-125b, miR-20, miR-155, and the miR-17-92 family) that inhibit the function of miRNAs are overexpressed in different types of cancers. In this case, miRNA antagonists such as synthetic anti-miRNAs or locked nucleic acids (LNAs) are used to inhibit the activity of oncogenic miRNAs. The usual method is to use the single-stranded oligonucleotides with sequences that are partial or complete complementary to endogenous mature miRNAs. The complementary binding of the antagonist to the endogenous miRNA prevents its processing by RISC. Anti-miRNAs are chemically modified to increase their binding affinity for the miRNA[42].

The delivery of nucleic acids requires a protection from serum endonucleases and an evasion from immune system detection. These could be accomplished by encapsulating nucleic acids inside the non-viral carriers and specific characterization of particles such as chemical modifications and adding polyethylene glycol (PEG) or specific ligands. After administration, these vectors have to avoid renal clearance, extravasate from the bloodstream to reach tumor sites, and mediate cell entry and endosomal escape. Different delivery approaches based on nanotechnology are described in **section 6**.

4. Biomedical imaging

Nowadays, biomedical imaging has numerous impacts on scientific discoveries and technological innovations. Advances in X-ray computed tomography (CT), magnetic resonance imaging (MRI), positron emission tomography (PET), single-photon emission computed tomography (SPECT), ultrasound, and optical-imaging techniques, play a crucial role in non-invasive experiments to obtain uniquely valuable information about tissue composition, morphology, and function (**Figure 7**). In research area, they are widely used for imaging small animals, being this understood as translational tools between animal models and human clinical applications. Furthermore, a variety of molecular devices and contrast agents have been created to drive cellular and molecular imaging for new inventions in biological research[43,44]. The capability to detect, diagnose, and monitor pathological, physiological, and molecular changes utilizing these techniques, is essential for disease management and personalized interventions.

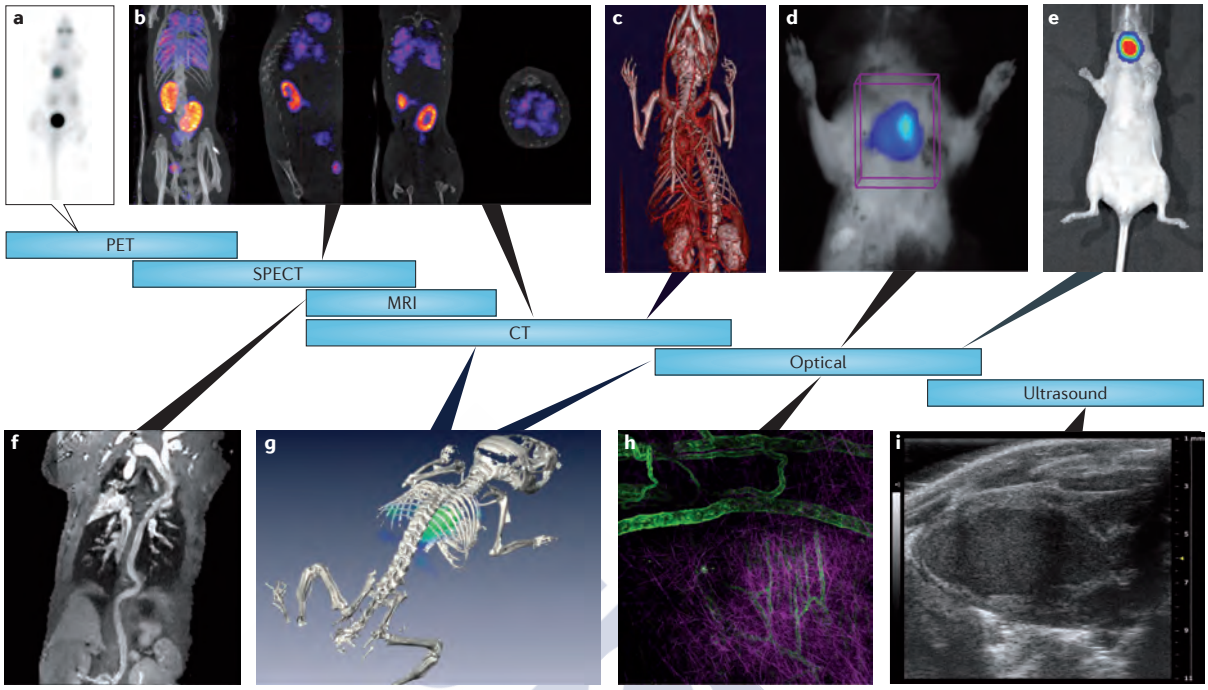

Figure 7. Various types of currently commercially available in vivo molecular multimodal imaging systems and applications. [Reproduced from De Jong, M., et al. (2014). Nat. Rev. Cancer[37] with permission]

Nevertheless, each imaging modality has its own advantages and disadvantages, and a single technique does not possess all the requirements for comprehensive imaging[45]. For instance, the major merits of radionuclide-based molecular imaging techniques (SPECT and PET) over other modalities are that they are quantitative and highly sensitive, and can detect tracer concentrations in the picomolar or nanomolar range. In addition, there is no tissue penetration limit. However, one disadvantage is that the resolution (typically >1 mm) of either SPECT or PET is not as high as for other imaging modalities such as MRI. On the contrary, the spatial resolution of MRI and CT is notably higher than that of SPECT, but they have the limitation in sensitivity. For optical imaging, they offer higher sensitivity and temporal resolution than PET at the same spatial resolution in small animals; however, it is limited to a few centimeters of tissue depth (**Table 3**).

Table 3. Advantages and disadvantages of each image modality.[45-47]

Imaging modality	Advantages	Disadvantages
Optical imaging	• High sensitivity • Easy labeling • Great variety of fluorescent molecules and detection wavelengths • No radiation exposure	• Low resolution • Limited tissue penetration • Potential incompatibility and toxicity of fluorescent probes • Relevant wavelength range limited to 700-900nm.
Computed tomography (CT)	• High spatial resolution • Ability to differentiate between tissues • Low radiation exposure	• Require contrast agent for enhanced tissue contrast • Radiation • Tissue non-specificity
Magnetic resonance imaging (MRI)	• High resolution • No ionizing radiation • Able to image physiological and anatomical details • Several contrast agents are widely used for clinical imaging	• Cost • Low sensitivity • Real-time imaging is difficult • Cannot be used in patients with metallic devices e.g. pacemakers
Positron emission tomography (PET)	• Ability to image biochemical process • High sensitive • Signals from radionuclides can be quantified precisely	• Radiation • Low resolution • Cost • Can give false results if chemical balances within the body are not normal • Radionuclides involved have relatively short half-lives
Single photon emission computed tomography (SPECT)	• Ability to image biochemical process • High sensitive • Signals from radionuclides can be quantified precisely	• Radiation • Low resolution • Cost
Ultrasound	• Non-invasive • Ease of procedure • No radiation exposure • Low cost	• Low resolution • Microbubbles as contrast agents have relatively large size and short blood circulation • Destruction of microbubbles ruptures vessel walls and causes hemolysis

Medical imaging enables rapid, longitudinal, and noninvasive visualization of the interior of living subjects. This technique is categorized into two main approaches. First is an anatomical imaging, which offers information on gross structure. Second is a molecular or functional imaging that provides data on physiology and cellular processes[48-50]. For instance, metabolism, protein expression, and DNA synthesis. While exogenous imaging agents are optional for anatomic imaging (e.g., MRI or CT contrast medium agents, which help improving tissue contrast), there is a requirement for molecular imaging, especially within the realm of nuclear medicine (SPECT or PET)[51-53]. Nanoparticles are a new and exciting class of imaging agents that can be used for both

anatomic and molecular imaging. An overview regarding the potential of nanotechnology for diagnostic applications is provided in **section 6**.

For CRC, imaging tests are examined to illustrate the site of tumor. They provide information for the doctor to evaluate the stage of cancer and plan treatment. Some imaging examinations use contrast agents to display tumor area, which are administered by injection into bloodstream[54]. Generally, this procedure is performed by the radiologist, who conveys imaging results to the oncologist. The common image modalities for CRC diagnosis are CT, MRI, and PET[55]. CT is usually advised when the cancer has spread beyond the second layer of the colon wall. Moreover, CT colonography has emerged as a potentially comfortable alternative for patients undergoing full structural screening of the colon and rectum[56,57]. Several studies suggest that CT colonography is able to depict colorectal neoplasms larger than 1 cm in diameter[58,59]. In certain cases that the CT scan are unclear, MRI can be required such as the evaluation of liver metastases[60]. The combination of PET/CT renders some benefits such as ability to find metastases and demonstrate the size of metastases tumor[61]. In addition, PET is a good option when the patients are not able to receive contrast agents of CT or MRI. It is administrated with glucose analog. Due to the high demand of sugar in cancer cells, it can have a high uptake, resulting in brighter image in tumor compared to normal cells[62].

4.1. Anatomical imaging

4.1.1 X-ray computed tomography (CT)

Anatomic imaging by CT can be performed without administration of any contrast agent; however, contrast administration can increase the sensitivity and specificity of lesion detection[63]. CT image contrast is dependent on tissue density, which determines the amount of x-ray beams that will be attenuated as they pass through the object of interest. Iodinated contrast agents are routinely used to visualize blood flow and washout, often delineating areas that can be used as a surrogate for neoplasm, infection, and inflammation[64,65].

The CT detectors measure the attenuation coefficient (μ) between the x-ray tube and detectors, which is a measure of how much x-rays are absorbed. The gray levels in a CT image

represent attenuation as Hounsfield units (HU). Bones or areas of calcification are the most attenuating (+1,000HU); whereas air is the least attenuating (−1,000 HU). Clinical CT scanners allows acquisition of whole-body images within a few seconds. Nevertheless, CT scans expose patients to ionizing radiation, which limits pediatric applications. For adults, short-time procedure is recommended[66,67].

4.1.2 Magnetic resonance imaging (MRI)

MRI is a noninvasive and nonionizing medical imaging for visualizing anatomical, physiological, and molecular information for internal structures of living subjects. Depending on the magnetic field strength, MRI can illustrate data with spatial resolutions down to 10 μm. Generally, clinical magnets provide ∼1 mm in resolution. Its penetration depth is adequate to image throughout the whole body of humans. Currently it is beneficial for image in brain, muscles, heart, and cancers because of its good contrast between the different soft tissues of the body[68,69].

The sensitivity of standard MRI is associated with the mechanism of signal detection, which measures the relaxation rates of water protons. It can also detect other nuclei with nonzero spins. However, the most common use is with protons. The precession of water hydrogen nuclei in an applied magnetic field changes after applying radiofrequency pulses. This causes changing in the alignment of the magnetization of atoms. The proton spin flips from being parallel to the external field to being transverse. After the removal of the pulse, the nuclei start to produce a rotating magnetic field and revert back to equilibrium. This is detectable by the scanner, which is recorded to construct an image. Strong magnetic field gradients affect nuclei at different locations to rotate at different speeds, hence giving 3D spatial information[70]. The different T_1 (spin–lattice/longitudinal relaxation) and T_2 (spin–spin/transverse) proton relaxation times in different tissues produce the endogenous contrast. To improve the differentiation between tissues, exogenous contrast agents are usually utilized to shorten the relaxation parameters (T_1 and T_2) of water resulting in a bright (positive) or dark (negative) contrast enhancement. Thus, contrast agents enhance the signal-noise ratio and provide the better detection sensitivity[71]. Paramagnetic molecules such as gadolinium (Gd) and manganese (Mn) can be chelated with small molecules or macromolecules creating T1 contrast agents. While gadolinium-based contrast agents shorten the

longitudinal relaxation times (T_1) of tissues and increase signal strength, iron oxide shortens transverse relaxation times (T_2) and darkens the contrast[72]. Currently, several Gd^{3+} contrast agents are FDA approved. Dextran-coated iron formulations are clinically approved for T2 contrast agents[73].

Although, conventional high resolution anatomic imaging modalities such as computed tomography (CT) and magnetic resonance imaging (MRI) can provide details regarding lesion location, size, morphology, and structural changes to adjacent tissues, these modalities offer little insight into tumor physiology. According to the increasing focus on molecularly targeted therapies, imaging radiolabelled agents are usually used to acquire information of tumor's biologic functions and its surrounding microenvironment.

4.2. Functional imaging

At the other end of the electromagnetic spectrum lied γ-ray emissions, which are the fundamental for PET and SPECT. Both modalities are based on administered radiopharmaceuticals and the detection by a camera. As the gamma rays have the megavolt energies, they require little signal amplification and are acquired over a nominally low background signal. Unlike MRI, they are quantitative techniques[74]. Biological molecules with labelling radionuclide can be tracked using PET or SPECT to obtain their biodistribution[75]. It is usually assumed that the labelling technique does not disturb the characteristics of those molecules regarding metabolism, specific binding or non-specific interactions.

4.2.1 Single-photon emission computed tomography (SPECT)

SPECT is a nuclear medicine tomographic imaging technique. It can create 3D information allowing accurate localization of organs[76]. It relies on the detection of gamma rays from radioisotopes, for example ^{99m}Tc, ^{111}In, ^{123}I, and ^{131}I. Several radionuclides can be multiplexed for use in SPECT because different isotopes emit different energies of gamma rays, while various isotopes for PET all emit the same energy in the form of positrons[77]. However, SPECT is an order of magnitude less sensitive than PET.

After *in vivo* administration, the isotope from the radiolabelled molecules emits gamma rays detected by a gamma camera. Normally, a marker radioisotope could be attached to an antibody or nanoparticles. As an example, one study was successfully accomplished in the liver to study the correlation between tumor accumulation of In-111-bevacizumab and VEGF-A expression in patients with colorectal liver metastases[78].

4.2.2. Positron emission tomography (PET)

The principle of PET relies on the administration of radiolabelled tracers to monitor their biodistribution, physiological processes, biochemical pathways, etc.[79]. This modality in clinical molecular imaging has a resolution of 1–2 mm. Although it suffers from low anatomical resolution compared to MRI, it perhaps has the highest sensitivity of the imaging techniques which is usually in a concentration of nanomolar. This enables quantification of the local concentration of radionuclide tracer and provides the possibility to detect a single abnormal cell labelled with only a few amount of trace isotopes. PET has no limit of the penetration depth. Thereby, it allows image, regardless of the location of the target. The advantage of PET is strengthened in cancer research for detection of molecular changes, which are occurring in the body before the macroscopic disease is shown. It is also helping in monitoring disease progression after treatment such as tumor response to therapy[80,81].

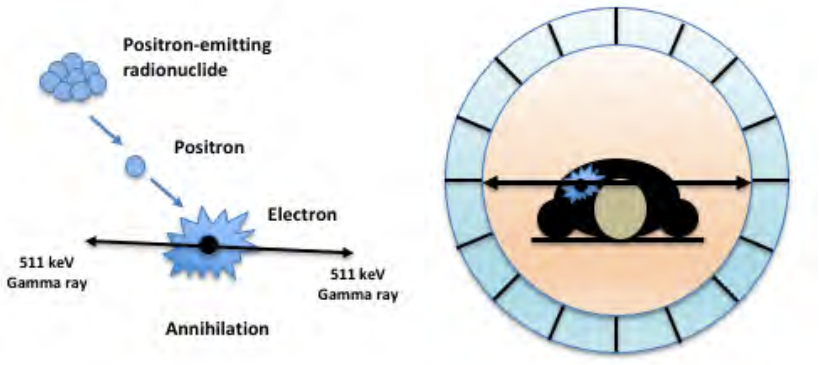

Figure 8. Principle of PET imaging

PET image is based on the emission of radioisotopes in the form of positrons without the need for external excitation. PET scans are acquired after the injection of the radiotracer, a molecule incorporated radionuclides during the radiosynthesis step. The radiotracer accumulates in tissues, and then its radionuclide decays by emission of a positron (anti-electron) contributing to *in vivo* tracking with a camera. Normally, after a positron travels a few millimeters, it will collide with an electron and simultaneously release two photons (gamma-rays) with energy of 511 keV into opposite directions **(Figure 8)**. This annihilation is detected by the PET camera[82]. By collecting a statistically significant number of radioactive events and mathematical algorithms, the distribution of the positron-emitting molecules in the tissues is reconstructed in three-dimensional image[83].

Radioisotopes for PET include both short-lived or long-lived positron-emitting radionuclides. These are examples of positron emitters and their half-lives: ^{11}C (20 minutes), ^{15}O (2 minutes), ^{18}F (2 hours), ^{68}Ga (68 minutes), ^{64}Cu (13 hours), and ^{76}Br (16 hours). Among those radioisotopes, ^{18}F could be an interesting choice for labelled-molecules to track tumor in whole-body and provide an efficient diagnosis. Its advantages are ease of production in large quantities with high specific activity, appropriated half-life (109.7 min), and high PET resolution[84]. [^{18}F]fluorodeoxyglucose (FDG) is a glucose analog approved for staging several cancers such as breast, colorectal, esophageal, head and neck cancers, melanomas and lymphomas[85]. In most of the malignancies that are rapidly metabolizing cells, it is selectively taken up. Nevertheless, in certain cases, imaging with FDG can be counter-productive as glucose metabolism is not only specific to tumors. Radiotracer with short half-life is also a double-edged sword. While this can reduce toxicity, it may be difficult to reach ample amounts at the target areas. Consequently, all pitfalls have driven researchers to develop more specific imaging molecules; for instance, antibodies, small proteins, peptides, and other targeted biological moieties.

Nonetheless, the benefits of using PET come with a relatively high price because the only approach to generate the positron-emitting isotopes is from a cyclotron. Thus, the laboratory operating PET image must be located near such a source in order to rapidly receive the radionuclides. Besides, preparing of appropriate storage and handling of these radioactive materials should be properly manipulated[86]. Lastly, the exposure to the ionizing radiation should be limited for both patients and clinicians.

5. Nanotechnology for treatment and diagnosis of cancer

Nanotechnology has been utilized in a wide spectrum of biomedical applications including imaging, bio-sensoring, and drug delivery, and have attracted a great deal of attention in cancer[87-90]. Some examples of nanoparticles with variable compositions and architectures are shown in **Figure 9.**

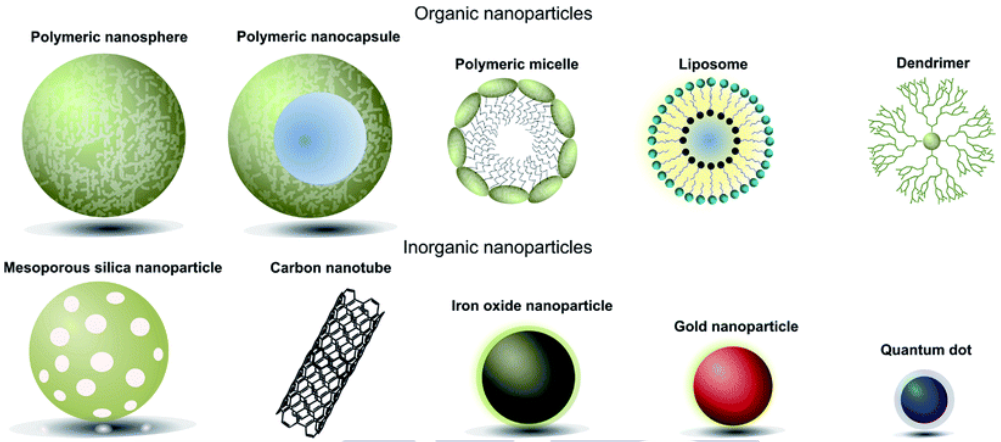

Figure 9. Nanotechnology-based carrier systems. [Reproduced from Richards, D. A., et al. (2016). Chem. Sci. Polym.[90] with permission].

5.1 Marketed nanoformulations in cancer therapy

Several nanomedicines have been approved for specific clinical indications related to cancer therapy (**Table 4**). Doxil/Caelyx® was the first FDA-approved anticancer nanomedicine. This liposomal doxorubicin rendered a distinct pharmacokinetic and biodistribution of the drug resulting in improvement of safety and effectiveness compared to the free doxorubicin. Currently, it has been approved for various indications including Kaposi's sarcoma, ovarian cancer, breast cancer, and multiple myeloma[91,92]. Similar improvements over the current treatments contributed to the approvals of other nanomedicines such as Abraxane®, DaunoXome®, Depocyt®, Genexol-PM®, and Myocet®[93]. Another advantage is the opportunity to develop a formulation without using dose-limiting toxic excipients. For example, patients using Abraxane® and Genexol-PM® can receive higher doses of paclitaxel because these formulations avoid the use of cremophor. As

a result, the maximum tolerated dose of the active ingredient can be augmented. Commonly, approved anti-cancer nanomedicines have been designed exploiting the concept of the EPR effect. Further development can be achieved via ligand-mediated targeting. Two targeted formulations are now in clinical trials such as BIND-014 (BIND Therapeutics) and MM-302 (Merrimack Pharmaceutical)[94-96].

Table 4. Anti-cancer nanomedicine clinically approved[91-94].

Trade Name	Company	Formulation / target	Indication
Abraxane	Abraxis Bioscience, Astra Zeneca, Celgene	Paclitaxel	Various cancers
DaunoXome	Galen	Daunorubicin	Kaposi's sarcoma, ovarian cancer, breast cancer, multiple myeloma
DepoCyt	Pacira	Cytarabine	Malignant lymphomatous meningitis
Doxil/Caelyx	Orthobiotech, Schering-Plough	Doxorubicin	Kaposi's sarcoma, ovarian cancer, breast cancer, multiple myeloma
Genexol-PM	Samyang Biopharm	Paclitaxel	Breast cancer, lung cancer, ovarian cancer
Lipo-Dox	Taiwan Liposome	Doxorubicin	Kaposi's sarcoma, ovarian cancer, breast cancer
Marqibo	Talon	Vincristine	Acute lymphoblastic leukemia
Mepact	Takeda	Mifamurtide MTP-PE	Osteosarcoma
Myocet	Cephalon	Doxorubicin	Breast cancer
NanoTherm	Magforce Nanotechnologies	Iron oxide nanoparticle	Thermal ablation of glioblastoma
Oncaspar	Enzon	PEG asparaginase	Acute lymphoblastic leukemia
Ontak	Eisai Medical Research	DAB_{389} IL-2	Recurrent CD25+ T cell lymphoma
Zinostatin stimalamer	Yamanouchi	SMANCS (styrene maleic acid neocarzinostatin)	Liver cancer, renal cancer

With respect to nanoformulations undergoing clinical trials, there is an increased number over the time, metallic and protein-based particles being the predominant types of studied nanomaterials (**Figure 10a and 10b)**[97]**.** In general, the whole clinical phase can last approximately 10–15 years with $1 billion per new drug. Nanoparticles have to be tested in animal to confirm efficacy, safety, and to identify suitable dose ranges in the preclinical phase. Subsequent human trials are composed of Phase I to Phase III including dosing, toxicity, excretion, safety, and efficacy. Further post-marketing (Phase IV) studies are regularly conducted on a request of the FDA according to particular questions raised during the Phase III trials. Hence, successfully translating anti-cancer nanomedicines from clinical study to the real market is a real challenge.

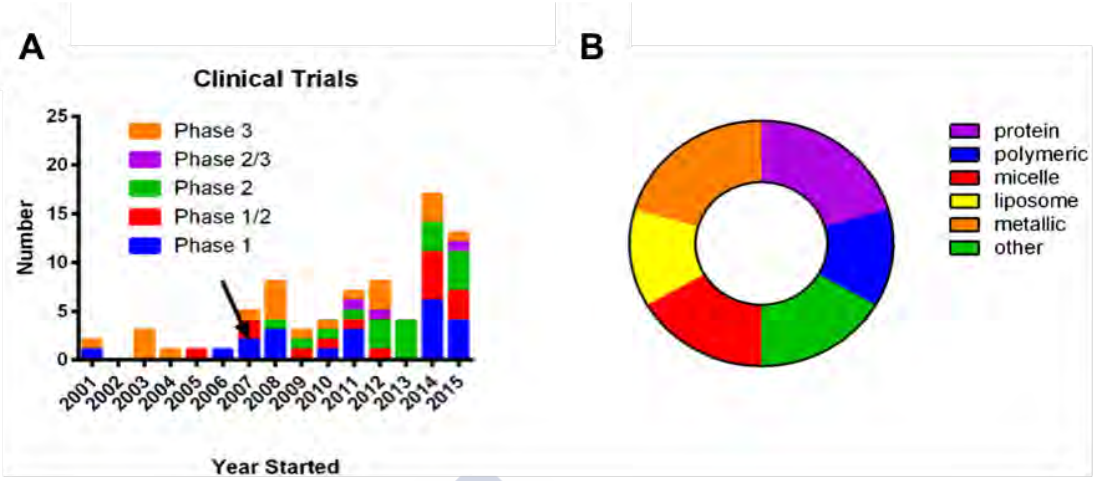

Figure 10. Trends in the development of nanomedicines. Clinical trials identified with arrow indicating approximate start date of US law (FDAAA 801) (a). Nanomedicines under clinical trial stratified by category overall (b). [Reproduced from Bobo, D., et al. (2016). Pharm. Res.[97] with permission]

5.2. Targeting nanoformulations to the tumor

The access of chemotherapeutic or diagnostic agents at tumor tissues is a critical step for achieving therapeutic and diagnostic efficacy[98]. Problems related to a poor access are mainly related to poor pharmacokinetics of low molecular weight anti-cancer drugs and medical diagnostic agents. They usually not only distribute to tumor areas but also go through healthy tissues after systemic administration. Therefore, improving biodistribution and reducing side effects is one of the big challenges relying in the application of nanotechnology to design improved anticancer therapies and diagnosis agents. **Figure 11** represent key steps in tumor delivery that can be improved making use of nanotechnology.

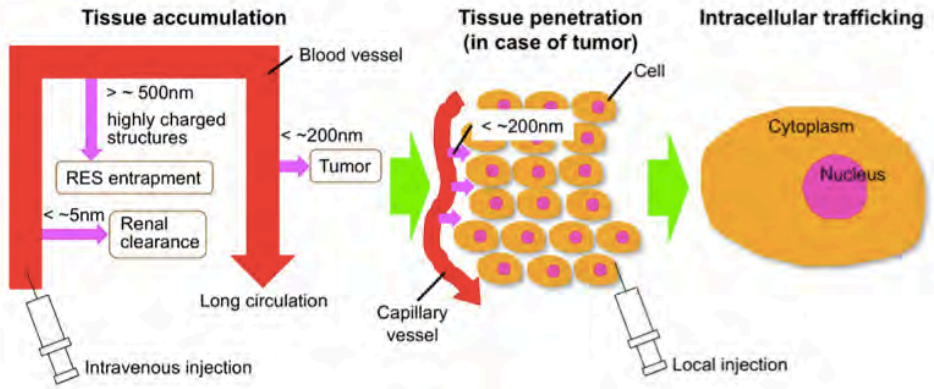

Figure 11. Three stages in the biodistribution of drugs. Tissue accumulation, tissue penetration, and intracellular trafficking. [Reproduced from Miyata, K., et al. (2011). React. Funct. Polym.[98] with permission]

To increase tissue accumulation, nanocarriers are designed to tackle fast renal excretion, and escape from the reticuloendothelial system (RES). For this problem, two of the most important criteria are size (or molecular weight) and the surface characteristics of the carrier. A molecular weight of approximately 45 kDa or between 4 and 9 nm in hydrodynamic diameter[99] is known to be the threshold of renal clearance; whereas, the RES usually captures highly-charged or large molecule (>several-hundred nanometer). Typically, and according to several reviews[100-102], <200 nm nanoparticles can efficiently penetrate and accumulate in tumor tissues owing to enhanced permeability and retention (EPR) effect (**Figure 12**). Finally, the drugs must be released at their targeted sites. The payload must be stably retained within the drug carrier until reaching the tumor to maximize efficacy and minimize off-target effects.

5.2.1 Enhanced permeability and retention (EPR) and stealth effect

The enhanced permeability and retention (EPR) effect is a unique phenomenon of solid tumors related to their anatomical and pathophysiological differences from normal tissues[103-105]. The neovasculature of tumors differs greatly from that of normal tissues due to their angiogenesis resulting in high vascular density in solid tumors with large gaps existing between endothelial cells in tumor blood vessels. Hence, macromolecules (nanometer-scale) can penetrate extensively into the tumor tissue. Furthermore, slow venous return in the tumor tissue and poor lymphatic drainage system cause macromolecules to be retained in the tumor. On the other hand, this concept does not

apply to low-molecular-weight agents because of their diffusion into the entire body with rapid renal clearance. Thus, EPR effect served as a basic concept for the delivery of anticancer nanodrugs.

Surface modification can modulate the fate of nanoparticles. The procedure of non-specific protein adsorption occurs when nanoparticles are exposed to the biological environment leading to a protein layer around the materials. It is practically impossible to completely avoid the formation of this protein corona. The major concern related to protein adsorption is the aggregation of nanoparticles and/or activation of macrophages though phagocytosis. This phenomenon leads to non-ideal biodistribution and unpredictable pharmacokinetics of nanocarriers. Coating with polyethylene glycol (PEG) derivatives can provide hydration shells at the solid-liquid interface[106]. Such coatings cause protein repulsion, hindering opsonization, and providing long circulation properties, what is called stealth effect[107-109]. This steric stabilization can prolong the half-life from less than a few minutes to several hours. Additionally, PEGylated nanocarriers are suitable to be further modified with targeted ligands[110].

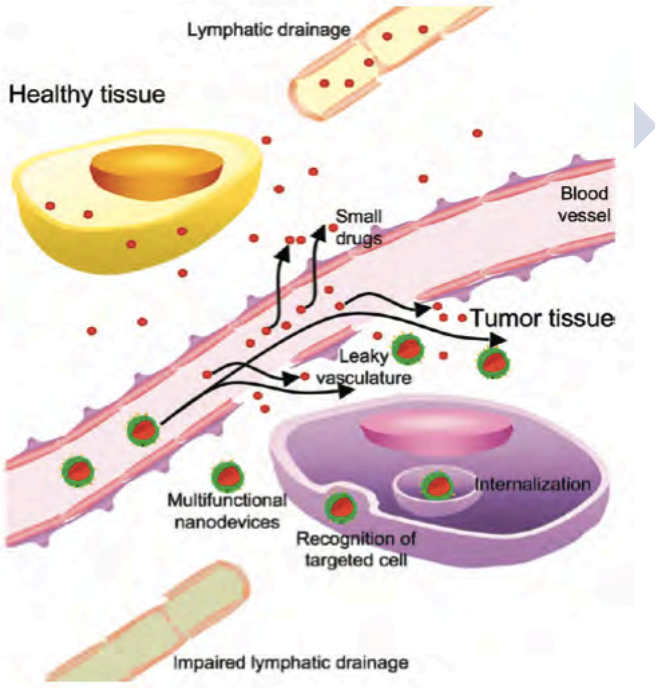

Figure 12. Schematic representation of the enhanced permeability and retention (EPR) effect. [Reproduced from Cabral, H., et al. (2011). Acc. Chem. Res.[103] with permission]

5.2.2. Targeted delivery

The conjugation of targeting ligands to nanocarriers, such as antibodies, peptides, aptamers, and proteins, has led to the development of targeted delivery strategies to tumors[111-114.] Active targeting nanocarriers enable specific binding to a receptor or antigen overexpressed on the cell surface of a malignant cell. Targeted receptors that are usually expressed on tumor and utilized in active targeting are folate receptor (folic acid)[115,116], CD-44 receptor (hyaluronic acid)[117,118], transferrin receptor (transferrin)[119], biotin receptor (biotin)[120], and integrin receptor (peptide)[121,122].

Peptides are short amino acid chains with the length of approximately 50 amino acids[123]. Their advantages as ligands relate to cost, ease of production, and high stability in a wide range of biological conditions. In general, selected peptides have high affinities at concentration down to nanomolar level for their receptors. Thereby, they offer a distinctive tool with desirable target-to-non-target ratios in the development of drug and gene delivery approaches[124]. As an example, the tripeptide Arg-Gly-Asp (RGD), which binds specifically to integrin receptors (integrin $\alpha V\beta 3$) related to tumor angiogenesis and metastasis[125,126], has been conjugated to radiolabelled iron oxide nanoparticles (RGD-^{64}Cu-DOTA-IO) showing and improved tumor uptake[127]. Modification of single-walled carbon nanotubes (SWNTs) with PEGylated phospholipids and RGD similarly demonstrated higher tumor uptake than those without RGD modification[128].

For colorectal cancer, CPIEDRPMC (RPM) peptide, first discovered in 2003 derived from a peptide library via phage display selection, specifically targets invasive colorectal cancer[129,130]. Enhanced cellular internalization of RPM-conjugated bioreducible gene carrier was confirmed by using targeted (IR820-SS-bPEI- PEG-RPM) and non-targeted (IR820-SS-bPEI- PEG) polyplexes. *In vivo* images at different time points after intravenously treatment of mice bearing HT-29 with the RPM-conjugated polyplex displayed a good targeting efficiency compared with the non-targeted polyplex (**Figure 13**)[131].

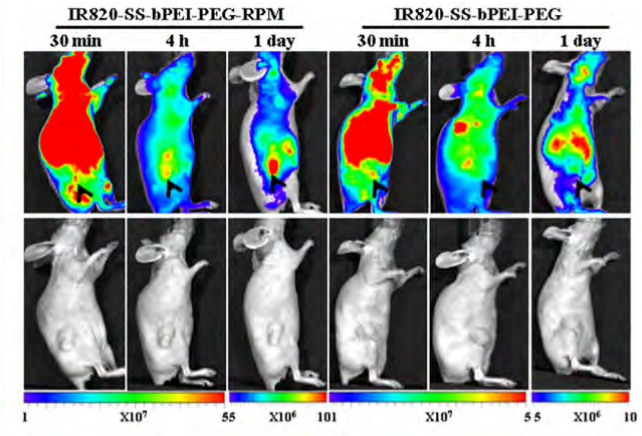

Figure 13. In vivo real-time images of mice bearing HT-29 tumor at 30 minutes, 4 hours, and the 1 day after injection with the RPM-conjugated or non-targeted polyplex. [Reproduced from Lee, Y., et al. (2015). J. Control. Release.[131] with permission]

5.3 Nanoemulsions

The development of lipid-based carriers has gained interest in research over the years, as they are versatile systems that typically show a good biocompatibility, safety, and efficacy[132-134]. They can be adapted to meet the requirements of the different routes of administration (e.g. topical, oral, pulmonary, or parenteral). Various kinds of lipid-based nanocarriers have been developed to date, including microemulsions, nanoemulsions, lipid nanocapsules, lipid nanoparticles, and liposome, in most cases with the purpose of enhancing the solubility of anti-cancer drugs,. Among them, nanoemulsions provide outstanding properties to encapsulate active compounds due to their flexible design, high kinetic stability, and good reproducibility[135,136].

5.3.1 Composition

The lipid selection is typically a compromise between its ability to solubilize the drug and its capacity to formulate nanoemulsions with desired characteristics. Nanoemulsions can be prepared from one lipid or a combination of lipids. The lipid in the formulations can be natural, semi-synthetic, or synthetic, and may also be biodegradable, such as based on triglycerides (tri-

stearic acid, tri-palmitic acid, tri-lauric acid and long-chain fatty acid), steroids, waxes (e.g. beeswax and carnauba wax), and phospholipids.

Phospholipids are one of the essential constituents of the cell membrane, and are widely used in the preparation of lipid-based nanosystems and nanoemulsions, as well as cholesterol [137]. They have solubilizing and polarity properties useful for engineering drug delivery nanosystems[138,139]. Other lipids of interest are non-bilayer lipids, such as triglycerides, waxes, vitamin E, and fixed oils (soybean oil and castor oil). Depending on their melting points, crystallinity, and polymorphic characteristics, their uses vary in the formulations. Usually long-chain triglycerides are difficult to nanoemulsify, while medium-chain triglycerides and fatty acid esters (e.g., ethyl oleate) are easy to nanoemulsify[140]. Additionally, the combination of lipids between long chain triglycerides and medium chain (mono- and diglycerides) can have a valuable benefit on self-emulsifying properties in comparison with a single lipid phase. Mixed lipid formulations can be created with lower levels of surfactants and no addition of co-solvents[141,142]. Vitamin E (D-α-tocopherol) has gained huge interest as an oily phase due to its ability to solubilize drugs such as paclitaxel, itraconazole, and saquinavir[143]. Thus, currently there is a great attempt to develop nanoemulsions based on Vitamin E[144-147].

Surfactants are necessary to stabilize lipid nanoparticle dispersions and prevent particle agglomeration. Based on their properties, for instance charge, molecular weight, chemical structure, and hydrophilic-lipophilic balance (HLB), surfactants can be selected for specific preparations. The HLB of an emulsifier is specified by the balance between the size and strength of the hydrophilic and lipophilic groups. The choice of the surfactant is based largely on the route of administration. For parenteral formulations, there are limits on the emulsifiers that can be used[148]. For topical routes, the concern of skin sensitization has to be considered, whereas for oral routes, the concentration of emulsifier used in the preparation should not create any physiological effects. Emulsifiers could as well be used in combination to produce synergistic effects and better stabilize the formulation. Examples of surfactants used in the production of nanoemulsions are Poloxamer 188 and 407, Polysorbate 20, 65, and 80, Cremophor EL, and Solutol HS 15. Non-ionic surfactants (HLB values between 12-16) are commonly utilized in the formulation of self-emulsifying systems.

Surfactants with a high HLB have a high hydrophilicity, which can promote the formation of O/W droplets and the rapid spreading of the formulation in the aqueous media. The usual surfactant strength ranges between 30-60% by weight of the formulation[149]. As a consequence, a major pitfall of these systems is the use of high concentrations of surfactants, leading to possible toxic effects. Nonetheless, in the case of ionic surfactants, toxicity problems are relatively more challenging compared with non-ionic surfactants. Thus, the selection of appropriate surfactants must be considered during the development of nanoemulsions.

The use of a single surfactant is usually not sufficient to lower the oil–water interfacial tension to yield a formulation. The addition of amphiphilic short chain molecules as co-surfactants aids in reducing surface tension nearly to zero. Moreover, incorporating co-surfactants in nanoemulsions aims to increase drug loading and modulate self-nanoemulsification in terms of time and droplet size. Co-surfactants penetrate into the surfactant monolayer giving additional fluidity to the interfacial film and disrupting the liquid crystalline phases[150]. Medium chain length alcohols (8 to 12 carbon atoms) and derivatives of ethylene- glycol, glycerol and propylene glycol are examples of co-surfactants.

5.3.2 Manufacturing

The methods used for fabrication of the nanoemulsionsare divided into high- and low-energy emulsification proceses (**Figure 14**).

5.3.2.1 High-energy emulsification methods

Typically, high-energy emulsification methods utilize mechanical devices to create nanoemulsions with high kinetic energy. These methods comprise high-pressure homogenization, microfluidization, and ultrasonic emulsification. High-pressure homogenization and microfluidization can be used for fabrication of nanoemulsions at both laboratory and industrial scale, whereas ultrasonic emulsification is predominantly used at laboratory scale.

High-pressure homogenization is most widely used to produce nanoemulsions of extremely low particle size (up to 1 nm). A high-pressure homogenizer passes the coarse macroemulsions

through a small orifice at an operating pressure in the range of 500 to 5000 psi. During this process, numerous forces, including hydraulic shear, intense turbulence and cavitation, perform together to generate nanoemulsions with extremely small droplet size. Recirculation of the emulsions through the region of high shear is important in order to obtain nanoemulsions with the desired droplet size and relatively low polydispersibility[151-153]. Owing to the higher shear rates, they are heated above room temperature during the process. Subsequently, they are cooled by a heat exchanger without affecting the size distribution or stability. The production rate of this strategy is several liters per hour.

The microfluidization process uses a high-pressure positive displacement pump operating at very high pressures, up to 20,000 psi. This pump forces macroemulsion droplets with high velocity through an interaction chamber, consisting of small channels called “microchannels”, resulting in very fine particle nanoemulsions. Nanoemulsions with the desired size range and dispersity can be acquired by varying the operating pressure and the number of passes through interaction chambers, as in high-pressure homogenization[154,155]. The development of water-soluble nanoemulsions for the highly lipid-soluble drug tamoxifen using microfluidization was reported by Tagne and coworkers[156]. Nanoemulsions with tamoxifen had mean particle sizes of 47 nm and could inhibit cell proliferation 20-fold greater and increase cell apoptosis 4-fold higher in the HTB-20 breast cancer cell line than the suspension of tamoxifen.

Ultrasonic emulsification uses a probe that produces ultrasonic waves to break up microscale droplets to nanoscale by means of cavitation forces. By varying the ultrasonic energy input and time, the nanoemulsions with desired properties can be gained. High-energy emulsification techniques can be employed to formulate both O/W and W/O nanoemulsions.

Although high-energy emulsification methods generate nanoemulsions with desired properties, and have industrial scalability, they are not suitable for thermolabile drugs and macromolecules such as proteins, enzymes, and nucleic acids[157,158]. In addition, high-energy methods involve sophisticated instruments and significant energy input, which affects the cost of the procedure. Therefore, researchers are now focusing in low-energy emulsification methods.

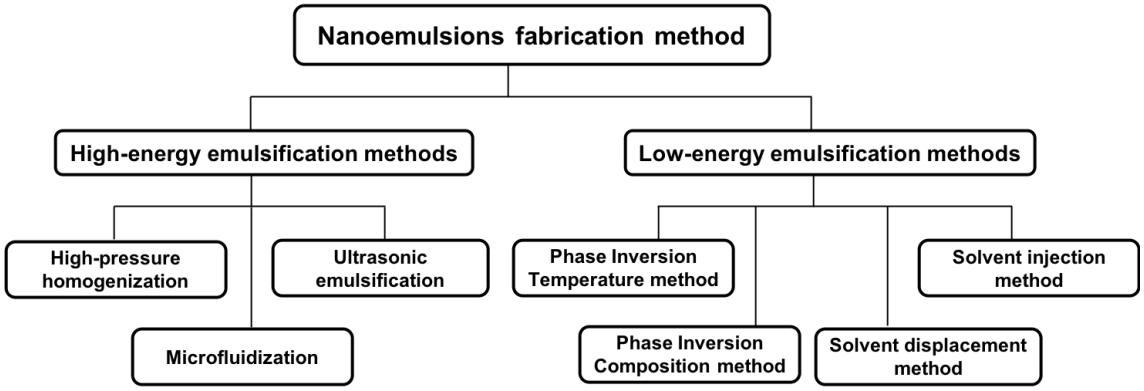

Figure 14. Nanoemulsions fabrication method

5.3.2.2 Low-energy emulsification methods

Low-energy emulsification methods are principally dependent on the modulation of interfacial phenomenon/phase transitions and intrinsic physicochemical properties of the oil, surfactants, and co-surfactants, to yield nanoemulsions.

The Phase Inversion Temperature (PIT) method employs the temperature-dependent solubility of nonionic surfactants to modify their affinities for water and oil[159]. For instance, the polyoxyethylene surfactants become lipophilic with rising temperature because of dehydration of the poly-oxyethylene chains. At low temperature, the surfactant monolayer has a large positive spontaneous curvature, thus forming emulsions of o/w type. When the temperature rises, the surfactant gets completely solubilized in the oily phase. The curvature becomes negative and initiates a phase inversion to w/o microemulsions. Nonetheless, this method involves heating the components, which may impact the stability of thermolabile molecules.

The Phase Inversion Composition (PIC) method, also known as the self-nanoemulsification method, can formulate nanoemulsions at room temperature without using any organic solvent or heat. Kinetically stable nanoemulsions with small droplet sizes (~50 nm) can be produced by the stepwise addition of water into a solution of surfactant in oil, with gentle stirring and at constant temperature[160]. Nanoemulsions obtained from the spontaneous nanoemulsification process can have high kinetic energy and long-term colloidal stability[161].

The solvent displacement method is an approach where the oily phase is dissolved in water-miscible organic solvents, such as acetone, ethanol and methyl ethyl ketone[162,163]. The organic phase is poured into an aqueous phase containing surfactant to produce spontaneous nanoemulsions owing to the rapid diffusion of organic solvent. The organic solvent can be removed from the nanoemulsions by a suitable means, such as vacuum evaporation. Spontaneous nanoemulsification can occur when a solution of organic solvents consisting of a small percentage of oil is poured into aqueous phase without any surfactant. Although this strategy can yield nanoemulsions at room temperature with simple stirring, the use of organic solvents such as acetone requires a removal process[164] that may hamper scale-up.

The solvent injection method is similar in principle to the solvent displacement method. Lipids are dissolved in a water miscible solvent. This system is then injected in an aqueous phase containing surfactants, which is carried out under continuous stirring. At the site of injection, nanoemulsions are formed by solvent diffusion. Typically, particle sizes prepared from the method range between 100–250 nm. Their sizes can be varied depending on the rate at which the organic solvent diffuses through the lipid-solvent barrier[165]. Lipid nanoformulations prepared by the ethanol injection method have been reported[166-168].

5.3.3 Sphingomyelin nanoemulsions

In most of mammalian cells, sphingomyelin (SM) is preferentially concentrated in the outer leaflet of the plasma membrane. It contains a long chain sphingoid base backbone (predominantly sphingosine), a fatty acid, and a phosphocholine head group. Hydrolysis of the phosphodiester bond by a sphingomyelinase yields ceramide and phosphocholine[169]. Various studies have proposed that the ability of ceramide to self-associate and mediate lipid raft reorganization is required for receptor capping and other signaling events leading to apoptosis[170,171]. The sphingomyelin metabolic pathway may play an essential role in cell growth, survival, and death. The number of aberrant crypts was significantly lower in 1,2-dimethylhydrazine-treated mice fed with sphingomyelin relative to controls reported by Dellehay and his groups[172]. These results demonstrate that consumption of sphingomyelin can affect the behavior of colon cells. Another study supported that SM cycle may play a role in growth inhibition of HT-29 cells[173].

SM has an inverted-cone shape due to its large headgroup and preferentially forms bilayers[174,175]. Liposomal nanoparticles (LN) from SM derivatives substantially improved drug retention properties both *in vitro* and *in vivo*[176]. Formulations based on SM have been prepared as lipid vesicles for delivery of anticancer drugs such as irinotecan, paclitaxel, and vinorelbine[177-179]. Antitumor effects of liposomal honokiol combined with cisplatin in colon cancer models were reported by Cheng and colleagues[180]. This finding indicated that the combination treatment revealed synergistic suppression in tumor progression in CT26 cells. Moreover, some of lipid-based formulations in clinic, as Marqibo®, are based on cholesterol and egg sphingomyelin (45:55 molar ratio)[181,182].

Considering these properties, SM could be an interesting candidate for the preparation of nanoemulsions since this lipid is essential for formation of specific lipid domains, such as lipid rafts in artificial lipid membranes or biological membranes[183]. Moreover, several SM-based formulations have supported its potential use as a drug carrier. SM nanoemulsions could serve as a suitable lipid structures in drug delivery systems.

6. Nanoemulsions for gene therapy applications.

Normally, oligonucleotides have a half-life of a couple of minutes in the bloodstream. In addition to their instability, their hydrophilic property with negative charge and high molecular weight hinders them from reaching tumor sites[184,185]. These problems can be overcomed by using non-viral vectors. Ideally, nanocarriers should be able to condense anionic oligonucleotides via charge interactions. In general, they have to reach tumor cells and escape endosomal degradation. The intracelullar targets depend on each type of molecule (**Figure 15)** [24,186].

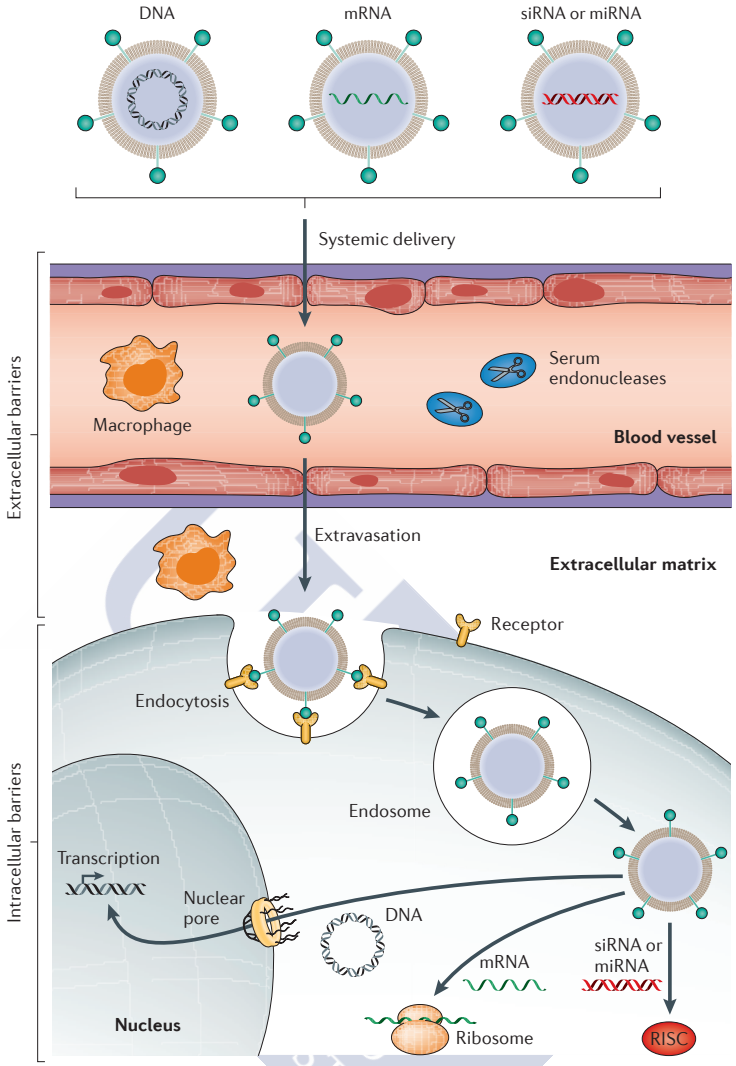

Figure 15. Diagram for nanoparticle-based gene delivery from IV administration to their own destinations. [Reproduced from Yin, H., et al. (2014). Nature reviews. Genetics[24] with permission]

Nanoparticles developed for gene delivery applications include both inorganic nanomaterials (gold/silver and calcium phosphate particles)[189,190] and organic nanocarriers (lipid-based, polymer-based, dendrimer).

6.1 Organic nanoparticles

In the past decade, lipid-based and polymer-based nanoparticles have been intensively developed for gene delivery. They have showed promising results in clinical studies[191].

6.1.1 Polymeric nanoparticles

Normally, cationic polymers used in gene delivery are classified into natural polymers and synthetic forms. Natural polymers are proteins, peptides and polysaccharides, whereas synthetic polymers comprise poly(l-lysine) (PLL), polyethylenimines (PEIs), polyphosphoesters, and dendrimers, among others. The amine groups in cationic polymers interact with the phosphate groups in the nucleic acids[192-197]. The ratio between the amine groups (N) in the polymer and phosphate (P) group in the nucleotide (N/P ratio) is calculated to determine the complexation such as size and morphology of the polyplexes[198].

PEGylated chitosan nanoparticles encapsulated anti-β-catenin siRNA could successfully enter colon cancer cells and decrease the level of a protein that promotes tumor progression[193]. Polyethyleneimine (PEI) are cationic synthetic polymers with protonatable amine groups, rendering a proton sponge effect[195]. PEG–PEI–cholesterol lipopolymer is under clinical investigation for immunotherapy of ovarian and colorectal cancers through forced expression of the cytokine interleukin-12 (IL-12)[196]. Similar to PEI, dendrimers can act as a proton sponge, thereby enabling endosomal escape into the cytoplasm. The development of combined EGFR and c-Src antisense oligodeoxynucleotides encapsulated with poly-amidoamine (PAMAM) dendrimers inhibited cell proliferation in HT-29 colon cancer[197].

6.1.2 Lipid-based nanoparticles

Lipid-based vectors are widely used as non-viral gene carriers. Cationic lipids consist of a cationic head group and a hydrophobic moiety attached by a linker. The positively charged head group interacts with nucleic acid at the phosphate groups. Monovalent lipids contain a single functional amine in their head group such as 1,2-dioleoyl-3-trimethylammonium-propane (DOTAP) and 1,2-di- O-octadecenyl-3-trimethylammonium propane (DOTMA). On the other

hand, multivalent aliphatic lipids have more than one amine group at the surface; for instance, di-ioctadecyl-amido-glycyl-spermine (DOGS). The lipoplexes synthesized from these lipids have high cationic surface charge and stability[199,200]. Neutral lipids, such as the fusogenic phospholipid DOPE or the membrane component cholesterol, have been incorporated in lipid-based formulations as 'helper lipids' to enhance transfection activity and nanoparticles stability[201,202]. Pitfalls of cationic lipids are poor stability, rapid clearance, inflammatory effects[203,204]. Besides, several lipid-based nanoparticles continue to be developed clinically, including DOTAP–cholesterol, GAP-DMORIE–DPyPE and GL67A–DOPE–DMPE–polyethylene glycol (PEG)[24]. Cationic liposomes (DOTAP:cholesterol) for a treatment of non-small-cell lung cancer (NSCLC) or small-cell lung cancer (SCLC) have completed phase I trials (DOTAP:Chol-fus1, NCT00059605). Currently, DOTAP: Chol-fus1 and erlotinib hydrochloride to control NSCLC, are undergoing phase I/II clinical trials[205].

Commercial available transfection agents from Invitrogen are composed of cationic lipids. Lipofectin™ is a 1:1 (w/w) mixture of DOTMA and di-oleoyl-phosphatidylethanolamine (DOPE). LipofectAMINE™ is a 3:1 (w/w) mixture of the polycationic lipid (2,3-Dioleyloxy-N-[2(sperminecarboxamido)ethyl]-N,N-dimethyl-l- propanaminium trifluoroacetate) (DOSPA), and DOPE. Both of them are normally used as transfection reagents for research[206,207]. **Figure 16** demonstrated common-used materials in lipid-based gene carriers.

Gene therapy has been defined as an interesting application for cationic nanoemulsions owing to the capability to complex with nucleic acids[208,209]. The cationic property of the lipid nanoemulsions is imposed by the cationic lipids. Common cationic lipids contain cholesteryl carboxyamidoethylenedimethylamine (DC-Chol), stearylamine, DOTAP, and DOTMA. Cationic emulsions were shown to successfully improve electrostatic-induced stability and enhance *in vivo* absorption, probably due to increased interactions with biological membranes. Recently, cationic nanoemulsions, composed of oil, surfactants, and cationic lipids, have been investigated as lipid carriers for gene delivery and DNA vaccines *in vivo*[210-212]. For example, (i) cationic nanoemulsions contained medium-chain triglycerides, sorbitan monooleate, and stearylamine and (ii) cationic nanoemulsions composed of medium chain triglycerides, DOTAP, DOPE, and DSPE-PEG have been studied for pDNA delivery[213,214].

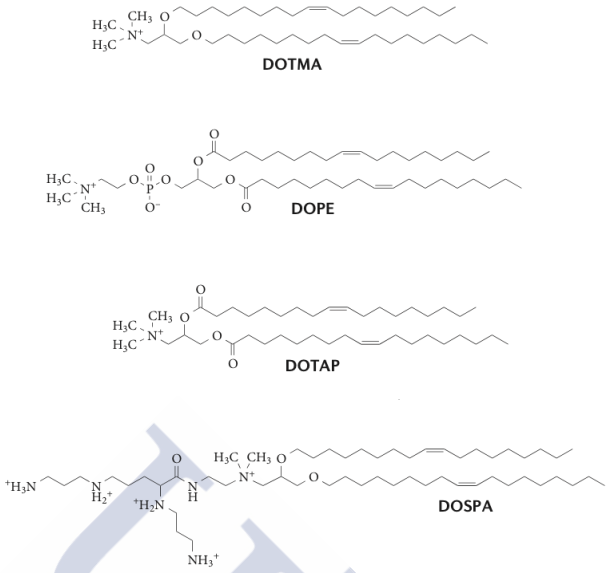

Figure 16. Common-used materials in lipid-based gene carriers. Abbreviation: DOTMA (1,2-di- O-octadecenyl-3-trimethylammonium propane), DOPE (di-oleoyl-phosphatidylethanolamine), DOTAP (1,2-dioleoyl-3-trimethylammonium-propane), and DOSPA (2,3-Dioleyloxy-N-[2(sperminecarboxamido)ethyl]-N,N-dimethyl-I-propanaminium trifluoroacetate).

6.2 miRNA-based nanoparticles

As stated in **Section 3**, the delivery of onco-suppressor miRNAs is a promising strategy for the development of innovative anticancer therapies. Systemic delivery of miR-34a mimics to orthotopic lung tumors was achieved with neutral lipid emulsion and showed inhibition of tumors in mice[215]. Indeed, MRX34, a miRNA-34a mimic (tumor suppressor and a component in the p53 signaling pathway), is currently in a phase I clinical trial (NCT01829971) of patients with primary liver cancer or liver metastases[216,217]. The formulation investigated in the trial is based on an ionizable liposome contained amphoteric lipids with a diameter of ~120 nm. However, the detailed structure of this liposome has not been revealed yet. Other interesting miRNA, miR-145, has also been proposed as a potential anticancer therapy, since loss of miR-145 function in several cancers lessened apoptosis and promoted proliferation. Successful examples of miRNA145-based nanoparticles are compiled in **Table 5**.

Table 5. miRNA145-based nanoparticles[218-225].

Delivery system	miRNA	Cancer type	Route	Ref.
Nanocomplexes (PLGA/PEI/miR-145/HA)	miR-145	Colon	Intratumoural	218
Polyarginine-modified PEI polyplexes	miR-145	Prostate	Intravenous	219
Polyurethane-short branch PEI polyplexes	miR-145	Lung	Intratumoural	220
Polymer-based systems PEI polyplexes	miR-145/33	Colon	Intravenous and Intratumoural	221
Pegylated-lipid nanoparticles (DOTAP:cholesterol:DSPE-PEG-OMe)	miR-143/145	Pancreas	Intravenous	222
Biodegradable Poly(caprolactone) Nanofibers	miR-145	Liver	*In vitro*	223
Chitosan nanocomplexes	miR-145	Breast	*in vitro*	224
Magnetic nanoparticles	miR-145	Pancreas	*In vitro*	225

7. Nanoparticles for nuclear imaging

Nanoparticle-based contrast agents are becoming valuable and potentially transformative tools for medical diagnostics in a wide range of *in vivo* imaging modalities. In comparison to conventional molecular-scale contrast agents, nanoparticles improve detection abilities and targeting efficiencies through longer engineered circulation times, designed clearance pathways, and multimeric binding capacities[226].

From a clinical perspective, nuclear imaging is feasible from cell culture to small animals in clinical systems, due to its tremendous sensitivity. Several attempts have been reported referring to the incorporation of radionuclides into nanoparticles[227,228]. Nanoparticles with surface-modified radioligands have also gained much attention[229]. The most common way to achieve radiolabelled nanoparticles is to attach a radioactive-metal via a metal chelator, such as 1,4,7-triazacyclononane-1,4,7- triacetic acid (NOTA), 1,4,7,10-tetraazacyclododecane-1,4,7,10- tetraacetic acid (DOTA), p-isothiocyanatobenzyl-desferrioxamine (Df- Bz-NCS), diethylene triamine pentaacetic acid (DTPA)[230-232].

Currently, there are several SPECT-based nanocarriers developed for cancer diagnosis. For example, Zhang and coworkers developed an ^{111}In-labelled nanoplatform, which allowed visualization of cancer cells overexpressing EphB4, a member of the largest family of receptor tyrosine kinases, in prostate cancer xenografts[233]. Deng *et al.* reported ^{125}I-radiolabelled cRGD-

USPIO (iron oxide nanoparticles) that had a long circulation half-life and high tumor uptake for breast cancer[234]. Other example refers to ^{99m}Tc-conjugated manganese-based mesoporous silica nanoparticles that could show tumor information in a breast tumor model as described by Gao and colleagues[235].

For PET, common isotopes that can be chelated on to, or incorporated within nanoparticles include ^{18}F, ^{11}C, ^{15}O, ^{13}N, ^{64}Cu, ^{124}I, ^{68}Ga, ^{82}Rb, and ^{86}Y. ^{18}F-labelling strategies are of high interest, due to its ideal imaging characteristics and good availability.^{18}F has become a well-known clinical instrument to monitor and quantify changes in receptor and enzyme levels *in vivo*. However, due to the short half-life of ^{18}F, fast conjugation with a high reaction yield between ^{18}F and its probe are required to improve the efficiency of the nuclide and to decrease cost. Unfortunately, most of the ^{18}F-labelled protocols suffer from harsh coupling conditions, such as high temperature and organic solvents, long reaction times, multistep procedures, complicated separation and purification methods, and poor overall yields[236]. Consequently, an efficient conjugation method of ^{18}F is urgently needed.

Radiolabelling with ^{18}F has been recently achieved via direct labelling by electrophilic, as well as nucleophilic, substitution by nucleophilic attack of activated ^{18}F. Nevertheless, direct radiolabelling frequently requires sophisticated and costly equipment with particularly suitable for metal oxide nanoparticles[237]. Therefore, the indirect labelling approach has to be considered by using prosthetic groups that are able to react with the target molecule. Numerous efforts have also been investigated on the mechanisms of the organic reactions for ^{18}F labelling. However, due to its complexity, the success rate is variable. Undoubtedly, the short half-life of ^{18}F has limited the number of labelling reports. ^{18}F-labelled nanoparticles have demonstrated their potential from biodistribution studies[238]. From a recent review, three main labelling strategies for ^{18}F can be described, (i) direct radiation method, (ii) ion exchange method (lanthanide-doped upconversion nanoparticles), and (iii) indirect labelling method (via a prosthetic group) (**Table 6**).

A direct way of labelling Al_2O_3 nanoparticles (Al_2O_3-NPs) with ^{18}F was developed by Pérez-Campaña and his groups[239]. Al_2O_3-NPs were directly activated in a cyclotron via the nuclear reaction ^{18}O (p,n)^{18}F. PET scans were performed and showed a renal excretion pathway. The long

retention of radioactivity in the heart implied a long blood circulation half-life. Insignificant uptake in bones suggested the slow leak of ^{18}F from the nanoparticles.

Another method was presented by Liu and his colleagues[240]. They used $NaYF_4$ to develop ^{18}F -labelled rare earth nanoparticles. The particles were surface-modified with Gd^{3+} by cation exchange with Y^{3+} for MRI and different rare earth elements (Yb, Er) for luminescence studies. ^{18}F was incorporated into the nanoparticles through interactions with the rare earth ions in an aqueous solution. *In vivo* studies showed a high uptake almost exclusively in the liver (80.9% ID/g) and spleen (36.6% ID/g) after 10 min. However, bone uptake of ~13% ID/g revealed the loss of ^{18}F from *the* nanoparticles.

The study by Guerrero and his groups exhibited ^{18}F-labelled gold nanoparticles using a prosthetic group named N-Succinimidyl-4-[^{18}F]fluorobenzoate ([^{18}F]SFB)[243]. It was observed that a considerable level of nanoparticles was trapped by the reticuloendothelial system (RES) in the spleen. The rapid renal clearance resulted in a rapid blood concentration drop during the first minutes after injection. Furthermore, [^{18}F]SFB conjugated with Ceria nanoparticles was reported[254]. The surface of the ceria nanoparticles was modified with silylation with 3-(aminopropyl)triethoxysilane enabling subsequent coupling to [^{18}F]SFB. High uptake values in liver, spleen and lungs were immediately observed after administration. Ducongé and his colleagues designed F-labelling of core/shell quantum dots (QDs)[245]. The QDs were encapsulated with polyethylene glycol (PEG-phospholipid micelles) and this coating was further functionalized with thiol groups. A coupling of these functionalities and a maleimido-based prosthetic group (1-[3(2-[^{18}F]fluoropyridin-3-xyloxy)propyl]pyrrole-2,5-dione ([^{18}F]FPyME)) was performed. Biodistribution indicated a long blood circulation time with a plasma half-life of 2 hours. In comparison to non-PEG-coated QDs, the uptake in liver and spleen could notably be reduced.

Table 6. An overview of ^{18}F-labelled nanoparticles and their important characteristics[237,239-246]

Labelling method	Nanostructure/system	Material	Size [nm]	Specific activity	Reaction time [min]	RCY [%]	Ref.
Direct radiation method	Al_2O_3 Nanoparticles	Al_2O_3 (alumina)	10/40/150/ 10000	1.85 MBq/mg	6 (only irradiation)	n.d	[237]
	Al_2O_3 Nanoparticles	Al_2O_3 (alumina)	n.d	2.3 ±0.2 MBq/mg	6 (only irradiation)	n.d	[239]
Ion exchange method (lanthanide-doped upconversion nanoparticles)	Nanophosphors	$NaYF_4$ (co-doped with Yb, Er, Tm, Gd)	10-20	n.d.	10 (only labeling)	92	[240]
	Nanophosphors	$NaYF_4$ (co-doped with Yb, Er, Gd)	28.2	n.d	10 (only labeling)	99	[241]
	Nanophosphors	$NaYF_4$ (co-doped with Yb, Er,TM, Gd)	20	n.d	5 (only labeling)	90	[242]
Indirect method	Nanoparticles/peptide	Gold/CLPFFD (peptide)	23 (h.r.)	27 atoms ^{18}F per NP*	60 (only labeling)	0.3-0.8	[243]
	Amino functionalized nanoparticles	CeO_2 (ceria)	5	n.d	n.d	17.7 ±0.3	[244]
	Phospholipid coated core/shell quantum dot	CdSe/CdZnS DSPE- PEG2000-NH_2	≥20	37-75 MBq/nmol	145	n.d	[245]
	Diamond nanoparticles	Diamond/peptide	340.6	n.d.	n.d	21.3 ±0.4	[246]

(n.d. = no data, RCY = radiochemical yield, h.r. = hydrodynamic radii, DSPE-PEG2000-NH_2 = 1,2-distearoyl-sn-glycero-3- phosphoethanolamine-N-[amino(polyethylene glycol)-2000], Cd = cadmium, Se = selenium, Zn = zinc, S = sulfur, Na = sodium, Y = yttrium, F = fluorine, Yb = ytterbium, Er = erbium, Tm = terbium, Gd = gadolinium, Ce = cerium, O = oxygen, Al = aluminium, Si = silicium), *Calculated from the radioactivity-to-mass-ratio.

References

(1) Siegel, R. L.; Miller, K. D.; Jemal, A. Colorectal Cancer Statistics, 2018. *CA Cancer J Clin* **2018**, *68*, 7–30.

(2) Bray, F.; Ferlay, J.; Soerjomataram, I.; Siegel, R. L.; Torre, L. A.; Jemal, A. Global Cancer Statistics 2018: GLOBOCAN Estimates of Incidence and Mortality Worldwide for 36 Cancers in 185 Countries. *CA Cancer J Clin* **2018**, *0*, 1–31.

(3) Takayama, T.; Miyanishi, K.; Hayashi, T.;Sato, Y.; Niitsu Y.Colorectal cancer: genetics of development and metastasis. *J Gastroenterol.* **2006**, *41*,185–192

(4) Church, J. Molecular Genetics of Colorectal Cancer. *Semin. Colon Rectal Surg.* **2016**, *27*, 172–175.

(5) Bhaw-Luximon, A.; Goonoo, N.; Jhurry, D. Nanotherapeutics Promises for Colorectal Cancer and Pancreatic Ductal Adenocarcinoma. *Nanobiomaterials in Cancer Therapy*. **2016**, *7*. 147-201.

(6) Banerjee, A.; Pathak, S.; Subramanium, V. D.; Dharanivasan, G.; Murugesan, R.; Verma, R. S. Strategies for Targeted Drug Delivery in Treatment of Colon Cancer: Current Trends and Future Perspectives. *Drug Discov. Today* **2017**, *22*, 1224–1232.

(7) Rex, D. K.; Johnson, D. A.; Anderson, J. C.; Schoenfeld, P. S.; Burke, C. A.; Inadomi, J. M. American College of Gastroenterology Guidelines for Colorectal Cancer Screening 2008. *Am. J. Gastroenterol.* **2009**, *104*, 739–750.

(8) Vogel, J. D.; Eskicioglu, C.; Weiser, M. R.; Feingold, D. L.; Steele, S. R. The American Society of Colon and Rectal Surgeons Clinical Practice Guidelines for the Treatment of Colon Cancer. *Dis. Colon Rectum* **2017**, *60*, 999–1017.

(9) Iqbal, A.; Gorge, T. J.; Randomized Clinical Trials in Colon and Rectal Cancer. *Surg. Oncol. Clin. N. Am.* **2017**, *17*.

(10) Salem, J. F.; Gummadi, S.; Marks, J. H. Minimally Invasive Surgical Approaches to Colon Cancer. *Surg. Oncol. Clin. N. Am.* **2018**, *27*, 303–318.

(11) Pearce, A.; Haas, M.; Viney, R.; Pearson, S.-A.; Haywood, P.; Brown, C.; Ward, R. Incidence and Severity of Self-Reported Chemotherapy Side Effects in Routine Care: A Prospective Cohort Study. *PLoS One* **2017**, *12*. 1-12

(12) Lorusso, D.; Bria, E.; Costantini, A.; Di Maio, M.; Rosti, G.; Mancuso, A. Patients' Perception of Chemotherapy Side Effects: Expectations, Doctor–patient Communication and Impact on Quality of Life – An Italian Survey. *Eur. J. Cancer Care (Engl).* **2017**, *26*, 1–9.

(13) Varghese, A. Chemotherapy for Stage II Colon Cancer. *Clin. Colon Rectal Surg.* **2015**, *28*, 256–261.

(14) Kim, J. H. Chemotherapy for Colorectal Cancer in the Elderly. *World J. Gastroenterol.* **2015**, *21*, 5158–5166.

(15) Aran, V.; Victorino, A. P.; Thuler, L. C.; Ferreira, C. G. Colorectal Cancer: Epidemiology, Disease Mechanisms and Interventions to Reduce Onset and Mortality. *Clin. Colorectal Cancer* **2016**, *15*, 195–203.

(16) Dienstmann, R.; Salazar, R.; Tabernero, J. Personalizing Colon Cancer Adjuvant Therapy: Selecting Optimal Treatments for Individual Patients. *J. Clin. Oncol.* **2015**, *33*, 1787–1796.

(17) Thi, E. P.; Mire, C. E.; Lee, A. C. H.; Geisbert, J. B.; Zhou, J. Z.; Agans, K. N.; Snead, N. M.; Deer, D. J.; Barnard, T. R.; Fenton, K. A.; *et al.* Lipid Nanoparticle siRNA Treatment of Ebola-Virus-Makona-Infected Nonhuman Primates. *Nature* **2015**, *521*, 362–365.

(18) Zuckerman, J. E.; Davis, M. E. Clinical Experiences with Systemically Administered siRNA-Based Therapeutics in Cancer. *Nat. Rev. Drug Discov.* **2015**, *14*, 843–856.

(19) Liu, Y.; Xu, C. F.; Iqbal, S.; Yang, X. Z.; Wang, J. Responsive Nanocarriers as an Emerging Platform for Cascaded Delivery of Nucleic Acids to Cancer. *Adv. Drug Deliv. Rev.* **2017**, *115*, 98–114.

(20) Kerr, D. Clinical Development of Gene Therapy for Colorectal Cancer. *Nat. Rev. Cancer* **2003**, *3*, 615–622.

(21) Van Etten, B.; Ten Hagen, T. L. M.; De Vries, M. R.; Ambagtsheer, G.; Huet, T.; Eggermont, A. M. M. Prerequisites for Effective Adenovirus Mediated Gene Therapy of Colorectal Liver Metastases in the Rat Using an Intracellular Neutralizing Antibody Fragment to P21-Ras. *Br. J. Cancer* **2002**, *86*, 436–442.

(22) Opalka, B.; Dickopp, A.; Kirch, H. C. Apoptotic Genes in Cancer Therapy. *Cells Tissues Organs* **2002**, *172*, 126–132.

(23) Liang, X.; Luo, M.; Wei, X.-W.; Ma, C.-C.; Yang, Y.-H.; Shao, B.; Liu, Y.-T.; Liu, T.; Ren, J.; Liu, L.; *et al.* A Folate Receptor-Targeted Lipoplex Delivering Interleukin-15 Gene for Colon Cancer Immunotherapy. *Oncotarget* **2016**, *7*, 52207–52217.

(24) Yin, H.; Kanasty, R. L.; Eltoukhy, A. A.; Vegas, A. J.; Dorkin, J. R.; Anderson, D. G. Non-Viral Vectors for Gene-Based Therapy. *Nat. Rev. Genet.* **2014**, *15*, 541–555.

(25) Sahin, U.; Karikó, K.; Türeci, Ö. MRNA-Based Therapeutics-Developing a New Class of Drugs. *Nat. Rev. Drug Discov.* **2014**, *13*, 759–780.

(26) Morse, M. A.; Nair, S. K.; Mosca, P. J.; Hobeika, A. C.; Clay, T. M.; Deng, Y.; Boczkowski, D.; Proia, A.; Neidzwiecki, D.; Clavien, P. A.; *et al.* Immunotherapy with Autologous, Human Dendritic Cells Transfected with Carcinoembryonic Antigen MRNA. *Cancer Invest.* **2003**, *21*, 341–349.

(27) Stein, C. A. The Experimental Use of Antisense Oligonucleotides: A Guide for the Perplexed. *J. Clin. Invest.* **2001**, *108*, 641–644.

(28) Ridge, O.; Que, L.; Que, L. Letters To Nature. **1998**, *396*, 563–567.

(29) Chen, Y.; Gao, D. Y.; Huang, L. In Vivo Delivery of miRNAs for Cancer Therapy: Challenges and Strategies. *Adv. Drug Deliv. Rev.* **2015**, *81*, 128–141.

(30) Bartel, D. P.; Lee, R.; Feinbaum, R. MicroRNAs : Genomics , Biogenesis , Mechanism , and Function Genomics : The miRNA Genes. **2004**, *116*, 281–297.

(31) Lee, Y.; Ahn, C.; Han, J.; Choi, H.; Kim, J.; Yim, J.; Lee, J.; Provost, P.; Radmark, O.; Kim, S.; *et al.* The Nuclear RNAse III Drosha Initates microRNA Processing. *Nature* **2003**, *425*, 415–419.

(32) Lim, L. P.; Lau, N. C.; Garrett-Engele, P.; Grimson, A.; Schelter, J. M.; Castle, J.; Bartel, D. P.; Linsley, P. S.; Johnson, J. M. Microarray Analysis Shows That Some microRNAs Downregulate Large Numbers of Target mRNAs. *Nature* **2005**, *433*, 769–773.

(33) Lam, J. K. W.; Chow, M. Y. T.; Zhang, Y.; Leung, S. W. S. siRNA versus miRNA as Therapeutics for Gene Silencing. *Mol. Ther. - Nucleic Acids* **2015**, *4*, 1–20.

(34) Wang, H.; Jiang, Y.; Peng, H.; Chen, Y.; Zhu, P.; Huang, Y. Recent Progress in microRNA Delivery for Cancer Therapy by Non-Viral Synthetic Vectors. *Adv. Drug Deliv. Rev.* **2015**, *81*, 142–160.

(35) Osaki, M.; Takeshita, F.; Sugimoto, Y.; Kosaka, N.; Yamamoto, Y.; Yoshioka, Y.; Kobayashi, E.; Yamada, T.; Kawai, A.; Inoue, T.; *et al.* MicroRNA-143 Regulates Human Osteosarcoma Metastasis by Regulating Matrix Metalloprotease-13 Expression. *Mol. Ther.* **2011**, *19*, 1123–1130.

(36) Henry, J. C.; Azevedo-Pouly, A. C. P.; Schmittgen, T. D. MicroRNA Replacement Therapy for Cancer. *Pharm. Res.* **2011**, *28*, 3030–3042.

(37) Bader, A. G.; Brown, D.; Stoudemire, J.; Lammers, P. Developing Therapeutic microRNAs for Cancer. *Gene Ther.* **2011**, *18*, 1121–1126.

(38) Bader, A. G.; Brown, D.; Winkler, M. The Promise of microRNA Replacement Therapy. *Cancer Res.* **2010**, *70*, 7027–7030.

(39) Chen, M. L.; Liang, L. Sen; Wang, X. K. MiR-200c Inhibits Invasion and Migration in Human Colon Cancer Cells SW480/620 by Targeting ZEB1. *Clin. Exp. Metastasis* **2012**, *29*, 457–469.

(40) Qin, Y.; Cheng, C.; Lu, H.; Wang, Y. MiR-4458 Suppresses Glycolysis and Lactate Production by Directly Targeting Hexokinase2 in Colon Cancer Cells. *Biochem. Biophys. Res. Commun.* **2016**, *469*, 37–43.

(41) Feng, Y.; Zhu, J.; Ou, C.; Deng, Z.; Chen, M.; Huang, W.; Li, L. MicroRNA-145 Inhibits Tumour Growth and Metastasis in Colorectal Cancer by Targeting Fascin-1. *Br. J. Cancer* **2014**, *110*, 2300–2309.

(42) Van Rooij, E.; Kauppinen, S. Development of microRNA Therapeutics Is Coming of Age. *EMBO Mol. Med.* **2014**, *6*, 851–864.

(43) Ding, H.; Wu, F. Image Guided Biodistribution and Pharmacokinetic Studies of Theranostics. *Theranostics* **2012**, *2*, 1040–1053.

(44) De Jong, M.; Essers, J.; Van Weerden, W. M. Imaging Preclinical Tumour Models: Improving Translational Power. *Nat. Rev. Cancer* **2014**, *14*, 481–493.

(45) Janib, S. M.; Moses, A. S.; MacKay, J. A. Imaging and Drug Delivery Using Theranostic Nanoparticles. *Adv. Drug Deliv. Rev.* **2010**, *62*, 1052–1063.

(46) Smith, B. R.; Gambhir, S. S. Nanomaterials for in Vivo Imaging. *Chem. Rev.* **2017**, *117*, 901–986.

(47) Cheng, Z.; Yan, X.; Sun, X.; Shen, B.; Gambhir, S. S. Tumor Molecular Imaging with Nanoparticles. *Engineering* **2016**, *2*, 132–140.

(48) Denecke, T.; Rau, B.; Hoffmann, K. T.; Hildebrandt, B.; Ruf, J.; Gutberlet, M.; Hünerbein, M.; Felix, R.; Wust, P.; Amthauer, H. Comparison of CT, MRI and FDG-PET in Response Prediction of Patients with Locally Advanced Rectal Cancer after Multimodal Preoperative Therapy: Is There a Benefit in Using Functional Imaging? *Eur. Radiol.* **2005**, *15*, 1658–1666.

(49) Glunde, K.; Pathak, A. P.; Bhujwalla, Z. M. Molecular-Functional Imaging of Cancer: To Image and Imagine. *Trends Mol. Med.* **2007**, *13*, 287–297.

(50) Torigian, D. A.; Huang, S. S.; Houseni, M.; Alavi, A. Functional Imaging of Cancer with Emphasis on Molecular Techniques. *CA. Cancer J. Clin.* **2007**, *57*, 206–224.

(51) Brendle, C.; Schwenzer, N. F.; Rempp, H.; Schmidt, H.; Pfannenberg, C.; la Fougère, C.; Nikolaou, K.; Schraml, C. Assessment of Metastatic Colorectal Cancer with Hybrid Imaging: Comparison of Reading Performance Using Different Combinations of Anatomical and Functional Imaging Techniques in PET/MRI and PET/CT in a Short Case Series. *Eur. J. Nucl. Med. Mol. Imaging* **2016**, *43*, 123–132.

(52) Sun, H.; Xin, J.; Zhang, S.; Guo, Q.; Lu, Y.; Zhai, W.; Zhao, L.; Peng, W.; Wang, B. Anatomical and Functional Volume Concordance between FDG PET, and T2 and Diffusion-Weighted MRI for Cervical Cancer: A Hybrid PET/MR Study. *Eur. J. Nucl. Med. Mol. Imaging* **2014**, *41*, 898–905.

(53) Pfannenberg, A. C.; Eschmann, S. M.; Horger, M.; Lamberts, R.; Vonthein, R.; Claussen, C. D.; Bares, R. Benefit of Anatomical-Functional Image Fusion in the Diagnostic Work-up of Neuroendocrine Neoplasms. *Eur. J. Nucl. Med. Mol. Imaging* **2003**, *30*, 835–843.

(54) Schaefer, O.; Langer, M. Detection of Recurrent Rectal Cancer with CT, MRI and PET/CT. *Eur. Radiol.* **2007**, *17*, 2044–2054.

(55) L., S.; H., W.; Y.-S., G. Colonography by CT, MRI and PET/CT Combined with Conventional Colonoscopy in Colorectal Cancer Screening and Staging. *World J. Gastroenterol.* **2008**, *14*, 853–863.

(56) Gluecker, T. M.; Johnson, C. D.; Harmsen, W. S.; Offord, K. P.; Harris, A. M.; Wilson, L. A.; Ahlquist, D. A. Colorectal Cancer Screening with CT Colonography, Colonoscopy, and Double-Contrast Barium Enema Examination: Prospective Assessment of Patient Perceptions and Preferences. *Radiology* **2003**, *227*, 378–384.

(57) Yee, J.; Akerkar, G. A.; Hung, R. K.; Steinauer-Gebauer, A. M.; Wall, S. D.; McQuaid, K. R. Colorectal Neoplasia: Performance Characteristics of CT Colonography for Detection in 300 Patients. *Radiology* **2001**, *219*, 685–692.

(58) Hara, a K.; Johnson, C. D.; MacCarty, R. L.; Welch, T. J.; McCollough, C. H.; Harmsen, W. S. CT Colonography: Single- versus Multi-Detector Row Imaging. *Radiology* **2001**, *219*, 461–465.

(59) Ferrucci, J. T. Eugene W . Caldwell Lecture Colon Cancer Screening with Virtual Colonoscopy : *Am. J. Roentgenol.* **2001**, *177*, 975–988.

(60) Kijima, S.; Sasaki, T.; Nagata, K.; Utano, K.; Lefor, A. T.; Sugimot, H. Preoperative Evaluation of Colorectal Cancer Using CT Colonography, MRI, and PET/CT. *World J. Gastroenterol.* **2014**, *20*, 16964–16975.

(61) Bipat, S.; Leeuwen, M. S. Van; Comans, E. F. I.; Bossuyt, P. M. M.; Zwinderman, A. H.; Stoker, J. Colorectal Liver Metastases : CT , MR Imaging , and PET For. *Radiology* **2005**, *237*, 123–131.

(62) Squillaci, E.; Manenti, G.; Mancino, S.; Cicciò, C.; Calabria, F.; Danieli, R.; Schillaci, O.; Simonetti, G. Staging of Colon Cancer: Whole-Body MRI vs. Whole-Body PET-CT - Initial Clinical Experience. *Abdom. Imaging* **2008**, *33*, 676–688.

(63) Bluemke, D. A.; Liu, S. Imaging in Clinical Trials. *Princ. Pract. Clin. Res.* **2012**, 597–617.

(64) Gorospe, L.; Raman, S.; Echeveste, J.; Avril, N.; Herrero, Y.; Herna´ndez, S. Whole-Body Pet/Ct: Spectrum of Physiological Variants, Artifacts and Interpretative Pitfalls in Cancer Patients. *Nucl. Med. Commun.* **2005**, *26*, 671–687.

(65) Wechalekar, K.; Sharma, B.; Cook, G. J. R. PET/CT in Oncology - A Major Advance. *Clin. Radiol.* **2005**, *60*, 1143–1155.

(66) Histed, S. N.; Lindenberg, M. L.; Mena, E.; Turkbey, B.; Choyke, P. L.; Kurdziel, K. A. Review of Functional / Anatomic Imaging in Oncology. **2013**, *33*, 349–361.

(67) Yaghoubi, S. S.; Gambhir, S. S.; John, M.; Md; Peter, M. H.; Mark, A. I.; Joe, W. G.; PhD; Craig, B. T. Imaging and Cancer. *Mol. Basis Cancer (Third Ed.* **2008**, 309–323.

(68) Li, M.; Kim, H. S.; Tian, L.; Yu, M. K.; Jon, S.; Moon, W. K. Comparison of Two Ultrasmall Superparamagnetic Iron Oxides on Cyto-Toxicity and MR Imaging of Tumors. *Theranostics* **2012**, *2*, 76–85.

(69) Ray, P.; De, A. Reporter Gene Imaging in Therapy and Diagnosis. *Theranostics* **2012**, *2*, 333–334.

(70) Savla, R.; Minko, T. Nanoparticle Design Considerations for Molecular Imaging of Apoptosis: Diagnostic, Prognostic, and Therapeutic Value. *Adv. Drug Deliv. Rev.* **2017**, *113*, 122–140.

(71) Kim, T. H.; Lee, S.; Chen, X. Nanotheranostics for Personalized Medicine. *Expert Rev. Mol. Diagn.* **2013**, *13*, 257–269.

(72) Bennett, K. M.; Jo, J. I.; Cabral, H.; Bakalova, R.; Aoki, I. MR Imaging Techniques for Nano-Pathophysiology and Theranostics. *Adv. Drug Deliv. Rev.* **2014**, *74*, 75–94.

(73) Thakor, A. S.; Jokerst, J. V.; Ghanouni, P.; Campbell, J. L.; Mittra, E.; Gambhir, S. S. Clinically Approved Nanoparticle Imaging Agents. *J. Nucl. Med.* **2016**, *57*, 1833–1837.

(74) Beer, A. J.; Schwaiger, M. Imaging of Integrin αvβ3 Expression. *Cancer Metastasis Rev.* **2008**, *27*, 631–644.

(75) Voss, S. D.; Smith, S. V; DiBartolo, N.; McIntosh, L. J.; Cyr, E. M.; Bonab, A. A.; Dearling, J. L.; Carter, E. A.; Fischman, A. J.; Treves, S. T.; *et al.* Positron Emission Tomography (PET) Imaging of Neuroblastoma and Melanoma with 64Cu-SarAr Immunoconjugates. *Proc Natl Acad Sci U S A* **2007**, *104*, 17489–17493.

(76) Pimlott, S. L.; Sutherland, A. Molecular Tracers for the PET and SPECT Imaging of Disease. *Chem. Soc. Rev.* **2011**, *40*, 149–162.

(77) Massoud, T. F.; Massoud, T. F.; Gambhir, S. S.; Gambhir, S. S. Molecular Imaging in Living Subjects: Seeing Fundamental Biological Processes in a New Light. *Genes Dev.* **2003**, *17*, 545–580.

(78) Schneider, D. W.; Heitner, T.; Alicke, B.; Light, D. R.; McLean, K.; Satozawa, N.; Parry, G.; Yoo, J.; Lewis, J. S.; Parry, R. In Vivo Biodistribution, PET Imaging, and Tumor Accumulation of 86Y- and 111In-antimindin/RG-1, Engineered Antibody Fragments in LNCaP Tumor-Bearing Nude Mice. *J. Nucl. Med.* **2009**, *50*, 435–443.

(79) Lancelot, S.; Zimmer, L. Small-Animal Positron Emission Tomography as a Tool for Neuropharmacology. *Trends Pharmacol. Sci.* **2010**, *31*, 411–417.

(80) Miller, P. W.; Long, N. J.; Vilar, R.; Gee, A. D. Synthesis of11C, 18F, 15O, and 13N Radiolabels for Positron Emission Tomography. *Angew. Chemie - Int. Ed.* **2008**, *47*, 8998–9033.

(81) Sioka, C.; Fotopoulos, A.; Kyritsis, A. P. Recent Advances in PET Imaging for Evaluation of Parkinson's Disease. *Eur. J. Nucl. Med. Mol. Imaging* **2010**, *37*, 1594–1603.

(82) Lewellen, T. K. Recent Developments in PET Detector Technology. *Phys. Med. Biol.* **2008**, *53*.

(83) Reddy, S.; Robinson, M. K. Immuno-Positron Emission Tomography in Cancer Models. *Semin. Nucl. Med.* **2010**, *40*, 182–189.

(84) Jacobson, O.; Kiesewetter, D. O.; Chen, X. Fluorine-18 Radiochemistry, Labeling Strategies and Synthetic Routes. *Bioconjug. Chem.* **2015**, *26*, 1–18.

(85) Pharmacogenomics, J.; Press, N. A.; Ramaswamy, S.; Ross, K. N.; Lander, E. S.; Golub, T. R.; Ransohoff, D. F.; Ransohoff, D. F.; Hartwell, L.; Hopfield, J. J.; *et al.* Molecular Imaging in Cancer. **2006**, 1168–1172.

(86) Xing, Y.; Zhao, J.; Conti, P. S.; Chen, K. Radiolabeled Nanoparticles for Multimodality Tumor Imaging. *Theranostics* **2014**, *4*, 290–306.

(87) Khan, H. A.; Sakharkar, M. K.; Nayak, A.; Kishore, U.; Khan, A. *Nanoparticles for Biomedical Applications: An Overview*; Elsevier Ltd., 2018.

(88) Sheikhpour, M.; Barani, L.; Kasaeian, A. Biomimetics in Drug Delivery Systems: A Critical Review. *J. Control. Release* **2017**, *253*, 97–109.

(89) Grossen, P.; Witzigmann, D.; Sieber, S.; Huwyler, J. PEG-PCL-Based Nanomedicines: A Biodegradable Drug Delivery System and Its Application. *J. Control. Release* **2017**, *260*, 46–60.

(90) Richards, D. A.; Maruani, A.; Chudasama, V. Antibody Fragments as Nanoparticle Targeting Ligands: A Step in the Right Direction. *Chem. Sci.* **2016**, *8*, 63–77.

(91) von Roemeling, C.; Jiang, W.; Chan, C. K.; Weissman, I. L.; Kim, B. Y. S. Breaking Down the Barriers to Precision Cancer Nanomedicine. *Trends Biotechnol.* **2017**, *35*, 159–171.

(92) Barenholz, Y. Doxil® - The First FDA-Approved Nano-Drug: Lessons Learned. *J. Control. Release* **2012**, *160*, 117–134.

(93) Allen, T. M.; Cullis, P. R. Liposomal Drug Delivery Systems: From Concept to Clinical Applications. *Adv. Drug Deliv. Rev.* **2013**, *65*, 36–48.

(94) Hare, J. I.; Lammers, T.; Ashford, M. B.; Puri, S.; Storm, G.; Barry, S. T. Challenges and Strategies in Anti-Cancer Nanomedicine Development: An Industry Perspective. *Adv. Drug Deliv. Rev.* **2017**, *108*, 25–38.

(95) Hrkach, J.; Hoff, D. Von; Ali, M. M.; Andrianova, E.; Auer, J.; Campbell, T.; Witt, D. De; Figa, M.; Figueiredo, M.; Horhota, A.; *et al*. PreClinical Development and Clinical Translation of a PMSA-Targeted Docetaxel Nanoparticle with a Differentiated Pharmacological Profile. **2012**, *4*.

(96) Geretti, E.; Leonard, S. C.; Dumont, N.; Lee, H.; Zheng, J.; De Souza, R.; Gaddy, D. F.; Espelin, C. W.; Jaffray, D. A.; Moyo, V.; *et al.* Cyclophosphamide-Mediated Tumor Priming for Enhanced Delivery and Antitumor Activity of HER2-Targeted Liposomal Doxorubicin (MM-302). *Mol. Cancer Ther.* **2015**, *14*, 2060–2071.

(97) Bobo, D.; Robinson, K. J.; Islam, J.; Thurecht, K. J.; Corrie, S. R. Nanoparticle-Based Medicines: A Review of FDA-Approved Materials and Clinical Trials to Date. *Pharm. Res.* **2016**, *33*, 2373–2387.

(98) Miyata, K.; Christie, R. J.; Kataoka, K. Polymeric Micelles for Nano-Scale Drug Delivery. *React. Funct. Polym.* **2011**, *71*, 227–234.

(99) Soo Choi, H.; Liu, W.; Misra, P.; Tanaka, E.; Zimmer, J. P.; Itty Ipe, B.; Bawendi, M. G.; Frangioni, J. V. Renal Clearance of Quantum Dots. *Nat. Biotechnol.* **2007**, *25*, 1165–1170.

(100) Maruyama, K. Intracellular targeting delivery of liposomal drugs to solid tumors based on EPR effects. *Advanced Drug Delivery Reviews*. **2011**,*63*, 161–169.

(101) Hatakeyama, H.; Akita, H.; Harashima, H. A Multifunctional Envelope Type Nano Device (MEND) for Gene Delivery to Tumours Based on the EPR Effect: A Strategy for Overcoming the PEG Dilemma. *Adv. Drug Deliv. Rev.* **2011**, *63*, 152–160.

(102) Wong, A. D.; Ye, M.; Ulmschneider, M. B.; Searson, P. C. Quantitative Analysis of the Enhanced Permeation and Retention (EPR) Effect. *PLoS One* **2015**, *10*, 1–13.

(103) Cabral, H.; Nishiyama, N.; Kataoka, K. Supramolecular Nanodevices: From Design Validation to Theranostic Nanomedicine. *Acc. Chem. Res.* **2011**, *44*, 999–1008.

(104) Bertrand, N.; Wu, J.; Xu, X.; Kamaly, N.; Farokhzad, O. C. Cancer Nanotechnology: The Impact of Passive and Active Targeting in the Era of Modern Cancer Biology. *Adv. Drug Deliv. Rev.* **2014**, *66*, 2–25.

(105) Maeda, H. Toward a Full Understanding of the EPR Effect in Primary and Metastatic Tumors as Well as Issues Related to Its Heterogeneity. *Adv. Drug Deliv. Rev.* **2015**, *91*, 3–6.

(106) Tavano, L.; Muzzalupo, R. Multi-Functional Vesicles for Cancer Therapy: The Ultimate Magic Bullet. *Colloids Surfaces B Biointerfaces* **2016**, *147*, 161–171.

(107) Suk, J. S.; Xu, Q.; Kim, N.; Hanes, J.; Ensign, L. M. PEGylation as a Strategy for Improving Nanoparticle-Based Drug and Gene Delivery. *Adv. Drug Deliv. Rev.* **2016**, *99*, 28–51.

(108) Rabanel, J. M.; Hildgen, P.; Banquy, X. Assessment of PEG on Polymeric Particles Surface, a Key Step in Drug Carrier Translation. *J. Control. Release* **2014**, *185*, 71–87.

(109) Kolate, A.; Baradia, D.; Patil, S.; Vhora, I.; Kore, G.; Misra, A. PEG - A Versatile Conjugating Ligand for Drugs and Drug Delivery Systems. *J. Control. Release* **2014**, *192*, 67–81.

(110) Torchilin, V. P. P -Nitrophenylcarbonyl-PEG-PE-Liposomes : Fast and Simple Attachment of Speci ¢ c Ligands , Including Monoclonal Antibodies , to Distal Ends of PEG Chains via P -Nitrophenylcarbonyl Groups. **2001**, *1511*, 397–411.

(111) Komin, A.; Russell, L. M.; Hristova, K. A.; Searson, P. C. Peptide-Based Strategies for Enhanced Cell Uptake, Transcellular Transport, and Circulation: Mechanisms and Challenges. *Adv. Drug Deliv. Rev.* **2017**, *110–111*, 52–64.

(112) Sun, X.; Li, Y.; Liu, T.; Li, Z.; Zhang, X.; Chen, X. Peptide-Based Imaging Agents for Cancer Detection. *Adv. Drug Deliv. Rev.* **2017**, *110–111*, 38–51.

(113) Pérez-Herrero, E.; Fernández-Medarde, A. Advanced Targeted Therapies in Cancer: Drug Nanocarriers, the Future of Chemotherapy. *Eur. J. Pharm. Biopharm.* **2015**, *93*, 52–79.

(114) Giribabu, N.; Rao, P. V.; Salleh, N. *Nanoparticle and Targeted Systems for Colon Cancer Therapy*; Elsevier Inc., **2016**.

(115) Sriraman, S. K.; Pan, J.; Sarisozen, C.; Luther, E.; Torchilin, V. Enhanced Cytotoxicity of Folic Acid-Targeted Liposomes Co-Loaded with C6 Ceramide and Doxorubicin: In Vitro Evaluation on HeLa, A2780-ADR, and H69-AR Cells. *Mol. Pharm.* **2016**, *13*, 428–437.

(116) Lin, J.; Li, Y.; Wu, H.; Yang, X.; Li, Y.; Ye, S.; Hou, Z.; Lin, C. Tumor-Targeted Co-Delivery of Mitomycin C and 10-Hydroxycamptothecin via Micellar Nanocarriers for Enhanced Anticancer Efficacy. *RSC Adv.* **2015**, *5*, 23022–23033.

(117) Zafar, S.; Negi, L. M.; Verma, A. K.; Kumar, V.; Tyagi, A.; Singh, P.; Iqbal, Z.; Talegaonkar, S. Sterically stabilized polymeric nanoparticles with a combinatorial approach for multi drug resistant cancer: In vitro and in vivo investigation. *Int. J. Pharmaceutics.* **2014**, *477*, 454-468.

(118) Luo, Y.; Cai, X.; Li, H.; Lin, Y.; Du, D. Hyaluronic Acid-Modified Multifunctional Q-Graphene for Targeted Killing of Drug-Resistant Lung Cancer Cells. *ACS Appl. Mater. Interfaces* **2016**, *8*, 4048–4055.

(119) Abouzeid, A. H.; Patel, N. R.; Sarisozen, C.; Torchilin, V. P. Transferrin-Targeted Polymeric Micelles Co-Loaded with Curcumin and Paclitaxel: Efficient Killing of Paclitaxel-Resistant Cancer Cells. *Pharm. Res.* **2014**, *31*, 1938–1945.

(120) Guo, S.; Lv, L.; Shen, Y.; Hu, Z.; He, Q.; Chen, X. A Nanoparticulate Pre-Chemosensitizer for Efficacious Chemotherapy of Multidrug Resistant Breast Cancer. *Sci. Rep.* **2016**, *6*, 1–11.

(121) Chen, Y.; Zhang, W.; Huang, Y.; Gao, F.; Fang, X. Dual-Functional c(RGDyK)-Decorated Pluronic Micelles Designed for Antiangiogenesis and the Treatment of Drug-Resistant Tumor. *Int. J. Nanomedicine* **2015**, *10*, 4863–4881.

(122) Liu, Y.; Mei, L.; Yu, Q.; Xu, C.; Qiu, Y.; Yang, Y.; Shi, K.; Zhang, Q.; Gao, H.; Zhang, Z.; *et al.* Multifunctional Tandem Peptide Modified Paclitaxel-Loaded Liposomes for the Treatment of Vasculogenic Mimicry and Cancer Stem Cells in Malignant Glioma. *ACS Appl. Mater. Interfaces* **2015**, *7*, 16792–16801.

(123) Sato, A. K.; Viswanathan, M.; Kent, R. B.; Wood, C. R. Therapeutic Peptides: Technological Advances Driving Peptides into Development. *Curr. Opin. Biotechnol.* **2006**, *17*, 638–642.

(124) Yao, V. J.; D'Angelo, S.; Butler, K. S.; Theron, C.; Smith, T. L.; Marchiò, S.; Gelovani, J. G.; Sidman, R. L.; Dobroff, A. S.; Brinker, C. J.; *et al.* Ligand-Targeted Theranostic Nanomedicines against Cancer. *J. Control. Release* **2016**, *240*, 267–286.

(125) Gaertner, F. C.; Kessler, H.; Wester, H. J.; Schwaiger, M.; Beer, A. J. Radiolabelled RGD Peptides for Imaging and Therapy. *Eur. J. Nucl. Med. Mol. Imaging* **2012**, *39*, 126–138.

(126) Cai, H.; Conti, P. S. RGD-Based PET Tracers for Imaging Receptor Integrin Avβ3expression. *J. Label. Compd. Radiopharm.* **2013**, *56*, 264–279.

(127) Lee, H.-Y.; Li, Z.; Chen, K.; Hsu, A. R.; Xu, C.; Xie, J.; Sun, S.; Chen, X. PET/MRI Dual-Modality Tumor Imaging Using Arginine-Glycine-Aspartic (RGD)-Conjugated Radiolabeled Iron Oxide Nanoparticles. *J. Nucl. Med.* **2008**, *49*, 1371–1379.

(128) Liu, Z.; Cai, W.; He, L.; Nakayama, N.; Chen, K.; Sun, X.; Chen, X.; Dai, H. In Vivo Biodistribution and Highly Efficient Tumour Targeting of Carbon Nanotubes in Mice. *Nat. Nanotechnol.* **2007**, *2*, 47–52.

(129) Kelly, K. A.; Jones, D. A. Isolation of a Colon Tumor Specific Binding Peptide Using Phage Display Selection. *Neoplasia* **2003**, *5*, 437–444.

(130) Kelly, K.; Alencar, H.; Funovics, M.; Mahmood, U.; Weissleder, R. Detection of Invasive Colon Cancer Using a Novel, Targeted, Library-Derived Fluorescent Peptide. *Cancer Res.* **2004**, *64*, 6247–6251.

(131) Lee, Y. M.; Lee, D.; Kim, J.; Park, H.; Kim, W. J. RPM Peptide Conjugated Bioreducible Polyethylenimine Targeting Invasive Colon Cancer. *J. Control. Release* **2015**, *205*, 172–180.

(132) Teixeira, M. C.; Carbone, C.; Souto, E. B. Beyond Liposomes: Recent Advances on Lipid Based Nanostructures for Poorly Soluble/Poorly Permeable Drug Delivery. *Prog. Lipid Res.* **2017**, *68*, 1–11.

(133) A., A.; A., M.; F., P. Lipid Nanoparticulate Drug Delivery Systems: A Revolution in Dosage Form Design and Development. *Recent Adv. Nov. Drug Carr. Syst.* **2012**, 107–140.

(134) Patidar, A.; Thakur, D. S.; Kumar, P.; Verma, J. A Review on Novel Lipid Based Nanocarriers. *Int. J. Pharm. Pharm. Sci.* **2010**, *2*, 30–35.

(135) Slovak, J. E.; Villarino, N. F. Safety of Oral and Intravenous Mycophenolate Mofetil in Healthy Cats. *J. Feline Med. Surg.* **2018**, *20*, 184–188.

(136) Kotta, S.; Khan, A. W.; Pramod, K.; Ansari, S. H.; Sharma, R. K.; Ali, J. Exploring Oral Nanoemulsions for Bioavailability Enhancement of Poorly Water-Soluble Drugs. *Expert Opin. Drug Deliv.* **2012**, *9*, 585–598.

(137) Adhikari, P.; Pal, P.; Das, A. K.; Ray, S.; Bhattacharjee, A.; Mazumder, B. Nano Lipid-Drug Conjugate: An Integrated Review. *Int. J. Pharm.* **2017**, *529*, 629–641.

(138) Singh, C.; Bhatt, T. D.; Gill, M. S.; Suresh, S. Novel Rifampicin-Phospholipid Complex for Tubercular Therapy: Synthesis, Physicochemical Characterization and in-Vivo Evaluation. *Int. J. Pharm.* **2014**, *460*, 220–227.

(139) Attama, A. A.; Reichl, S.; Müller-Goymann, C. C. Sustained Release and Permeation of Timolol from Surface-Modified Solid Lipid Nanoparticles through Bioengineered Human Cornea. *Curr. Eye Res.* **2009**, *34*, 698–705.

(140) Date, A. A.; Desai, N.; Dixit, R.; Nagarsenker, M. Self-Nanoemulsifying Drug Delivery Systems: Formulation Insights, Applications and Advances. *Nanomedicine* **2010**, *5*, 1595–1616.

(141) Čerpnjak, K.; Zvonar, A.; Gašperlin, M.; Vrečer, F. Lipid-Based Systems as a Promising Approach for Enhancing the Bioavailability of Poorly Water-Soluble Drugs. *Acta Pharm.* **2013**, *63*, 427–445.

(142) Bolko, K.; Zvonar, A.; Gašperlin, M. Mixed Lipid Phase SMEDDS as an Innovative Approach to Enhance Resveratrol Solubility. *Drug Dev. Ind. Pharm.* **2014**, *40*, 102–109.

(143) Constantinides, P. P.; Tustian, A.; Kessler, D. R. Tocol Emulsions for Drug Solubilization and Parenteral Delivery. *Adv. Drug Deliv. Rev.* **2004**, *56*, 1243–1255.

(144) Saberi, A. H.; Fang, Y.; McClements, D. J. Fabrication of Vitamin E-Enriched Nanoemulsions: Factors Affecting Particle Size Using Spontaneous Emulsification. *J. Colloid Interface Sci.* **2013**, *391*, 95–102.

(145) Ozturk, B.; Argin, S.; Ozilgen, M.; McClements, D. J. Formation and Stabilization of Nanoemulsion-Based Vitamin e Delivery Systems Using Natural Surfactants: Quillaja Saponin and Lecithin. *J. Food Eng.* **2014**, *142*, 57–63.

(146) Mehmood, T. Optimization of the Canola Oil Based Vitamin E Nanoemulsions Stabilized by Food Grade Mixed Surfactants Using Response Surface Methodology. *Food Chem.* **2015**, *183*, 1–7.

(147) Morais, J. M.; Burgess, D. J. In Vitro Release Testing Methods for Vitamin e Nanoemulsions. *Int. J. Pharm.* **2014**, *475*, 393–400.

(148) Severino, P.; Andreani, T.; Macedo, A. S.; Fangueiro, J. F.; Santana, M. H. A.; Silva, A. M.; Souto, E. B. Current State-of-Art and New Trends on Lipid Nanoparticles (SLN and NLC) for Oral Drug Delivery. *J. Drug Deliv.* **2012**, *2012*, 1–10.

(149) Khunt, B.; Koradiya, B. Self Emulsifying Drug Delivery System. *International Journal of Pharmacy and Pharmaceutical Sciences.* **2012**, *2*,4.

(150) Sigward, E.; Mignet, N.; Rat, P.; Dutot, M.; Muhamed, S.; Guigner, J. M.; Scherman, D.; Brossard, D.; Crauste-Manciet, S. Formulation and Cytotoxicity Evaluation of New Self-Emulsifying Multiple W/O/W Nanoemulsions. *Int. J. Nanomedicine* **2013**, *8*, 611–625.

(151) Date, A. A.; Nagarsenker, M. S. Parenteral Microemulsions: An Overview. *Int. J. Pharm.* **2008**, *355*, 19–30.

(152) Anton, N.; Benoit, J. P.; Saulnier, P. Design and Production of Nanoparticles Formulated from Nano-Emulsion Templates-A Review. *J. Control. Release* **2008**, *128*, 185–199.

(153) Gutiérrez, J. M.; González, C.; Maestro, A.; Solè, I.; Pey, C. M.; Nolla, J. Nano-Emulsions: New Applications and Optimization of Their Preparation. *Curr. Opin. Colloid Interface Sci.* **2008**, *13*, 245–251.

(154) Tadros, T.; Izquierdo, P.; Esquena, J.; Solans, C. Formation and Stability of Nano-Emulsions. *Adv. Colloid Interface Sci.* **2004**, *108–109*, 303–318.

(155) Mason, T. G.; Wilking, J. N.; Meleson, K.; Chang, C. B.; Graves, S. M. Nanoemulsions: Formation, Structure, and Physical Properties. *J. Phys. Condens. Matter* **2006**, *18*.

(156) Tagne, J. B.; Kakumanu, S.; Ortiz, D.; Shea, T.; Nicolosi, R. J. A Nanoemulsion Formulation of Tamoxifen Increases Its Efficacy in a Breast Cancer Cell Line. *Mol. Pharm.* **2008**, *5*, 280–286.

(157) Tang, G. Q.; Tanaka, N.; Kunugi, S. In Vitro Increases in Plasmid DNA Supercoiling by Hydrostatic Pressure. *Biochim. Biophys. Acta - Gene Struct. Expr.* **1998**, *1443*, 364–368.

(158) Hernández, A.; Cano, M. P. High-Pressure and Temperature Effects on Enzyme Inactivation in Tomato Puree. *J. Agric. Food Chem.* **1998**, *46*, 266–270.

(159) Kunieda, H.; Fukui, Y.; Uchiyama, H.; Solans, C. Spontaneous Formation of Highly Concentrated Water-in-Oil Wmulsions (Gel-Emulsions). *Langmuir* **1996**, *12*, 2136–2140.

(160) Forgiarini, A.; Esquena, J.; González, C.; Solans, C. Formation of Nano-Emulsions by Low-Energy Emulsification Methods at Constant Temperature. *Langmuir* **2001**, *17*, 2076–2083.

(161) Jaworska, M.; Sikora, E.; Zielina, M.; Ogonowski, J. Studies on the Formation of O/W Nano-Emulsions, by Low-Energy Emulsification Method, Suitable for Cosmeceutical Applications. *Acta Biochim. Pol.* **2013**, *60*, 779–782.

(162) Ganachaud, F.; Katz, J. L. Nanoparticles and Nanocapsules Created Using the Ouzo Effect: Spontaneous Emulsification as an Alternative to Ultrasonic and High-Shear Devices. *ChemPhysChem* **2005**, *6*, 209–216.

(163) Bouchemal, K.; Briançon, S.; Perrier, E.; Fessi, H. Nano-Emulsion Formulation Using Spontaneous Emulsification: Solvent, Oil and Surfactant Optimisation. *Int. J. Pharm.* **2004**, *280*, 241–251.

(164) Kelmann, R. G.; Kuminek, G.; Teixeira, H. F.; Koester, L. S. Carbamazepine Parenteral Nanoemulsions Prepared by Spontaneous Emulsification Process. *Int. J. Pharm.* **2007**, *342*, 231–239.

(165) Ekambaram, P.; Abdul Hasan Sathali, A. Formulation and Evaluation of Solid Lipid Nanoparticles of Ramipril. *J. Young Pharm.* **2011**, *3*, 216–220.

(166) Pons, M.; Foradada, M.; Estelrich, J. Liposomes Obtained by the Ethanol Injection Method. *Int. J. Pharm.* **1993**, *95*, 51–56.

(167) Li, D. C.; Zhong, X. K.; Zeng, Z. P.; Jiang, J. G.; Li, L.; Zhao, M. M.; Yang, X. Q.; Chen, J.; Zhang, B. S.; Zhao, Q. Z.; *et al.* Application of Targeted Drug Delivery System in Chinese Medicine. *J. Control. Release* **2009**, *138*, 103–112.

(168) Shin, G. H.; Chung, S. K.; Kim, J. T.; Joung, H. J.; Park, H. J. Preparation of Chitosan-Coated Nanoliposomes for Improving the Mucoadhesive Property of Curcumin Using the Ethanol Injection Method. *J. Agric. Food Chem.* **2013**, *61*, 11119–11126.

(169) Kolesnick, R.; Golde, D. W. The Sphingomyelin Pathway in Tumor Necrosis Factor and Interleukin-1 Signaling. *Cell* **1994**, *77*, 325–328.

(170) Kolesnick, R. The Therapeutic Potential of Modulating the Ceramide/Sphingomyelin Pathway. *J. Clin. Invest.* **2002**, *110*, 3–8.

(171) Levade, T.; Malagarie-Cazenave, S.; Gouazé, V.; Ségui, B.; Tardy, C.; Betito, S.; Andrieu-Abadie, N.; Cuvillier, O. Ceramide in Apoptosis: A Revisited Role. *Neurochem. Res.* **2002**, *27*, 601–607.

(172) Dillehay, D. L.; Webb, S. K.; Andalfred, E. S.; Merrill, H. Biochemical and Molecular Roles of Nutrients Dietary Sphingomyelin Inhibits Colon Cancer in CF1 Mice. *J. Nutr.* **1994**, 615–620.

(173) Awad, A.B.; von Holtz, R.L.; Cone, J. P.; Fink, C. S.; Chen, Y. C. beta-Sitosterol inhibits growth of HT-29 human colon cancer cells by activating the sphingomyelin cycle. *Anticancer Research.* **1998**,18, 471-473.

(174) Frolov, V. A.; Shnyrova, A. V.; Zimmerberg, J. Lipid Polymorphisms and Membrane Shape. *Cold Spring Harb. Perspect. Biol.* **2011**, *3*.

(175) Peetla, C.; Vijayaraghavalu, S.; Labhasetwar V. Biophysics of cell membrane lipids in cancer drug resistance: Implications for drug transport and drug delivery with nanoparticles. *Adv. Drug Deliv. Rev.* **2013**, *65*, 1686–1698.

(176) Johnston, M. J. W.; Semple, S. C.; Klimuk, S. K.; Ansell, S.; Maurer, N.; Cullis, P. R. Characterization of the Drug Retention and Pharmacokinetic Properties of Liposomal Nanoparticles Containing Dihydrosphingomyelin. *Biochim. Biophys. Acta - Biomembr.* **2007**, *1768*, 1121–1127.

(177) Tiwari, S. B.; Amiji, M. M. Improved Oral Delivery of Paclitaxel Following Administration in Nanoemulsion Formulations. *J. Nanosci. Nanotechnol.* **2006**, *6*, 3215–3221.

(178) Carter, K. A.; Luo, D.; Razi, A.; Geng, J.; Shao, S.; Ortega, J.; Lovell, J. F. Sphingomyelin Liposomes Containing Porphyrin-Phospholipid for Irinotecan Chemophototherapy. *Theranostics* **2016**, *6*, 2329–2336.

(179) Semple, S. C.; Leone, R.; Wang, J.; Leng, E. C.; Klimuk, S. K.; Eisenhardt, M. L.; Yuan, Z. N.; Edwards, K.; Maurer, N.; Hope, M. J.; *et al.* Optimization and Characterization of a Sphingomyelin/Cholesterol Liposome Formulation of Vinorelbine with Promising Antitumor Activity. *J. Pharm. Sci.* **2005**, *94*, 1024–1038.

(180) Cheng, N.; Xia, T.; Han, Y.; He, Q. J.; Zhao, R.; Ma, J. R. Synergistic Antitumor Effects of Liposomal Honokiol Combined with Cisplatin in Colon Cancer Models. *Oncol. Lett.* **2011**, *2*, 957–962.

(181) Press, D. Clinical Development of Liposome-Based Drugs : Formulation , Characterization , and Therapeutic Efficacy. **2012**, 49–60.

(182) Lamichhane, N.; Udayakumar, T. S.; D'Souza, W. D.; Simone, C. B.; Raghavan, S. R.; Polf, J.; Mahmood, J. Liposomes: Clinical Applications and Potential for Image-Guided Drug Delivery. *Molecules* **2018**, *23*, 1–17.

(183) Quinn, P. J. A Lipid Matrix Model of Membrane Raft Structure. *Prog. Lipid Res.* **2010**, *49*, 390–406.

(184) Wang, K.; Kievit, F. M.; Zhang, M. Nanoparticles for Cancer Gene Therapy: Recent Advances, Challenges, and Strategies. *Pharmacol. Res.* **2016**, *114*, 56–66.

(185) Parlea, L.; Puri, A.; Kasprzak, W.; Bindewald, E.; Zakrevsky, P.; Satterwhite, E.; Joseph, K.; Afonin, K. A.; Shapiro, B. A. Cellular Delivery of RNA Nanoparticles. *ACS Comb. Sci.* **2016**, *18*, 527–547.

(186) Zhou, Z.; Liu, X.; Zhu, D.; Wang, Y.; Zhang, Z.; Zhou, X.; Qiu, N.; Chen, X.; Shen, Y. Nonviral Cancer Gene Therapy: Delivery Cascade and Vector Nanoproperty Integration. *Adv. Drug Deliv. Rev.* **2017**, *115*, 115–154.

(187) Crew, E.; Rahman, S.; Razzak-Jaffar, A.; Mott, D.; Kamundi, M.; Yu, G.; Tchah, N.; Lee, J.; Bellavia, M.; Zhong, C.-J. MicroRNA Conjugated Gold Nanoparticles and Cell Transfection. **2011**, 8–11.

(188) Frede, A.; Neuhaus, B.; Klopfleisch, R.; Walker, C.; Buer, J.; Müller, W.; Epple, M.; Westendorf, A. M. Colonic Gene Silencing Using SiRNA-Loaded Calcium Phosphate/PLGA Nanoparticles Ameliorates Intestinal Inflammation in Vivo. *J. Control. Release* **2016**, *222*, 86–96.

(189) Cullis, P. R.; Hope, M. J. Lipid Nanoparticle Systems for Enabling Gene Therapies. *Mol. Ther.* **2017**, *25*, 1467–1475.

(190) Xiao, Y.; Shi, K.; Qu, Y.; Chu, B.; Qian, Z. Engineering Nanoparticles for Targeted Delivery of Nucleic Acid Therapeutics in Tumor. *Mol. Ther. - Methods Clin. Dev.* **2018**, *12*, 1–18.

(191) Wong, J. K.L.; Mohseni, R.; Hamidieh, A. A.; MacLaren, R. E.; Habib, N.; Seifalian, A. M. Will Nanotechnology Bring New Hope for Gene Delivery?. *Trends in Biotechnology*. **2017**, *35*, 5

(192) Raftery, R. M.; Tierney, E. G.; Curtin, C. M.; Cryan, S. A.; O'Brien, F. J. Development of a Gene-Activated Scaffold Platform for Tissue Engineering Applications Using Chitosan-PDNA Nanoparticles on Collagen-Based Scaffolds. *J. Control. Release* **2015**, *210*, 84–94.

(193) Rudzinski, W. E.; Palacios, A.; Ahmed, A.; Lane, M. A.; Aminabhavi, T. M. Targeted Delivery of Small Interfering RNA to Colon Cancer Cells Using Chitosan and PEGylated Chitosan Nanoparticles. *Carbohydr. Polym.* **2016**, *147*, 323–332.

(194) Jin, H.; Yu, Y.; Chrisler, W. B.; Xiong, Y.; hu, D.; Lei, C. Delivery of MicroRNA-10b with polylysine nanoparticles for Inhibition of Breast cancer cell Wound Healing. *Breast Cancer: Basic and Clinical Research.* **2012**, *6*, 9–19

(195) Lungwitz, U.; Breunig, M.; Blunk, T.; Göpferich, A. Polyethylenimine-Based Non-Viral Gene Delivery Systems. *Eur. J. Pharm. Biopharm.* **2005**, *60*, 247–266.

(196) Alvarez, R. D.; Sill, M. W.; Davidson, S. A.; Muller, C. Y.; Bender, D. P.; Debernardo, R. L.; Behbakht, K.; Huh, W. K. A Phase II Trial of Intraperitoneal EGEN-001, an IL-12 Plasmid Formulated with PEG-PEI-Cholesterol Lipopolymer in the Treatment of Persistent or Recurrent Epithelial Ovarian, Fallopian Tube or Primary Peritoneal Cancer: A Gynecologic Oncology Group Study. *Gynecol. Oncol.* **2014**, *133*, 433–438.

(197) Nourazarian, A. R.; Najar, A. G.; Farajnia, S.; Khosroushahi, A.Y.; Pashaei-Asl, R.; Omidi, Y. Combined EGFR and c-Src Antisense Oligodeoxynucleotides Encapsulated with PAMAM Denderimers Inhibit HT-29 Colon Cancer Cell Proliferation. *Asian Pacific J Cancer Prev*, **2012,**13 (9), 4751-4756

(198) Muthiah, M.; Park, I.-K.; Cho, C.-S. Nanoparticle-Mediated Delivery of Therapeutic Genes: Focus on MiRNA Therapeutics. *Expert Opin. Drug Deliv.* **2013**, *10*, 1259–1273.

(199) Ahmad, A.; Evans, H. M.; Ewert, K.; George, C. X.; Samuel, C. E.; Safinya, C. R. New Multivalent Cationic Lipids Reveal Bell Curve for Transfection Efficiency versus Membrane Charge Density: Lipid - DNA Complexes for Gene Delivery. *J. Gene Med.* **2005**, *7*, 739–748.

(200) Anderson, D. M.; Hall, L. L.; Ayyalapu, A. R.; Irion, V. R.; Nantz, M. H.; Hecker, J. G. Stability of MRNA/Cationic Lipid Lipoplexes in Human and Rat Cerebrospinal Fluid: Methods and Evidence for Nonviral MRNA Gene Delivery to the Central Nervous System. *Hum. Gene Ther.* **2003**, *14*, 191–202.

(201) Li, W.; Szoka, F. C. Lipid-Based Nanoparticles for Nucleic Acid Delivery. *Pharm. Res.* **2007**, *24*, 438–449.

(202) Yu, W.; Liu, C.; Ye, J.; Zou, W.; Zhang, N.; Xu, W. Novel Cationic SLN Containing a Synthesized Single-Tailed Lipid as a Modifier for Gene Delivery. *Nanotechnology* **2009**, *20*.

(203) Whitehead, K. A.; Langer, R.; Anderson, D. G. Knocking down Barriers: Advances in SiRNA Delivery. *Nat. Rev. Drug Discov.* **2009**, *8*, 129–138.

(204) Lonez, C.; Vandenbranden, M.; Ruysschaert, J. M. Cationic Liposomal Lipids: From Gene Carriers to Cell Signaling. *Prog. Lipid Res.* **2008**, *47*, 340–347.

(205) Lu, C.; Stewart, D. J.; Lee, J. J.; Ji, L.; Ramesh, R.; Jayachandran, G.; Nunez, M. I.; Wistuba, I. I.; Erasmus, J. J.; Hicks, M. E.; *et al.* Phase I Clinical Trial of Systemically Administered TUSC2(FUS1)-Nanoparticles Mediating Functional Gene Transfer in Humans. *PLoS One* **2012**, *7*, e34833.

(206) Cardarelli, F.; Digiacomo, L.; Marchini, C.; Amici, A.; Salomone, F.; Fiume, G.; Rossetta, A.; Gratton, E.; Pozzi, D.; Caracciolo, G. The Intracellular Trafficking Mechanism of Lipofectamine-Based Transfection Reagents and Its Implication for Gene Delivery. *Sci. Rep.* **2016**, *6*, 1–8.

(207) Lin, C. W.; Jan, M. S.; Kuo, J. H. S. The Vector-Related Influences of Autophagic MicroRNA Delivery by Lipofectamine 2000 and Polyethylenimine 25K on Mouse Embryonic Fibroblast Cells. *Eur. J. Pharm. Sci.* **2017**, *101*, 11–21.

(208) Saharjo, B. H.; Sudo, S.; Yonemura, S.; Tsuruta, H. Greenhouse Gasses Produced during Burning in the Land Preparation Area Using Fire in Peat Area Belong to the Community. *For. Ecol. Manage.* **2006**, *234*, S247.

(209) Verissimo, L. M.; Agnez Lima, L. F.; Monte Egito, L. C.; De Oliveira, A. G.; Do Egito, E. S. T. Pharmaceutical Emulsions: A New Approach for Gene Therapy. *J. Drug Target.* **2010**, *18*, 333–342.

(210) Liu, C. H.; Yu, S. Y. Cationic Nanoemulsions as Non-Viral Vectors for Plasmid DNA Delivery. *Colloids Surfaces B Biointerfaces* **2010**, *79*, 509–515.

(211) Kwon, S. M.; Nam, H. Y.; Nam, T.; Park, K.; Lee, S.; Kim, K.; Kwon, I. C.; Kim, J.; Kang, D.; Park, J. H.; *et al.* In Vivo Time-Dependent Gene Expression of Cationic Lipid-Based Emulsion as a Stable and Biocompatible Non-Viral Gene Carrier. *J. Control. Release* **2008**, *128*, 89–97.

(212) Ott, G.; Singh, M.; Kazzaz, J.; Briones, M.; Soenawan, E.; Ugozzoli, M.; O'Hagan, D. T. A Cationic Sub-Micron Emulsion (MF59/DOTAP) Is an Effective Delivery System for DNA Vaccines. *J. Control. Release* **2002**, *79*, 1–5.

(213) Fraga, M.; Carvalho, T. G. De; Diel, S.; Bruxel, F.; Alexandre, N.; Filho, K.; Teixeira, H. F.; Matte, U. Cationic Nanoemulsions as a Gene Delivery System : Proof of Concept in the Mucopolysaccharidosis I Murine Model. **2015**.

(214) Silva, A. L.; Alexandrino, F.; Verissimo, L. M.; Agnez-Lima, L. F.; Egito, L. C. M.; de Oliveira, A. G.; do Egito, E. S. T. Physical Factors Affecting Plasmid DNA Compaction in Stearylamine-Containing Nanoemulsions Intended for Gene Delivery. *Pharmaceuticals* **2012**, *5*, 643–654.

(215) Trang, P.; Wiggins, J. F.; Daige, C. L.; Cho, C.; Omotola, M.; Brown, D.; Weidhaas, J. B.; Bader, A. G.; Slack, F. J. Systemic Delivery of Tumor Suppressor MicroRNA Mimics Using a Neutral Lipid Emulsion Inhibits Lung Tumors in Mice. *Mol. Ther.* **2011**, *19*, 1116–1122.

(216) Beg, M. S.; Brenner, A. J.; Sachdev, J.; Borad, M.; Kang, Y. K.; Stoudemire, J.; Smith, S.; Bader, A. G.; Kim, S.; Hong, D. S. Phase I Study of MRX34, a Liposomal MiR-34a Mimic, Administered Twice Weekly in Patients with Advanced Solid Tumors. *Invest. New Drugs* **2017**, *35*, 180–188.

(217) Bader, A. G. MiR-34 - a MicroRNA Replacement Therapy Is Headed to the Clinic. *Front. Genet.* **2012**, *3*, 1–9.

(218) Liang, G.; Zhu, Y.; Jing, A.; Wang, J.; Hu, F.; Feng, W.; Xiao, Z.; Chen, B. Cationic MicroRNA-Delivering Nanocarriers for Efficient Treatment of Colon Carcinoma in Xenograft Model. *Gene Ther.* **2016**, *23*, 829–838.

(219) Zhang, T.; Xue, X.; He, D.; Hsieh, J. T. A Prostate Cancer-Targeted Polyarginine-Disulfide Linked PEI Nanocarrier for Delivery of MicroRNA. *Cancer Lett.* **2015**, *365*, 156–165.

(220) Chiou, G. Y.; Cherng, J. Y.; Hsu, H. S.; Wang, M. L.; Tsai, C. M.; Lu, K. H.; Chien, Y.; Hung, S. C.; Chen, Y. W.; Wong, C. I.; *et al.* Cationic Polyurethanes-Short Branch PEI-Mediated Delivery of Mir145 Inhibited Epithelial-Mesenchymal Transdifferentiation and Cancer Stem-like Properties and in Lung Adenocarcinoma. *J. Control. Release* **2012**, *159*, 240–250.

(221) Ibrahim, A. F.; Weirauch, U.; Thomas, M.; Gruñweller, A.; Hartmann, R. K.; Aigner, A. MicroRNA Replacement Therapy for MiR-145 and MiR-33a Is Efficacious in a Model of Colon Carcinoma. *Cancer Res.* **2011**, *71*, 5214–5224.

(222) Pramanik, D.; Campbell, N. R.; Karikari, C.; Chivukula, R.; Kent, O. A.; Mendell, J. T.; Maitra, A. Restitution of Tumor Suppressor MicroRNAs Using a Systemic Nanovector Inhibits Pancreatic Cancer Growth in Mice. *Mol. Cancer Ther.* **2011**, *10*, 1470–1480.

(223) Che, H.-L.; Lee, H. J.; Uto, K.; Ebara, M.; Kim, W. J.; Aoyagi, T.; Park, I.-K. Simultaneous Drug and Gene Delivery from the Biodegradable Poly(ε-Caprolactone) Nanofibers for the Treatment of Liver Cancer. *J. Nanosci. Nanotechnol.* **2015**, *15*, 7971–7975.

(224) Santos-Carballal, B.; Aaldering, L. J.; Ritzefeld, M.; Pereira, S.; Sewald, N.; Moerschbacher, B. M.; Götte, M.; Goycoolea, F. M. Physicochemical and Biological Characterization of Chitosan-MicroRNA Nanocomplexes for Gene Delivery to MCF-7 Breast Cancer Cells. *Sci. Rep.* **2015**, *5*, 1–15.

(225) Setua, S.; Khan, S.; Yallapu, M. M.; Behrman, S. W.; Sikander, M.; Khan, S. S.; Jaggi, M.; Chauhan, S. C. Restitution of Tumor Suppressor MicroRNA-145 Using Magnetic Nanoformulation for Pancreatic Cancer Therapy. *J. Gastrointest. Surg.* **2017**.

(226) Hahn, M. A.; Singh, A. K.; Sharma, P.; Brown, S. C.; Moudgil, B. M. Nanoparticles as Contrast Agents for in-Vivo Bioimaging: Current Status and Future Perspectives. *Anal. Bioanal. Chem.* **2011**, *399*, 3–27.

(227) Sun, G.; Xu, J.; Hagooly, A.; Rossin, R.; Li, Z.; Moore, D. A.; Hawker, C. J.; Welch, M. J.; Wooley, K. L. Strategies for Optimized Radiolabeling of Nanoparticles for in Vivo PET Imaging. *Adv. Mater.* **2007**, *19*, 3157–3162.

(228) Devaraj, N. K.; Keliher, E. J.; Thurber, G. M.; Nahrendorf, M.; Weissleder, R. 18 F Labeled Nanoparticles for in Vivo PET-CT Imaging. *Bioconjug. Chem.* **2009**, *20*, 397–401.

(229) Debbage, P.; Jaschke, W. Molecular Imaging with Nanoparticles: Giant Roles for Dwarf Actors. *Histochem. Cell Biol.* **2008**, *130*, 845–875.

(230) Cheng, Z.; Yan, X.; Sun, X.; Shen, B.; Gambhir, S. S. Tumor Molecular Imaging with Nanoparticles. *Engineering* **2016**, *2*, 132–140.

(231) Cutler, C. S.; Hennkens, H. M.; Sisay, N.; Huclier-Markai, S.; Jurisson, S. S. Radiometals for Combined Imaging and Therapy. *Chem. Rev.* **2013**, *113*, 858–883.

(232) Wadas, T. J.; Wong, E. H.; Weisman, G. R.; Anderson, C. J. Coordinating Radiometals of Copper , Gallium , Indium , Yttrium , and Zirconium for PET and SPECT Imaging of Disease. **2010**, 2858–2902.

(233) Zhang, R.; Xiong, C.; Huang, M.; Zhou, M.; Huang, Q.; Wen, X.; Liang, D.; Li, C. Peptide-Conjugated Polymeric Micellar Nanoparticles for Dual SPECT and Optical Imaging of EphB4 Receptors in Prostate Cancer Xenografts. *Biomaterials* **2011**, *32*, 5872–5879.

(234) Deng, S.; Zhang, W.; Zhang, B.; Hong, R.; Chen, Q.; Dong, J.; Chen, Y.; Chen, Z.; Wu, Y. Radiolabeled Cyclic Arginine-Glycine-Aspartic (RGD)-Conjugated Iron Oxide Nanoparticles as Single-Photon Emission Computed Tomography (SPECT) and Magnetic Resonance Imaging (MRI) Dual-Modality Agents for Imaging of Breast Cancer. *J. Nanoparticle Res.* **2015**, *17*.

(235) Gao, H.; Liu, X.; Tang, W.; Niu, D.; Zhou, B.; Zhang, H.; Liu, W.; Gu, B.; Zhou, X.; Zheng, Y.; *et al.* 99mTc-Conjugated Manganese-Based Mesoporous Silica Nanoparticles for SPECT, PH-Responsive MRI and Anti-Cancer Drug Delivery. *Nanoscale* **2016**, *8*, 19573–19580.

(236) Ametamey, S. M.; Honer, M.; Schubiger, P. A. Molecular Imaging with PET. *Chem. Rev.* **2008**, *108*, 1501–1516.

(237) Pérez-Campaña, C.; Gómez-Vallejo, V.; Puigivila, M.; Martín, A.; Calvo-Fernández, T.; Moya, S. E.; Ziolo, R. F.; Reese, T.; Llop, J. Biodistribution of Different Sized Nanoparticles Assessed by Positron Emission Tomography: A General Strategy for Direct Activation of Metal Oxide Particles. *ACS Nano* **2013**, *7*, 3498–3505.

(238) Stockhofe, K.; Postema, J. M.; Schieferstein, H.; Ross, T. L. Radiolabeling of Nanoparticles and Polymers for PET Imaging. *Pharmaceuticals* **2014**, *7*, 392–418.

(239) Pérez-Campaña, C.; Gómez-Vallejo, V.; Martin, A.; San Sebastián, E.; Moya, S. E.; Reese, T.; Ziolo, R. F.; Llop, J. Tracing Nanoparticles in Vivo: A New General Synthesis of Positron Emitting Metal Oxide Nanoparticles by Proton Beam Activation. *Analyst* **2012**, *137*, 4902–4906.

(240) Liu, Q.; Sun, Y.; Li, C.; Zhou, J.; Li, C.; Yang, T.; Zhang, X.; Yi, T. F-Labeled Magnetic-Upconversion. **2011**, 3146–3157.

(241) Zhou, J.; Yu, M.; Sun, Y.; Zhang, X.; Zhu, X.; Wu, Z.; Wu, D.; Li, F. Fluorine-18-Labeled Gd3+/Yb3+/Er3+ Co-Doped NaYF4 Nanophosphors for Multimodality PET/MR/UCL Imaging. *Biomaterials* **2011**, *32*, 1148–1156.

(242) Sun, Y; Yu, M.; Liang, S.; Zhang, Y.; Li, C.; Mou, T.; Yang, W.; Zhang, X.; Li, B.; Huang, C.; *et al.* Fluorine-18 Labeled Rare-Earth Nanoparticles for Positron Emission Tomography (PET) Imaging of Sentinel Lymph Node. *Biomaterials* **2011**, *32*, 2999–3007.

(243) Guerrero, S.; Herance, J. R.; Rojas, S.; Mena, J. F.; Gispert, J. D.; Acosta, G. A.; Albericio, F.; Kogan, M. J. Synthesis and in Vivo Evaluation of the Biodistribution of a 18F-Labeled Conjugate Gold-Nanoparticle-Peptide with Potential Biomedical Application. *Bioconjug. Chem.* **2012**, *23*, 399–408.

(244) Rojas, S.; Gispert, J. D.; Abad, S.; Buaki-Sogo, M.; Victor, V. M.; Garcia, H.; Herance, J. R. In Vivo Biodistribution of Amino-Functionalized Ceria Nanoparticles in Rats Using Positron Emission Tomography. *Mol. Pharm.* **2012**, *9*, 3543–3550.

(245) Ducongé, F.; Pons, T.; Pestourie, C.; Hérin, L.; Thézé, B.; Gombert, K.; Mahler, B.; Hinnen, F.; Kühnast, B.; Dollé, F.; *et al.* Fluorine-18-Labeled Phospholipid Quantum Dot Micelles for in Vivo Multimodal Imaging from Whole Body to Cellular Scales. *Bioconjug. Chem.* **2008**, *19*, 1921–1926.

(246) Rojas, S.; Gispert, J. D.; Martín, R.; Abad, S.; Menchón, C.; Pareto, D.; Víctor, V. M.; Álvaro, M.; García, H.; Herance, J. R. Biodistribution of Amino-Functionalized Diamond Nanoparticles. in Vivo Studies Based On18F Radionuclide Emission. *ACS Nano* **2011**, *5*, 5552–5559.

Background, hypothesis and objectives

USC
UNIVERSIDADE
DE SANTIAGO
DE COMPOSTELA

Background

1. Nanotechnology has played an important role in the development of improved anticancer therapies in the last few decades. The development of engineered nanoparticles has been studied to diagnose and treat cancer more effectively[1,2]. Nanoparticles can enhance the stability of the encapsulated molecules against degradation in the biological environment, prolong their circulation half-life, improve biodistribution, promote accumulation into the targeted tumor, and reduce systemic toxicity[3,4]. The application of nanoparticles for gene therapy purposes has also been explored, through the incorporation of different molecules with different activities such as pDNA, mRNA, siRNA, and miRNA[5,6]. Nanoparticles can additionally be used for *in vivo* diagnosis since they can incorporate different molecules allowing tracking for multiple image modalities such as MRI, PET, and SPECT[7,8].

2. Nanoemulsions have been widely explored in the drug delivery field. They are thermodynamically stable isotropic systems in which two immiscible liquids (oil and water) are mixed to form a single phase and stabilized by surfactants[9]. They offer several advantages, (i) simple, (ii) suitable for the incorporation of labile molecules, and (iii) easy for scale-up. Their compositions can be adjusted according to specific needs[10]. Cationic lipids can be included to improve the association of nucleic acids by electrostatic interaction[11]. The ethanol injection method is a low-energy emulsification technique typically used for the preparation of liposomes, which has been adapted for the formulation of nanoemulsions[12].

3. Gene therapy offers a lot of potential for the development of targeted anticancer treatments[13,14]. Mature microRNAs (miRNAs) are naturally small non-coding RNA molecules, 21–25 nucleotides in length. MicroRNAs are partially complementary to one or more messenger RNA (mRNA) molecules[15]. Their major utility is to downregulate or upregulate gene expression in various ways. However, there remain several challenges in miRNA delivery due to the poor stability of these molecules in biological environment, and limited access to the intracellular compartment. Association to nanocarriers can offer an opportunity for successful translation[16].

4. Positron Emission Tomography (PET), a technique that detects gamma rays from positron-emitting isotopes, is widely use in clinic diagnosis. The high sensitivity and specificity of PET result from the high sensitivity of radioisotopes compared with other diagnostic modules[17,18]. Numerous studies have been focused on development of radiolabelled nanoparticles for non-invasive PET cancer diagnosis, to increase patients' survival rate. In both clinical and preclinical research, ^{18}F is the most frequently used radioisotope for the development of PET radiopharmaceuticals. It has high specific activity and ease of large-scale production contributing to its widely use in molecular imaging. Generally, introduction of ^{18}F into molecules of interest is achieved through ^{18}F-prosthetic group. Currently, there are significant needs required for the establishing of simple and efficient methods for ^{18}F-labeling procedures for nanoparticles[19]. Tracking of radiolabelled nanoparticles provides valuable information that can pave the way for future cancer diagnosis[20,21].

Hypothesis

On the basis of general knowledge in clinical use and pharmaceutical science, we set out the following hypotheses (H) for this work.

- It is possible to optimize the composition of sphingomyelin nanoemulsions (SNs) for the development of miRNA replacement therapies to interfere cancer progression.

H1. SNs can be prepared by a mild method without the use of heat or high-energy input, being suitable for the association of labile biomolecules.

H2. The composition of SNs can be conveniently modulated to mediate an efficient association of oncosuppressor miRNA mimics.

H3. SNs can efficiently interact with colorectal cancer cells to deliver their miRNA cargo.

H4. Delivery of oncosuppressor miRNA can interfere tumor progression.

- It is possible to radiolabel SNs with Fluorine-18 for *in vivo* imaging by PET.

H5. SNs and surface decorated SNs (targeted SNs) can be radiolabelled with Fluorine-18 (^{18}F) following a simple methodology using a prosthetic group, [^{18}F]FBEM.

H6. Radiolabelled SNs can be tracked after intravenous injection to provide biodistribution information, and be of interest for the future development of innovative diagnosis methodologies and nanotheranostics.

USC
UNIVERSIDADE
DE SANTIAGO
DE COMPOSTELA

Objectives

Considering the previous background information and the established hypothesis, the main goal of this thesis was to develop innovative nanosystems, of application in the treatment and molecular diagnosis of colorectal cancer. We aim to explore the full potential of sphingomyelin nanoemulsions (SNs) for association and delivery of oncosuppressor miRNAs, and additionally optimize a procedure for radiolabelling of SNs with ^{18}F for imaging and diagnosis purposes. This goal has been pursued after setting up specific objectives (O) that are disclosed next:

- Development of SNs for miRNA replacement therapies to interfere cancer progression

O1. To optimize the composition of SNs to favor the association of miRNAs.

O2. To fully characterize the resultant miRNA-loaded SNs.

O3. To perform *in vitro* studies which allow studying the transfection efficiency of the developed miRNA-loaded SNs and prove the potential of the proposed anticancer therapy.

Corresponding results are presented in Chapter 2.

- Radiolabelling strategy of SNs with ^{8}F for *in vivo* imaging by PET

O4. To radiolabel SNs and peptide-decorated SNs (targeted SNs) with ^{18}F-prosthetic group, [^{18}F]FBEM.

O5. To characterize the resultant products and the efficiency of the radiolabelling process.

O6. To evaluate the biodistribution of the ^{18}F-radiolabelled SNs *ex vivo.*

O7. To determine the potential of ^{18}F-radiolabelled SNs for the development of innovative diagnosis proofs for PET scan.

Corresponding results are presented in chapter 3.

USC
UNIVERSIDADE
DE SANTIAGO
DE COMPOSTELA

References

(1) Khan, H. A.; Sakharkar, M. K.; Nayak, A.; Kishore, U.; Khan, A. Nanoparticles for Biomedical Applications: An Overview. *Nanobiomaterials* **2018**. 357-384.

(2) Bobo, D.; Robinson, K. J.; Islam, J.; Thurecht, K. J.; Corrie, S. R. Nanoparticle-Based Medicines: A Review of FDA-Approved Materials and Clinical Trials to Date. *Pharm. Res.* **2016**, *33*, 2373–2387.

(3) Rizzo, L. Y.; Theek, B.; Storm, G.; Kiessling, F.; Lammers, T. Recent Progress in Nanomedicine: Therapeutic, Diagnostic and Theranostic Applications. *Current Opinion in Biotechnology*, **2013**, *24*. 1159-1166

(4) Roy C.; M.; Schumann, C.; Bhakta-Guha, D.; Guha, G. Cancer Nanotheranostics: Strategies, Promises and Impediments. *Biomedicine and Pharmacotherapy*, **2016**, *84*. 291-304

(5) Li, W.; Szoka, F. C. Lipid-Based Nanoparticles for Nucleic Acid Delivery. *Pharm. Res.* **2007**, *24*, 438–449.

(6) Wang, K.; Kievit, F. M.; Zhang, M. Nanoparticles for Cancer Gene Therapy: Recent Advances, Challenges, and Strategies. *Pharmacol. Res.* **2016**, *114*, 56–66.

(7) Vazquez-Rios, A. J; Alonso-Nocelo M; Bouzo B. L.; Ruíz J; de la Fuente, M. Nanotheranostics and Their Potential in the Management of Metastatic Cancer. *Handbook of Nanomaterials for Cancer Theranostics*. **2018**, 199-244.

(8) Thakor, A. S.; Jokerst, J. V.; Ghanouni, P.; Campbell, J. L.; Mittra, E.; Gambhir, S. S. Clinically Approved Nanoparticle Imaging Agents. *J. Nucl. Med.* **2016**, *57*, 1833–1837.

(9) Mason, T. G.; Wilking, J. N.; Meleson, K.; Chang, C. B.; Graves, S. M. Nanoemulsions: Formation, Structure, and Physical Properties. *J. Phys. Condens. Matter* **2006**, *18*.

(10) Gutiérrez, J. M.; González, C.; Maestro, A.; Solè, I.; Pey, C. M.; Nolla, J. Nano-Emulsions: New Applications and Optimization of Their Preparation. *Curr. Opin. Colloid Interface Sci.* **2008**, *13*, 245–251.

(11) Verissimo, L. M.; Agnez Lima, L. F.; Monte Egito, L. C.; De Oliveira, A. G.; Do Egito, E. S. T. Pharmaceutical Emulsions: A New Approach for Gene Therapy. *J. Drug Target.* **2010**, *18*, 333–342.

(12) Pons, M.; Foradada, M.; Estelrich, J. Liposomes Obtained by the Ethanol Injection Method. *Int. J. Pharm.* **1993**, *95*, 51–56.

(13) Sahin, U.; Karikó, K.; Türeci, Ö. MRNA-Based Therapeutics-Developing a New Class of Drugs. *Nat. Rev. Drug Discov.* **2014**, *13*, 759–780.

(14) Bader, A. G.; Brown, D.; Stoudemire, J.; Lammers, P. Developing Therapeutic MicroRNAs for Cancer. *Gene Ther.* **2011**, *18*, 1121–1126.

(15) Bartel, D. P.; Lee, R.; Feinbaum, R. MicroRNAs : Genomics , Biogenesis , Mechanism , and Function Genomics : The MiRNA Genes. **2004**, *116*, 281–297.

(16) Fernandez-Piñeiro, I.; Badiola, I.; Sanchez, A. Nanocarriers for MicroRNA Delivery in Cancer Medicine. *Biotechnol. Adv.* **2017**, *35*, 350–360.

(17) Ametamey, S. M.; Honer, M.; Schubiger, P. A. Molecular Imaging with PET. *Chem. Rev.* **2008**, *108*, 1501–1516.

(18) Bluemke, D. A.; Liu, S. Imaging in Clinical Trials. *Princ. Pract. Clin. Res.* **2012**, 597–617.

(19) Devaraj, N. K.; Keliher, E. J.; Thurber, G. M.; Nahrendorf, M.; Weissleder, R. 18 F Labeled Nanoparticles for in Vivo PET-CT Imaging. *Bioconjug. Chem.* **2009**, *20*, 397–401.

(20) Ding, H.; Wu, F. Image Guided Biodistribution and Pharmacokinetic Studies of Theranostics. *Theranostics* **2012**, *2*, 1040–1053.

(21) Xing, Y.; Zhao, J.; Conti, P. S.; Chen, K. Radiolabeled Nanoparticles for Multimodality Tumor Imaging. *Theranostics* **2014**, *4*, 290–306.

Chapter 2

Sphingomyelin nanoemulsions for miRNA replacement therapies to interfere cancer progression

This work has been done in collaboration with Belen L. Bouzo, Abi Judit Vazquez-Rios, Rafael Lopez, and Maria de la Fuente from the university of Santiago de Compostela (Spain)

USC
UNIVERSIDADE
DE SANTIAGO
DE COMPOSTELA

Chapter 2

Sphingomyelin nanoemulsions for miRNA replacement therapies to interfere cancer progression

Abstract

Gene replacement therapies with oncosuppressor miRNA mimics have been described as promising alternatives to stop cancer progression. However, miRNA mimics are highly unstable in a biological environment hampering a successful translation to clinics. Naked RNA requires a protection from serum endonucleases and renal excretion. Furthermore, RNA administration may induce innate immune responses, resulting in unwanted toxicities. These constraints can be overcome upon association to biocompatible delivery systems able to transport intact RNAs to the targeted cancer cells. The main objective of this work has been the development of a new nanotechnology adapted for the intracellular delivery of miRNA. In this study, self-assembled sphingomyelin nanoemulsions (SNs) were adapted to achieve a good association efficiency of miRNA mimics and favour their interaction with colorectal cancer cells. Two different approaches were pursued. On the one hand, the cationic lipid stearylamine was included as an additional component to favour the association of the miRNA by establishment of electrostatic interactions (SNs-ST-miRNA). On the other hand, freeze-dried DOTAP-miRNA, lipid complexes were encapsulated into SNs (SNs-DOTAP-miRNA). Both approaches were successful for promoting the access of oncosuppressor miRNA145 to colorectal cancer cells, SNs-DOTAP-miRNA showing superior transfection efficiencies and an improved ability to interfere tumor progression. Our results suggest that SNs have the potential for miRNA delivery to develop innovative-targeted anticancer therapies.

Keywords*:* Sphingomyelin**,** nanoemulsions, gene therapy, oncosuppressor miRNA, colorectal cancer.

1.Introduction

Nowadays, cancer is one of the leading causes of death[1]. Cancer treatments can still be improved making use of novel technologies and biotechnological drugs. Advances in nanotechnology have shown a prompt impact in numerous applications in cancer, as nano-scaled carriers have the potential for incorporating various kinds of molecules into their architecture, including anticancer drugs and contrast agents, as well as macromolecules such as proteins, peptides, or oligonucleotides[2-4]. Indeed, several nanoformulations are already routine use in clinics[5-8].

RNA-based therapeutics such as small interfering RNA (siRNA) and microRNA mimics (miRNA) provide a promising approach to treat cancer by targeting specific proteins involved in the mechanism of proliferation, invasion, antiapoptosis, drug resistance, and metastasis[9,10]. MicroRNAs (miRNA) are small (17 to 25 nucleotides) non-coding RNA molecules, which specifically interact with target messenger RNA (mRNAs), resulting in inhibiting translation or mRNA cleavage and degradation[11,12]. It is well-known that various miRNAs, for instance miR145, miR143, miR137, miR10a, and miR34b/c, are downregulated in colorectal cancer cells compared to healthy tissues, and modulation of the corresponding gene expressions is gaining interest in cancer therapy[13-19]. However, the major barriers of miRNA delivery are their poor systemic stability, rapid clearance, degradation by nucleases, risk of systemic toxicity, elimination by phagocytic immune cells, and lack of efficient delivery to targeted cells to achieve the desired therapeutic outcome. Those obstructed phenomena can be avoided by using non-viral vectors. MRX34 (NCT01829971) is first-in-class miRNA mimic therapy for cancer, was tested in phase I clinical trial for patients with refractory advanced solid tumors. Besides this liposomal miR-34a mimic formulation showed evidence of antitumor activity, unfortunately it was halted because of immune responses[20,21]. Different types of nanoplatforms have also been evaluated in the last years with promising results, such as PLGA/PEI/miRNA/HA nanoparticles and miRNA-145-based magnetic nanoparticles[22,23]. Therefore, delivery of safe miRNA-nanotherapeutics might represent a promising alternative for the development of cancer therapeutics.

For the design of nanostructures, it is possible to use organic biodegradable materials that do not accumulate in the body and do not cause toxicity. Lipidic sphingomyelin nanoemulsions (SNs), which main components are sphingomyelin (SM), present in cell membranes, vitamin E, widely used in different formulations that are of clinical use, and a lipid derivative of polyethylene glycol (PEG), to modulate the surface properties of SNs and prolong half-life in the blood circulation[24-27]. We aim to develop novel nanosystems, based on SNs, for the efficient association of miRNA145 mimics and delivery to colorectal cancer cells to interefere cancer progression. We pursue two different strategies. Firstly, the cationic lipid sterylamine was incorporated to the nanoemulsions, in order to obtian cationic SNs and favour the association of miRNA mimics (SNs-ST-miRNA)[28-30]. Secondly, we propose the encapsulation of preformed DOTAP-miRNA complexes into SNs (SNs-DOTAP-miRNA) to provide additional protection for the associated miRNA mimics[31,32]. Transfection experiments and functional in vitro assays will be performed to determine the potential of the proposed formulations to developed innovative oncosuppressor therapies to colorectal cancer.

2. Materials and methods

2.1 Materials

Vitamin E (DL-α-tocopherol) was obtained from Merck (Darmstadt, Germany). Sphingomyelin and N-[1-(2,3-Dioleoyloxy)propyl]-N,N,N-trimethylammonium methylsulfate (DOTAP) were acquired from Lipoid (Ludwigshafen, Germany). Stearylamine (ST), agarose, 3-(4,5-Dimethyl-2-thiazolyl)-2,5-diphenyl-2H-tetrazolium bromide (MTT), Triton-X, heparin, *Mowiol*® 4-88, Minimum Essential Media (MEM), Dulbecco's Modified Eagle's Medium (DMEM), and Dulbecco's Phosphate Buffered Saline (PBS) were purchased from Sigma Aldrich (St.Louis, MO, United States). SH-PEG_{12}-C_{18} was supplied by Creative PEGworks (North Carolina, United States). N-[11-(dipyrrometheneboron difluoride)undecanoyl]-D-*erythro* sphingosylphosphoryl choline (C11 TopFluor® Sphingomyelin) was purchased from Avanti Polar

Lipids (Alabama, United States). miRNA145, miRNA145 scramble, and Cy5-modified miRNA145 were bought from Eurofins Scientific (Luxembourg) **(Table 1)**.

Table 1. Sequence of the different RNAs used in this study

RNAs	Sequence
miRNA 145	5'GUCCAGUUUUCCCAGGAAUCCCU 3'
miRNA scrambled	5'UUCUCCGAACGUGUCACGUUU 3'
Cy5-modified miRNA145	5'Cy5-GUCCAGUUUUCCCAGGAAUCCCU 3'

SYBR® Gold Nucleic Acid Gel Stain, RNAse free water, DNA ladder, penicillin and streptomycin were obtained from Invitrogen (Madrid, Spain). microRNA Purification Kit was acquired from Norgen Biotek Corporation (Zaragoza, Spain). qScript™ microRNA cDNA Synthesis kit, PerfeCta® Universal PCR Primer and PerfeCta® SYBR® Green SuperMix, Low Rox™ were bought from Quantabio, VWR International Eurolab (Barcelona, Spain). Primers, has-miR145-5p (5'GUCCAGUUUUCCCAGGAAUCCCU 3') and the house keeping small RNA control primer RNU6 (5'CTCGCTTCGGCAGCACA3', 5'AACGCTTCACGAATTTGCGT3') was purchased from IDT, (A Coruna, Spain) and Fisher Scientific (Madrid, Spain) respectively. Ultrapure Mili-Q water was used all throughout the experiments. Ethanol was of analytical grade and supplied from Thermo Fisher Scientific (Madrid, Spain). All other chemicals used were of reagent grade.

2.2 Preparation and characterization of SNs

SNs were formulated from vitamin E (VitE), sphingomyelin (SM), and SH-PEG_{12}-C_{18} (PEG) in a ratio VitE:SM:PEG of 10:1:0.1 w/w, by ethanol injection. In brief, the components were dissolved in a final volume of 110 µL in ethanol (organic phase, total lipid concentration 5.05 mg/mL) and injected with a syringe (0.5 mL) into 1 mL of ultrapure water under magnetic stirring. SNs were isolated from non-interacted compounds by ultracentrifugation (Beckman, California, United state) at 35000 rpm for 1 h at 15ºC in a 70.1 Ti rotor.

2.2.1 Size and zeta-potential measurements

Nanoemulsions were analyzed for their hydrodynamic size and polydispersity index (PDI) by dynamic light scattering (DLS) using a Zetasizer Nano ZS (Malvern Instruments, Worcestershire, UK) equipped with a standard λ = 633 nm laser as the incident beam. Nanoemulsions were diluted in ultrapure water and loaded into a disposable solvent resistant microcuvette (ZEN0040). The obtained data were analyzed based on cumulative analysis method for determination of mean hydrodynamic diameter and PDI. ζ–potential, a parameter indicative of the surface charge of the nanoemulsions, was measured by Lasser Doppler Anemometry (LDA) in the same equipment, using a dip-cell (DTS 1060). Each analysis was performed in triplicate.

2.2.2 Transmission electron microscopic (TEM)

The morphology of SNs was investigated using Transmission electron microscopy, TEM (JEOL JEM-2010) high-resolution microscope (Peabody, MA, USA). 10 µL of diluted nanoemulsions (1/10 in Mili-Q water) were placed on 400-mesh copper grids, incubated for 3 minutes at room temperature, and stained with 10 µL of 2% phosphotungstic acid solution for 1 minute. Excessing of phosphotungstic solution was removed with filter paper. The grids were washed five times in water droplets for 1 minute (each time) and dried overnight.

2.2.3 Nanoparticle tracking analysis (NTA)

NTA measurements were achieved with a NanoSight NS300 (Malvern Instruments, Worcestershire, UK), equipped with a sample chamber with a 488-nm laser. Samples were diluted 1/1000 in Mili-Q water. Samples were then injected in the sample chamber with sterile syringes (Omnifix®-F 1ml, Melsungen, Germany) until the liquid reached the tip of the nozzle. All measurements were performed at room temperature. The software used for capturing and analyzing the data was the NTA 3.3 Build 3.3.104. The samples were measured for 60 seconds. Three measurements of the same sample were performed for all of the formulations 3 times. The error bars displayed on the NTA graphs were obtained by the standard deviation of the different measurements of each sample. The mean particle size and SD values obtained by the NTA software

correspond to the arithmetic values calculated with the sizes of all the particles analyzed by the software.

2.3 Preparation and characterization of cationic stearylamine SNs and association of miRNA (SNs-ST-miRNA)

Cationic SNs were prepared upon addition of the cationic lipid, stearylamine (ST) to the organic phase at a ratio VitE:SM:PEG:ST 10:1:0.1:1 (w/w). Cationic SNs-ST were fully characterized as described in the previous section (2.2). miRNA was subsequently associated to SNs-ST by the establishment of electrostatic interactions by simple incubation. 10 µg of miRNA were incubated with SNs-ST at different miRNA:ST mass ratios (1:1, 1:2.5, 1:5, 1:7.5, and 1:10) in 100 µL of H_2O. The association of miRNA was analyzed by agarose gel electrophoresis (1% w/v in Tris-Acetate-EDTA (TAE) Buffer). Briefly, 0.5 µg of nucleic acids labeled with SYBR® Gold from solution, associated to the nanoemulsions, and the displacement with an excess of heparin were loaded into each well. Gel electrophoresis was run at 100V, 40 minutes in an electrophoresis cell, Ecogen (Barcelona, Spain). Gel images were obtained with a Molecular Imager® Gel Doc™ XR System (UV light 302 nm; Bio-Rad, Madrid, Spain). To ensure a correct association, displacement experiments were addiationlly peformed upon incubation of the formulations with a 25-fold heparin (with respect to the amount of miRNA) for 2 h at 37 °C.

2.4 Preparation and characterization of miRNA complexes with cationic lipids

Preparation of lipid complexes was attempted with miRNA and cationic lipids (ST or DOTAP). 10 µg of miRNA were incubated with cationic lipid at different miRNA: cationic lipid mass ratios (1:1, 1:5, 1:10, 1:15, and 1:20) in a total solution of 500 µL (H_2O 450 µL and EtOH 50 µL). They were characterized for their physicochemical properties as described in sections 2.2.

2.5 Loading of lipid complexes into SNs (SNs-DOTAP-miRNA)

miRNA:DOTAP complexes in a ratio of 1:15 were lyophilized using a VirTis genesis Lyophilizer (Warminster, PA, United States). Lyophilization steps contained thermal treatment, freezing, primary drying, and secondary drying. During freezing step, it had a condenser temperature of −40 °C and vacuum set point 200 mTorr for 60 min. At the end of the cycle, lipid complexes were finally obtained. Lyophilized lipid complexes were then suspended in 100 µL the organic phase containing VitE, SM, and SH-PEG_{12}-C_{18}, in a ratio of 10:1:0.1 (w/w), and this suspension was inmediatly injected to water (1mL) following the same methology reported in section 2.2. for the preparation of SNs, finally rendering lipid complex-loaded SNs (SNs-DOTAP-miRNA). Characterization was performed as disclosed in section 2.3. DOTAP-miRNA lipid complexes and broken SNs-DOTAP-miRNA formulation (upon incubation with a 25-fold heparin with respect to the amount of miRNA, for 2 h at 37 °C) were additionally placed as controls in the heparin displacement experiment.

2.6 *In vitro* cell uptake

Confocal laser-scanning microscope (TCS SP5, Leica Microsystems GmbH, Heidelberg) was used to observe cell uptake of fluorescent nanoemulsions. 24 h before the experiment SW480 cells (1×10^5 cells/well) were seeded onto 12 mm diameter glass coverslips in a 24-well plate in 0.5 mL of supplemented cell culture medium. SNs-ST-miRNA and SNs-DOTAP-miRNA were labelled with C11 TopFluor® Sphingomyelin (0.2 ng/µl), and Cy5-labelled miRNA (0.2 ng/µl) was also used to allow direct observation of the molecule of interest. After addition of 20 µl to the cells (500 ul of supplemented cell culture medium), they were incubated for 4 h at 37 ºC in the cell incubator. After that, cells were exhaustively washed with PBS and then fixed with paraformaldehyde (PFA; 4% v/v in PBS) in the dark at room temperature for 15 minutes. Cells were rinsed again with PBS, and cell nuclei were then counterstained with Hoechst 33342 (1:1000 in PBS) for 5 minutes. Then washed again with PBS. Lastly, 8 µL of *Mowiol*® 4-88 were used for mounting samples on coverslips. Preparations were conserved in the dark at -20ºC. The confocal laser scanning microscopic images were obtained with a 63×oil immersion objective for Hoechst 33342 (blue), TopFluor® Sphingomyelin (green), and Cy5 (red) respectively. (scanning speed 600

Hz, with an image resolution of 1024x1024 pixels). The colocalization ratio of Cy5 and TopFluor® Sphingomyelin was determined by LAS AF software (Barcelona, Spain).

Studies were also accomplished by Fluorescence-Activated Cell Sorting (FACScan flow cytometer, BD biosciences, San Jose, CA, United States). For this experiment, the cells were transfected with same amount of fluorescent formulations as mentioned in confocal study. They were incubated for 4 h at 37 ºC in the cell incubator and washed with PBS. Then, the cells were trypsinized and resuspended in 0.5 mL of PFA (approx. $1x10^5$ cells/mL) prior to analysis. The results were analysed using Flowjo 8.7 (Ashland, OR, United States).

2.7 Transfection efficiency

SNs-ST-miRNA and SNs-DOTAP-miRNA were evaluated for their transfection efficacy in SW480 human coloreatal cancer cells. Both types of nanoemulsions were formulated with miRNA145, and with a scrambled sequence miRNAScr. SW480 cells were seeded in 6-well plates (5×10^5 cells/well) and incubated in DMEM for 24 h. Formulations were then added (SNs-ST-miRNA145, SNs-ST-miRNAScr, SNs-DOTAP-miRNA145, and SNs-DOTAP-miRNAScr), being the dose 2 µg of miRNA in a final volume of 2 mL of fresh cell culture medium. The nanoemulsions were removed after 4 h of incubation, cells washed, and fresh media added (2 mL). The transfection efficiency was determined 72 h post transfection by quantitative real-time PCR (qRT-PCR) (Stratagene Mx 3000, Agilent Technologies). According to the manufacturer's protocol of Norgen Biotek Corporation, microRNA Purification Kit (ON, Canada), the total miRNA was extracted from SW480 cells. miRNA concentration and purity were evaluated with UV spectrophotometry (Nanodrop, Spectrophotometer ND-100, Thermo Scientific). Extracted RNA samples were measured and diluted to have the same amount of RNA (120 ng). Next, the reverse RNA transcription to cDNA was carried out using qScript™ microRNA cDNA Synthesis Kits (Quanta Biosciences). The qRT-PCR was performed using PerfeCta® MicroRNA Assays (Quanta Biosciences), with a primer for miR 145 (has-miR145-5p, IDT). Small nuclear RNA, RNU-6 was employed as an endogenous house-keeping gene to normalize the miRNA amount (5'CTCGCTTCGGCAGCACA3', 5'AACGCTTCACGAATTTGCGT3'). PCR cycle consisted of activation at 95ºC (2 min), denaturation at 95ºC (5 sec), and annealing at 60 ºC (30 sec) for 40

cycles. Quantitative data were analyzed by utilizing the MxPro software (Agilent Tecgnologies). The relative miRNA145 expression level was calculated based on comparative $2^{-\Delta\Delta CT}$ method in relation to RNU6 and normalized to that obtained from non-treated cells.

2.8 Functional assays

SW480 cells were seeded in 24-well plates (2.5×10^4 cells/well) and incubated in DMEM for 24 h. Then the cells were transfected as described in the previous section. For cell proliferation, cells were harvested at 72 h post transfection and then counted manually in neubauer-improved cell counting chamber, depth 0.100 mm, 0.0025mm^2 (Marienfeld, germany). With respect to the cell migration assay, after the transfection, the cells were trypsinized and counted. Then 2×10^5 cells/well were planted onto 24-well plate, artificail wounds were created on the confluent cell monolayer using 200 µL pipette tip. Wounded cells were gently washed PBS for 3 times to remove the detached cells and cultures in 5% CO_2 at 37 ºC. The wound closer was observed and photographed at time point 0,24,48,72, and 96 h under microscope (Leica type 090-135.00, Germany). For colony forming assay, transfected cells were seeded at a density of 200 cells/well in 12-well plates and cultured at 37°C for 2 weeks. Cells were stained with MTT solution (5mg/ml) and photographed. The images were analyzed using ImageJ software.

2.8 Statistic analysis

Differences were statistically determined by two-way ANOVA. All statistical analysis was perfomed using GraphPad Prism (Version 6.0 software). A p value < 0.05 was considered to be significant (**** $p \leq 0.0001$, *** $p \leq 0.001$, and ** $p \leq 0.01$).

3. Results and discussion

3.1 Development and characterizations of sphingomyelin nanoemulsions loaded with miRNA mimics

Nanoemulsions are thermodynamically stable isotropic systems in which two immiscible liquids, usually oil and water, are mixed to form a single phase with the help of suitable surfactants[33,34]. They have been extensively applied throughout the pharmaceutical industry for delivery of poorly water-soluble drugs. For cationic nanoemulsions, they were widely used for gene delivery by utilizing cationic lipids such as DOTMA, DOTAP, linear polyethylenimine grafted with cholesterols, and stearylamine, allowing association of nucleic acids on the surface of nanoemulsions[35-39]. In this work, we aim to study the potential of SNs for the delivery of oncosuppressor miRNAs to cancer cells. SNs are very simple biocompatible and biodegradable formulations produced by ethanol injection in a simple step, which main components are the oil vitamin E (VitE) and the sphingolipid sphingomyelin (SM) acting as a surfactant. Lipid PEG derivatives (SH-PEG_{12}-C_{18}) were also included in a smaller proportion to improve the stability of the formulation after intravenous injection[40,41]. In this particular work, we additionally incorporated small amounts of cationic lipids to increase the association efficiency of miRNA mimics and the capacity of the resulting formulation to efficiently transfect colorectal cancer cells[42-44]. Our first strategy for association of miRNA mimics was to incubate the nucleic acids onto the surface of preformed cationic SNs. The second approach was to prepare lipid complexes (DOTAP and miRNA) for subsequent encapsulation into SNs. A schematic representation of both approaches is shown in **Figure 1**.

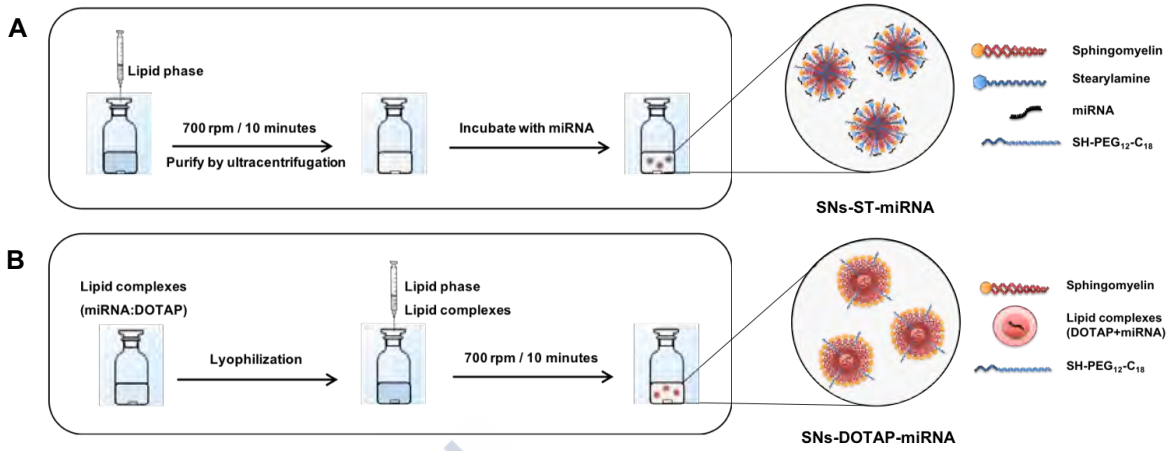

Figure 1. Preparation and Scheme illustrated components of SNs-ST-miRNA (A) and SNs-DOTAP-miRNA (B).

3.2. Adsorption of miRNA to preformed cationic SNs

Blank SNs were prepared upon injection of lipids VitE:SM:PEG dissolved in ethanol (in a proportion 10:1:0.1 w/w), into ultrapure water. This is a green and simple procedure that renders reproducible formulations. SNs have a mean average size of 131 ± 8 nm, a PDI of 0.2, and a slightly negative surface charge of -13 ± 7. NTA analysis correlates with DLS analysis, confirming the size and the relatively mono-disperse size distribution (**Figure 2)**, and giving a concentration of $4.2x10^{12} \pm 2.1x10^{10}$ particles/ml.

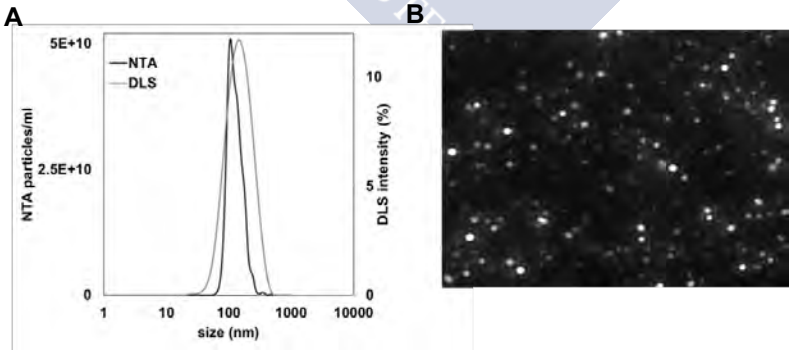

Figure 2. Size distribution graph of SNs measured from nanoparticle tracking analysis (NTA) and dynamic light scattering (DLS) (A) and video frame of SNs acquired by NTA (B).

Next step consisted in the addition of a cationic lipid to get cationic SNs. Because the interaction between cationic lipids and nucleic acids is intensely influenced by charge-charge interaction, lipid pK_a is expected to play a significant role affecting the association efficiency of nucleic acids in lipidic nanosystems[45]. We selected stearylamine (pK_a=10.6) to formulate cationic SNs, since it presents a positively charged primary ammonium group over a wide range of pH[46,]. Additionally, steraylamine has already been reported for the preparation of cationic nanoemulsions for delivery of nucleic acids[47,48]. As shown in **Table 2**, nanoemulsions with VitE:SM:PEG:ST ratios from 10:1:0.1:0.1 to 10:1:0.1:1 rendered monodispersed populations with a mean size of around 100 nm. However, SNs-ST with a ratio VitE:SM:PEG:ST above 10:1:0.1:1.5 had a higher dispersion. As expected, SNs-ST were positively charged, and the zeta potential increased as the amount of ST does. Based on this physicochemical properties, VitE:SM:PEG:ST 10:1:0.1:1 (SNs-ST) were selected for further studies

Table 2. Hydrodynamic size, polydispersity index (PDI), and zeta potential (ζ-potential) of SNs-ST

Formulations	Ratio (w/w) VitE:SM:PEG:Cationic lipid	Size (nm)	PDI	ζ-Potential (mV)
SNs-ST	10:1:0.1:0.1	104 ± 10	0.2	+40 ± 12
	10:1:0.1:0.5	115 ± 11	0.2	+44 ± 4
	10:1:0.1:1	109 ± 11	0.2	+46 ± 6
	10:1:0.1:1.5	99 ± 12	0.3	+48 ± 11
	10:1:0.1:2	104 ± 22	0.3	+51 ± 3

Association of miRNA mimics was attempted next. Increasing amounts of SNs-ST were added over a solution of miRNA (10 μg) (miRNA:ST ratios from 1:1 to 1:10) and incubated under magnetic stirring. The characteristics of the resulting formulations are shown in **Table 3**. Increasing the proportion of SNs-ST, and therefore of cationic groups, mainly affect the surface properties of the nanosystems. While proportions of miRNA:ST 1:1 and 1:2.5 rendered negative nanosystems, there is an inversion on the zeta potential for formulations prepared with the highest proportion of ST (miRNA:ST 1:10). These variations in the surface properties are an evidence of the efficient adsorption of the oligonucleotides to SNs-ST, in agreement with other reports in the field[49]. Sizes

are around 150-170nm, with low polidispersity indexes, in all cases except for the ratios miRNA:ST 1:5 and 1:7.5, for which a massive aggregation is observed. This can be related to the neutralization of the surface charge, as reported for other cationic lipid-based nanopaticles[50-52]. Liu *et al*., demonstrated that when the ζ-potential values was closed to zero, the size of solid lipid nanoparticles/miRNAcomplexes became larger. This was probably because the nanoparticles with this weight ratio were in an unstable state and easily aggregated. This also supported by Martini *et al*., that the highest size of nanoemulsions was observed when the ζ-potential values were closer to neutrality. Teixeira *et al*., explained about the electrostatic interaction between positively charged stearylamine and negatively charged nucleotides that as long as the positive amine groups from the stearylamine are not neutralized by ion pairing with DNA phosphate groups, the overall droplet zeta potential will remain positive, preventing flocculation.

The efficient association of the miRNA to the surface of SNs-ST-miRNA was confirmed by a gel electrophoresis assay (data not shown). SNs-ST-miRNA with a miRNA:ST mass ratio 1:10 were selected for the transfection experiments. Analysis by transmission electron microscopy (TEM) show a spherical morphology, comparable to plain SNs-ST, and analystis by NTA corroborated the data obtained by DLS (**Figure 3**).

Table 3. Hydrodynamic size, polydispersity index (PDI), and zeta potential (ζ-potential) of SNs-ST-miRNA.

Formulations	Mass ratio (w/w)* miRNA:ST	Size (nm)	PDI	ζ-Potential (mV)
SNs-ST-miRNA	1:1	155 ± 2	0.2	-30 ± 3
	1:2.5	172 ± 4	0.2	-15 ± 2
	1:5		Aggregate	
	1:7.5		Aggregate	
	1:10	148 ± 8	0.2	+26± 3

*miRNA was maintained constant (10 ug per formulation).

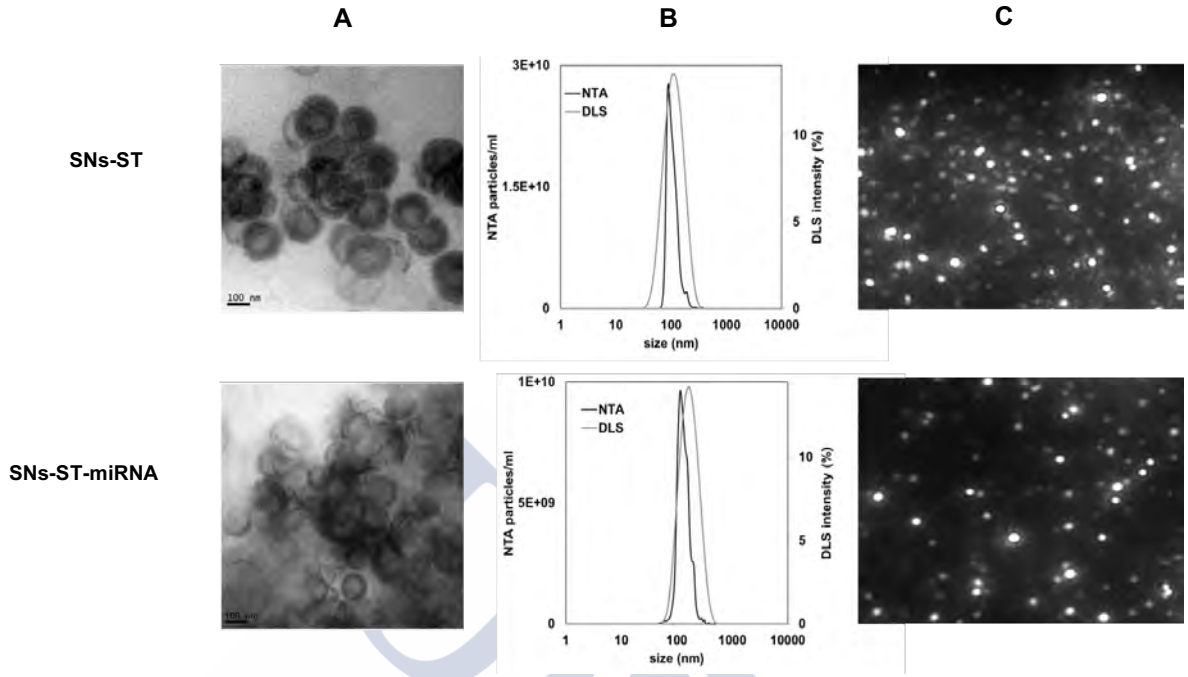

Figure 3. Characterization of SNs-ST and SNs-ST-miRNA. Transmission electron microscopy (TEM) images (A). Size distribution graph measured from nanoparticle tracking analysis (NTA) and dynamic light scattering (DLS) (B), and video frame acquired by NTA (C).

3.3 Development and characterizations of of lipid complexes and encapsulation into SNs

Lipid complexes of miRNA-ST and miRNA-DOTAP, prepared at different miRNA:cationic lipid mass ratios were characterized with respect to their size, PDI, and surface charge (**Table 4**). In general, most of the complexes had a broad PDI, and were therefore disregarded. Complexes with a PDI of 0.3 were obtained for complexes with a miRNA:cationic lipid ratio 1:15. Due to the smallest size of the miRNA:DOTAP complexes 1:15, around 80 nm, these were selected for futher association to SNs. The incorporation of DOTAP into cationic nanocarriers is commonly described. It is available as GMP material for clinical studies and able to hold a positive charge at a pharmaceutically relevant pH. Due to the anionic electrostatic charge on the lipid bilayers, cationic nanoplatforms prepared from DOTAP have been shown to be the

effective carriers for the anionic nucleotides RNA and DNA. They mediate high encapsulation efficiencies for nucleotides and high cellular uptakes and transfection efficiencies[53].

Table 4. Hydrodynamic size, polydispersity index (PDI), and zeta potential (ζ-potential) of lipid complexes

Lipid complexes	Mass ratio (w/w)* miRNA:Cationic lipid	Size (nm)	PDI	ζ-Potential (mV)
miRNA-ST	1:1	466± 91	0.4	-9 ± 4
	1:5	76 ± 86	0.7	+17 ± 4
	1:10	158 ± 96	0.6	+28 ± 6
	1:15	189 ± 54	0.3	+29± 4
	1:20	164 ± 45	0.3	+31 ± 3
miRNA-DOTAP	1:1	15 ± 18	0.7	-10 ± 4
	1:5	68 ± 73	0.7	+6 ± 7
	1:10	46 ± 34	0.4	+20 ± 7
	1:15	83 ± 16	0.3	+32 ± 3
	1:20	123 ± 80	0.5	+32 ± 3

*miRNA was maintained constant (10 ug per formulation)

The pre-condensation of DNA with polycations has been described to be a favorable method to increase *in vitro* and *in vivo* transfection efficiency of lipid emulsions. This enhancement is due to the formation of compacted complexes supporting encapsulation of nucleic acid and additional protection against enzymatic degradation[54-56]. For example, the complexation of a model plasmid with different cationic lipids via hydrophobic ion pairing (HIP), reduced hydrophilicity and enabled its incorporation into a lipophilic carrier, which provided additional protection in biological environment[57]. A similar strategy has also been described for encapsulation of other hydrophilic biomolecules to be uploaded into lipid nanosystems. The modification by HIP has been described to increase the lipohilicity of peptides, allowing further association to lipid nanosystems and improving protection against enzymatic degradation as well as bioavailability[58].

In our case, we follow a similar approach for complexation of miRNA mimics and further association to SNs. Within this study, HIP was established among the amino group of the cationic lipid DOTAP and the negatively charged phosphate group of the RNA backbone. Resulting

complexes were freezed-dried and subsequently resuspended in the ethanol phase containing the lipid mixture (VitE:SM:PEG 10:1:0.1), prior injection onto ultrapure water (see Figure 1B). SNs-DOTAP-miRNA nanosystems exhibited a mean particle size of 124 ± 9 nm, a PDI of 0.2, and a postivie ζ-potential of +37 ± 3. We performed a gel electrophoresis assay to prove that miRNA was efficiently complexed by the cationic DOTAP, and that association to SNs actually provide an additional protection. As it can be observed in **Figure 4**, no free RNA was shown in both formulations. Free miRNA was only observed in broken SNs-DOTAP-miRNA with heparin, not in SNs-DOTAP-miRNA, indicating the dissociation was prevented due to the association of the complexes to SNs. Transmission electron microscopy (TEM) reveal the spherical morphology of SNs-DOTAP-miRNA (**Figure 5**). DLS and NTA data prove that SNs-DOTAP-miRNA nanosystems are homogenoenous in size and monodisperse.

.

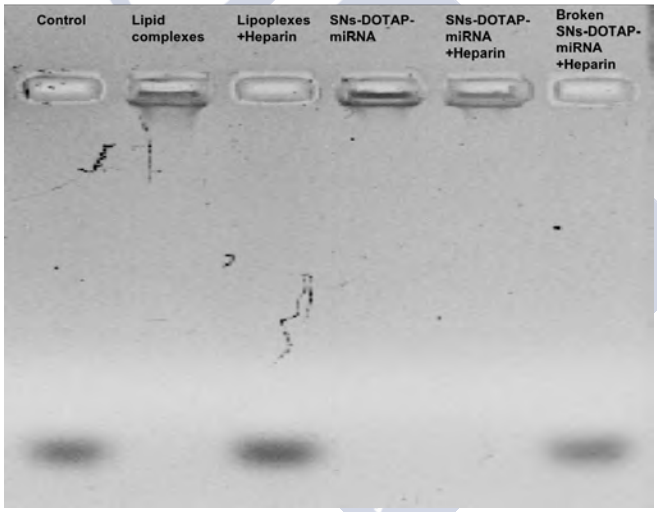

Figure 4. Electrophoresis of lipid complexes and SNs-DOTAP-miRNA. A displacement experiment upon incubation with a 25-fold excess of heparin (w/w) for 2 hours at 37 °C allowed the migration of the associated miRNA. Experiment was carried in agrarose gel 1% 100 Volts, 40 minutes (control miRNA 0.5µg).

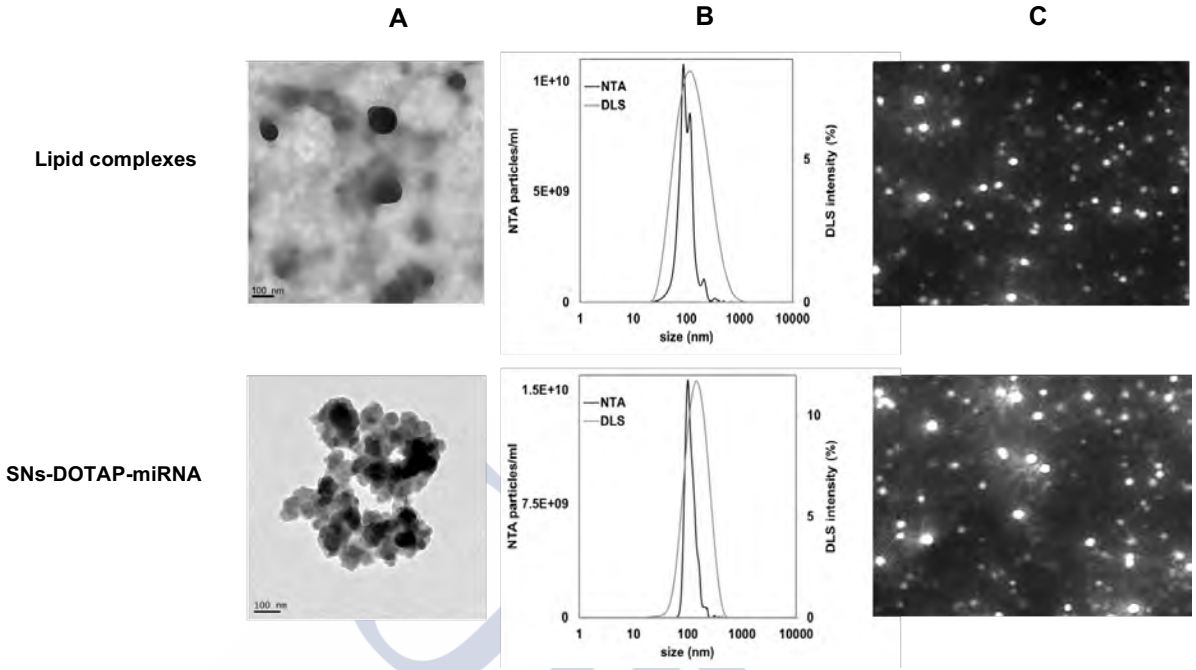

Figure 5. Characterization of lipid complexes and SNs-DOTAP-miRNA. Transmission electron microscopy (TEM) images (A). Size distribution measured from nanoparticle tracking analysis (NTA) and dynamic light scattering (DLS) (B), and video frame acquired by NTA (C).

3.4 *In vitro* cell uptake and transfection efficiency

It is recognized that the physicochemical properties of nanoparticles impact their cellular uptake mechanism. The surface charge of nanocarriers plays an important role in their cellular uptake and internalization pathway. Cationic nanocarriers can bind to sulfated proteoglycan of cell surfaces through electrostatic interactions and subsequently be internalized by pinocytosis and endocytosis[59]. We wanted to investigate if the developed nanosystems were able to efficiently interact with cancer cells and deliver their payload with a similar efficiency. Main differences are related to the location of the miRNA (disposed at the nanoparticle surface for SNs-ST-miRNA nanosystems and complexed with cationic lipids and further entrapped into SNs for SNs-DOTAP-miRNA nanosystems) and to their negative or positive surface charge, for SNs-ST-miRNA and SNs-DOTAP-miRNA nanosystems, respectively.

Cell uptake studies with double fluorescent SNs-ST-miRNA and SNs-DOTAP-miRNA (miRNA was labelled with Cy5, Cy5-miRNA, and SM with green TopFluor®, TopFluor®-SM) in SW480 (human colon cancer cells; cell nuclei counterstained with Hoechst) were performed by confocal laser-scanning microscopy. As it can be obsvered (**Figure 6A**), both formulations were efficiently internalized by the cells (green signal), and the associated Cy5-miRNA was transported to the cell cytoplams (red signal). Importantly, merged images illustrated that SNs-ST-miRNA and SNs-DOTAP-miRNA were uptaken in assembled form of stable nanoemulsions, as we can see a good co-localization of the green and red signals in both cases.

Complementary FACS analysis was used to verify the results and provide quantitative data (**Figure 6B-C**). Three controls were established in the FACS experiment to observe the signal of fluorescent dyes on nanoemulsion and distinguish from double-negative control cells (Cy5 -, TopFluor® -) located in quadrant 4 (Q4) (cells without treatment), cells positive for Cy5 (Cy5 +, TopFluor® -) localized in quadrant 1 (Q1) (cells incubated with SNs-ST-miRNA prepared only with miRNA-Cy5), and cells cells positive for TopFluor® (Cy5 -, TopFluor® +) localized in quadrant 3 (Q3) (cells incubated with SNs-ST-miRNA prepared only with TopFluor®-SM). Double positive cells (Cy5 +, TopFluor® +), were observed in the double-positive quadrant 2 (Q2). Importantly, cells treated with double labeled nanoemulsions (either SNs-ST-miRNA and SNs-DOTAP-miRNA), were indeed observed in Q2, indicating that the nanoemulsions labeled with TopFluor® effectively delivered miRNA-Cy5 into the cells, both molecules travelling together. SNs-DOTAP-miRNA showed higher co-localization of Cy5-miRNA and TopFluor®-SM signals compared to SNs-ST-miRNA, related to a higher population in Q2 (92.8% compared with 57.7% respectively). The signal of TopFluor®-SM showed almost the same intensity for both formulations stating the ability of the SNs-based formulation to penetrate the tumor cells. On the contrary, SNs-DOTAP-miRNA showed higher intensity of Cy5-miRNA compared to SNs-ST-miRNA (**Figure 6B-C**). This suggest that our second approach, preparation of miRNA-lipid complexes prior to the synthesis of SNs-DOTAP-miRNA, is more efficient for the intracellular delivery of miRNA, than having it adsoverd onto the surface of SNs (SNs-ST-miRNA), which may lead to a partial detachement from the nanostructure and subsequent enzymatic degradation.

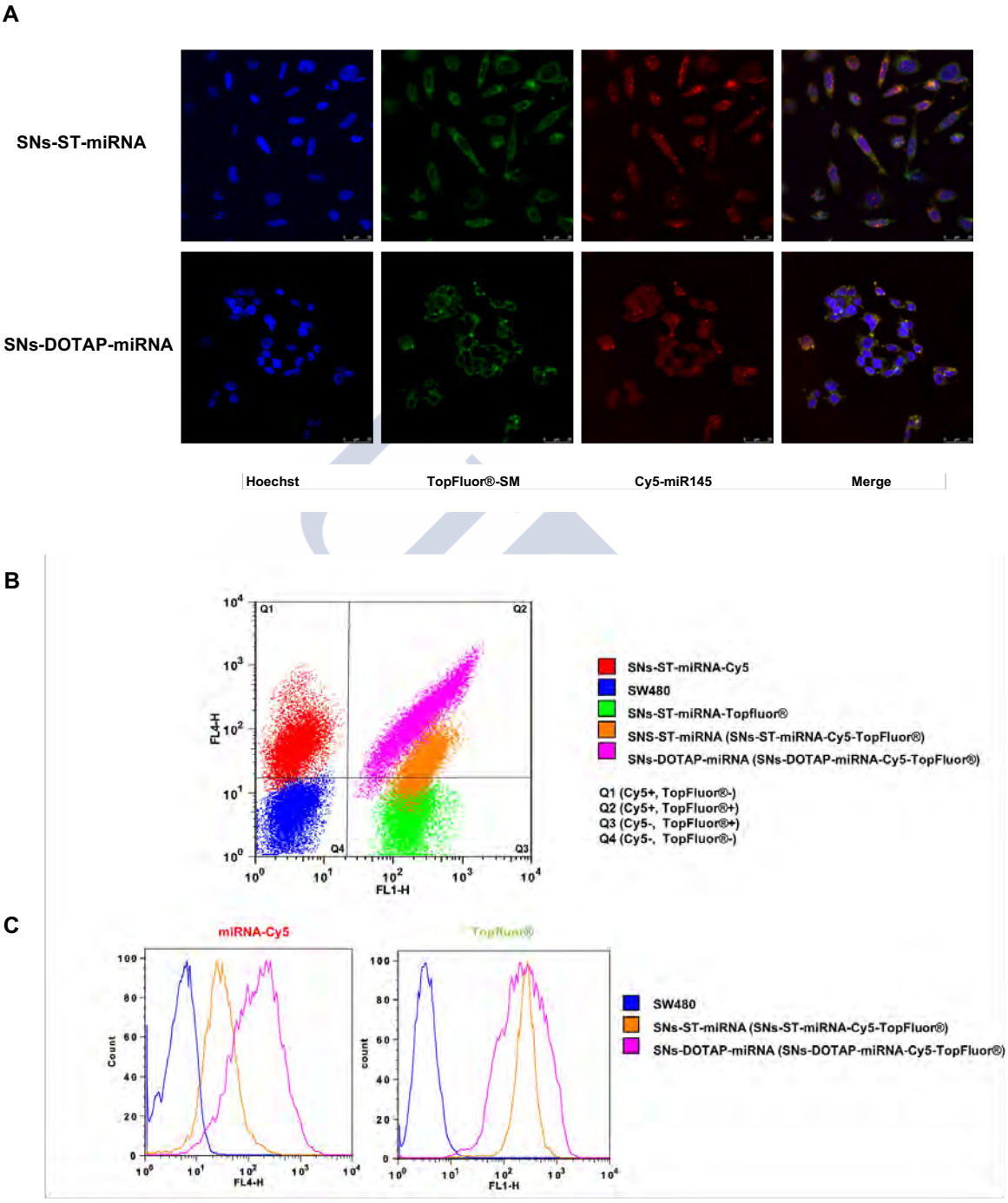

Figure 6. Internalization of SNs-ST-miRNA and SNs-DOTAP-miRNA in SW480. Maximal projection of confocal images upon incubation of nanoemulsions labeled with TopFluor® Sphingomyelin (green), and Cy5-miRNA (red) (4 h at 37 ºC). Cell nuclei were counterstained with Hoechst (blue) (A). FACS results showing controls of untreated control cells (Q4, blue), cells positive for Cy5 (treated with SNs-ST-miRNA-Cy5, Q1, red), cells positive for TopFluor® (treated

with SNs-ST-miRNA-TopFluor®, Q3, green), and double positive cells for Cy5 and TopFluor® (treated with either SNs-ST-miRNA-Cy5-TopFluor®, Q2, orange, or SNs-DOTAP-miRNA-Cy5-TopFluor®, Q2, pink) (B). FACS Histogram of two different fluorophores, TopFluor® and Cy5, obtained for cells treated with double labeled nanoemulsions, (SNs-ST-miRNA-Cy5-TopFluor®, orange, or SNs-DOTAP-miRNA-Cy5-TopFluor®, pink) (C).

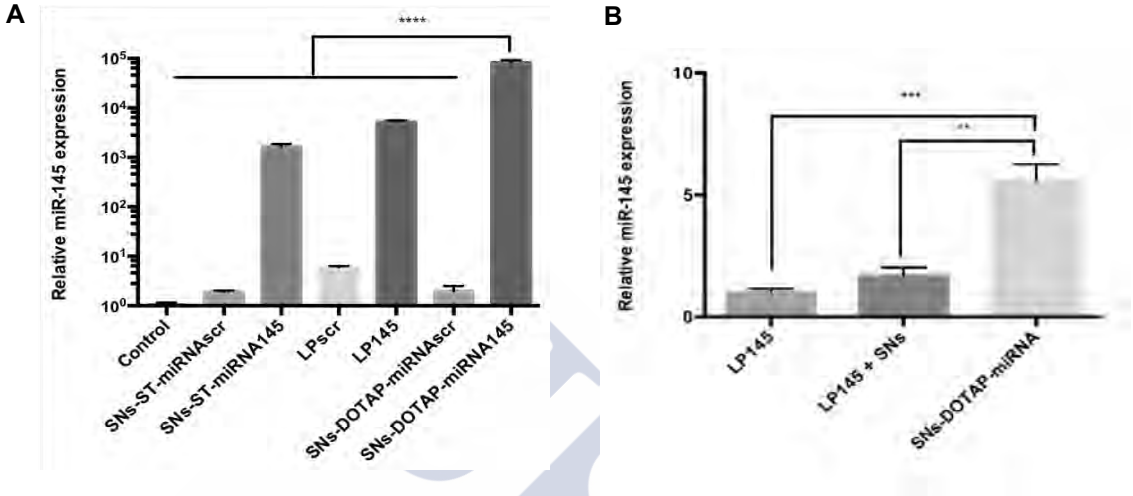

Figure. 7. Expression of miR145 after transfection with SNs-ST-miRNA145, Lipid complexes145 (LP145), and SNs-DOTAP-miRNA145 nanosystems (as well as nanosystems prepared with the scrambled sequence, SNs-ST-miRNAscr, LP scr, and SNs-DOTAP-miRNAscr (A). Relative expression of miR145 after transfection with LP145, a physical mixture of LP145 and SNs, and SNs-DOTAP-miRNA145 in SW480 cells (B). (2 µg miRNA/well in 6-well plates, 4 h incubation, 72 h post-transfection, data normalized against RNU6) (**** $p \leq 0.0001$, *** $p \leq 0.001$, and ** $p \leq 0.01$).

To study the transfection efficiency, and ability to incrase the levels of intracellular miRNA145, SW480 cells were transfected with SNs-ST-miRNA and SNs-DOTAP-miRNA, lipid DOTAP-miRNA145 complexes (LP145) for control, and with the same formulations but with a scrambled sequence, and samples analysed by qRT-PCR. (**Figure 7A**). Results show that all formulations were able to efficiently increase intracellular miRNA 145 levels compared to control cells, SNs-DOTAP-miRNA145 showing the higher transfection efficiency (64-fold higher than SNs-ST-miRNA). This is because the preformed lipid complexes later encapsulated in SNs-DOTAP-miRNA, provide a supportive protection for miRNA145 and mediate an improved miRNA145 delivery. Moreover, these cationic lipid complexes might be able to destabilize the cell membranes by themselves and penetrate into the cells even if dissociated from the nanoemulsions[60]. Despite of this, when we compared the transfection efficiency of the cationic lipid complexes (LP145), a physical mixture of LP145 and SNs, and SNs-DOTAP-miRNA, results highlighted the

the benefits of incorporating lipid complexes into SNs (**Figure 7B**). The results obtained with SNs-DOTAP-miRNA nanoemulsions are superior to those recently published with cationic microRNA-loaded nanoparticles in HTC-116 cells (11-fold increase)[22], miRNA-145-loaded magnetic nanoparticles in AsPC-1cells (19-fold increase) and HPAF-II cells (4-fold increase)[23], miRNA145-loaded cationic liposomes in HepG2 cells (9-fold increase)[61], and miRNA145 associated to a lentiviral vector in SW620 cells (8.2-fold increase)[62]. Therefore, SNs-DOTAP-miRNA145 nanosystems were selected for further anticancer activity experiments.

3.4 Anticancer activity

Finally, to determine whether SNs-DOTAP-miRNA145 can suppress growth in SW480 colorectal cancer cells, cell proliferation assays were conducted. The cell number of cells treansfected with SNs-DOTAP-miRNA145 was significantly reduced with respect to both untreated control cells and cells treated with their scramble formulations (**Figure 8A**). In addition, a colony formation assay was subsequently performed. Our data indicated a significant reduction in colony formation in SNs-DOTAP-miRNA145 cells as compared to control cells (**Figure 8B**). Wound-healing studies finally confirmed that our proposed treatment also affects cell migration. Indeed, the artificially created wound of SW480 treated with SNs-DOTAP-miRNA145 remained almost inalterable at the end of the study, opposibtel to what observed in the case of untreated cells and cells treated with the scrambled sequence SNs-DOTAP-miRNAscr (the wound closure was superior to 50%) (**Figure 8C**). These results are in agreement with previously published work with biodegradable PLGA and magnetic nanoparticles[22, 23], and clearly indicated that SNs-DOTAP-miRNA145 inhibited cell growth and migration in colorectal cancer cells and is a potential treatment for avoiding tumor progression in colorectal cancer.

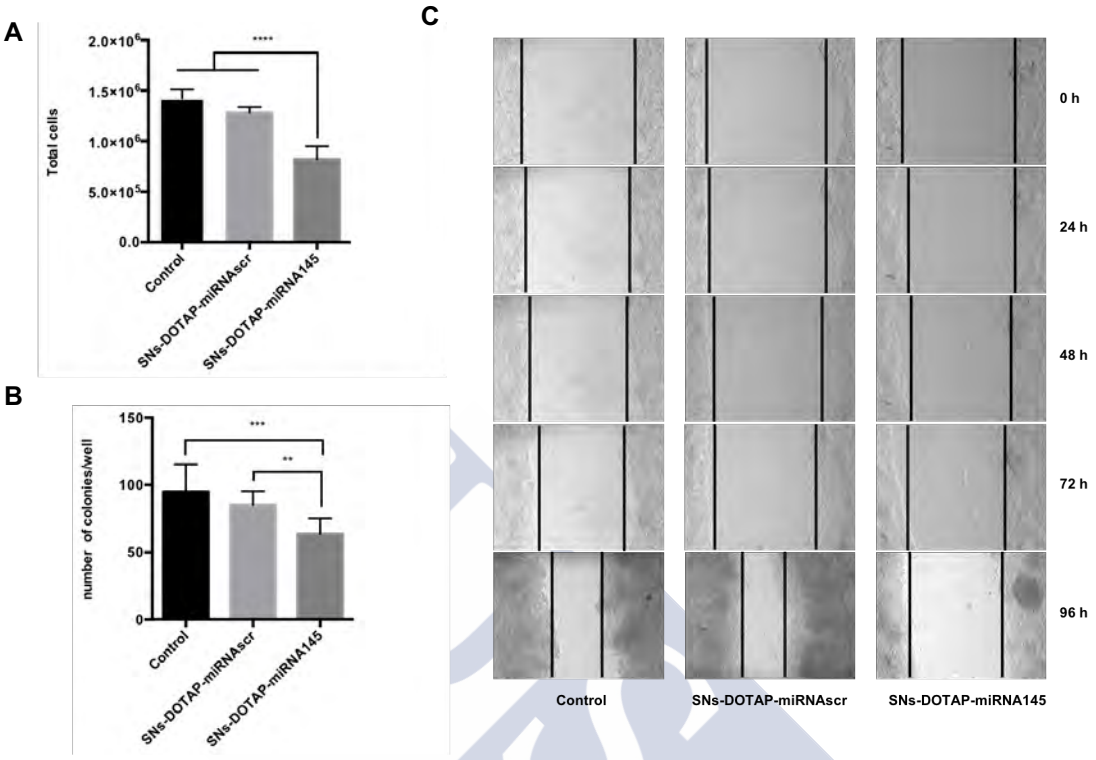

Figure. 8. Anticancer activity of SNs-DOTAP-miRNA145 in SW480 transfected cells. Proliferation of SW480 cells 72 h post-transfection (**** $p \leq 0.0001$) (A). Quantitative analysis of colony numbers, 2 weeks after transfection is shown (*** $p \leq 0.001$ and ** $p \leq 0.01$) (B). Representative images showing cell migration in wound healing assay, of untreated control cells and cells treated with SNs-DOTAP-miRNA145 and the same formulation with the scrambled sequence (SNs-DOTAP-miRNAscr). Images were taken 0,24,48,72, and 96 h after treatment. The dark lines designated the rough margins of the SW480 cells (C).

5. Conclusion

We have successfully proved the potential of SNs for the efficient association of miRNA145 mimics to interfere cancer progression in colorectal cancer. We pursue two different strategies to associate miRNA (adsorption to the surface of SNs, SNs-ST-miRNA, and preformation of lipid complexes for further encapsulation, SNs-DOTAP-miRNA). Both formulations showed capacity to deliver miRNA145 intracellularly and thereafter efficiently restore its expression. Restitution of miRNA145 from the delivery of SNs-DOTAP-miRNA demonstrated to be related to a decreasing tumor proliferation, colony forming, and migration capacity. Further investigation of this SNs-DOTAP-miRNA in an animal models of colorectal cancer is required to confirm the potential of this platform for the development of efficient miRNA replacement therapies.

References

(1) Miller, K. D.; Siegel, R. L.; Lin, C. C.; Mariotto, A. B.; Kramer, J. L.; Rowland, J. H.; Stein, K. D.; Alteri, R.; Jemal, A. Cancer Treatment and Survivorship Statistics, 2016. *CA. Cancer J. Clin.* **2016**, *66*, 271–289.

(2) Chen, H.; Zhang, W.; Zhu, G.; Xie, J.; Chen, X. Rethinking Cancer Nanotheranostics. *Nat. Rev. Mater.* **2017**, *2*, 17024.

(3) Cui, H.; Wang, J. Progress in the Development of Nanotheranostic Systems. *Theranostics* **2016**, *6*, 915–917.

(4) Jasinski, D.; Haque, F.; Binzel, D. W.; Guo, P. Advancement of the Emerging Field of RNA Nanotechnology. *ACS Nano* **2017**, *11*, 1142–1164.

(5) Von Roemeling, C.; Jiang, W.; Chan, C. K.; Weissman, I. L.; Kim, B. Y. S. Breaking Down the Barriers to Precision Cancer Nanomedicine. *Trends Biotechnol.* **2017**, *35*, 159–171.

(6) Barenholz, Y. Doxil® - The First FDA-Approved Nano-Drug: Lessons Learned. *J. Control. Release* **2012**, *160*, 117–134.

(7) Allen, T. M.; Cullis, P. R. Liposomal Drug Delivery Systems: From Concept to Clinical Applications. *Adv. Drug Deliv. Rev.* **2013**, *65*, 36–48.

(8) Hare, J. I.; Lammers, T.; Ashford, M. B.; Puri, S.; Storm, G.; Barry, S. T. Challenges and Strategies in Anti-Cancer Nanomedicine Development: An Industry Perspective. *Adv. Drug Deliv. Rev.* **2017**, *108*, 25–38.

(9) Bartel, D. P.; Lee, R.; Feinbaum, R. MicroRNAs : Genomics , Biogenesis , Mechanism , and Function Genomics : The miRNA Genes. **2004**, *116*, 281–297.

(10) Bader, A. G.; Brown, D.; Stoudemire, J.; Lammers, P. Developing Therapeutic microRNAs for Cancer. *Gene Ther.* **2011**, *18*, 1121–1126.

(11) Chen, Y.; Gao, D. Y.; Huang, L. In Vivo Delivery of miRNAs for Cancer Therapy: Challenges and Strategies. *Adv. Drug Deliv. Rev.* **2015**, *81*, 128–141.

(12) Conde, J.; Edelman, E. R.; Artzi, N. Target-Responsive DNA/RNA Nanomaterials for microRNA Sensing and Inhibition: The Jack-of-All-Trades in Cancer Nanotheranostics? *Adv. Drug Deliv. Rev.* **2015**, *81*, 169–183.

(13) Liu, Y.; Zhang, Y.; Wu, H.; Li, Y.; Zhang, Y.; Liu, M.; Li, X.; Tang, H. MiR-10a Suppresses Colorectal Cancer Metastasis by Modulating the Epithelial-To-Mesenchymal Transition and Anoikis. *Cell Death Dis.* **2017**, *8*.

(14) Dong, J.; Xiao, D.; Zhao, Z.; Ren, P.; Li, C.; Hu, Y.; Shi, J.; Su, H.; Wang, L.; Liu, H.; et al. Epigenetic Silencing of microRNA-137 Enhances ASCT2 Expression and Tumor Glutamine Metabolism. *Oncogenesis* **2017**, *59*.

(15) Zhang, Y.; Wang, Z.; Chen, M.; Peng, L.; Wang, X.; Ma, Q.; Ma, F.; Jiang, B. MicroRNA-143 Targets MACC1 to Inhibit Cell Invasion and Migration in Colorectal Cancer. *Mol. Cancer* **2012**, *11*. 1-9

(16) Slaby, O.; Svoboda, M.; Fabian, P.; Smerdova, T.; Knoflickova, D.; Bednarikova, M.; Nenutil, R.; Vyzula, R. Altered Expression of miR-21, miR-31, miR-143 and miR-145 Is Related to Clinicopathologic Features of Colorectal Cancer. *Oncology* **2008**, *72.* 397-402

(17) Akao, Y.; Nakagawa, Y.; Naoe, T. MicroRNA-143 and -145 in Colon Cancer. *DNA Cell Biol.* **2007**, *26.*311-320.

(18) Chen, X.; Guo, X.; Zhang, H.; Xiang, Y.; Chen, J.; Yin, Y.; Cai, X.; Wang, K.; Wang, G.; Ba, Y.; et al. Role of miR-143 Targeting KRAS in Colorectal Tumorigenesis. *Oncogene* **2009**, *28.* 1385-1392.

(19) Xie, Y.; Zong, P.; Wang, W.; Liu, D.; Li, B.; Wang, Y.; Hu, J.; Ren, Y.; Qi, Y.; Cui, X.; et al. Hypermethylation of Potential Tumor Suppressor miR-34b/c Is Correlated with Late Clinical Stage in Patients with Soft Tissue Sarcomas. *Exp. Mol. Pathol*. **2015**, *98.* 446-454.

(20) Beg, S. M.; Brenner, J. A.; Sachdev, J; Borad, M;. Kang, Y.; Stoudemire, J.; Smith, S.; Bader, G. A.; Kim, S.; Hong, S. D.; Phase I study of MRX34, a liposomal miR-34a mimic, administered twice weekly in patients with advanced solid tumors. *Invest New Drugs.* **2017**, *35*. 180-188.

(21) Chakraborty, C.; Sharma, A. R.; Sharma, G.; Doss, C. G. P.; Lee, S. S. Therapeutic MiRNA and SiRNA: Moving from Bench to Clinic as Next Generation Medicine. *Molecular Therapy - Nucleic Acids*, **2017**, *8*. 132-143.

(22) Liang, G.; Zhu, Y.; Jing, A.; Wang, J.; Hu, F.; Feng, W.; Xiao, Z.; Chen, B. Cationic MicroRNA-Delivering Nanocarriers for Efficient Treatment of Colon Carcinoma in Xenograft Model. *Gene Ther*. **2016**, *23*. 829-838.

(23) Setua, S.; Khan, S.; Yallapu, M. M.; Behrman, S. W.; Sikander, M.; Khan, S. S.; Jaggi, M.; Chauhan, S. C. Restitution of Tumor Suppressor MicroRNA-145 Using Magnetic Nanoformulation for Pancreatic Cancer Therapy. *J. Gastrointest. Surg.* **2017**, *21*. 94-105.

(24) Saberi, A. H.; Fang, Y.; McClements, D. J. Fabrication of Vitamin E-Enriched Nanoemulsions: Factors Affecting Particle Size Using Spontaneous Emulsification. *J. Colloid Interface Sci.* **2013**, *391.* 95-102.

(25) Samsonov, A. V.; Mihalyov, I.; Cohen, F. S. Characterization of Cholesterol-Sphingomyelin Domains and Their Dynamics in Bilayer Membranes. *Biophys. J.* **2001**, *81*. 1486-1500.

(26) Langesq, Y.; Swaisgoodllii, M. H.; Ramoss, B. V; Steckn, T. L. Plasma Membranes Contain Half the Phospholipid and 90% of the Cholesterol and Sphingomyelin in Cultured Human Fibroblasts. *J. Biological chemistry.* **1989**, *264*. 3786-3793

(27) Sadzuka, Y.; Nakade, A.; Hirama, R.; Miyagishima, A.; Nozawa, Y.; Hirota, S.; Sonobe, T. Effects of Mixed Polyethyleneglycol Modification on Fixed Aqueous Layer Thickness and Antitumor Activity of Doxorubicin Containing Liposome. *Int. J. Pharm.* **2002**, *238*. 171-180.

(28) Pedersen, N.; Hansen, S.; Heydenreich, A. V.; Kristensen, H. G.; Poulsen, H. S. Solid Lipid Nanoparticles Can Effectively Bind DNA, Streptavidin and Biotinylated Ligands. *Eur. J. Pharm. Biopharm.* **2006**, *62*, 155–162.

(29) Vighi, E.; Ruozi, B.; Montanari, M.; Battini, R.; Leo, E. PDNA Condensation Capacity and in Vitro Gene Delivery Properties of Cationic Solid Lipid Nanoparticles. *Int. J. Pharm.* **2010**, *389*, 254–261.

(30) Pramanik, D.; Campbell, N. R.; Karikari, C.; Chivukula, R.; Kent, O. A.; Mendell, J. T.; Maitra, A. Restitution of Tumor Suppressor MicroRNAs Using a Systemic Nanovector Inhibits Pancreatic Cancer Growth in Mice. *Mol. Cancer Ther.* **2011**, *10*, 1470–1480.

(31) Kim, T. W.; Chung, H.; Kwon, I. C.; Sung, H. C.; Shin, B. C.; Jeong, S. Y. Polycations Enhance Emulsion-Mediated in Vitro and in Vivo Transfection. *Int. J. Pharm.* **2005**, *295*, 35–45.

(32) He, S. N.; Li, Y. L.; Yan, J. J.; Zhang, W.; Du, Y. Z.; Yu, H. Y.; Hu, F. Q.; Yuan, H. Ternary Nanoparticles Composed of Cationic Solid Lipid Nanoparticles, Protamine, and DNA for Gene Delivery. *Int. J. Nanomedicine* **2013**, *8*, 2859–2869.

(33) Xue, H. Y.; Guo, P.; Wen, W. C.; Wong, H. L.; Lipid-Based Nanocarriers for RNA Delivery. *Current Pharmaceutical Design* **2015**, *21*, 3140-3147

(34) Souto, E. B.; Nayak, A. P.; Murthy, R. S. R. Lipid Nanoemulsions for Anti-Cancer Drug Therapy. *Pharmazie* **2011**, *66*, 473–478.

(35) Brito, L. A.; Chan, M.; Shaw, C. A.; Hekele, A.; Carsillo, T.; Schaefer, M.; Archer, J.; Seubert, A.; Otten, G. R.; Beard, C. W.; *et al.* A Cationic Nanoemulsion for the Delivery of Next-Generation RNA Vaccines. *Mol. Ther.* **2014**, *22*, 2118–2129.

(36) Oh, M. H.; Kim, J. S.; Lee, J. Y.; Park, T. G.; Nam, Y. S. Radio-Opaque Theranostic Nanoemulsions with Synergistic Anti-Cancer Activity of Paclitaxel and Bcl-2 SiRNA. *RSC Adv.* **2013**, *3*, 14642–14651.

(37) Kaneda, M. M.; Sasaki, Y.; Lanza, G. M.; Milbrandt, J.; Wickline, S. A. Mechanisms of Nucleotide Trafficking during SiRNA Delivery to Endothelial Cells Using Perfluorocarbon Nanoemulsions. *Biomaterials* **2010**, *31*, 3079–3086.

(38) Bondì, M. L.; Craparo, E. F. Solid Lipid Nanoparticles for Applications in Gene Therapy: A Review of the State of the Art. *Expert Opin. Drug Deliv.* **2010**, *7*, 7–18.

(39) Bivas-Benita, M.; Oudshoorn, M.; Romeijn, S.; Van Meijgaarden, K.; Koerten, H.; Van Der Meulen, H.; Lambert, G.; Ottenhoff, T.; Benita, S.; Junginger, H.; *et al.* Cationic Submicron Emulsions for Pulmonary DNA Immunization. *J. Control. Release* **2004**, *100*, 145–155.

(40) Kolate, A.; Baradia, D.; Patil, S.; Vhora, I.; Kore, G.; Misra, A. PEG - A Versatile Conjugating Ligand for Drugs and Drug Delivery Systems. *J. Control. Release* **2014**, *192*, 67–81.

(41) Suk, J. S.; Xu, Q.; Kim, N.; Hanes, J.; Ensign, L. M. PEGylation as a Strategy for Improving Nanoparticle-Based Drug and Gene Delivery. *Adv. Drug Deliv. Rev.* **2016**, *99*, 28–51.

(42) Wang, X.; Yu, B.; Ren, W.; Mo, X.; Zhou, C.; He, H.; Jia, H.; Wang, L.; Jacob, S. T.; Lee, R. J.; *et al.* Enhanced Hepatic Delivery of SiRNA and MicroRNA Using Oleic Acid Based Lipid Nanoparticle Formulations. *J. Control. Release* **2013**, *172*, 690–698.

(43) Chen, Y.; Zhu, X.; Zhang, X.; Liu, B.; Huang, L. Nanoparticles Modified with Tumor-Targeting ScFv Deliver SiRNA and MiRNA for Cancer Therapy. *Mol. Ther.* **2010**, *18*, 1650–1656.

(44) Silva, A. L.; Marcelino, H. R.; Veríssimo, L. M.; Araujo, I. B. Stearylamine-Containing Cationic Nanoemulsion. *J. Nanoscience and Nanotechnology*. **2016**, *16*. 1339-1345.

(45) Zhang, J.; Fan, H.; Levorse, D. A.; Crocker, L. S. Ionization Behavior of Amino Lipids for SiRNA Delivery: Determination of Ionization Constants, SAR, and the Impact of Lipid p K a on Cationic Lipid-Biomembrane Interactions. *Langmuir* **2011**, *27*, 1907–1914.

(46) Jeong, M. W.; Oh, S. G.; Kim, Y. C. Effects of Amine and Amine Oxide Compounds on the Zeta-Potential of Emulsion Droplets Stabilized by Phosphatidylcholine. *Colloids Surfaces A Physicochem. Eng. Asp.* **2001**, *181*, 247–253.

(47) Fraga, M.; Laux, M.; Zandoná, B.; Santos, G. R.; dos Santos Giuberti, C.; de Oliveira, M. C.; Matte, U.; Teixeira, H. F. Optimization of Stearylamine-Based Nanoemulsions Obtained by Spontaneous Emulsification Process as Nucleic Acids Delivery Systems. *J. Drug Deliv. Sci. Technol.* **2008**, *18*, 398–403.

(48) Teixeira, H.; Dubernet, C.; Chacun, H.; Rabinovich, L.; Boutet, V.; Deverre, J. R.; Benita, S.; Couvreur, P. Cationic Emulsions Improves the Delivery of Oligonucleotides to Leukemic P388/ADR Cells in Ascite. *J. Control. Release* **2003**, *89*, 473–482.

(49) Bivas-Benita, M.; Oudshoorn, M.; Romeijn, S.; Van Meijgaarden, K.; Koerten, H.; Van Der Meulen, H.; Lambert, G.; Ottenhoff, T.; Benita, S.; Junginger, H.; *et al.* Cationic Submicron Emulsions for Pulmonary DNA Immunization. *J. Control. Release* **2004**, *100*, 145–155.

(50) Liu, J.; Meng, T.; Yuan, M.; Wen, L. J.; Cheng, B. L.; Liu, N.; Huang, X.; Hong, Y.; Yuan, H.; Hu, F. Q. MicroRNA-200c Delivered by Solid Lipid Nanoparticles Enhances the Effect of Paclitaxel on Breast Cancer Stem Cell. *Int. J. Nanomedicine* **2016**, *11*, 6713–6725.

(51) Martini, É.; Fattal, E.; de Oliveira, M. C.; Teixeira, H. Effect of Cationic Lipid Composition on Properties of Oligonucleotide/Emulsion Complexes: Physico-Chemical and Release Studies. *Int. J. Pharm.* **2008**, *352*, 280–286.

(52) Teixeira, H.; Dubernet, C.; Puisieux, F. ; Benita, F. ; Couvreur, P. ; Submicron Cationic Emulsions as a New Delivery System for Oligonucleotides. *Pharmaceutical Research*. **1999,** *16*, 1.

(53) Lee, H. Y.; Mohammed, K. A.; Kaye, F.; Sharma, P.; Moudgil, B. M.; Clapp, W. L.; Nasreen, N. Targeted Delivery of Let-7a MicroRNA Encapsulated Ephrin-A1 Conjugated Liposomal Nanoparticles Inhibit Tumor Growth in Lung Cancer. *Int. J. Nanomedicine* **2013**, *8*, 4481–4494.

(54) Delgado, D.; Del Pozo-Rodríguez, A.; Angeles Solinís, M.; Bartkowiak, A.; Rodríguez-Gascón, A. New Gene Delivery System Based on Oligochitosan and Solid Lipid Nanoparticles: “In Vitro” and “in Vivo” Evaluation. *Eur. J. Pharm. Sci.* **2013**, *50*, 484–491.

(55) Chen, J.; Yu, Z.; Chen, H.; Gao, J.; Liang, W. Transfection Efficiency and Intracellular Fate of Polycation Liposomes Combined with Protamine. *Biomaterials* **2011**, *32*, 1412–1418.

(56) Yuan, H.; Zhang, W.; Du, Y. Z.; Hu, F. Q. Ternary Nanoparticles of Anionic Lipid Nanoparticles/Protamine/DNA for Gene Delivery. *Int. J. Pharm.* **2010**, *392*, 224–231.

(57) Hauptstein, S.; Prüfert, F.; Bernkop-Schnürch, A. Self-Nanoemulsifying Drug Delivery Systems as Novel Approach for PDNA Drug Delivery. *Int. J. Pharm.* **2015**, *487*, 25–31.

(58) Hintzen, F.; Perera, G.; Hauptstein, S.; Müller, C.; Laffleur, F.; Bernkop-Schnürch, A. In vivo evaluation of an oral self-microemulsifying drug delivery system (SMEDDS) for leuprorelin. *Int. J. Pharm.* **2014**, *472*, 20–26.

(59) Hillaireau, H.; Couvreur, P. Nanocarriers’ Entry into the Cell: Relevance to Drug Delivery. *Cell. Mol. Life Sci.* **2009**, *66*, 2873–2896.

(60) Mahmood, A.; Bernkop-Schnürch, A. SEDDS: A Game Changing Approach for the Oral Administration of Hydrophilic Macromolecular Drugs. *Adv. Drug Deliv. Rev.* **2018**.

(61) Tao, J.; Ding, W. F.; Che, X. H.; Chen, Y. C.; Chen, F.; Chen, X. D.; Ye, X. L.; Xiong, S. Bin. Optimization of a Cationic Liposome-Based Gene Delivery System for the Application of MiR-145 in Anticancer Therapeutics. *Int. J. Mol. Med.* **2016**, *37*, 1345–1354.

(62) Li, C.; Xu, N.; Li, Y. Q.; Wang, Y.; Zhu, Z. T. Inhibition of SW620 Human Colon Cancer Cells by Upregulating MiRNA-145 Basic Study. *World J. Gastroenterol.* **2016**, *22*, 2771–2778.

Chapter 3

A radiolabelling strategy with Fluorin-18 for in vivo imaging of lipid-based nanosystems by PET

This work has been done in collaboration with Guillaume Becker, Sylvestre Dammicco, Melisa Serrano, Natacha Leroi, François Lallemand, Mohamed Ali Bahri, Alain Plenevaux, Christian Lemaire, and André Luxen from the university of Liege (Belgium)

USC
UNIVERSIDADE
DE SANTIAGO
DE COMPOSTELA

Chapter 3

A radiolabelling strategy with Fluorine-18 for *in vivo* imaging of lipid-based nanosystems by PET

Abstract

Organic nanoparticles made out of biodegradable and biocompatible materials have attracted increased attention in the diagnostic and therapeutic fields. In this study, we attempted to explore the potential of biocompatible sphingomyelin nanoemulsions (SNs) for clinical positron emission tomography (PET) imaging after radiolabelling with Fluorine-18 (^{18}F), a radioisotope regularly used in clinic. [^{18}F] fluoride was produced by the cyclotron and was incorporated into 4-[^{18}F]fluorobenzamido-N-ethylmaleimide ([^{18}F]FBEM), which was coupled next to SNs previously functionalized with a thiol group, via inclusion either of a lipid-PEG-thiol derivative (SNs), or a lipid-PEG-peptide (SNs-RPM). Radiolabelling of SNs and SNs-RPM was obtained through facile-conjugated chemistry with simple purification and without the use of organic solvents, providing a simple platform for rapid and efficient nanoparticle labelling. PET imaging and biodistribution studies in BALB/c mice allowed obtaining the pharmacokinetics of both formulations and determining the clearance pathways. Altogether, we confirmed the potential of this new technique for the radiolabelling of lipid-based drug nanocarriers for application in drug delivery and diagnosis.

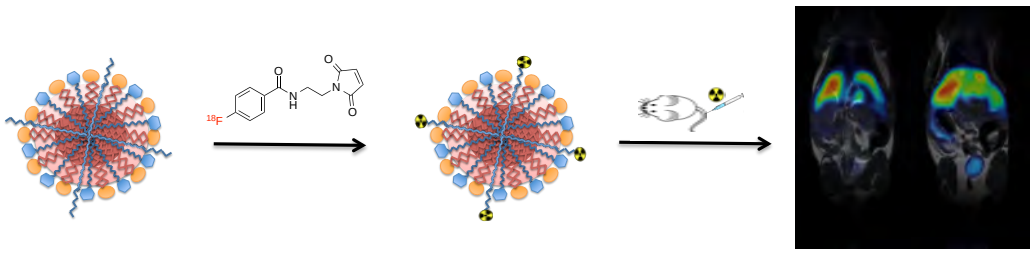

Keywords*:* nanoemulsions, radiolabelling, [^{18}F]FBEM, PET, biodistributuion

USC
UNIVERSIDADE
DE SANTIAGO
DE COMPOSTELA

1.Introduction

Nanotechnology offers promising standpoints for diagnosis of a number of diseases such as cancer, atherosclerosis, leukemia, and tuberculosis, by providing innovative non-invasive methodologies[1-3]. Most typically, nanoparticles designed for *in vivo* whole-body imaging purposes are inorganic, such as quantum dots (fluorescent nanocrystals) for optical image, iron oxide and manganese oxide nanoparticles (magnetic nanoparticles) for Magnetic Resonance Imaging (MRI), and gold nanorods (plasmonic nanoparticles) for photonics[4-6]. In the case of molecular imaging, apart from inorganic nanoparticles, polymeric micelles, liposomes, and dendrimers are generally used as basic materials labeled with radionuclides for Positron Emission Tomography (PET) and Single-Photon Emission Computed Tomography (SPECT)[7-11]. The use of biodegradable organic nanoparticles has several advantages with respect to inorganic materials. For example, no toxicity is observed, oppositely to other materials such as heavy metal ions (CdSe/CdTe) present in quantum dots (QDs). More importantly, since QDs are efficient energy donors, they could transfer energy to nearby oxygen molecules, resulting in the generation of reactive oxygen species (ROS), causing cell damage or death[12,13]. While many iron oxide nanoparticles have shown excellent results *in vitro*, many of them had failed *in vivo* due to toxicity via plentiful mechanisms including the disruption of cytoskeletons, inducement of oxidative stress, generation of free radicals, impairment of mitochondrial function, damage of DNA, and altering of cell signaling pathways among others[14]. On the other hand, organic nanoparticles can provide an upper edge in terms of biocompatibility and biodegradability over inorganic nanoparticles.

Among all various imaging modalities currently used in clinical applications, one of the prevalent techniques at the hospital is PET due to its own merits, such as high sensitivity, feasible functional image, and precise quantification of signals from radionuclides[15,16]. ^{18}F-fluorodeoxyglucose (FDG) is broadly used clinically for tumor imaging based on increased glucose metabolism in most types of tumors. This clinical approved agent by the Food and Drug Administration (FDA) helps improving diagnosis and treatment of cancers[17,18]. Nonetheless, in certain cases, imaging with FDG can be counter-productive as glucose metabolism is not only specific to tumors. It may be difficult to reach sufficient amounts at the target area. Consequently, this drawback has driven researchers to develop more specific delivery systems for imaging[19,20].

Radiolabelled nanocarriers can increase the signal, sensitivity, and resolution of the acquired image compared to the current standard radiotracer e.g. FDG[21]. Additionally, radiolabeled nanoparticles can be tailored to have long blood circulation times and be stable in plasma, therefore holding a great potential for clinical applications[22-24]. Harrington *et al*. demonstrated that ^{111}In-DTPA-labeled pegylated liposomes were able to accumulate in solid tumors at high concentrations and remained there for prolonged periods in patients with locally advanced cancers particularly in head and neck cancer[25]. ^{64}Cu-DOTA-loaded pegylated liposomes, reported by A.L. Petersen *et al*., showed a high retention stability and a high degree of tumor accumulation in HT29 (colon adenocarcinoma) xenografts[26]. In another study by Zhang *et al.*, ^{99m}Tc-labeled dendrimers conjugated with folic acid improved the tumor targeting in human oral epidermoid carcinoma[27]. Therefore, developments of targeted-radiolabeled nanocarriers can lead to imaging tools with high potential in cancer diagnosis.

To date, the development of radiolabeled nanoparticles is widely based on chelation principles by means of a bifunctional chelator (BFC)[28-30]. However, the attachment of a radionuclide using BFCs has some disadvantages. The coordination chemistry of common radiometals and their chelators may be hampered due to steric hindrance of nanoparticles. Along the production, the presence of non-radioactive metals may interfere the chelation, leading to less radiochemical yield. One alternative for the use of radiometals is labelling nanoparticles with fluorine-18 (^{18}F). ^{18}F can be considered as promising positron emitter for PET, resulting from its half-life of 110 min allowing performing scans over several hours, together with a low positron energy allowing for images of high resolution, and a large-scale production with high specific activity[31-33]. Therefore, ^{18}F seems to be an interesting choice for radiolabelling of nanoparticles. There have been several attempts for radiolabeling biologically active compounds with ^{18}F, such as peptides, neuro-transmitter ligands, and enzyme targets[34,35]. So far, labeling methods are often described and characterized by multi-step synthetic pathways. First of all, ^{18}F-labeled molecule (^{18}F-prosthetic group) have to be synthesized in advance by intricate techniques. Then the conjugation of the ^{18}F-prosthetic group with the biomarker is achieved for the last step[36-38]. Such a conjugation usually targets primary amino groups either at the N-terminus of peptides (α-NH2) or

at internal lysine residues (α-NH2). Nevertheless, this process still has pitfalls related to non-selective radio-labeling because of the relative abundance of lysine in proteins.

Thus, the peptide labelling at thiol groups has emerged as a method offering the opportunity to accomplish efficient and site-specific radiolabeling. Since a free thiol group is only present in cysteine residues, radiolabeling of thiol functional groups definitively renders a regio-specific modification of peptides. In addition, under physiological conditions, the thiol group is more nucleophilic than amines. The common approaches for synthesis thiol labeling precursors are counted on a maleimide group via Michael addition reaction. Consequently, numerous labeling precursors containing a maleimide functional group have been developed, as for example 4-[^{18}F]fluorobenzamido-N-ethylmaleimide ([^{18}F]FBEM)[39], and N-[4-[(4-[^{18}F] fluorobenzylidene)aminooxy]butyl]-maleimide[40].

We describe here a new methodology for radiolabelling organic lipid-based nanosystems with ^{18}F, and provide an example with biocompatible and biodegradable SNs and SNs-RPM. We started by the synthesis of a ^{18}F-labeled prosthetic group, [^{18}F]FBEM, which was later conjugated to thiol groups located at the surface of SNs, or to the cysteine residue of the SNs-RPM via Michael addition reaction. Both radiolabelled nanoemulsions (SNs-[^{18}F]FBEM and SNs-RPM-[^{18}F]FBEM) were then purified at room temperature without organic solvents, and fully characterized for their physicochemical properties. The labeling was confirmed by ultra-performance liquid chromatography (UPLC) in both UV and gamma detectors. SNs-[^{18}F]FBEM and SNs-RPM-[^{18}F]FBEM were eventually injected to healthy mice, to determine their potential for future PET imaging studies. This strategy could represent a step-forward towards the development of innovative diagnostic nanotools.

2. Materials and methods

2.1 Materials

Vitamin E (DL-α-tocopherol), stearylamine, potassium carbonate (K_2CO_3), N,N-diisopropylethylamine (DIPEA), diethyl cyanophosphonate (DECP), and N-(2-Aminoethyl)maleimide trifluoroacetate salt were purchased from Sigma Aldrich (St.Louis, MO, United States). Sphingomyelin was acquired from Lipoid (Ludwigshafen, Germany). SH-PEG_{12}-C_{18} was supplied by Creative PEGworks (North Carolina, United States). Cys-Pro-Ile-Glu-Asp-Arg-Pro-Met-Cys-PEG_8-C_{18} (RPMpeptide-PEG_8-C_{18}) was obtained from ChinaPeptides (Shanghai, China). Both of SH-PEG_{12}-C_{18} and RPMpeptide-PEG_8-C_{18} were used as references for UPLC analysis, Ref-SH-PEG_{12}-C_{18} (Ref-lipid), and Ref-RPMpeptide-PEG_8-C_{18} (Ref-peptide). Tris (2-carboxyethyl) phosphine hydrochloride (TCEP.HCl) was purchased from Pierce Biotechnology. Kryptofix® 222 was supplied by Merck KGaA (Darmstadt, Germany). 2,5-Dioxopyrrolidin-1-yl 4-fluorobenzoate (N-succinimidyl 4-fluorobenzoate) was provided from AK Scientific (California, United States). PD-10 desalting column was obtained from GE healthcare (Chicago, IL, United States). Water used in all experiments was deionized from Milli-Q Integral Water Purification System.

2.2 Nanoemulsions preparation by ethanol injection method

SNs functionalized with a thiol group (SNs) were formulated from vitamin E, sphingomyelin, stearylamine, and SH-PEG_{12}-C_{18} in a ratio of 10:1:1:0.06 w/w. In the case of peptide-decorated SNs (SNs-RPM) they were formulated from vitamin E, sphingomyelin, stearylamine, and RPMpeptide-PEG_8-C_{18} in a ratio of 10:1:1:0.1 w/w.

All components were dissolved in a final volume of 110 µL of ethanol (organic phase, sphingomyelin concentration 0.45 mg/mL) and injected with syringe pump (0.5 mL) into 1 mL of ultrapure water under magnetic stirring. SNs and SNs-RPM were spontaneously formed and maintained in agitation for 10 minutes at room temperature. Both formulations were isolated from

non-interacted compounds by ultracentrifugation (Beckman, California, United states) at 35000 rpm for 1 hour at 15ºC in a 70.1 Ti rotor.

2.3 Size and zeta-potential measurements

Nanoemulsions were analyzed for their hydrodynamic size by dynamic laser scattering (DLS) (Zetasizer Nano ZS, Malvern Instruments, Worcestershire, UK). Measurements were performed at 25 ºC with a detection angle of 173º.The obtained data were analyzed based on cumulative analysis method for determination of mean hydrodynamic diameter and polydispersity index (PDI). ζ–potential was measured by Lasser Doppler Anemometry (LDA). Nanoemulsions were diluted with filtered ultrapure water and loaded into a Disposable Solvent Resistant Micro Cuvette (ZEN0040) and a dip-cell (DTS 1060) for size and ζ-potential analysis, respectively.

2.4 Synthesis of [^{18}F]FBEM

The automated radiosynthesis of [^{18}F]FBEM was conducted on a GE Healthcare FastLab® in three-steps, and then purified by the semipreparative HPLC on a SymmetryPrep C18 column (**Figure 1A and 1B**)[41]. In brief, the [^{18}F]fluoride obtained from the cyclotron (23 ± 0.8 GBq) was recovered and trapped on an ion exchange resin QMA Carbonate Cartridge. The activity was eluted with the solution of a Kryptofix® (K2.2.2., 37.5 mg in 630 µL of ACN) and K_2CO_3 (7.5 mg in 70 µL of water) into the reactor. Water was azeotropically evaporated by heating at 105 °C and 120 °C under vacuum and nitrogen flow. Precurrsor **1** (**Figure 1A**) was prepared according to a previously described methodology[42]. 10 mg of Precurrsor **1** in anhydrous DMF 1.0 mL was then added to the reactor. The labeling was performed for 10 min at 130 °C. After that NaOH (1 mL, 2 M) was added to the bulk reaction to hydrolyze the ester for 10 min. HCl (2 mL, 4 M) was added to quench the reaction. After dilution with water (6 mL), the bulk solution is trapped on an HLB cartridge. The cartridge was washed afterwards with water (6 mL) and dry with hexane (5 mL). The reactor was washed three times with ACN (4 mL). Then **3** was eluted with N,N-diisopropylethylamine (20 µL) in a 1:1 mixture of ACN/Et_2O (4 mL) to the reactor. After evaporation the solution at 60 °C under N_2 flow for 5 min, maleimidetrifluoroacetate salt (10 mg, 16 µmol) and diethyl cyanophosphonate

DECP (20 µL, 60 µmol) in a 1:1 mixture of ACN/Et_2O (3 mL) was added to the reactor. The reaction was heated at 60 °C for 20 min under N_2 flow until the volume was reached 1 mL. The bulk solution was diluted with water (4 mL) and injected in a semi-preparative HPLC to separate [^{18}F]FBEM from by-products that may interfere with the labeling with the nanoemulsions. The peak of purified [^{18}F]FBEM was collected in water (15 ml) and transferred back to the FastLab module through a second HLB cartridge. Then this cartridge was washed with water (6 mL), dried with hexane (5 mL) and then eluted with ACN (4 mL). A fraction (0.74 GBq) of this solution was evaporated under N_2 to dryness, which was ready for nanoemulsions labeling.

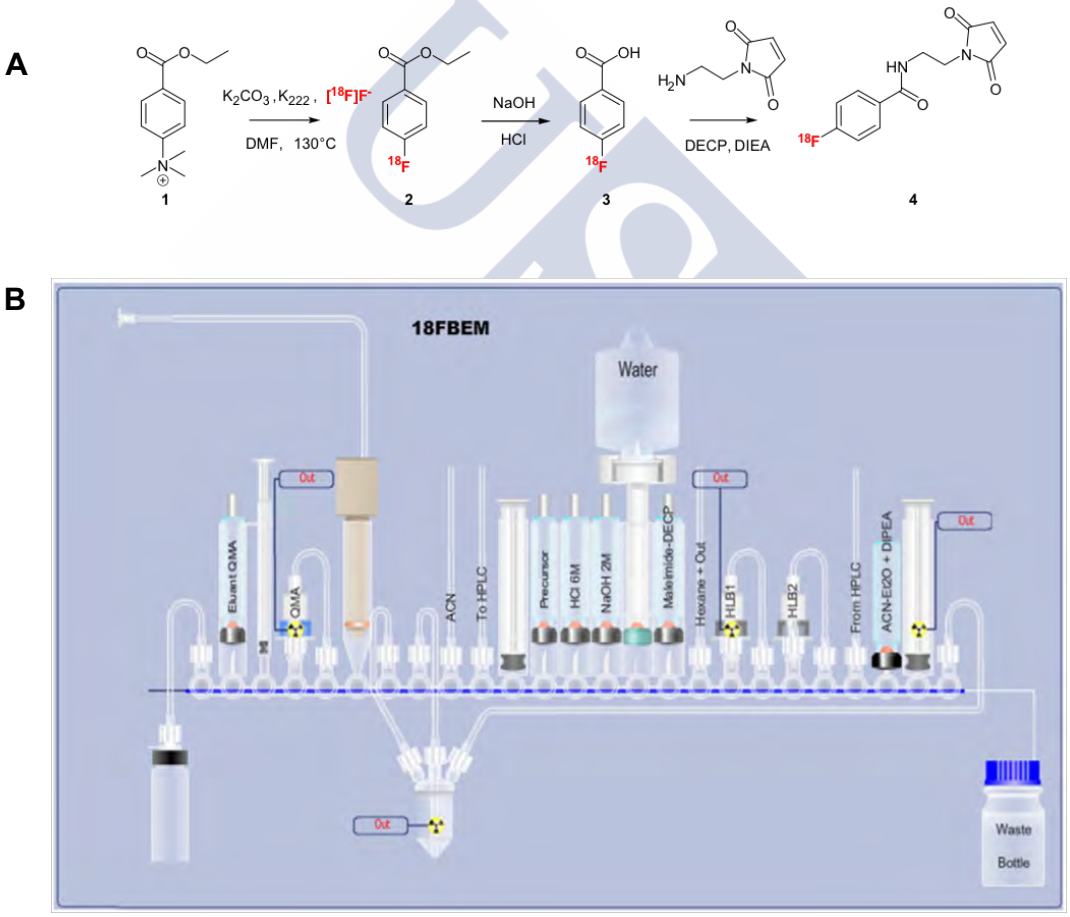

Figure 1. Radiosynthesis of [^{18}F]FBEM (A). Cassette layout for [^{18}F]FBEM preparation on a FastLab module (B). [Reproduced from Dammicco S., et al. (2017). Nucl. Med. Biol.[41] with permission.]

2.5 Synthesis of [^{18}F]FBEM-labelled nanoemulsions

SNs and SNs-RPM were firstly treated with TCEP.HCl (20 eq.) during 20 min at room temperature (RT) to reduce the disulfide bond. Nanoemulsions were then purified using a PD-10 desalting column with Sephadex G-25 resin. 5 fractions of 500 µL. They were collected and characterized by DLS. Nanoemulsions were eluted in a total volume of 1 ml, added to the thin film of evaporated [^{18}F]FBEM (see section 2.4), mixed for 30 min at RT, and purified by a PD-10 desalting column. The fractions of [^{18}F]FBEM-labelled nanoemulsions were collected and the amount of radioactivity was measured by ionization chamber. Furthermore, [^{18}F]FBEM-labelled SNs and SNs-RPM (SNs-[^{18}F]FBEM and SNs-RPM-[^{18}F]FBEM), as well as free [^{18}F]FBEM, Ref-[^{19}F]FBEM, Ref-SH-PEG$_{12}$-C$_{18}$ (Ref-lipid), and Ref-RPMpeptide-PEG$_8$-C$_{18}$ (Ref-peptide), were subsequently analyzed by UPLC (**Figure 4**). The analysis was implemented on ACQUITY UPLC BEH C18 Column, 130Å, 1.7 µm, 2.1 mm X 50 mm with a flow rate of 0.7 mL/min. Eluent A: H_2O + 0.1%TFA, Eluent B: ACN. The gradient was linear 1.9 min from 90/10 to 40/60, linear 1.2 min from 60/40 to 0/100 and the washout linear 0.9 min from 0/100 to 90/10.

2.6 Biodistribution studies and PET imaging

All animal studies were performed in compliance with the European Ethics Committee. The study protocol was approved by the local Animal Experimental Ethical Committee of the University of Liège (Belgium). The mice were anesthetized with 1–2% isoflurane, placed in the MINERVE animal cell bed (Equipement Veterinaire Minerve, Esternay, France) and continuously received anesthesia via a nose cone system. Temperature was controlled at 37 ± 0.5 °C by an air warming system (Minerve, France). PET studies were obtained using a Siemens FOCUS 120 microPET scanner (Siemens, Knoxville, TN, USA). PET data acquisition started with a 10-min transmission scan using a ^{57}Co point source with single event acquisition mode. Afterward SNs-SH-[^{18}F]FBEM and SNs-RPM-[^{18}F]FBEM nanoemulsions, suspended in 0.1 mL of 0.5% Glucose (280 mOsm/kg, 6 ± 2.2 MBq), were injected via the lateral tail vein of male BALB/c mice. Dynamic microPET scans over 120 minutes were started few seconds before the tracer injection. The list-mode data was histogrammed into three-dimentional (3D) sonograms by Fourier rebinning (Defrise M, et al. IEEE Trans Med Imag 1997, 16:145-158) and reconstructed by filtered

backprojection with all corrections, except for scatter events (Bahri *et al*. 2009)[43]. A set of 2D images was reconstructed in a 256 x 256 x 95 matrix with a pixel size of 0.433 x 0.433 x 0.796 mm. the dynamic time framing was as follow 6 x 5 s, 6 x 10s, 3 x 20 s, 5 x 30s, 5 x 60 s, 8 x 150 s, 6 x 300s, and 6 x 600 s. The obtained images were then analyzed for the kinetic studies.

For anatomical whole-body imaging, the anesthetized mice were transferred into a 9.4 Tesla MRI DirectDrive VNMRS horizontal bore system with a shielded gradient system (Agilent Technologies, Palo Alto, CA). The used sequence parameters were as follows: 25 contiguous coronal slices, slice thickness = 1 mm, TR/TE = 2000/ 23.68 ms, FOV = 80 × 40 mm, matrix = 256 × 128. By using PMOD software version 3.6 (PMOD Technologies Ltd., Zurich, Switzerland), dynamic PET images were co-registered to the corresponding MRI structural image (guided by the fiducial markers) in each mouse. Then regions of interest (ROIs) were drawn over major organs using PMOD software on the structural MRI image and transferred into the whole-body dynamic PET images in order to extract their time activity curves (TACs).

The mice were sacrificed at the end of the imaging experiment. Their blood and organs were harvested 3 h after injection. All the collected organs were weighed and the radioactivity was measured with a γ-counter (2480 Wizard^2 Gamma counter, Perkin Elmer). The output measures were expressed as the percentage injected dose per gram of tissue (%ID/g).

3. Results and discussion

3.1 Physiochemical characterizations of nanoemulsions

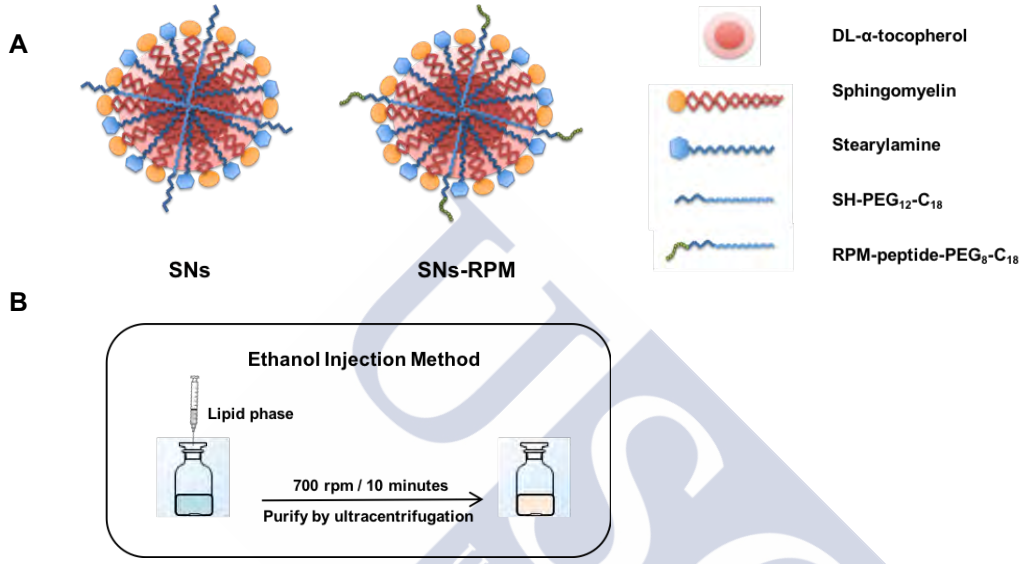

Figure 2. Components (A). and Scheme of preparation of SNs and SNs-RPM (B).

Currently, lipid-based systems have gained greatly interest owing to their ability to allow efficient drug delivery system [44,45]. Nanoemulsions are thermodynamically stable isotropic systems in which two immiscible liquids (oil and water) are mixed to formulate a single phase. They are typically composed of an oily core and stabilized by surfactants such as phospholipids and cationic lipids. In this report, SNs and SNs-RPM were prepared by a low-energy method, using the ethanol injection procedure[46]. Nanoemulsions were spontaneously formed after injection of the lipid phase (containing all components dissolved in ethanol) into the aqueous phase (in this particular study, ultrapure water) (**Figure 2A and 2B**). SNs and SNs-RPM had a vitamin E core stabilized by sphingomyelin and stearylamine. A lipid-PEG-thiol derivative (SH-PEG_{12}-C_{18}), or a lipid-PEG-peptide (RPMpeptide-PEG_8-C_{18}) were incorporated to the formulations, for further labelling with [^{18}F]FBEM. RPMpeptide was selected to provide a basic information of radiolabelling of peptides that could be incorporated to the formulations for targeting purposes. RPM has been described as a ligand of interest for targeting colorectal cancer[47-49]. The physicochemical properties of SNs and

SNs-RPM are described in **Table 1**. As it can be observed, nanoemulsions formed monodispersed populations with a mean size of 120-140 nm and are positively charged.

Table 1. Hydrodynamic size, polydispersity index (PDI), and zeta potential (ζ-potential) of SNs and SNs-RPM (n=3).

Formulation	Size (nm)	PDI	ζ-Potential (mV)
SNs	125 ± 3	0.2	+37± 2
SNs-RPM	138 ± 5	0.2	+41 ± 7

3.2 Synthesis of [^{18}F]FBEM-labelled nanoemulsions

Following a previous published methodology[41], we proceed to the synthesis of [^{18}F]FBEM. All steps and HPLC purification were automated on a FastLab from GE Healthcare. Time of radiosynthesis was approximately 85 min. This radiosynthesis was reproducible, reliable and rendered sufficient yields for multi-step procedures. The specific radioactivity of [^{18}F]FBEM (830 GBq/μmol) was analyzed on one batch for quality control. With respect to the labelling of the nanoemulsions, after [^{18}F]FBEM was synthesized, it was evaporated as a thin film. Nanoemulsions were added onto this film, after reduction of the disulfide bond was performed to reactivate the free thiol function[41], and subsequent purification to remove the reducing agent.

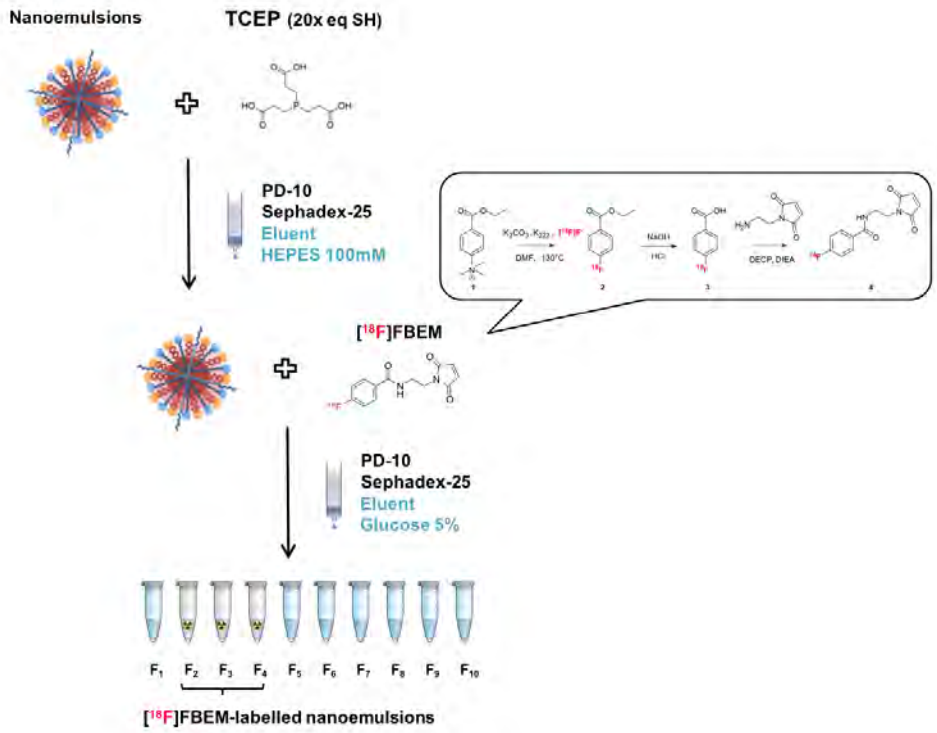

Figure 3. Labelling Process of SNs-[^{18}F]FBEM and SNs-RPM-[^{18}F]FBEM.

Radiolabeling was performed by chemical reaction between a maleimide group of [^{18}F]FBEM and the free thiol groups at the surface of SNs and SNs-RPM. Radiolabelled nanoemulsiones were purified again rendering SNs-[^{18}F]FBEM and SNs-RPM-[^{18}F]FBEM (**Figure 3**). Radiochemical yields (RCY) (decay corrected) of SNs-[^{18}F]FBEM and SNs-RPM-[^{18}F]FBEM were 35.1 $\pm$ 5.7% (n=4) and 39.4 $\pm$ 5.5% (n=4) respectively. The radioactivity amounts were sufficient for injection and observation *in vivo* biodistribution in mice during 2 hours. Both [^{18}F]FBEM-labelled nanoemulsions had hydrodynamic sizes of 130-150 nm with narrow PDI and positive ζ-Potential. No significant changes with respect to the unlabeled nanoemulsions are reported, allowing us to conclude that the radiolabeling process is mild and do not compromise the structure and stability of the nanosystems. SNs-[^{18}F]FBEM and SNs-RPM-[^{18}F]FBEM also have a pH between pH 7-8 and an osmolarity between 280-290 mOsm/kg, characteristics that make them suitable for parenteral injection (**Table 2**).

Table 2. Radiochemical yields, hydrodynamic size, polydispersity index (PDI), zeta potential (ζ-potential), pH, and osmolality of SNs-[^{18}F]FBEM and SNs-RPM-[^{18}F]FBEM (n=4).

Formulation	RCY	Size (nm)	PDI	ζ-Potential (mV	pH	Osmolality (mOsm/kg)
SNs-[^{18}F]FBEM	35.1 ± 5.7	136 ± 9	0.2	+38 ± 6	7.6 ± 0.2	287 ± 5
SNs-RPM-[^{18}F]FBEM	39.4 ± 5.5	149 ± 8	0.2	+37 ± 5	7.8 ± 0.3	285 ± 6

This study reported the successful labelling of lipid-based nanoparticles with [^{18}F]FBEM, using indirect labelling method and in absence of organic solvents. The chemical reaction was based on thiol-maleimide groups via Michael addition reaction. Generally, radiolabelling of nanoparticles could be accomplished either before or after the synthesis of nanoparticles. Labelling with different ^{18}F-prosthetic groups after the formation of nanoparticles have already been reported[50-52]. On the other hand, (4-[^{18}F]fluorobenzyl-2-bromoacetamide ([^{18}F]FBBA) conjugated to polymers before the preparation of nanoparticles (RCY = 5-14%, decay corrected) has been described[53]. Due to the short half-life of ^{18}F, the method of post-labelling may display an advantage allowing high radiochemical yields in relation to the pre-labelling method. In addition, the labelling process was performed under controlled pH and osmolarity to prepare the appropriated characteristics of radiolabelled nanoemulsions for injection in animal[54].

To confirm the radiolabelling results, the signals of non-labelled products, Ref-[^{19}F]FBEM, Ref-SH-PEG$_{12}$-C$_{18}$ (Ref-lipid), and Ref-RPMpeptide-PEG$_8$-C$_{18}$ (Ref-peptide) were analyzed with UV detector. Then [^{18}F]FBEM-labelled nanoemulsions were broken in ethanol and evaluated by gamma detector to confirm the signal of labelled products with the references mentioned above. No free [^{18}F]FBEM peak was detected from both chromatograms of broken labelled nanoemulsions, stating that the purification was completely accomplished to separate labelled nanoemulsions and free [^{18}F]FBEM (**Figure 4A, 4B, 4D, and 4F**). Broken SNs-[^{18}F]FBEM confirmed that they were conveniently labeled, as a signal of [^{18}F]FBEM-PEG$_{12}$-C$_{18}$ ([^{18}F]FBEM-lipid) was detected at 3.1 min, in agreement with the chromatograph of the Ref-lipid (**Figure 4C and 4D**). The corresponding of Ref-peptide with conjugated product [^{18}F]FBEM-RPMpeptide-PEG$_8$-C$_{18}$ ([^{18}F]FBEM-peptide)

in the broken of SNs-RPM-[^{18}F]FBEM at 2.5 min was confirmed by UPLC chromatogram (**Figure 4E and 4F**). From these results, the labelling position was confirmed at thiol functional groups either on lipid or peptide. Non-specific labelling was not observed from both labelled nanoemulsions. Lastly, the purification process was successfully performed for obtaining purified labelled nanoemulsions.

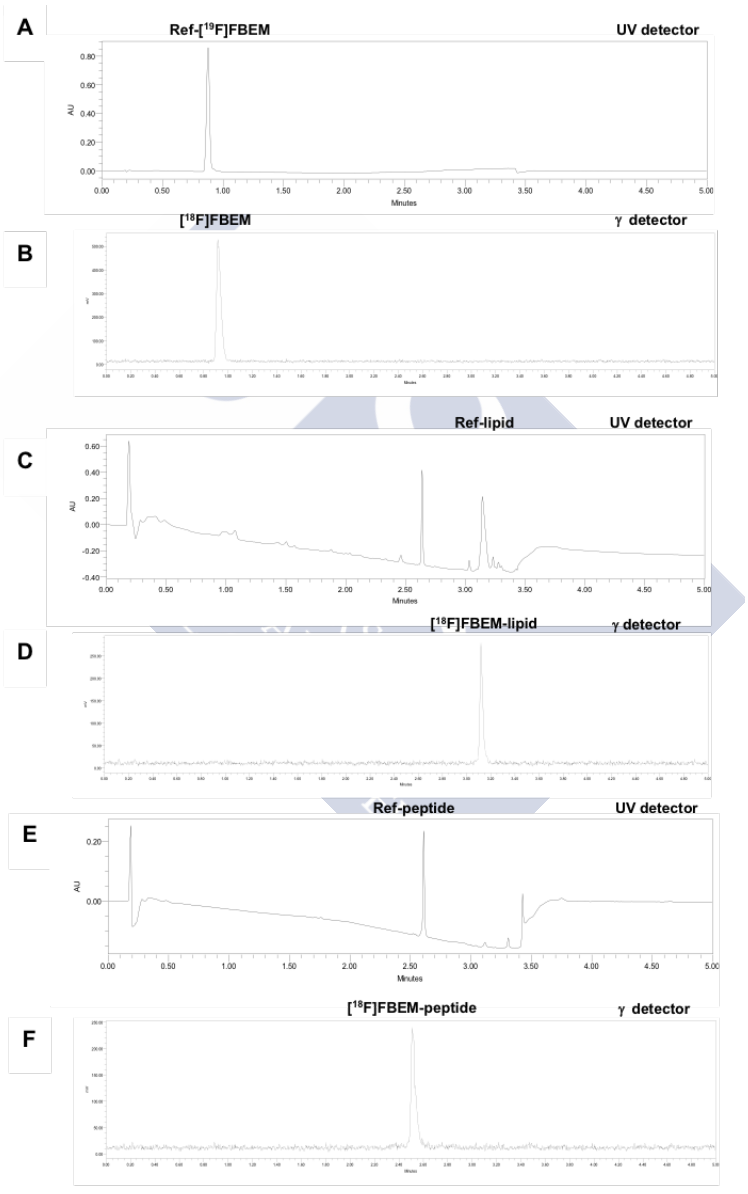

Figure 4. Chromatogram UPLC in UV and gamma detector of Ref-[^{19}F]FBEM) (A). [^{18}F]FBEM (B). Ref-lipid(C). [^{18}F]FBEM-lipid (D). Ref-peptide (E) and [^{18}F]FBEM-peptide (F).

3.3 Biodistribution studies and PET imaging nanoemulsions

To determine the *in vivo* behavior of the radiolabelled nanoemulsions, they were administered via tail injection to healthy mice. On the one side, the radioactivity was measured in dissected organs, to determine the biodistribution *ex vivo*. On the other side, PET-MRI studies were carried out to prove the potential of the developed nanoemulsions as contrast agents for in vivo imaging, and also to perform pharmacokinetic studies.

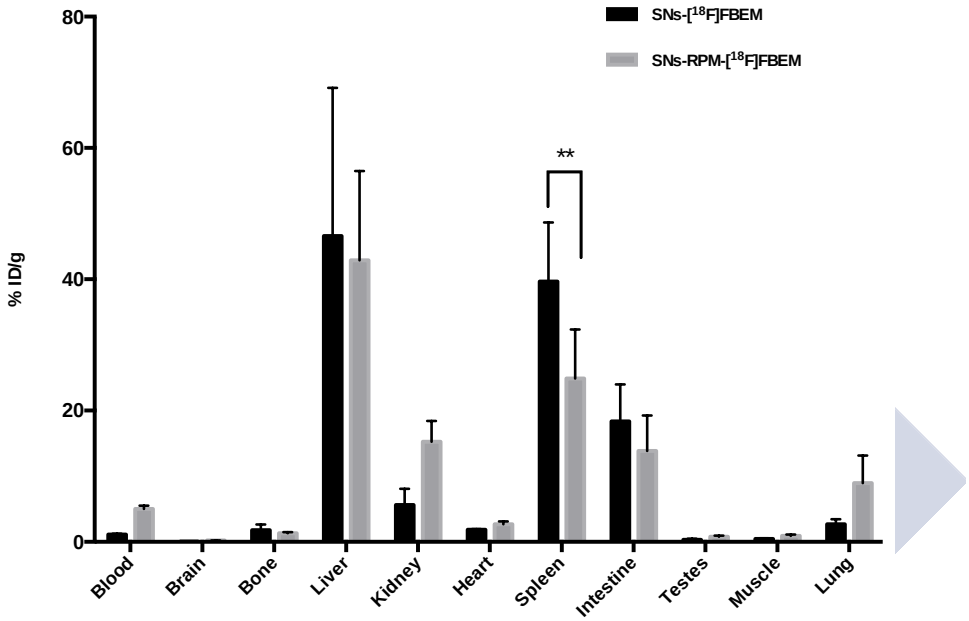

Figure 5. *Ex vivo* biodistribution profile of SNs-[^{18}F]FBEM and SNs-RPM-[^{18}F]FBEM in organs of male BALB/c mice 3h after injection.

The *ex vivo* biodistribution of SNs-[^{18}F]FBEM (n=4) and SNs-RPM-[^{18}F]FBEM (n=5) in organs of male BALB/C 3 h post injection, demonstrated an uptake in liver (46.6 ± 22.6% and 47.4 ± 10.7%ID/g), kidneys (5.6 ± 2.5 and 16.1 ± 2.9%ID/g), spleen (39.6 ± 9.0 and 26.4 ± 7.6%ID/g) and intestine (18.4 ± 5.6% and 11.6 ± 2.2%ID/g) **(Figure 5)**. The presence of radioactivity in the intestine might originate from liver excretion via gallbladder within feces. The radioactivity in the kidney showed that parts of the radiolabelled nanoemulsions were eliminated via urine. The low amount of radioactivity detected in bone indicated that no defluorination occurs as free $^{18}F^-$ has a

native bone targeting capability, this suggesting that most of the ^{18}F radiolabel remained on nanoemulsions[55,56]. In general, the uptake in different organs depends on the stability of the nanostructures, which resulted from the nanomaterial composition, size, and surface functionalization[57]. The *ex vivo* pattern of both SNs-[^{18}F]FBEM and SNs-RPM-[^{18}F]FBEM displayed different pharmacokinetic profiles compared to the free labelled-peptide ([^{18}F]FBEM-peptide) from preliminary study. The capture of [^{18}F]FBEM-peptide was lower than both [^{18}F]FBEM-nanoemulsions in liver, spleen, and intestine demonstrated with the uptake of 27.73%ID/g, 12.92%ID/g, and 6.39 %ID/g respectively. Form all these results, the radiolabelled nanoemulsions were stable *in vivo* upon intravenous injection.

According to nanoparticles viewpoints, a possible explanation for the high uptake in liver and spleen might be described by the action of mononuclear phagocyte system (MPS). The protein adsorption might occur on the surface of nanoemulsions, stimulating the elimination of foreign particles[58-60]. Similar distribution patterns from lipid-based nanoparticles has been reported from ^{52}Mn-DOTA and ^{64}Cu-DOTA liposomes, ^{159}Gd-DTPA liposomes, and ^{99m}Tc-labelled solid lipid nanoparticles[61-63]. One strategy to modulate biodistribution and interaction with MPS could be the modification of the surface of nanoparticles[64,65]. For instance, the decoration of the nanoparticles with a PEG layer could prevent opsonization and sequestration by the MPS, resulting in prolonged blood circulation as reported from ([^{18}F]FBBA) labelled nanoparticles and [^{18}F]FPyME (1-[3-(2-fluoropyridin-3-yloxy)propyl]pyrrole-2,5-dione) labelled quantum dot micelles[53,66]. Indeed, SNs decorated with the hydrophilic peptide RPM (SNs-RPM-[^{18}F]FBEM) had a decreased accumulation in spleen and liver.

In vivo biodistribution studies with PET-MRI were accomplished to evaluate the potential of the nanoemulsions to be used for in vivo diagnosis, as well as to determine the pharmacokinetics of SNs-[^{18}F]FBEM and SNs-RPM-[^{18}F]FBEM. **Figure 6** shows images acquired by PET-MRI, 2h after intravenous injection of both types of nanosystems. It is possible to observe a high accumulation of nanoemulsions in liver and spleen. Certain amounts of radioactivity appeared in urinary bladder indicating that radiolabelled nanoemulsions or their radiolabeled metabolic products were excreted through urinary tracts. With respect to the ROI drawn on the heart ventricles confirmed the success of the injection in the tail vein since the radioactivity decreased after the

administration. Time-activity curves (**Figure 7**) indeed show a quick uptake in the liver and spleen. Two ways of clearance (liver and kidney) can be observed, being the predominant liver excretion. The progressive increase in the bladder could indicate that a fraction of the labelled nanoemulsions was circulating in the bloodstream being later excreted through the kidney into urine[51]. Time-activity curves in the lung, heart, and kidney followed a similar way, and remained lower compared to liver and kidney. Overall, these results correlate well with the *ex vivo* at 2 hours after injection.

In conclusion, *in vivo* biodistribution and pharmacokinetic studies proved that our approach resulted adequate radiolabelling for SNs and SNs-RPM, paving the way for the future delivery of biodegradable and biocompatible organic nanoemulsions for tumor diagnosis.

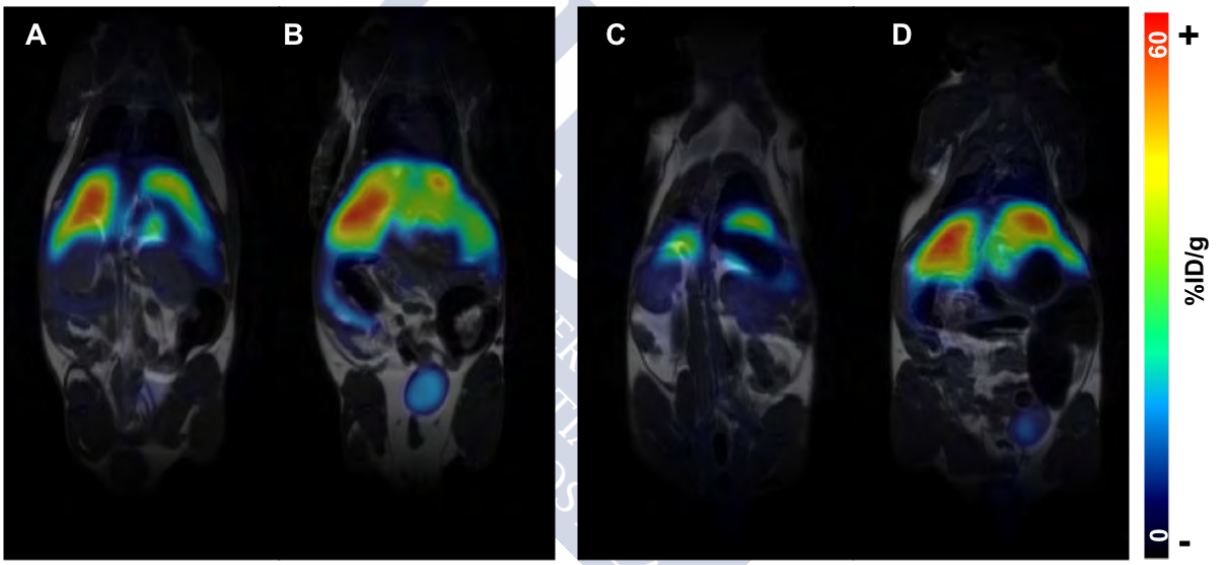

Figure 6. Whole body *in vivo* biodistribution of SNs-[^{18}F]FBEM (left) and SNs-RPM-[^{18}F]FBEM (right) in male BALB/c mice 2h p.i. using PET and MRI: two different coronal slides showing respectively the kidneys (A,C) and the liver and bladder (B,D).

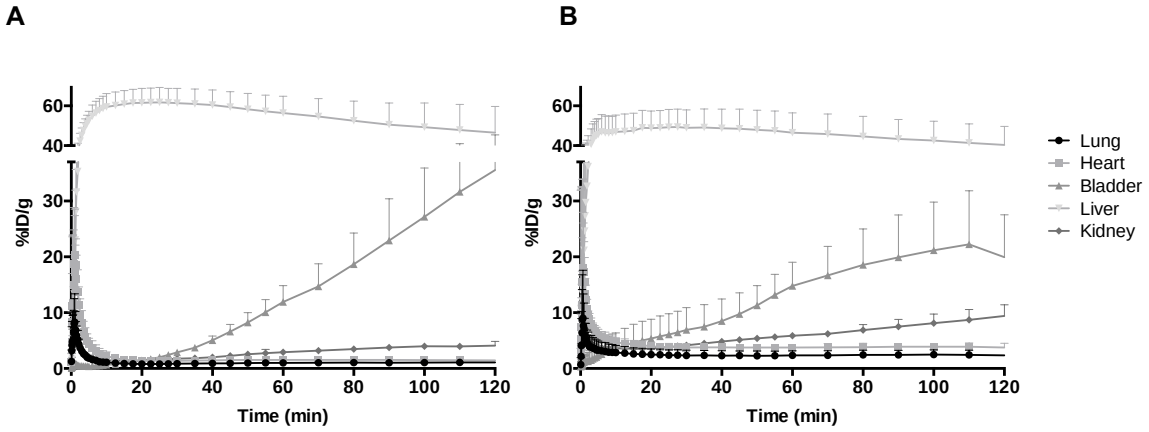

Figure 7. Graphical representation of the whole body in vivo biodistribution of SNs-[^{18}F]FBEM (A) and SNs-RPM-[^{18}F]FBEM (B) in male BALB/c mice using PET in different organs after single intravenous injection. Data are given in mean ± SD (standard deviation) in % of the injected dose per gram (%ID/g).

4. Conclusion

Radiolabeling of lipid-based nanocarriers was successfully developed for both biodegradable lipid nanoemulsions (SNs-[^{18}F]FBEM) and peptide-decorated nanoemulsions (SNs-RPM-[^{18}F]FBEM) by a simple method under mild conditions, without altering their physicochemical properties, and rendering acceptable radiolabelling yields. Radiolabelled nanoemulsions can be followed by PET-MRI and could be exploited for further development of nanoemulsions for molecular imaging diagnosis. Additionally, this strategy could be applied for other nanoparticle compositions, if they are functionalized with a thiol group on their surface.

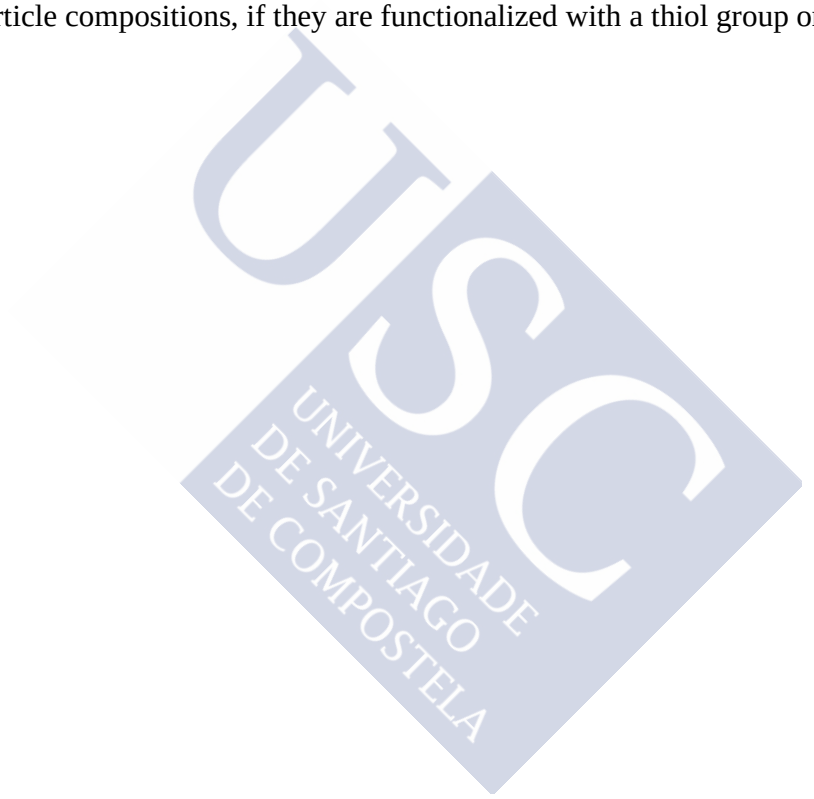

Supplementary

1. Synthesis of [^{19}F]FBEM (Ref-[^{19}F]FBEM)

Synthesis of [^{19}F]FBEM (also used as Ref-[^{19}F]FBEM) was described in previous report[67]. Briefly, N-(2-Aminoethyl)maleimide (20 µmol) in 800 µL of acetonitrile, N-succinimidyl 4-fluorobenzoate (18 µmol) in 400 µL of acetonitrile, and 2 mL of 50 mmol/L of K_3PO_4 buffer (pH 8.5) were mixed. The reaction was continued at 50°C for 20 minutes. The solution was purified with the semipreparative HPLC on C18 column (110Å, 5 µm, 10 mm × 250 mm) at a flow rate of 4 mL/min (Eluent A: ACN/H_2O 5/95+0.1%TFA, Eluent B: ACN. The gradient was linear 25 min from 100/0 to 0/100 and the washout linear 10 min from 0/100 to 100/0. After the collection of the [^{19}F]FBEM and further lyophilization, the characteristic of [^{19}F]FBEM was confirmed by UPLC-MS. Analytical UPLC was accomplished on ACQUITY UPLC BEH C18 Column **(**130Å, 1.7 µm, 2.1 mm X 50 mm**)** controlled by Empower® software. They were performed with a flow rate of 0.5 mL/min (Eluent A: H_2O + 0.1%TFA, Eluent B: ACN). The gradient was linear 3.8 min from 90/10 to 0/100 and the washout linear 1.2 min from 0/100 to 90/10. The synthesis of [^{19}F]FBEM was confirmed by Mass spectrum analysis with molecular weight of 262.98 g/mol.

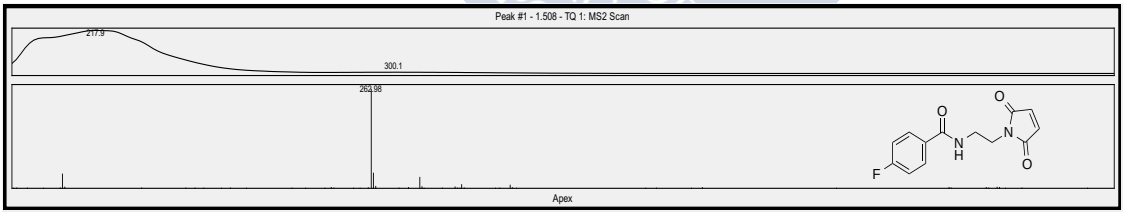

S1. MS analysis (electospray, negative ionization mode) of [^{19}F]FBEM.

2. Synthesis of [^{18}F]FBEM-RPMpeptide-PEG$_8$-C$_{18}$ ([^{18}F]FBEM-peptide)

RPMpeptide-PEG$_8$-C$_{18}$ firstly treated with TCEP.HCl (20 eq.) during 20 min at room temperature (RT) to reduce the disulfide bond. The solution then purified using semipreparative HPLC on C18 column (110Å, 5 µm, 10 mm × 250 mm) at a flow rate of 4 mL/min (Eluent A:

Ethanol/H_2O 5/95+0.1%TFA, Eluent B: Ethanol. The gradient was linear 25 min from 100/0 to 0/100 and the washout linear 10 min from 0/100 to 100/0. It was collected and added to the thin film of evaporated [^{18}F]FBEM (see section 2.4). [^{18}F]FBEM-peptide was analyzed with gamma detector in UPLC and injected to observe biodistribution in healthy mice.

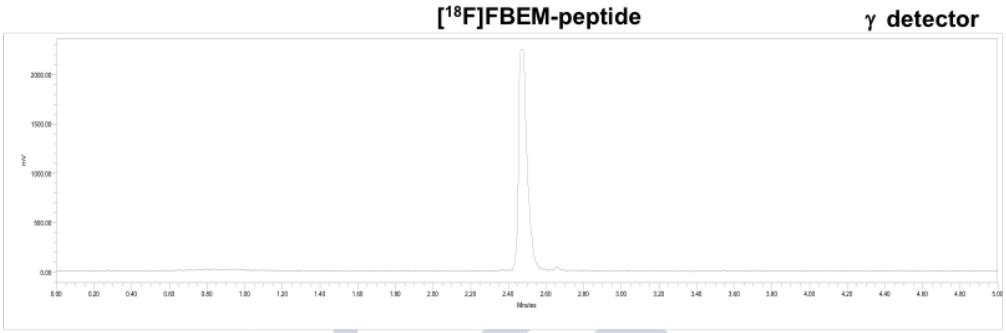

S2. Chromatogram UPLC in gamma detector of [^{18}F]FBEM-peptide.

References

(1) Lee, C.-N.; Wang, Y.-M.; Lai, W.-F.; Chen, T.-J.; Yu, M.-C.; Fang, C.-L.; Yu, F.-L.; Tsai, Y.-H.; Chang, W. H.-S.; Zuo, C. S.; *et al.* Super-Paramagnetic Iron Oxide Nanoparticles for Use in Extrapulmonary Tuberculosis Diagnosis. *Clin. Microbiol. Infect.* **2012**, *18*, E149–E157.

(2) Parvanian, S.; Mostafavi, S. M.; Aghashiri, M. Multifunctional Nanoparticle Developments in Cancer Diagnosis and Treatment. *Sens. Bio-Sensing Res.* **2017**, *13*, 81–87.

(3) Montiel Schneider, M. G.; Lassalle, V. L. Magnetic Iron Oxide Nanoparticles as Novel and Efficient Tools for Atherosclerosis Diagnosis. *Biomed. Pharmacother.* **2017**, *93*, 1098–1115.

(4) Cheng, Z.; Yan, X.; Sun, X.; Shen, B.; Gambhir, S. S. Tumor Molecular Imaging with Nanoparticles. *Engineering* **2016**, *2* (1), 132–140.

(5) Giner-Casares, J. J.; Henriksen-Lacey, M.; Coronado-Puchau, M.; Liz-Marzán, L. M. Inorganic Nanoparticles for Biomedicine: Where Materials Scientists Meet Medical Research. *Mater. Today* **2016**, *19* (1), 19–28.

(6) Xu, K.; Shi, J.; Pourmand, A.; Udayakumar, T. S.; Dogan, N.; Zhao, W.; Pollack, A.; Yang, Y. Plasmonic Optical Imaging of Gold Nanorods Localization in Small Animals. *Scientific reports* **2018**, 1-12

(7) Xing, Y; Zhao, J; Conti, P.S; Chen. K; Radiolabeled Nanoparticles for Multimodality Tumor imaging. *Theranostics* **2014**, *4* (3), 290-306.

(8) Abou, D. S.; Pickett, J. E.; Thorek, D. L. J. Nuclear Molecular Imaging with Nanoparticles: Radiochemistry, Applications and Translation. *Br. J. Radiol.* **2015**, *88* (1054), 1–18.

(9) Marik, J.; Tartis, M. S.; Zhang, H.; Fung, J. Y.; Kheirolomoom, A.; Sutcliffe, J. L.; Ferrara, K. W. Long-Circulating Liposomes Radiolabeled with [18F]fluorodipalmitin ([18F]FDP). *Nucl. Med. Biol.* **2007**, *34* (2), 165–171.

(10) Narmani, A.; Yavari, K.; Mohammadnejad, J. Imaging, Biodistribution and in Vitro Study of smart99mTc-PAMAM G4 Dendrimer as Novel Nano-Complex. *Colloids Surfaces B Biointerfaces* **2017**, *159*, 232–240.

(11) Rossin, R.; Pan, D.; Qi, K.; Turner, J. L.; Sun, X.; Wooley, K. L.; Welch, M. J. Folate-Conjugated Shell Cross-Radiotherapy: Synthesis, Radiolabeling, and Biologic Evaluation. **2005**, *46* (7), 1210–1219.

(12) Drobintseva, A. O.; Matyushkin, L. B.; Aleksandrova, O. a.; Drobintsev, P. D.; Kvetnoy, I. M.; Mazing, D. S.; Moshnikov, V. a.; Polyakova, V. O.; Musikhin, S. F. Colloidal CdSe and ZnSe/Mn Quantum Dots: Their Cytotoxicity and Effects on Cell Morphology. *St. Petersbg. Polytech. Univ. J. Phys. Math.* **2015**, *1* (3), 272–277.

(13) Lovrić, J.; Cho, S. J.; Winnik, F. M.; Maysinger, D. Unmodified Cadmium Telluride Quantum Dots Induce Reactive Oxygen Species Formation Leading to Multiple Organelle Damage and Cell Death. *Chem. Biol.* **2005**, *12* (11), 1227–1234.

(14) Revia, R. A.; Zhang, M. Magnetite Nanoparticles for Cancer Diagnosis, Treatment, and Treatment Monitoring: Recent Advances. *Mater. Today* **2016**.

(15) Cabral, H.; Nishiyama, N.; Kataoka, K. Supramolecular Nanodevices: From Design Validation to Theranostic Nanomedicine. *Acc. Chem. Res.* **2011**, *44*, 999–1008.

(16) Ding, H.; Wu, F. Image Guided Biodistribution and Pharmacokinetic Studies of Theranostics. *Theranostics* **2012**, *2*, 1040–1053.

(17) Zhu, A.; Daniel Lee, A.; Shim, H. Metabolic PET Imaging in Cancer Detection and Therapy Response. *Semin Oncol* **2011**, *38* (1), 55–69.

(18) Jadvar, H; Is There Utility for FDG PET in Prosate Cancer. *Semin Nucl Med* . **2016**, *46* (6), 502–506.

(19) Goel,S.; England, C. G.; Chen, F.; Cai, W.; Positron emission tomography and nanotechnology: A dynamic duo for cancer theranostics. *Adv. Drug Deliv. Rev.* **2017.** *113* 157–176

(20) Gambhir, S. S.; Molecular Imaging of Cancer with Positron Emission Tomography. *Nature Rev. Cancer.* **2002**, *2* 683-693

(21) Thakor, A. S.; Jokerst, J. V.; Ghanouni, P.; Campbell, J. L.; Mittra, E.; Gambhir, S. S. Clinically Approved Nanoparticle Imaging Agents. *J. Nucl. Med.* **2016**, *57*, 1833–1837.

(22) Madru, R.; Kjellman, P.; Olsson, F.; Wingardh, K.; Ingvar, C.; Stahlberg, F.; Olsrud, J.; Latt, J.; Fredriksson, S.; Knutsson, L.; et al. 99mTc-Labeled Superparamagnetic Iron Oxide Nanoparticles for Multimodality SPECT/MRI of Sentinel Lymph Nodes. *J. Nucl. Med.* **2012**.

(23) Psimadas, D.; Baldi, G.; Ravagli, C.; Bouziotis, P.; Xanthopoulos, S.; Franchini, M. C.; Georgoulias, P.; Loudos, G. Preliminary Evaluation of a 99mTc Labeled Hybrid Nanoparticle Bearing a Cobalt Ferrite Core: In Vivo Biodistribution. *J. Biomed. Nanotechnol.* **2012**.

(24) Zeng, J.; Jia, B.; Qiao, R.; Wang, C.; Jing, L.; Wang, F.; Gao, M. In situ111In-Doping for Achieving Biocompatible and Non-Leachable 111In-Labeled Fe3O4 Nanoparticles. *Chem. Commun.* **2014**.

(25) Harrington, K. J.; Mohammadtaghi, S.; Uster, P. S.; Glass, D.; Peters, A. M.; Vile, R. G.; Stewart, J. S. W. Effective Targeting of Solid Tumors in Patients With Locally Advanced Cancers by Radiolabeled Pegylated Liposomes. **2001**, *7*, 243–254.

(26) Petersen, A. L.; Binderup, T.; Rasmussen, P.; Henriksen, J. R.; Elema, D. R.; Kjær, A.; Andresen, T. L. 64Cu Loaded Liposomes as Positron Emission Tomography Imaging Agents. *Biomaterials* **2011**, *32* (9), 2334–2341.

(27) Zhang, Y.; Sun, Y.; Xu, X.; Zhang, X.; Zhu, H.; Huang, L.; Qi, Y.; Shen, Y. M. Synthesis, Biodistribution, and Microsingle Photon Emission Computed Tomography (SPECT) Imaging Study of Technetium-99m Labeled PEGylated Dendrimer Poly(amidoamine) (PAMAM)-Folic Acid Conjugates. *J. Med. Chem.* **2010**, *53* (8), 3262–3272.

(28) Stockhofe, K.; Postema, J. M.; Schieferstein, H.; Ross, T. L. Radiolabeling of Nanoparticles and Polymers for PET Imaging. *Pharmaceuticals*. **2014**, *7*, 392-418.

(29) Miura, Y.; Tsuji, A. B.; Sugyo, A.; Sudo, H.; Aoki, I.; Inubushi, M.; Yashiro, M.; Hirakawa, K.; Cabral, H.; Nishiyama, N.; et al. Polymeric Micelle Platform for Multimodal Tomographic Imaging to Detect Scirrhous Gastric Cancer. *ACS Biomater. Sci. Eng.* **2015**, *1* (11), 1067–1076.

(30) Hervella, P.; Parra, E.; Needham, D. Encapsulation and Retention of Chelated-Copper inside Hydrophobic Nanoparticles: Liquid Cored Nanoparticles Show Better Retention than a Solid Core Formulation. *Eur. J. Pharm. Biopharm.* **2016**, *102*, 64–76.

(31) Okarvi, S. M. Recent Progress in Fluorine-18 Labeled Peptide Radiopharmaceuticals. *Eur. J. Nucl. Med.* **2001**, *28*, 929–938.

(32) Pretze, M.; Große-Gehling, P.; Mamat, C. Cross-Coupling Reactions as Valuable Tool for the Preparation of PET Radiotracers. *Molecules* **2011**, *16*, 1129–1165.

(33) Van der Born, D.; Pees, A.; Poot, A. J.; Orru, R. V. A.; Windhorst, A. D.; Vugts, D. J. Fluorine-18 Labeled Building Blocks for PET Tracer Synthesis. *Chem. Soc. Rev.* **2017**, *46*, 4709–4773.

(34) Okarvi, S. M. Peptide-Based Radiopharmaceuticals: Future Tools for Diagnostic Imaging of Cancers and Other Diseases. *Med. Res. Rev.* **2004**, *24*, 357–397.

(35) Pourghiasian, M.; Liu, Z.; Pan, J.; Zhang, Z.; Colpo, N.; Lin, K. S.; Perrin, D. M.; Bénard, F. ^{18}F-AmBF<inf>3</Inf>-MJ9: A Novel Radiofluorinated Bombesin Derivative for Prostate Cancer Imaging. *Bioorganic Med. Chem.* **2015**, *23*, 1500–1506.

(36) Bolton, R. Radiohalogen Incorporation into Organic Systems. *J. Label. Compd. Radiopharm.* **2002**, *45*, 485–528.

(37) Schirrmacher, R.; Wangler, C.; Schirrmacher, E. Recent Developments and Trends in 18F-Radiochemistry: Syntheses and Applications. *Mini. Rev. Org. Chem.* **2007**, *4*, 317–329.

(38) Fani, M.; Maecke, H. R.; Okarvi, S. M. Radiolabeled Peptides: Valuable Tools for the Detection and Treatment of Cancer. *Theranostics* **2012**, *2*, 481–501.

(39) Cai, W.; Zhang, X.; Wu, Y.; Chen, X. A Thiol-Reactive 18F-Labeling Agent, N-[2-(4-18F-Fluorobenzamido)ethyl]maleimide, and Synthesis of RGD Peptide-Based Tracer for PET Imaging of Alpha v Beta 3 Integrin Expression. *J. Nucl. Med.* **2006**, *47*, 1172–1180.

(40) Toyokuni, T.; Walsh, J. C.; Dominguez, A.; Phelps, M. E.; Barrio, J. R.; Gambhir, S. S.; Satyamurthy, N. Synthesis of a New Heterobifunctional Linker, N-[4-(Aminooxy)butyl]maleimide, for Facile Access to a Thiol-Reactive 18F-Labeling Agent. *Bioconjug. Chem.* **2003**, *14*, 1253–1259.

(41) Dammicco, S.; Goux, M.; Lemaire, C.; Becker, G.; Bahri, M. A.; Plenevaux, A.; Cinier, M.; Luxen, A. Regiospecific Radiolabeling of Nanofitin on Ni Magnetic Beads with [^{18}F]FBEM and in Vivo PET Studies. *Nucl. Med. Biol.* **2017**, *51*, 33–39.

(42) Haka, M. S.; Kilbourn, M. R.; Leonard Watkins, G.; Toorongian, S. A. Aryltrimethylammonium Trifluoromethanesulfonates as Precursors to Aryl [18F]fluorides: Improved Synthesis of [18F]GBR-13119. *J. Label. Compd. Radiopharm.* **1989**, *27*, 823–833.

(43) Bahri, M. a; Plenevaux, A.; Warnock, G.; Luxen, A.; Seret, A. NEMA NU4-2008 Image Quality Performance Report for the microPET Focus 120 and for Various Transmission and Reconstruction Methods. *J. Nucl. Med.* **2009**, *50*, 1730–1738.

(44) Teixeira, M. C.; Carbone, C.; Souto, E. B. Beyond Liposomes: Recent Advances on Lipid Based Nanostructures for Poorly Soluble/Poorly Permeable Drug Delivery. *Prog. Lipid Res.* **2017**, *68*, 1–11.

(45) A., A.; A., M.; F., P. Lipid Nanoparticulate Drug Delivery Systems: A Revolution in Dosage Form Design and Development. *Recent Adv. Nov. Drug Carr. Syst.* **2012**, 107–140.

(46) Shin, G. H.; Chung, S. K.; Kim, J. T.; Joung, H. J.; Park, H. J. Preparation of Chitosan-Coated Nanoliposomes for Improving the Mucoadhesive Property of Curcumin Using the Ethanol Injection Method. *J. Agric. Food Chem.* **2013**, *61*, 11119–11126.

(47) Kelly, K. a; Jones, D. a. Isolation of a Colon Tumor Specific Binding Peptide Using Phage Display Selection. *Neoplasia* **2003**, *5*, 437–444.

(48) Kelly, K.; Alencar, H.; Funovics, M.; Mahmood, U.; Weissleder, R. Detection of Invasive Colon Cancer Using a Novel, Targeted, Library-Derived Fluorescent Peptide. *Cancer research.* **2004**, 64, 6247–6251.

(49) Lee, Y. M.; Lee, D.; Kim, J.; Park, H.; Kim, W. J. RPM Peptide Conjugated Bioreducible Polyethylenimine Targeting Invasive Colon Cancer. *J. Control. Release* **2015**, *205*, 172–180.

(50) Rojas, S.; Gispert, J. D.; Martín, R.; Abad, S.; Menchón, C.; Pareto, D.; Víctor, V. M.; Álvaro, M.; García, H.; Herance, J. R. Biodistribution of Amino-Functionalized Diamond Nanoparticles. in Vivo Studies Based On18F Radionuclide Emission. *ACS Nano* **2011**, *5*, 5552–5559.

(51) Rojas, S.; Gispert, J. D.; Abad, S.; Buaki-Sogo, M.; Victor, V. M.; Garcia, H.; Herance, J. R. In Vivo Biodistribution of Amino-Functionalized Ceria Nanoparticles in Rats Using Positron Emission Tomography. *Mol. Pharm.* **2012**, *9*, 3543–3550.

(52) Guerrero, S.; Herance, J. R.; Rojas, S.; Mena, J. F.; Gispert, J. D.; Acosta, G. A.; Albericio, F.; Kogan, M. J. Synthesis and in Vivo Evaluation of the Biodistribution of a 18F-Labeled Conjugate Gold-Nanoparticle-Peptide with Potential Biomedical Application. *Bioconjug. Chem.* **2012**, *23*, 399–408.

(53) Di Mauro, P. P.; Gómez-Vallejo, V.; Baz Maldonado, Z.; Llop Roig, J.; Borrós, S. Novel 18F Labeling Strategy for Polyester-Based NPs for in Vivo PET-CT Imaging. *Bioconjug. Chem.* **2015**, *26*, 582–592.

(54) Stranz, M.; Kastango, E. S. A Review of pH and Osmolarity. *International Journal of Pharmaceutical Compounding*. **2013**.

(55) Schirrmeister, H.; Guhlmann, A.; Elsner, K.; Kotzerke, J.; Glatting, G.; Rentschler, M.; Neumaier, B.; Träger, H.; Nüssle, K.; Reske, S. N. Sensitivity in Detecting Osseous Lesions Depends on Anatomic Localization: Planar Bone Scintigraphy versus 18F PET. *J. Nucl. Med.* **1999**, *40*, 1623–1629.

(56) Zhou, J.; Yu, M.; Sun, Y.; Zhang, X.; Zhu, X.; Wu, Z.; Wu, D.; Li, F. Fluorine-18-Labeled Gd3+/Yb3+/Er3+ Co-Doped NaYF4 Nanophosphors for Multimodality PET/MR/UCL Imaging. *Biomaterials* **2011**, *32*, 1148–1156.

(57) Harper, S.; Usenko, C.; Hutchison, J. E.; Maddux, B. L. S.; Tanguay, R. L. In Vivo Biodistribution and Toxicity Depends on Nanomaterial Composition, Size, Surface Functionalisation and Route of Exposure. *J. Exp. Nanosci.* **2008**, *3*, 195–206.

(58) Mailänder, V.; Landfester, K. Interaction of Nanoparticles with Cells. *Biomacromolecules* **2009**, *10*, 2379–2400.

(59) Cho, E. C.; Xie, J.; Wurm, P. A.; Xia, Y.; Understanding the Role of Surface Charges in Cellular Adsorption versus Internalization by Selectively Removing Gold Nanoparticles on the Cell Surface with a I_2/KI Etchant. *Nano Letter.* **2009**, *9*, 3, 1080-1084

(60) Xiao, W.; Chen, W. H.; Xu, X. D.; Li, C.; Zhang, J.; Zhuo, R. X.; Zhang, X. Z. Design of a Cellular-Uptake-Shielding "Plug and Play" Template for Photo Controllable Drug Release. *Adv. Mater.* **2011**, *23*, 3526–3530.

(61) Jensen, A. I.; Severin, G. W.; Hansen, A. E.; Fliedner, F. P.; Eliasen, R.; Parhamifar, L.; Kjær, A.; Andresen, T. L. Remote-Loading of Liposomes with Manganese-52 and in Vivo Evaluation of the Stabilities of 52 Mn-DOTA and 64 Cu-DOTA Using Radiolabelled Liposomes and PET Imaging. *J. Control. Release* **2018**, *269*, 100–109.

(62) Crístian, D.; Soares, F.; Oliveira, M. C. De; Luís, A.; Barros, B. De; Cardoso, V. N.; Ramaldes, G. A. European Journal of Pharmaceutical Sciences Liposomes Radiolabeled with 159 Gd : In Vitro Antitumoral Activity , Biodistribution Study and Scintigraphic Image in Ehrlich Tumor Bearing Mice. **2011**, *43*, 290–296.

(63) Eroglu, H.; Yenilmez, A. An Investigation of the Usability of Solid Lipid Nanoparticles Radiolabelled with Tc-99m as Imaging Agents in Liver-Spleen Scintigraphy. **2016**, *12*, 1501–1509.

(64) Blanco, E.; Shen, H.; Ferrari, M. Principles of Nanoparticle Design for Overcoming Biological Barriers to Drug Delivery. *Nat. Biotechnol.* **2015**, *33*, 941–951.

(65) Rao, L.; Xu, J. H.; Cai, B.; Liu, H.; Li, M.; Jia, Y.; Xiao, L.; Guo, S. S.; Liu, W.; Zhao, X. Z. Synthetic Nanoparticles Camouflaged with Biomimetic Erythrocyte Membranes for Reduced Reticuloendothelial System Uptake. *Nanotechnology* **2016**, *27*, 85106.

(66) Ducongé, F.; Pons, T.; Pestourie, C.; Hérin, L.; Thézé, B.; Gombert, K.; Mahler, B.; Hinnen, F.; Kühnast, B.; Dollé, F.; *et al.* Fluorine-18-Labeled Phospholipid Quantum Dot Micelles for in Vivo Multimodal Imaging from Whole Body to Cellular Scales. *Bioconjug. Chem.* **2008**, *19*, 1921–1926.

(67) Chen, X.; Tohme, M.; Park, R.; Hou, Y.; Bading, J. R.; Conti, P. S. Micro-PET Imaging of A v B 3 -Integrin Expression with Dimeric RGD Peptide F-Labeled. *Mol. Imaging* **2004**, *3*, 96–104.

Chapter 4

Overall discussion and conclusions

USC
UNIVERSIDADE
DE SANTIAGO
DE COMPOSTELA

Overall Discussion

Colorectal cancer is one of the most common causes of cancer deaths worldwide. Poor patient survival rates result from poor prognosis, drug resistance, tumor invasion and migration, and inefficient therapeutic methods. Although survival rates are high at early stages of the disease, survival in the metastatic setting continues to be low[1,2]. Furthermore, due to the broad effect of conventional chemotherapeutic drugs, a number of patients are suffering from side-effects[3]. Therefore, improvements are necessary to specifically deliver drugs to tumor cells while avoiding systemic toxicity. Delivery based on nanotechnology can tackle this drawback[4]. Currently, there are FDA-approved nanoparticle-based therapies in oncology, and several formulations are under clinical investigation[5,6].

The potential of nanotechnology for delivery of innovative therapeutics such as polynucleotides has already been stated[7-9]. Due to its ability to interfere with tumor progression, invasion, and dissemination, oncosuppressor miRNAs become one of the choices for designing novel nanocarriers in the battle against colorectal cancer. miRNAs are endogenously expressed RNAs 18-24 nucleotides that can regulate gene expression through translational repression by binding to a target mRNA[10,11]. As previously reported, nanotechnology-based delivery systems have enabled the development of promising miRNAs to clinical trials[12]. We selected miRNA145 because it was frequently found to be downregulated in various kinds of neoplasia including colon cancer and could act as tumor suppressor[13-15].

Nanoparticles can also be of utility for the association of molecular agents prompting their application in molecular diagnosis, either for direct application in clinical diagnosis, for example to determine the efficiency of a particular treatment and/or follow-up of the diseas[16-18], or for *in vivo* tracking of the nanotherapeutics, rendering what are currently known as nanotheranostics[19]. The use of ^{18}F for radiolabelling has numerous benefits related to specific properties, such as (i) half-life of 109.8min, (ii) low β^+-energy (0.64 MeV), (iii) ease of production, (iv) availability as clinical routine use in the hospital. ^{18}F half-life is long enough to allow synthesis, transportation, and imaging procedure to be extended over hours, while limits the amount of radiation doses to patients in relation to other PET radionuclides. In addition, ^{18}F has a short positron linear range in

tissue because of its low positron energy, leading to particularly high resolution in PET imaging[20]. Unfortunately, direct labelling of peptide/protein with ^{18}F is difficult as the basic conditions of nucleophilic introduction of ^{18}F usually cause proton abstraction from the precursor molecules. The harsh labelling conditions may denature the sensitive biomolecules[21]. Hence, most ^{18}F labelling techniques utilize the use of ^{18}F-prosthetic groups, which could be activated and coupled to specific functional groups within the proteins (such as amino, carboxylate or sulfhydryl groups)[22,23]. The prosthetic group 4-[^{18}F]fluorobenzamido-N-ethylmaleimide ([^{18}F]FBEM) has been widely used for labelling peptides[24,25].

In the scope of this work, we have focused on the engineering and evaluation of nanoemulsions for gene delivery and radio-imaging purposes. Structurally, nanoemulsions are thermodynamically stable isotropic systems in which two immiscible liquids, usually oil and water, are mixed to form a single phase with the help of surfactants[26,27]. Nanoemulsions have already been explored for gene therapy applications and have already been decorated with target ligands such as peptides and proteins[28,29]. Adding cationic lipids such as DOTAP, DOTMA, and ST to the formulation mediates the association/complexation with nucleic acids, serving as a suitable gene carrier system[30,31]. A variety of targeting ligands can be attached to the surface of nanoemulsions to enable recognition by appropriate receptors expressed at the target site. Several articles relate to targeting receptors that are overexpressed on cancer cells including epidermal growth factor receptor (EGFR), folate, and transferrin[32-34]. We selected nanoemulsions formulated from natural lipid compounds, such as sphingomyelin and vitamin E, which are indeed being used in different formulations in clinical research[35,36]. Sphingomyelin nanoemulsions, SNs, were formulated following a very mild methodology, conveniently adapted to associate oncosuppressor miRNA mimics, and successfully radiolabeled with ^{18}F for PET. *In vitro* and *in vivo* assays were performed to determine their potential in the treatment and diagnosis of colorectal cancer.

SNs can be conveniently modulated to meet specific biomedical applications

The composition of SNs was conveniently adapted for each specific purpose. In the case of the development of SNs for miRNA replacement therapies to interfere cancer progression, cationic lipids were included in the formulation, either as part of the composition (stearylamine, (SNs-ST-

miRNA)), or as condensing agents for miRNAs, to obtain complexes that will eventually be encapsulated into SNs (SNs-DOTAP-miRNA) (**Figure 1**).

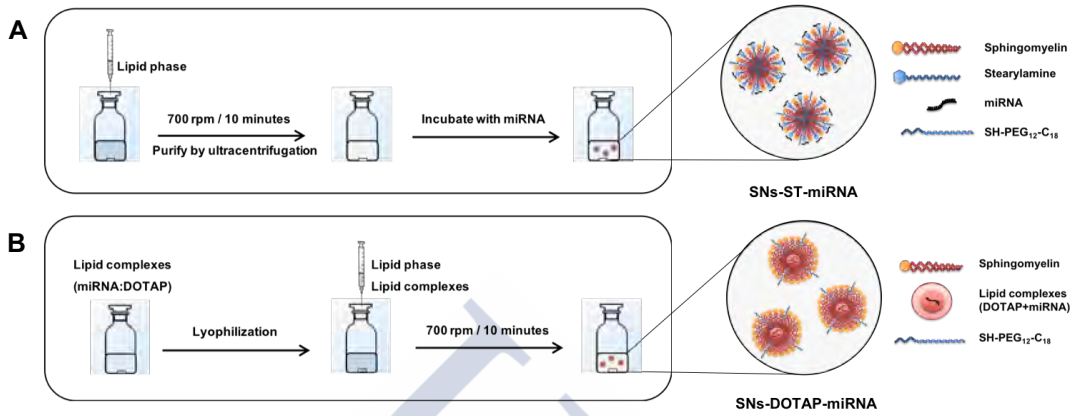

Figure 1. Preparation and illustration of SNs-ST-miRNA (A) and SNs-DOTAP-miRNA (B).

In the case of radiolabelling of SNs with ^{18}F for *in vivo* imaging by PET, thiol groups had to be exposed at the nanoparticle surface. For this, a lipid-PEG-SH derivative was included in the preparation of SNs. Other approach was to surface-decorated SNs with a targeted peptide that has already been proposed in colorectal cancer, the RPM peptide, with a thiol group in its structure (**Figure 2**).

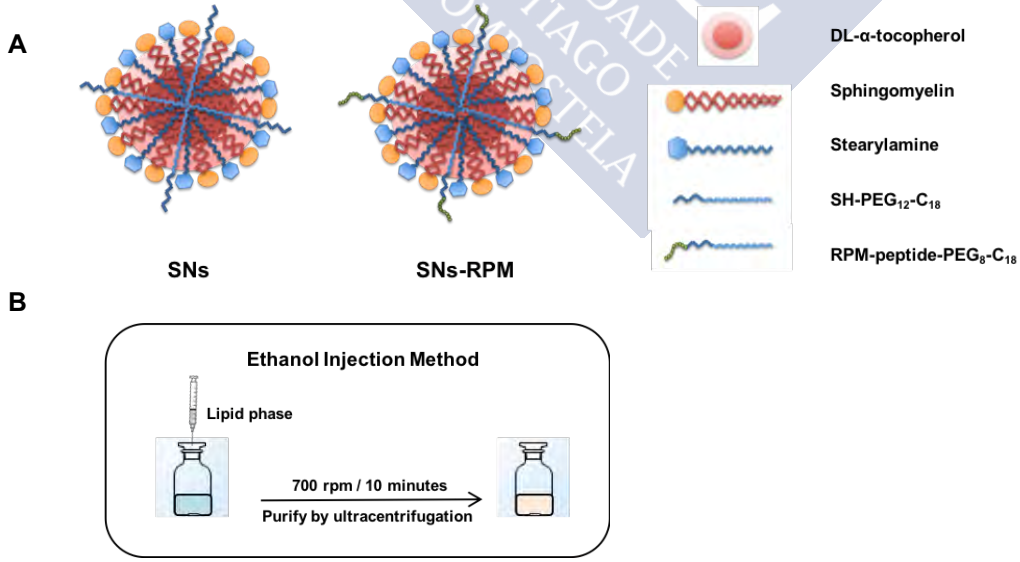

Figure 2. Components (A). and Scheme of preparation of SNs and SNs-RPM (B).

By adding a cationic lipid (stearylamine) during the formulation of SNs-ST, we were able to obtain monodisperse nanoemulsions with cationic charge suitable for miRNA association on their surface. The association was achieved by the establishment of electrostatic interactions between the positive charge of the cationic lipid and the negative charge of the phosphate groups of miRNA[37,38]. SNs-ST-miRNA with mass ratio of miRNA:ST 1:10 has suitable properties and a good association efficiency, being therefore selected for *in vitro* testing of their antitumor activity (**Figure 3**). Modifications of the preparation methodology allowed the development of a second type of formulation. SNs-DOTAP-miRNA were synthesized from the encapsulation of preformed lipid complexes into SNs. Lipid complexes were formulated employing hydrophobic ion pairing between the positively charged amino-functionalized lipids (DOTAP) and the negatively charged phosphate group of the RNA backbone. The complexes formation could increase the lipophilicity of the hydrophilic molecule, subsequently favoring its incorporation into lipid-based nanoformulations, similar to what reported with other type of hydrophilic molecules[39].

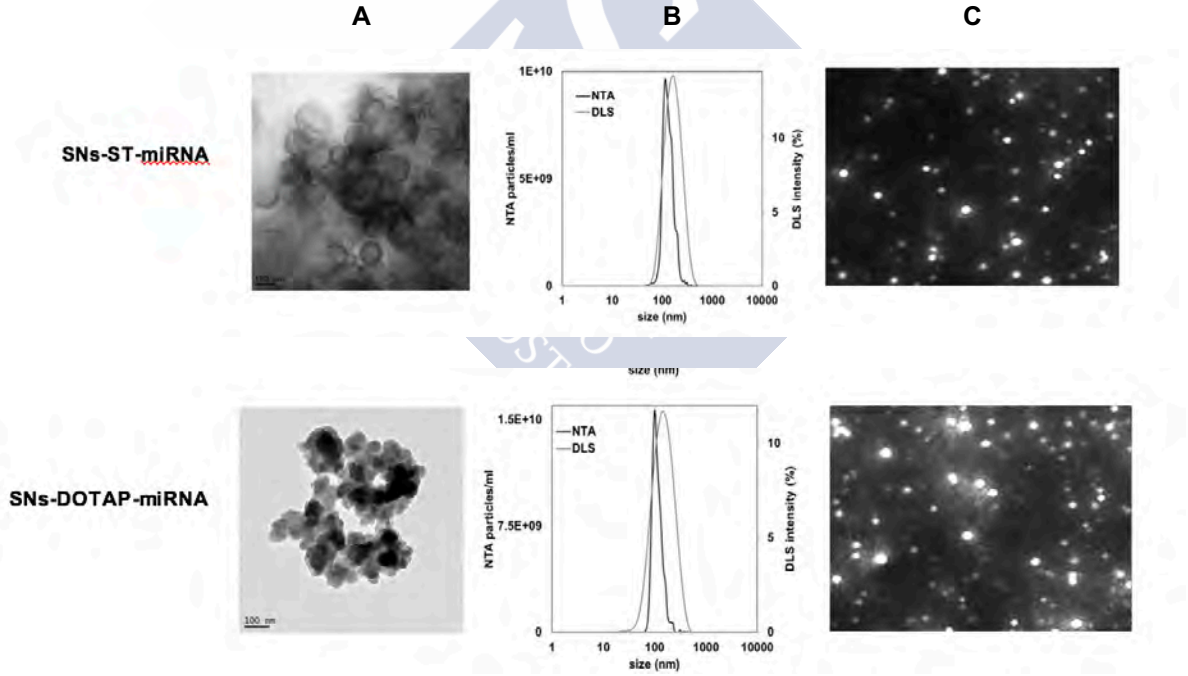

Figure 3. Characterization of SNs-ST-miRNA and SNs-DOTAP-miRNA. Transmission electron microscopy (TEM) images (A). Size distribution graph measured from nanoparticle tracking analysis (NTA) and dynamic light scattering (DLS) (B), and video frame acquired by NTA (C).

With respect to the radiolabelling, the strategy was to add the required functionalities to SNs for further conjugation of ^{18}F-prosthetic group, [^{18}F]FBEM. Thiol functional groups were incorporated via the inclusion of a lipid-PEG-thiol derivative into SNs, or upon surface decoration with the RPM peptide, which on the other hand has already proved to be an interesting ligand for targeted delivery to colorectal cancer cells expressing the integrin $\alpha_5\beta_1$ receptor[40-42]. **Table 1** shows the physicochemical properties of SNs with a thiol group and SNs-RPM. They maintained a small size and form monodisperse formulations, proving that it is possible to introduce the desired functionalities in the formulation without altering the physicochemical properties.

Table 1. Hydrodynamic size, polydispersity index (PDI), and zeta potential (ζ-potential) of SNs and SNs-RPM (n=3).

Formulation	Size (nm)	PDI	ζ-Potential (mV)
SNs	125 ± 3	0.2	+37± 2
SNs-RPM	138 ± 5	0.2	+41 ± 7

Altogether, SNs proved to provide a nanoplatform that can be tailored according to specific medical needs, in this particular case to allow the association of oncosuppressor miRNA mimics and radiolabelling with ^{18}F, to develop new strategies for treatment and diagnosis of colorectal cancer.

SNs can mediate a therapeutic effect after intracellular delivery of oncosuppressor miRNAs to colorectal cancer cells

The capability of SNs-loaded with miRNA to interact with colorectal cancer cells and deliver their cargo was analyzed. SNs-ST-miRNA and SNs-DOTAP-miRNA showed colocalization of two fluorescence dyes labelled with miRNA and lipid parts, demonstrating the ability to deliver miRNA to tumor. It is worth mentioning that SNs-DOTAP-miRNA exhibited higher internalization of miRNA145 compared to SNs-ST-miRNA (**Figure 4**). This confirmed the improvement of greatly compacted complexes to support encapsulation of nucleic acid and to protect them against enzymatic digestion[43,44]. Furthermore, tumor activity was suppressed by transfection of SNs-DOTAP-miRNA, in reference to untreated control cells and cells treated with

the scrambled sequence. These results are in agreement with previously published work with miRNA145-based biodegradable PLGA and magnetic nanoparticles[45, 46], providing potential for further development of gene replacement therapies for colorectal cancer. From these results, it can be considered that SNs can be conveniently modulated and adapted to the specific requirements of a certain therapy.

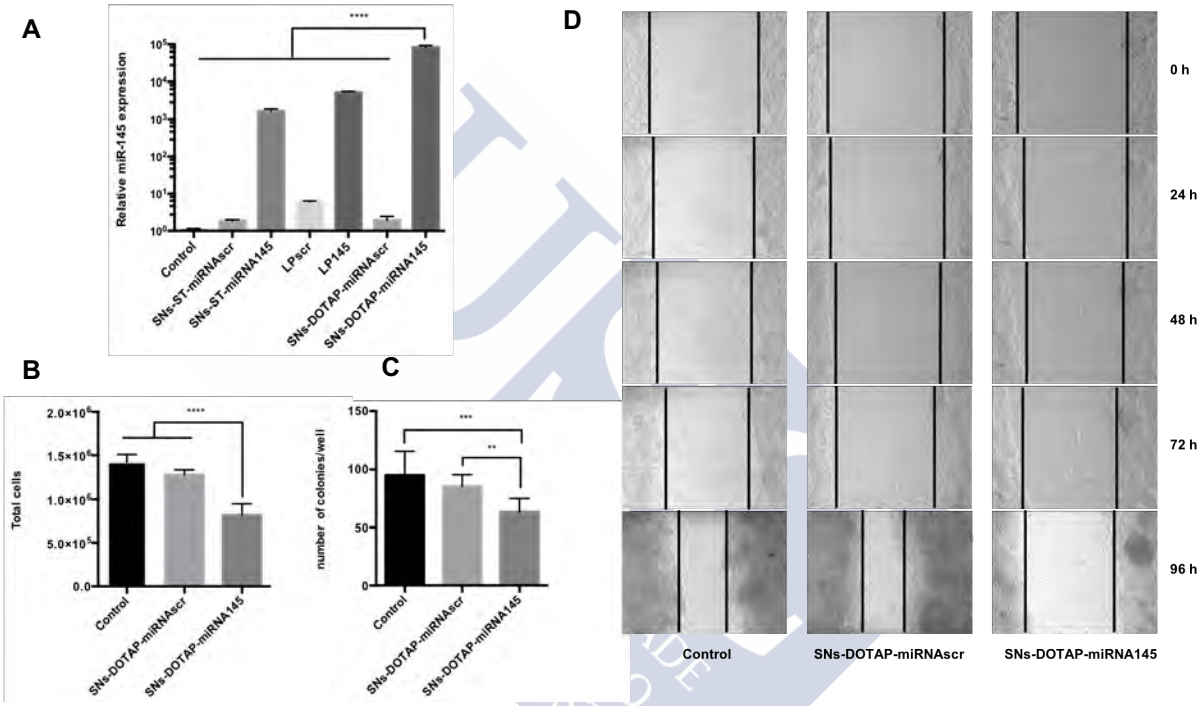

Figure 4. Expression of miR145 after transfection with SNs-ST-miRNA145, Lipid complexes145 (LP145), and SNs-DOTAP-miRNA145 nanosystems (as well as nanosystems prepared with the scrambled sequence, SNs-ST-miRNAscr, LPscr, and SNs-DOTAP-miRNAscr (A). Proliferation of SW480 cells 72 h post-transfection (**** $p \leq 0.0001$) (B). Quantitative analysis of colony numbers, 2 weeks after transfection is shown (*** $p \leq 0.001$ and ** $p \leq 0.01$) (C). Representative images showing cell migration in wound healing assay, of untreated control cells and cells treated with SNs-DOTAP-miRNA145 and the same formulation with the scrambled sequence (SNs-DOTAP-miRNAscr). Images were taken 0,24,48,72, and 96 h after treatment. The dark lines designated the rough margins of the SW480 cells (D).

SNs can be radiolabelled with 18F for PET imaging

Radiolabelled SNs and SNs-RPM were obtained through facile-conjugated chemistry with simple purification and without the use of organic solvents. Moreover, the labelling process was performed under controlled pH and osmolarity to obtain a formulation with suitable characteristics for further intravenous injection[47].

We started from the synthesis of [^{18}F]FBEM, which was later coupled to the nanoemulsions. It is a reproducible and reliable automated synthesis, which renders adequate yields at the end of the procedure for further experiments[48]. The conjugation of [^{18}F]FBEM to SNs and SNs-RPM was performed after the reduction of the disulfide bond when free thiol groups were available for radiolabelling[49,50]. Further experiments specifically confirmed that the labelling position occurred at thiol functional groups either coming from the lipid-PEG derivative or the peptide. Non-specific labelling was not observed in any case. Lastly, the purification process was successfully performed. In general, radiolabelling of nanoparticles could be accomplished either before or after the synthesis of nanoparticles. Other reports of post-labelled nanoparticles using different ^{18}F-prosthetic groups have been reported[51-53]. Due to the short half-life of ^{18}F, the method of post-labelling may display an advantage allowing high radiochemical yields in relation to the pre-labelling method.

Both SNs-[^{18}F]FBEM and SNs-RPM-[^{18}F]FBEM were characterized and injected to healthy mice to determine their biodistribution by PET scan. Generally, the uptake in different organs depends on the stability of the nanostructures resulted from the nanomaterial composition, size, and surface functionalization[54]. The *ex vivo* pattern of both radiolabelled nanoemulsions exhibited different pharmacokinetic profiles compared with the free labelled-peptide ([^{18}F]FBEM-peptide) from preliminary study. The capture of [^{18}F]FBEM-peptide was lower than both [^{18}F]FBEM-nanoemulsions in liver, spleen, and intestine, stating that the radiolabelled nanoemulsions were stable after injection.

A possible explanation for the high uptake in liver and spleen might be due to the interaction of mononuclear phagocyte system (MPS), stimulating the elimination of foreign particles[55,56]. Other reports from lipid-based nanoparticles have displayed similar distribution patterns[57-59]. Hence, further optimizations such as surface modification with PEG layer may be required to prolong blood circulation time[60,61]. *In vivo* biodistribution studies with PET-MRI exhibited that other than liver, radiolabelled nanoemulsions or their radiolabeled metabolic products were also excreted through urinary tracts (**Figure 5**). Overall, these results were in agreement with the results of the *ex vivo* study. Biodistribution and pharmacokinetic of this labelled nanoemulsions could pave the way for promising tumor diagnosis.

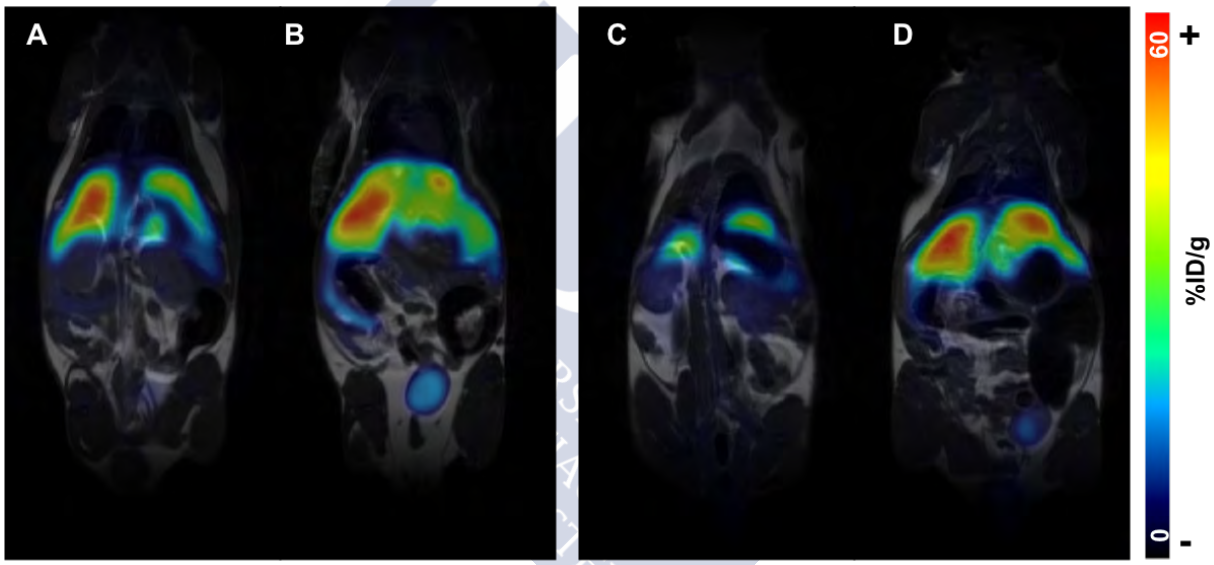

Figure 5. Whole body *in vivo* biodistribution of SNs-[^{18}F]FBEM (left) and SNs-RPM-[^{18}F]FBEM (right) in male BALB/c mice 2h p.i. using PET and MRI: two different coronal slides showing respectively the kidneys (A,C) and the liver and bladder (B,D).

Conclusions

The experimental work described in this thesis was aimed to develop nanoemulsions as multifunctional platforms for treatment and molecular diagnosis of colorectal. Overall, the results allowed us to withdraw the following conclusions:

1. SNs can be conveniently tailored to incorporate molecules of interest for their application in cancer therapy and diagnosis. They can be produced by low energy methods, and their composition can be adjusted to mediate an efficient association of biomolecules and radionuclides.
2. Association of oncosuppressor miRNAs was successfully achieved by incorporation of cationic lipids in the nanostructure. Stearylamine was included as an additional lipid in the original formulation, and DOTAP was used for previous complexation of miRNA previous addition to SNs. Both strategies successfully mediated the internalization of the associated miRNA by the targeted cancer cells, being the second strategy more efficient.
3. The increase in the intracellular levels of oncosuppressor miRNAs translated into demonstrated anticancer activity. miRNA-loaded SNs are efficient nanosystems for the development of innovative gene therapy strategies to treat colorectal cancer.
4. Radiolabelling of SNs was successfully accomplish after incorporation of a thiol group at the nanoparticle surface, either by the inclusion of a PEG surfactant functionalized with thiol, or a targeted peptide with thiol residues.
5. A Michael addition reaction was set among the –SH groups of SNs and a ^{18}F-prosthetic group, [^{18}F]FBEM. The properties of SNs were maintained after the radiolabelling process.
6. ^{18}F-radiolabelled SNs proved to render an adequate signal for PET scan and allowed studying their biodistribution both *ex vivo* and *in vivo*.
7. Radiolabeling SNs opens an entire new horizon towards the development of biocompatible nanoemulsions for *in vivo* diagnosis purposes, and more sophisticated entities such as nanotheranostics.

References

(1) Smith, J. J.; Deane, N. G.; Wu, F.; Merchant, N. B.; Zhang, B.; Jiang, A.; Lu, P.; Johnson, J. C.; Schmidt, C.; Bailey, C. E.; *et al.* Experimentally Derived Metastasis Gene Expression Profile Predicts Recurrence and Death in Patients With Colon Cancer. *Gastroenterology* **2010**, *138*, 958–968.

(2) Lordick, F.; Mariette, C.; Haustermans, K.; Obermannová, R.; Arnold, D.; on behalf of the ESMO Guidelines Committee, clinicalguidelines@esmo org. Oesophageal Cancer: ESMO Clinical Practice Guidelines for Diagnosis, Treatment and Follow-Up. *Ann. Oncol.* **2016**, *27*, v50–v57.

(3) Lorusso, D.; Bria, E.; Costantini, A.; Di Maio, M.; Rosti, G.; Mancuso, A. Patients' Perception of Chemotherapy Side Effects: Expectations, Doctor–Patient Communication and Impact on Quality of Life – An Italian Survey. *Eur. J. Cancer Care (Engl).* **2017**, *26*, 1–9.

(4) Shi, J.; Kantoff, P. W.; Wooster, R.; Farokhzad, O. C. Cancer Nanomedicine: Progress, Challenges and Opportunities. *Nat. Rev. Cancer* **2017**, *17*, 20–37.

(5) Bobo, D.; Robinson, K. J.; Islam, J.; Thurecht, K. J.; Corrie, S. R. Nanoparticle-Based Medicines: A Review of FDA-Approved Materials and Clinical Trials to Date. *Pharm. Res.* **2016**, *33*, 2373–2387.

(6) Hare, J. I.; Lammers, T.; Ashford, M. B.; Puri, S.; Storm, G.; Barry, S. T. Challenges and Strategies in Anti-Cancer Nanomedicine Development: An Industry Perspective. *Adv. Drug Deliv. Rev.* **2017**, *108*, 25–38.

(7) Muthiah, M.; Park, I.-K.; Cho, C.-S. Nanoparticle-Mediated Delivery of Therapeutic Genes: Focus on MiRNA Therapeutics. *Expert Opin. Drug Deliv.* **2013**, *10*, 1259–1273.

(8) Fernandez-Piñeiro, I.; Badiola, I.; Sanchez, A. Nanocarriers for MicroRNA Delivery in Cancer Medicine. *Biotechnol. Adv.* **2017**, *35*, 350–360.

(9) Wang, H.; Jiang, Y.; Peng, H.; Chen, Y.; Zhu, P.; Huang, Y. Recent Progress in MicroRNA Delivery for Cancer Therapy by Non-Viral Synthetic Vectors. *Adv. Drug Deliv. Rev.* **2015**, *81*, 142–160.

(10) Ganju, A.; Khan, S.; Hafeez, B. B.; Behrman, S. W.; Yallapu, M. M.; Chauhan, S. C.; Jaggi, M. MiRNA Nanotherapeutics for Cancer. *Drug Discov. Today* **2017**, *22*, 424–432.

(11) Lin, S.; Gregory, R. I. MicroRNA Biogenesis Pathways in Cancer. *Nat. Rev. Cancer* **2015**, *15*, 321–333.

(12) Rupaimoole, R.; Slack, F. J. MicroRNA Therapeutics: Towards a New Era for the Management of Cancer and Other Diseases. *Nat. Rev. Drug Discov.* **2017**, *16*, 203–221.

(13) Wang, Z.; Zhang, X.; Yang, Z.; Du, H.; Wu, Z.; Gong, J.; Yan, J.; Zheng, Q. MiR-145 Regulates PAK4 via the MAPK Pathway and Exhibits an Antitumor Effect in Human Colon Cells. *Biochem. Biophys. Res. Commun.* **2012**, *427*. 444-449.

(14) Feng, Y.; Zhu, J.; Ou, C.; Deng, Z.; Chen, M.; Huang, W.; Li, L. MicroRNA-145 Inhibits Tumour Growth and Metastasis in Colorectal Cancer by Targeting Fascin-1. *Br. J. Cancer* **2014**, *110*. 2300-2309.

(15) Panza, A.; Votino, C.; Gentile, A.; Valvano, M. R.; Colangelo, T.; Pancione, M.; Micale, L.; Merla, G.; Andriulli, A.; Sabatino, L.; *et al.* Peroxisome Proliferator-Activated Receptor γ-Mediated Induction of MicroRNA-145 Opposes Tumor Phenotype in Colorectal Cancer. *Biochim. Biophys. Acta - Mol. Cell Res.* **2014**, *1843*. 1225-1236.

(16) Ding, H.; Wu, F. Image Guided Biodistribution and Pharmacokinetic Studies of Theranostics. *Theranostics* **2012**, *2*, 1040–1053.

(17) Savla, R.; Minko, T. Nanoparticle Design Considerations for Molecular Imaging of Apoptosis: Diagnostic, Prognostic, and Therapeutic Value. *Adv. Drug Deliv. Rev.* **2017**, *113*, 122–140.

(18) Hahn, M. A.; Singh, A. K.; Sharma, P.; Brown, S. C.; Moudgil, B. M. Nanoparticles as Contrast Agents for In-Vivo Bioimaging: Current Status and Future Perspectives. *Anal. Bioanal. Chem.* **2011**, *399*, 3–27.

(19) Vázquez-Ríos, A. J.; Alonso-Nocelo, M.; Bouzo, B. L.; Ruiz-Bañobre, J.; de la Fuente, M. Nanotheranostics and Their Potential in the Management of Metastatic Cancer. *Handbook of Nanomaterials for Cancer Theranostics*. **2018**, 199-244

(20) Coenen, H. H.; Elsinga, P. H.; Iwata, R.; Kilbourn, M. R.; Pillai, M. R. A.; Rajan, M. G. R.; Wagner, H. N.; Zaknun, J. J. Fluorine-18 Radiopharmaceuticals beyond [18F]FDG for Use in Oncology and Neurosciences. *Nucl. Med. Biol.* **2010**, *37*, 727–740.

(21) Littich, R.; Scott, P. J. H. Novel Strategies for Fluorine-18 Radiochemistry. *Angew. Chemie - Int. Ed.* **2012**, *51*, 1106–1109.

(22) Jacobson, O.; Zhu, L.; Ma, Y.; Weiss, I. D.; Sun, X.; Niu, G.; Kiesewetter, D. O.; Chen, X. Rapid and Simple One-Step F-18 Labeling of Peptides. *Bioconjug. Chem.* **2011**, *22*, 422–428.

(23) Wu, Z.; Kandeel, F. F-Labeled Proteins. *Current Pharmaceutical Biotechnology*, **2010**, *11*, 572-580

(24) Kiesewetter, D. O.; Jacobson, O.; Lang, L.; Chen, X. Automated Radiochemical Synthesis of [18F]FBEM: A Thiol Reactive Synthon for Radiofluorination of Peptides and Proteins. *Appl. Radiat. Isot.* **2011**, *69*, 410–414.

(25) Lim, K.; Ropchan, J.; Kiesewetter, D. O.; Chen, X.; Huang, Y. Automated Radiosynthesis of [18F]FBEM, a Sulfhydryl Site Specific Labeling Agent for Peptides and Proteins. *Appl. Radiat. Isot.* **2018**, *140*, 294–299.

(26) Sutradhar, K. B.; Amin, L. Nanoemulsions: Increasing Possibilities in Drug Delivery. *Eur. J. Nanomedicine* **2013**, *5*, 97–110.

(27) Gupta, A.; Eral, H. B.; Hatton, T. A.; Doyle, P. S. Nanoemulsions: Formation, Properties and Applications. *Soft Matter* **2016**, *12*, 2826–2841.

(28) Verissimo, L. M.; Agnez Lima, L. F.; Monte Egito, L. C.; De Oliveira, A. G.; Do Egito, E. S. T. Pharmaceutical Emulsions: A New Approach for Gene Therapy. *J. Drug Target.* **2010**, *18*, 333–342.

(29) Ganta, S.; Talekar, M.; Singh, A.; Coleman, T. P.; Amiji, M. M. Nanoemulsions in Translational Research—Opportunities and Challenges in Targeted Cancer Therapy. *AAPS PharmSciTech* **2014**, *15*, 694–708.

(30) Teixeira, H. F.; Bruxel, F.; Fraga, M.; Schuh, R. S.; Zorzi, G. K.; Matte, U.; Fattal, E. Cationic Nanoemulsions as Nucleic Acids Delivery Systems. *Int. J. Pharm.* **2017**, *534*, 356–367.

(31) Liu, C. H.; Yu, S. Y. Cationic Nanoemulsions as Non-Viral Vectors for Plasmid DNA Delivery. *Colloids Surfaces B Biointerfaces* **2010**, *79*, 509–515.

(32) Loureiro, A.; Nogueira, E.; Azoia, N. G.; Sárria, M. P.; Abreu, A. S.; Shimanovich, U.; Rollett, A.; Härmark, J.; Hebert, H.; Guebitz, G.; *et al.* Size Controlled Protein Nanoemulsions for Active Targeting of Folate Receptor Positive Cells. *Colloids Surfaces B Biointerfaces* **2015**, *135*, 90–98.

(33) Ganta, S.; Singh, A.; Kulkarni, P.; Keeler, A. W.; Piroyan, A.; Sawant, R. R.; Patel, N. R.; Davis, B.; Ferris, C.; O'Neal, S.; *et al.* EGFR Targeted Theranostic Nanoemulsion for Image-Guided Ovarian Cancer Therapy. *Pharm. Res.* **2015**, *32*, 2753–2763.

(34) Afzal, S. M.; Shareef. M. Z.; Kishan, V. Transferrin tagged lipid nanoemulsion of docetaxel for enhanced tumor targeting. *Journal of Drug Delivery Science and Technology*. **2016**, *36.* 175-182

(35) Press, D. Clinical Development of Liposome-Based Drugs : Formulation , Characterization , and Therapeutic Efficacy. **2012**, 49–60.

(36) Lamichhane, N.; Udayakumar, T. S.; D'Souza, W. D.; Simone, C. B.; Raghavan, S. R.; Polf, J.; Mahmood, J. Liposomes: Clinical Applications and Potential for Image-Guided Drug Delivery. *Molecules* **2018**, *23*, 1–17.

(37) Wang, X.; Yu, B.; Ren, W.; Mo, X.; Zhou, C.; He, H.; Jia, H.; Wang, L.; Jacob, S. T.; Lee, R. J.; *et al.* Enhanced Hepatic Delivery of SiRNA and MicroRNA Using Oleic Acid Based Lipid Nanoparticle Formulations. *J. Control. Release* **2013**, *172*, 690–698.

(38) Hsu, S. hao; Yu, B.; Wang, X.; Lu, Y.; Schmidt, C. R.; Lee, R. J.; Lee, L. J.; Jacob, S. T.; Ghoshal, K. Cationic Lipid Nanoparticles for Therapeutic Delivery of SiRNA and MiRNA to Murine Liver Tumor. *Nanomedicine Nanotechnology, Biol. Med.* **2013**, *9*, 1169–1180.

(39) Hintzen, F.; Perera, G.; Hauptstein, S.; Müller, C.; Laffleur, F.; Bernkop-Schnürch, A. In vivo evaluation of an oral self-microemulsifying drug delivery system (SMEDDS) for leuprorelin. *Int. J. Pharm.* **2014**, *472*, 20–26.

(40) Kelly, K. a; Jones, D. a. Isolation of a Colon Tumor Specific Binding Peptide Using Phage Display Selection. *Neoplasia* **2003**, *5*, 437–444.

(41) Kelly, K.; Alencar, H.; Funovics, M.; Mahmood, U.; Weissleder, R. Detection of Invasive Colon Cancer Using a Novel, Targeted, Library-Derived Fluorescent Peptide. *Cancer research.* **2004**, 64, 6247–6251.

(42) Lee, Y. M.; Lee, D.; Kim, J.; Park, H.; Kim, W. J. RPM Peptide Conjugated Bioreducible Polyethylenimine Targeting Invasive Colon Cancer. *J. Control. Release* **2015**, *205*, 172–180.

(43) Yuan, H.; Zhang, W.; Du, Y. Z.; Hu, F. Q. Ternary Nanoparticles of Anionic Lipid Nanoparticles/Protamine/DNA for Gene Delivery. *Int. J. Pharm.* **2010**, *392*, 224–231.

(44) Hauptstein, S.; Prüfert, F.; Bernkop-Schnürch, A. Self-Nanoemulsifying Drug Delivery Systems as Novel Approach for PDNA Drug Delivery. *Int. J. Pharm.* **2015**, *487*, 25–31.

(45) Liang, G.; Zhu, Y.; Jing, A.; Wang, J.; Hu, F.; Feng, W.; Xiao, Z.; Chen, B. Cationic MicroRNA-Delivering Nanocarriers for Efficient Treatment of Colon Carcinoma in Xenograft Model. *Gene Ther.* **2016**.

(46) Setua, S.; Khan, S.; Yallapu, M. M.; Behrman, S. W.; Sikander, M.; Khan, S. S.; Jaggi, M.; Chauhan, S. C. Restitution of Tumor Suppressor MicroRNA-145 Using Magnetic Nanoformulation for Pancreatic Cancer Therapy. *J. Gastrointest. Surg.* **2017**.

(47) Stranz, M.; Kastango, E. S. A Review of pH and Osmolarity. *International Journal of Pharmaceutical Compounding.* **2013**, *6.* 216-220

(48) Dammicco, S.; Goux, M.; Lemaire, C.; Becker, G.; Bahri, M. A.; Plenevaux, A.; Cinier, M.; Luxen, A. Regiospecific Radiolabelling of Nanofitin on Ni Magnetic Beads with [18F]FBEM and in Vivo PET Studies. *Nucl. Med. Biol.* **2017**, *51*, 33–39.

(49) Erel, O.; Neselioglu, S. A Novel and Automated Assay for Thiol/Disulphide Homeostasis. *Clin. Biochem.* **2014**, *47*, 326–332.

(50) Zwyssig, A.; Schneider, E. M.; Zeltner, M.; Rebmann, B.; Zlateski, V.; Grass, R. N.; Stark, W. J. Protein Reduction and Dialysis-Free Work-Up through Phosphines Immobilized on a Magnetic Support: TCEP-Functionalized Carbon-Coated Cobalt Nanoparticles. *Chem. - A Eur. J.* **2017**, *23*, 8585–8589.

(51) Rojas, S.; Gispert, J. D.; Martín, R.; Abad, S.; Menchón, C.; Pareto, D.; Víctor, V. M.; Álvaro, M.; García, H.; Herance, J. R. Biodistribution of Amino-Functionalized Diamond Nanoparticles. in Vivo Studies Based On18F Radionuclide Emission. *ACS Nano* **2011**, *5*, 5552–5559.

(52) Rojas, S.; Gispert, J. D.; Abad, S.; Buaki-Sogo, M.; Victor, V. M.; Garcia, H.; Herance, J. R. In Vivo Biodistribution of Amino-Functionalized Ceria Nanoparticles in Rats Using Positron Emission Tomography. *Mol. Pharm.* **2012**, *9*, 3543–3550.

(53) Guerrero, S.; Herance, J. R.; Rojas, S.; Mena, J. F.; Gispert, J. D.; Acosta, G. A.; Albericio, F.; Kogan, M. J. Synthesis and in Vivo Evaluation of the Biodistribution of a 18F-Labeled Conjugate Gold-Nanoparticle-Peptide with Potential Biomedical Application. *Bioconjug. Chem.* **2012**, *23*, 399–408.

(54) Harper, S.; Usenko, C.; Hutchison, J. E.; Maddux, B. L. S.; Tanguay, R. L. In Vivo Biodistribution and Toxicity Depends on Nanomaterial Composition, Size, Surface Functionalisation and Route of Exposure. *J. Exp. Nanosci.* **2008**, *3*, 195–206.

(55) Cho, E. C.; Xie, J.; Wurm, P. A.; Xia, Y.; Understanding the Role of Surface Charges in Cellular Adsorption versus Internalization by Selectively Removing Gold Nanoparticles on the Cell Surface with a I_2/KI Etchant. *Nano Letter.* **2009**, *9*, 3, 1080-1084

(56) Xiao, W.; Chen, W. H.; Xu, X. D.; Li, C.; Zhang, J.; Zhuo, R. X.; Zhang, X. Z. Design of a Cellular-Uptake-Shielding "Plug and Play" Template for Photo Controllable Drug Release. *Adv. Mater.* **2011**, *23*, 3526–3530.

(57) Jensen, A. I.; Severin, G. W.; Hansen, A. E.; Fliedner, F. P.; Eliasen, R.; Parhamifar, L.; Kjær, A.; Andresen, T. L. Remote-Loading of Liposomes with Manganese-52 and in Vivo Evaluation of the Stabilities of 52 Mn-DOTA and 64 Cu-DOTA Using Radiolabelled Liposomes and PET Imaging. *J. Control. Release* **2018**, *269*, 100–109.

(58) Crístian, D.; Soares, F.; Oliveira, M. C. De; Luís, A.; Barros, B. De; Cardoso, V. N.; Ramaldes, G. A. European Journal of Pharmaceutical Sciences Liposomes Radiolabeled with 159 Gd : In Vitro Antitumoral Activity , Biodistribution Study and Scintigraphic Image in Ehrlich Tumor Bearing Mice. **2011**, *43*, 290–296.

(59) Eroglu, H.; Yenilmez, A. An Investigation of the Usability of Solid Lipid Nanoparticles Radiolabelled with Tc-99m as Imaging Agents in Liver-Spleen Scintigraphy. **2016**, *12*, 1501–1509

(60) Blanco, E.; Shen, H.; Ferrari, M. Principles of Nanoparticle Design for Overcoming Biological Barriers to Drug Delivery. *Nat. Biotechnol.* **2015**, *33*, 941–951.

(61) Rao, L.; Xu, J. H.; Cai, B.; Liu, H.; Li, M.; Jia, Y.; Xiao, L.; Guo, S. S.; Liu, W.; Zhao, X. Z. Synthetic Nanoparticles Camouflaged with Biomimetic Erythrocyte Membranes for Reduced Reticuloendothelial System Uptake. *Nanotechnology* **2016**, *27*, 85106.

Abbreviation list

USC
UNIVERSIDADE
DE SANTIAGO
DE COMPOSTELA

Abbreviation list

^{18}F	Fluorine-18
[^{18}F]FBEM	4-[^{18}F]fluorobenzamido-N-ethylmaleimide
[^{18}F]SFB	N-Succinimidyl-4-[^{18}F]fluorobenzoate
AuNPs	Gold nanoparticles
BFC	Bifunctional chelator
CaP	Calcium phosphate
CRC	Colorectal cancer
CT	Computed tomography
DDS	Drug delivery system
DLS	Dynamic laser scattering
DOGS	di-ioctadecyl-amido-glycyl-spermine
DOPE	di-oleoyl-phosphatidyl ethanolamine
DOSPA	2,3-Dioleyloxy-N-[2(sperminecarboxamido)ethyl]-N,N-dimethyl-l-propanaminium trifluoroacetate);
DOTA	1,4,7,10-tetraazacyclododecane-1,4,7,10- tetraacetic acid
DOTAP	1,2-dioleoyl-3-trimethylammonium-propane
DOTMA	1,2-di- O-octadecenyl-3-trimethylammonium propane
DTPA	Diethylene triamine pentaacetic acid
EGFR	Epidermal growth factor receptor
EPR	Enhance permeability and retention
FACS	Fluorescence-Activated Cell Sorting
FDG	^{18}F-fluorodeoxyglucose
Gd	Gadolinium
miRNA	MicroRNA
MPS	Mononuclear phagocyte system
MRI	Magnetic resonance imaging
mRNA	Messenger RNA
NOTA	1,4,7-triazacyclononane-1,4,7- triacetic acid

NTA	Nanoparticle tracking analysis
pDNA	Plasmid DNA
PDI	Polydispersity index
PEG	Polyethylene glycol
PEI	Polyethyleneimine
PET	Positron emission tomography
PLGA	Poly(D,L-lactide-co-glycolide acid
PLL	Poly(l-lysine)
QDs	Quantum dots
ROS	Reactive oxygen species
siRNA	Small interfering RNA
SM	Sphingomyelin
SNs	Sphingomyelin nanoemulsions
SPECT	Single-photon emission computed tomography
ST	Stearylamine
SWNTs	single-walled carbon nanotubes
TEM	Transmission electron microscopy
UPLC	Ultra-performance liquid chromatography
Vit E	Vitamin E (DL-α-tocopherol)
VEGF	Vascular endothelial growth factor

Ethical considerations

USC
UNIVERSIDADE
DE SANTIAGO
DE COMPOSTELA

Annex

USC
UNIVERSIDADE
DE SANTIAGO
DE COMPOSTELA